Wind Farm Efficiency

Design Synthesis Exercise Spring 2011

Group S12: Final Report

Principal Tutor	*Wim Bierbooms*
Coach	*Roger Groves*
	Coen de Visser
Daniel Boonman	*(1375776)*
Carsten Broich	*(1544373)*
Ronald Deerenberg	*(1398288)*
Koen Groot	*(1507060)*
Ash Hamraz	*(1312278)*
Roelant Kalthof	*(1324675)*
Gijs Nieuwint	*(1376500)*
Jan Schneiders	*(1513095)*
Yu Tang	*(1507915)*
Jord Wiegerink	*(1521837)*

Date: June 28th 2011

TU Delft Delft University of Technology

{This page is intentionally left blank.}

Change record

Issue	Date	Pages affected	Brief description of change
1	13-6-2011	all	First version of report body
2	14-6-2011	all	First revision of report (body)
3	16-6-2011	all	Added frontmatter and backmatter
4	17-6-2011	all	Second revision of report (full)
5	17-6-2011	all	Exclude compilation errors
6	17-6-2011	all	Finalize report
7			

Preface

This technical report was written as a part of the Design Synthesis Exercise (DSE), part of the third year Aerospace Engineering Bachelor curriculum of the Delft University of Technology. Ten students, together forming DSE group S12, have worked together for eleven weeks to come to this result.

The report describes the design of an innovative system to increase wind farm efficiency. After reading this report, the reader should understand the design process and the design itself.

When reading this report, some prior knowledge of the working principles of wind farms, economics, aerodynamics and structures is helpful to fully understand the content and derivations. However, without this prior knowledge the general outline should be understandable for most readers.

DSE group S12 likes to thank principle tutor dr. ir. W.A.A.M. Bierbooms and the coaches ir. C.C. de Visser and dr. R.M. Groves for their support and sharp remarks. Also ir. R. van der Vlugt, ir A. de Wachter, dr. S.J. Hulshoff, dr.ir. L.L.M. Veldhuis and dr.ir. B.W. van Oudheusden are thanked for their advises on kites and aerodynamics. Furthermore, ir. M.L.A. Segeren is thanked for his advises on offshore engineering.

{This page is intentionally left blank.}

Contents

List of symbols

Symbol	Description	Unit	Symbol	Description	Unit
A	Scale parameter Weibull	[m/s]	Re	Reynolds number	[-]
A	Surface Area	[m^2]	r	Distance between kite and buoy	[m]
a	Speed of sound	[m/s]	S	Surface area	[m^2]
AR	Aspect ration	[-]	s	Non-dimensional horizontal distance	[-]
b	Span	[m]	T	Temperature	[K]
C	Coefficient	[-]	t	Thickness	[m]
c	Fitting parameter	[-]	V	Wind speed	[m/s]
c	Wind direction correction factor	[-]	W	Weight	[N]
c	Chord length	[m]	w	Width	[m]
c	Characteristic length	[m]	X	Horizontal distance	[m]
D	Rotor disc area	[m^2]	y	Vertical distance	[m]
D	Drag	[N]	z_0	Roughness coefficient	[-]
d	Diameter	[m]	α	Frandsen parameter	[-]
d	Depth	[m]	α	Entrainment coefficient	[-]
E	Modulus of elasticity	[Pa]	α	Chain force angle	[deg]
F	Force	[N]	α_i	Induced angle of attack	[deg]
f	Velocity factor	[-]	α	Thermal expansion coefficient	[K^{-1}]
g	Gravitational acceleration	[m/s^2]	β	Frandsen parameter	[-]
H	Needed height	[m]	β	Slope of solar panel	[rad]
h	Height	[m]	β	Buoy tether force angle	[rad]
I	Solar Intensity	[W/m^2]	γ	Azimuth angle	[rad]
I	Second area moment of inertia	[m^4]	γ	Buoy chain angle	[rad
K	Column effective length factor	[-]	δ	Thickness boundary layer	[m]
k	Shape parameter	[-]	δ	Declination angle	[rad]
k	Decay factor	[-]	δ	Displacement	[m]
L	Lift	[N]	ϵ	Downwash angle	[deg]
l	Length	[m]	ϵ	Strain	[-]
M	Mach number	[-]	η	Efficiency	[-]
M	Moment	[Nm]	θ	Angle	[rad]
m	Fitting parameter	[-]	μ	Viscosity	[kg/m/s]
$\dot{m}$	Mass flow	[m/s]	μ	Friction coefficient	[-]
P	Power	[W]	ν	Poission's ratio	[-]
P	Profit	[€]	ρ	Density	[kg/m^3]
p	Pressure	[Pa]	σ	Stress	[Pa]
p	Calculation parameter	[-]	ϕ	Latitude	[rad]
R	Universal gas constant	[J/mol·K]	ω	Argument of perigee	[rad]

List of subscripts

Symbol	Description
anchor	Anchor
av	Average
b	Bending
buoy	Buoy
buoyancy	Buoyancy
chain	Chain
concrete	Concrete
controlpod	Control pod
corr	Corrected
correction factor	Correction factor
current	Current
cl	Control line
D	Drag
D	Departing flow
disturbed	Disturbed
dw	Downwash
E	Entering free stream
extreme	Extreme
flat	Flat
friction	Friction
IJmuiden	Weather station IJmuiden
inf	Free stream
jet expansion	Jet expansion
hub	Wind turbine hub
Independent	Independent
Initial	Initial
kite	kite
K13	Weather station K13
L	Lift
maint.kite	Maintenance kite
mast	Mast
max	Maximum
mix	Mixing
N	Number of wind turbines
Noordwijk	Weather station Noordwijk

Symbol	Description
operational	During operation
optimal	Optimal
P	Power
pl	Power line
power rating	Power rating
projected	Projected
r	Reality
rated	Rated
rating correction	Rating correction
req	Required
rotor	Rotor
rotor disk	Rotor disk
solar	Solar
stall	Stall
suspended	Suspended on the mast
T	Thrust
t	Wind tunnel
undisturbed	Undisturbed
vector	In direction of
w	Wake
water	Water
weight	Weight
wf	Wind farm
winch	Winch
wind dir.	Wind direction
wind	wind
x,	X-direction of
y,	Y-direction of
0	Initial
0.x	From 0 to x
1	First wind turbine
2	Second wind turbine
3	After second wind turbine
*	Dimensionless velocity

List of Abbreviations

Full Name	Abbreviation
Alternating Current	AC
Attitude Control System	ACS
Applied Sustainable Science Engineering and Technology	ASSET
Bisphenol A	BPA
Business to Business	B2B
Center of Buoyancy	CB
Center of Gravity	CG
Computational Fluid Dynamics	CFD
Commercially Off-The-Shelf	COTS
Cumulative Density Function	CDF
Direct Current	DC
Dutch Offshore Wind Energy Converter	DOWEC
Environmental Observation System	EOS
Finite Element Method	FEM
Fault Tree Analysis	FTA
Global Positioning System	GPS
Health Monitoring System	HMS
Koninklijk Nederlands Meteorologisch Instituut	KNMI
Kite Steering Unit	KSU
Kamer van Koophandel	KvK
Mission Need Statement	MNS
MacNeal-Schwendler Corporation	MSC
Mean Time Between Maintenance	MTBM
Mean Time To Maintain	MTTM
Polyethylene Terephthalate	PET
Polyvynil Fluoride	PVF
Probability Density Function	PDF
Particle Image Velocimetry	PIV
Project Objective Statement	POS
Reliability, Availability, Maintenance and Safety	RAMS
Requirements Discovery Tree	RDT
Return on Investment	ROI
Safety Factor	SF
Sound Pressure Level	SPL
Thanet Wind Farm	TWF
Thermal Expansion Coefficient	TEC
Offshore Windpark Egmond aan Zee	OWEZ
Strength Weakness Opportunities Threads	SWOT
Technical Performance Measurement	TPM
Tether Retraction System	TRS
Ultra Violet	UV
Vertical distance Leading Edge Curvature	VLEC
Wind Speed	WS

Summary

Within wind farms wind turbines are located in arrays. The wind turbines induce wakes which propagate within these arrays, causing a velocity decrease experienced by the wind turbines downstream, resulting in a reduced wind farm efficiency. The objective is to reduce this deficit by at least 3%, by mixing the outer undisturbed flow with the wake of the wind turbines.

The purpose of this report is to come up with a detailed design of a device that can fulfil all requirements set by the client. It can be stated that the design of the kite system is founded by the Project Objective Statement (POS) and the Mission Need Statement (MNS), presented below. From these statements the design of the kite system starts with the identification of the different requirements, followed by the generation of the first concepts. Finally, from these concepts, one is selected to be worked out further in the detailed design phase, this report.

The Project Objective Statement (POS) of the design is as follows:

> "Design a device, with 10 students within 11 weeks, resulting in a total of 3500 man hours, to increase the efficiency of a wind farm, cost effectively, by at least 3%, by mixing the undisturbed outer flow into the wake region of the wind farm."

The Mission Need Statement (MNS) of the design is as follows:

> "Increase the efficiency of the wind farm by mixing the undisturbed outer flow into the wake of the wind turbines autonomously, in a sustainable manner, within the OWEZ wind farm, providing a high availability with maintenance cycles of 2 years and recyclability with a life cycle of 20 years."

The design option, that was selected to be worked out in this report, is the generation of downwash with the use of kites. This concept is called: the *Daeolus kite system.* A kite is suspended at a height of approximately 145 [m], in the middle of two wind turbines at the boundary of the wake region and the undisturbed flow. The kite is connected by a tether to a buoy floating at sea level. This buoy, together with an attitude control system, keeps the kite at its designated location, while feeding the kite with power and important environmental data. The kite generates lift and therefore downwash, bending the outer undisturbed flow into the wake region, yielding a wind velocity increase at the turbine downstream. This wind velocity increase, in turn, results in a higher power output of the downstream turbine, yielding a wind farm efficiency increase.

The design of the kite system is done for the Offshore Windpark Egmond aan Zee (OWEZ), afterwards the applicability of the device to other wind farms is verified. When looking at the kite concept, three main structural parts can be identified, these are stated below:

- The ground segment
- The tether
- The aerial segment

Each of these is worked out in detail. This is done in the following way. From aerodynamic calculations, considering the given requirements, the loads and stresses present in the subsystems are identified. From these the structures and materials are selected and the overall system performance is evaluated. From the achieved efficiency increase and the system costs, the overall profit of applying the kite system to OWEZ is estimated.

By iterating the aforementioned method for different wind farm efficiency increases, the design is optimized.

For this project, there were several requirements set by the client that had to be fulfilled. These are shown in

Table 1: Results

Requirement	Result
$\geq$ 3% wind farm efficiency increase	4% increase
20 years lifetime	20 years
2 years maintenance interval	2 years
cost efficient	> €6M profit
applicable to OWEZ	yes
scalable to other wind farms	to be determined

the first column of table 27.1. The second column shows the results.
When looking at the results it can be stated that all requirements, when applying the kite system to OWEZ, are satisfied. A wind farm efficiency increase of 4% is achieved by a kite with a projected surface of 128 [m^2] and a projected span of 16 [m]. This kite is actively controlled by a control pod. The main materials used in the different segments are: Dacron for the kite, Dyneema for the tether and Glass fibres for the Buoy. This system yields a profit of more than €6M, while the device performs its functions for 20 years. The first subsystem that has to be maintained is the kite, which will be after two years, satisfying the corresponding requirement. Next to the fact that the kite system is applicable to OWEZ, it can be applied to other wind farms, depending on their characteristics. Whether the kite can be scaled and in what sense this can be done, to apply it to other wind farms is yet to be determined.

All functions can be performed in a sustainable way, posing negligible risks to its surroundings and human beings.

Chapter 1

Introduction

Within wind farms wind turbines are located in arrays. The wind turbines induce wakes which propagate within these arrays, causing a velocity decrease experienced by the wind turbines downstream. In figure 1.1 this effect is shown. The light shaded areas indicate relatively low air velocity; the dark shaded areas indicate high air velocity. This causes a decrease in efficiency of the entire wind farm.

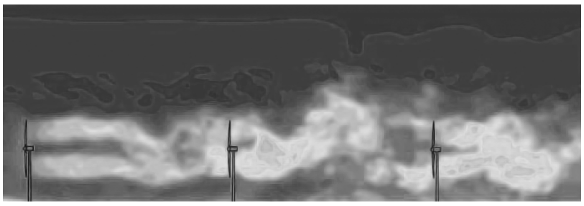

Figure 1.1: Velocity deficit produced by the wind turbines (source: [1])

The decrease in efficiency is a loss for this sustainable way of power generation. Many attempts to reduce this loss have failed or succeeded only partially, because mostly they turned out to be ineffective or too costly. If the efficiency would be increased, this would make wind farms more sustainable and profitable. Luckily, fresh undisturbed air is present above the wind turbines. A device can be designed to use this fact. This device can mix the undisturbed outer flow with the wake regions of the wind farm. Thus, it can increase the velocity in front of the wind turbines downstream, yielding a higher efficiency.

The purpose of this report is to come up with a detailed design of a device that can fulfil all requirements set by the client, which are listed in table 1.1. The main goal is to increase the efficiency of the OWEZ wind farm by at least 3%. This report deals with the detailed design of the concept that was selected out of many others. By performing multiple trade-offs in the Mid-term Report, the best option was chosen: the *Daeolus kite system*. In the end, the design should be able to perform its functions, being sustainable and profitable, posing little or no risks to its surroundings and human beings.

Table 1.1: Requirements

Requirement
$\geq$ 3% wind farm efficiency increase
20 years lifetime
2 years maintenance interval
cost efficient
applicable to OWEZ
scalable to other wind farms

The design of the kite system is done for the Offshore Windpark Egmond aan Zee (OWEZ), afterwards the applicability of the device to other wind farms is verified. Figure 1.2 shows a map of this wind farm. When looking at the kite concept, three main structural parts can be identified, namely the ground segment, the tether and the aerial segment.

Each of these is worked out in detail. This is done in the following way. From aerodynamic calculations, considering the given requirements, the loads and stresses present in the subsystems are identified. From these the structures and materials are selected and the overall system performance is evaluated. From the achieved efficiency increase and the system costs, the overall profit of applying the kite system to OWEZ is estimated.

By iterating the aforementioned method for different wind farm efficiency increases, the design is optimized.

Firstly, a short recap on what is done during the earlier stages of the project is presented. This is done by describing the general characteristics of OWEZ in chapter 2, followed by a recap of the requirements in chapter 3 and a recap of the design options in chapter 4.

Secondly, a description of the final concept is presented. Chapter 5 describes what the system should do and how it should do this. Followed by chapter 6 in which way the different subsystem communicate is presented. Thereafter, chapter 7 shows the functional analysis of the system, by presenting a functional flow diagram and a functional breakdown structure. Next, the technical constraints and resource allocation are presented in chapter 8.

Thirldy, after the concept is described, the technical analysis of the system is performed. This starts with the technical risk assessment in chapter 9. Extensive aerodynamic calculations are performed in chapter 10, followed by a performance analysis in chapter 11. Next, the way the kite is controlled and is kept stable is described in chapter 12. Following this, the structural characteristics of the system are described in chapter 13, presenting the aerial segment's and the tether's structures, and in chapter 14, handling the ground segment's structures. After this is done, the materials used in the aforementioned structures are described in chapter 15.

Fourthly, the production of the kite system is presented. This is done by describing the manufacturing, integration and maintenance in chapter 16. Next, the reliability, availability, maintainability and safety are evaluated in chapter 17. Technical drawings and descriptions of the kite system are given in chapter 18, where the aerial segment (and tether) are presented, and in chapter 19, where the ground segment is presented. Next, the sustainability of the kite system is evaluated in chapter 20.

Fifthly, the potential of the system is evaluated by looking at its costs. This is done by performing a market analysis in chapter 21, followed by a cost breakdown and a return on investment analysis in chapter 22.

Finally, the detailed design is concluded by verifying different other aspects. The applicability of the system to other wind farms is presented in chapter 23. Next, the requirements set in the beginning of the report are evaluated in the compliance matrix in chapter 24. This is followed by the description of what to perform in the future, to come to a fully operating and effective device in chapter 25. An advise on what research should be performed in the future is given in chapter 26.

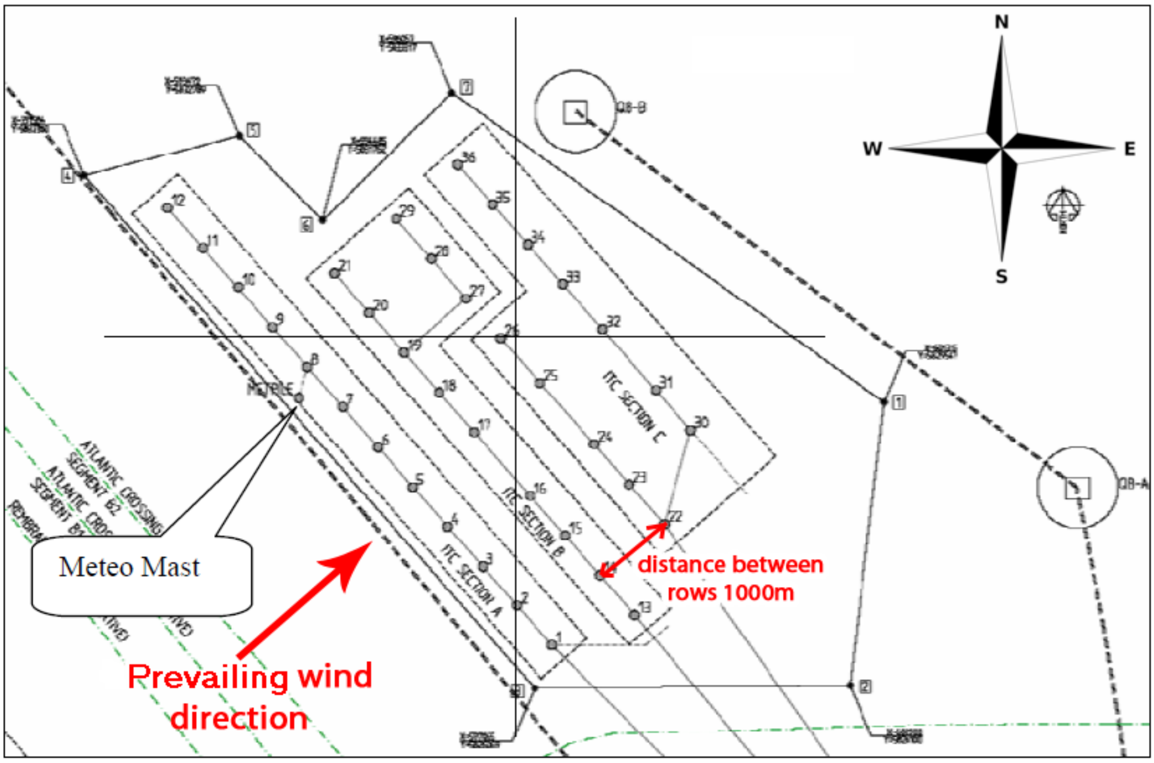

Figure 1.2: Layout of the OWEZ wind farm [2]

Chapter 2

Introduction to OWEZ

In this chapter a short introduction to the Offshore Windpark Egmond aan Zee (OWEZ), exploited by Nuon and Shell, is presented. The kite system is designed for the OWEZ wind farm, however it should be applicable to other wind farms as well. Firstly, section 2.1 describes the layout of the wind farm. Secondly, section 2.2 presents the environmental characteristics of the wind farm.

2.1 Layout

The OWEZ wind farm consists of 36 Vestas V90-3MW wind turbines and is located in the North Sea, 10-18 [km] of the coasts of Egmond aan Zee, in the Netherlands [3]. Figure 1.2 shows a schematic map of the OWEZ wind farm. Four rows, consisting of 7 to 12 wind turbines, can be distinguished. Near wind turbine no. 8 a 116 [m] high meteorological mast is present, measuring the environmental conditions. The wind farm is oriented in the direction, from which the wind comes most of the time, namely south-west [2]. This is done, such that a wind stream passes through four wind turbines, standing behind each other, only. The distance between the wind turbines [4] in this direction is 1000 [m]. The spacing between two parallel turbine rows is 645 [m].

Now the dimensions and performance of an individual wind turbine are considered [5]. The hub height of a Vestas V90-3MW wind turbine is 70 [m]. The rotor diameter equals 90 [m]. Noting that the hub at the center of the rotor is located at the top of the tower, the turbine rises 115 [m] above the mean sea level. The yawing nacelle can position the rotor in the optimal direction. The wind turbine has a rated velocity of 15 [m/s]. If the wind velocity increases above this level, this yields no increase in power output. The cut-out velocity of the OWEZ turbines is 25 [m/s], while the cut-in velocity is 4 [m/s], which means that within this range the wind turbines are operative.

2.2 Environment

In this section the environmental conditions at the OWEZ wind farm location are presented.

OWEZ is an offshore wind farm, meaning that the wind turbines are embedded in the sea, a salt water environment. The local depth [5][6] of the North Sea at the wind farm fluctuates between 15 and 20 [m], with wave heights that fluctuate from 0 to 5 [m]. The water temperature lies between 7 °C during winter time and 20 °C during summer. As stated in section 2.1 the prevailing wind direction is south-west. The average wind velocity [2] from this direction is 8.9 [m/s].

Chapter 3

Recap on Requirements

In the Baseline and Mid-Term report of this DSE project much attention was paid to the requirements, which the device should fulfil. This chapter briefly summarizes this previous research in order to provide a complete overview of the system. If one wants to know more about the requirements analysis, one is advised to read the previous reports.

First the top level requirements as set by the client are presented in section 3.1. Thereafter the Requirements Discovery Tree (RDT), which shows all set and inherent requirements, is presented in section 3.2.

3.1 Top Level Requirements

Five top level requirements were set by the clients. These are briefly discussed one by one.

Increase of wind farm efficiency by 3%
Installing the device should lead to a 3% efficiency increase. This increase is reached by mixing the outer, undisturbed flow with the wake flow. This wake flow is turbulent and has a decreased velocity, so mixing it with an undisturbed flow increases the output of downstream wind turbines. This increases wind farm efficiency. The 3 % should be seen as a minimum efficiency increase and as is stated in chapter 11.

Applicable to the OWEZ wind farm, but also scalable to other wind farms
The system is designed for OWEZ, which is an offshore wind farm. More information on this wind farm is given in chapter 2. Since OWEZ is an offshore wind farm, this poses design challenges. The device should function in a harsh environment without human interaction. Furthermore, it should be possible to scale the system to apply it to another (offshore or onshore) wind farm. Chapter 23 treats the multi-applicability in detail.

Cost effective
The system should be cost effective or in other words, installing the device should lead to a profit. This profit should be large enough to cover budget uncertainties to be able to ensure profitability. The revenue can be determined by evaluating the efficiency increase and deriving the revenue of the extra energy output. The project costs must be estimated in order to determine the profitability. Chapter 22 treats the cost estimation and chapter 22 treats the revenue increase and the profit.

Required maintenance less than once every two years
The device should need maintenance less than once every two years, since maintenance in an offshore environment is very expensive. That is why the device should be made robust. The system should be able to withstand environmental influences such as corrosion, extreme weather and UV radiation without a decrease of performance. Section 16.3 treats the maintenance, while section 17.2 describes measures to increase the maintainability.

Recyclable with a lifetime of 20 years
The device should be recyclable to reduce the environmental impact to a minimum. The more parts are recyclable, biodegradable and do no harm to their environment, the more sustainable will the device be. This means that special care should be taken when selecting the different resources and materials used for the manufacturing, installation and operation of the system. Next to this, the device should be able to operate for 20 years, as is the lifetime of an average wind farm. This sets high demands for the design. These requirements are dealt with in chapter 15.

From the aforemetioned top level requirements the Project Objective Statement (POS) and the Mission Need Statement (MNS) are derived, which are presented below.

The Project Objective Statement (POS) of the design is as follows:

> "Design a device, with 10 students within 11 weeks, resulting in a total of 3500 man hours, with a maximum budget of €12.7M, to increase the efficiency of a wind farm by at least 3%, by mixing the undisturbed outer flow into the wake region of the wind farm."

The Mission Need Statement (MNS) of the design is as follows:

> "Increase the efficiency of the wind farm by mixing the undisturbed outer flow into the wake of the wind turbines autonomously, in a sustainable manner, within the OWEZ wind farm, providing a high availability with maintenance cycles of 2 years and recyclability with a life cycle of 20 years."

3.2 Requirements Discovery Tree (RDT)

From the top level requirements described in section 3.1, inherent requirements can be derived. These and the aforementioned set requirements can be seen in the Requirements Discovery Tree in figure 3.2. This will be a guide for the design of the kite system. Afterwards, the compliance with the requirements is verified in chapter 24.

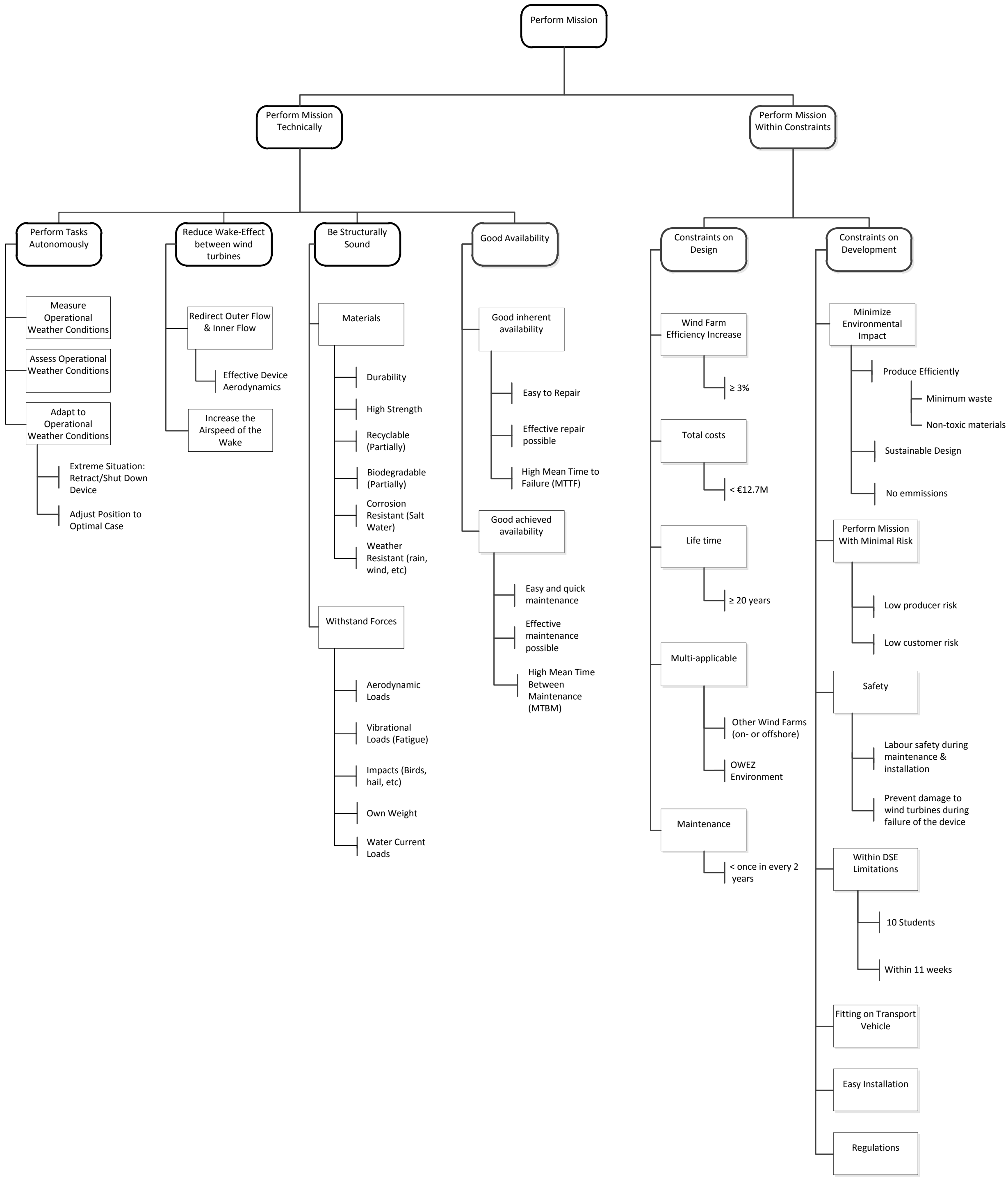

Figure 3.1: Requirements Discovery Tree

Chapter 4

Recap design options

In this chapter a short description of the different design options, that were derived during the conceptual design phase, an earlier stage of the project is presented. Three trade-offs were made in the Mid-term Report, from which the best solution was chosen: *the Daeolus kite system*. Main reasons for not choosing a different design option are mostly based on the required size of these concepts. Large structures will result in large manufacturing, integration, installation and retirement costs. To come up with a profitable design, a relatively cheap solution is required as stated in chapter 22. A second reason for rejecting many design options is that they require a significant amount of energy to perform their functions, from which endangers the requirement of increasing the wind farm efficiency with 3% point. Figure 4.1 displays the different principles on which all design options are based.

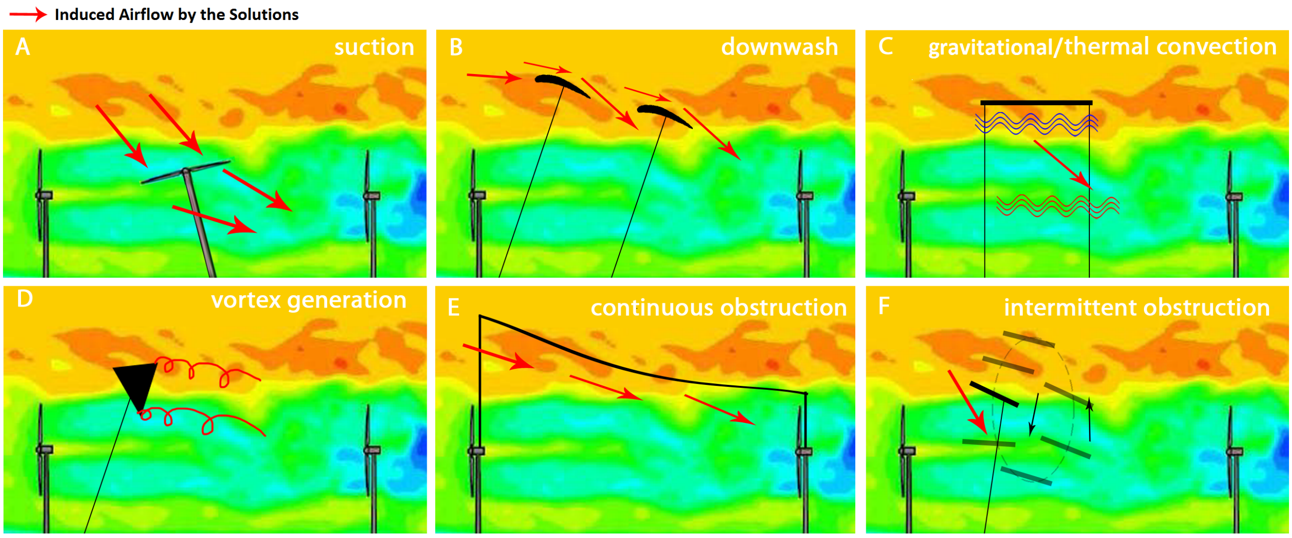

Figure 4.1: Design options

4.1 Suction

The principle of suction is to suck down the undisturbed flow above the wind turbines to the wake region. The critical factor for this principle is the size and energy consumption of this concept. To meet the requirements, the size of a suction device should be in the same order as the wind turbine itself, which is very infeasible. The second aspect is the energy consumption in operation, short calculations point out that this device can not result in a cost efficient and efficiency increasing device and can thus not meet the project requirements.

4.2 Downwash

Wings generate aerodynamic lift by pushing the air down behind the wing; this is known as downwash. Whereas normally lift is the objective, for this design option the objective is to create a large downwash to bend the outer flow downwards into the inner flow. Different concepts for generating downwash are proposed. A fixed structure can be made with an aerodynamically shaped structure on top of it, or an arrangement of kites or kytoons can be used. Also, downwash can be created with a rotating object through the Magnus effect.

The fixed structure concept was easily eliminated because of its size and costs. The other three design options looked feasible, and an extensive trade-off was made, from which the concept of generating downwash with a kite came out best. This design option is worked out in this report.

4.3 Gravitational & thermal convection

The principles of gravitational and thermal convection are to create a cycle in which air moves up and down in a cyclic manner. The cycle desired for this application is that the air above the wake region moves down, while the air next to the wake region goes up. The undisturbed flow is bent down by the convection cycle which will result in a flow velocity increase in the wake region of the wind turbine. The two ways in which this convection cycle can be created is either by increasing the temperature of the air or by reducing the weight of air, respectively yielding thermal convection and gravitational convection. This design option might be feasible, however the forming of both convection cycles consumes a lot of energy, as either the air needs to be heated or water has to be evaporated.

4.4 Vortex generation

This principle is based on the generation of vortices in the upper undisturbed flow, by creating turbulence: the upper flow and the wake flow will mix more easily, which will increase the wind speed in the wake. To realize this, a permanent vortex generating obstruction should be positioned in front of each wind turbine. To realize this design option, a large fixed foundation is necessary. This, as mentioned before, is not feasible since a foundation of this size will not be cost effective.

4.5 Continuous obstruction

This principle is based on Bernoulli's principle: decreasing the area results in an increased flow velocity. This design option requires are very large obstruction which results in relative high costs, therefore this design option is not feasible.

4.6 Intermittent obstruction

This principle is based on scooping the undisturbed air downwards into the wake region like an inverse watermill and increasing the mass flow and thus the flow velocity. This principle will require a complex construction up in the air, which will be too costly. If this device would be placed right above the wind turbine a large risk is present of hitting the turbine blades. This is very undesirable.

4.7 Design options overview

Table 4.1 gives an overview of the different design options that were derived in the earlier phases of the project.

Table 4.1: Design options overview

Principle	**Design option**	**Principle**	**Design option**
Suction:		*Vortex generation:*	
	using water currents		with an obstruction
	with a fan		with a delta wing
Downwash:		*Continuous obstruction:*	
	with kites		with a convergent duct
	with kytoons		with a sail
	with a fixed structure	*Intermittent obstruction:*	
	with a rotating cylinder		with a rotating cylinder
Thermal convection:			with a moving kite
	using active heating	*Gravitational convection:*	
	with a passive solar heating		with water vapour spraying

Chapter 5

Concept description

In this chapter the operations and logistics of the whole system are described. The focus of this chapter is on what the system should do and how this is done. The actual lay-out will be discussed in chapter 18 and 19. Note that the full system, which consists of five subsystems, will be discussed. The first subsystem, the kite itself, is discussed in section 5.1. The environmental observation system, the attitude control system, the retraction system and the health monitoring system are discussed in sections 5.2, 5.3, 5.4 and 5.5 respectively. The relations and the data stream between these subsystems are treated in chapter 6.1.

5.1 The Kite

In this section the kite subsystem is briefly described. Note that the different characteristics of the kite are treated in detail throughout the report (e.g. chapter 11 on the performance and chapter 18 on the lay-out). For this reason this section will only give a brief overview of the kite.

Three possible kite structures are evaluated: the C-kite, the bow kite and the sled kite. Figure 5.1 shows a front view of the first two possible kite structures: the C-kite and the bow kite. An advantage of the C-kite is that it is easily controllable. However, for this application the bow kite will be used. This is because this kite type is more stable and most lift is directed upwards (causing downwash), due to the mainly horizontal orientation of the airfoils. The C-kite, on the contrary, has vertical airfoils at the sides, which do not generate downwash. The bow kite is not fully stable and thus needs an active attitude control mechanism. Furthermore, the bow kite obtains its rigidity from an inflated leading edge and inflated struts in chordwise direction.

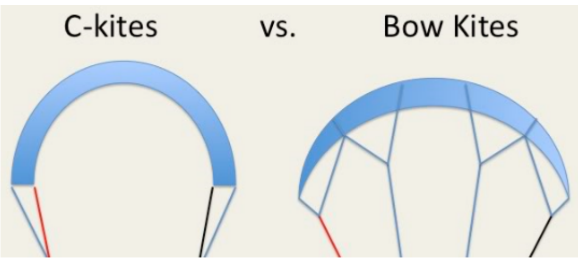

Figure 5.1: Kite shape: C-kite and bow kite [7]

Figure 5.2: A Sled kite

The third kite shape which was considered was the sled kite. This kite type obtains its shape by ram air inflated chambers and is shown in figure 5.2. The advantage of this kite is that it is fully stable by itself and thus no active attitude control is needed. Note that this implies the absence of an active control system. This is not an advantage however, since the possibility of steering the kite to an optimal position is lost. Another large disadvantage is that the kite looses its shape when wind is absent. Also the bridle system (all the attachment cables) is complex, in order to control the shape of the kite. This complex bridle system is a large disadvantage, since the bridle lines might get strangled during retraction. Since the device must function autonomously, this is unacceptable.

All in all, the bow kite type is used for the device since it provides the best aerodynamic performance, with a simple bridle system. Now first the inflatable tubes are discussed, after that the bridle system is presented. The inflatable tubes are needed to provide rigidity. The rigid kite retains its shape which yields good aerodynamic characteristics and more stability. Furthermore, the bridle system does not get entangled, since the kite never folds up. The pressure inside the tubes will however decrease over time, due to the porosity of the material and due to seasonal differences in temperature. A pressure regulation system will be installed in the control pod (see section 5.3) to address the depressurisation problem. This system is shown in figure 5.4. It is a passive system, which uses typical valves and springs to keep the pressure in the tubes within the wanted range. A high pressure gas cylinder is installed in the control pod. This is presented by the combination of the reservoir and the gas pump in the figure (note that there is no physical gas pump, this just indicates that the reservoir pressure is high). If the pressure in the inflatable tubes drops, the pressure regulator allows air to pass through it to inflate the tube again. If the pressure in the inflatable tubes becomes to high (e.g. due to a temperature increase in the spring) the pressure relief valve lets some gas escape. These two valve types must be designed to keep the pressure within the wanted range. Note that there will be two inflatable tubes inside the kite, to have a fail-safe system. The two tubes both have a semi-circular cross-section and both tubes together give the circular tube, which is discussed in later chapters. The check valves prevent air from flowing in the wrong direction and the flow rate regulators prevent air from flowing out to quickly if the tube pressure is high. Small tubes run from the pressure regulation system (in the control pod) to the inflatable tubes. These tubes transfer air and pressure between the two. Note that the inflatable tubes in the kite are further discussed in chapter 13.

The bridle system is used to attach the kite to the control pod. Furthermore, by pulling the control lines the kite can be steered. More on this in chapter 12.

5.2 Environmental Observation System

To ensure a safe operation of the kite system, an environmental observation system or EOS is essential. This system is used to assess current and future weather conditions. If the weather is too extreme, the kite must be retracted to a lower position where the wind speed is lower [8]. If the wind speed is almost lower than the stall speed of the kite, the kite must be fully retracted and suspended on the buoy. Since the device will be deployed in the OWEZ wind farm environment, the OWEZ weather monitoring system is used. This station has 48 weather measuring instruments and is located very close to the wind turbines. Next to this, the different data gathered by the anemometers on the yawing nacelle's are used to assess the environmental conditions.
As can be seen in figure 5.2, the OWEZ environmental observation system is located close to the "K13", "meetpost Noordwijk" and the "IJmuiden" envoronmental observation systems [9].

Figure 5.3: Weather station locations

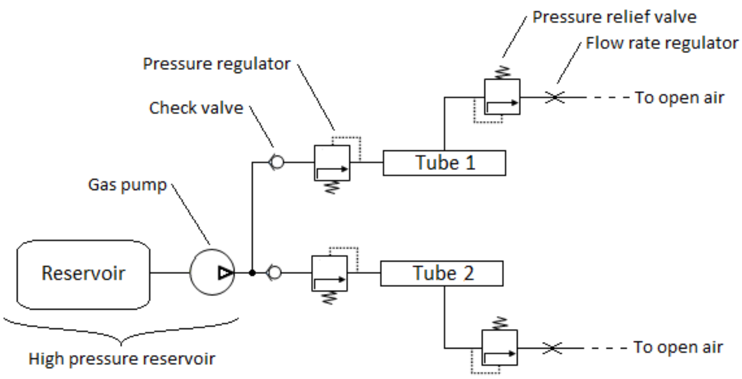

Figure 5.4: The pressure regulation system

The information gathered from these stations is combined to form more accurate weather observations, in chapter 6 the data handling is discussed. This is also done by the Dutch weather forecasting institute, the KNMI [9]. The kite system uses information from the four observation systems. This yields a more accurate weather forecast and prevents unnecessary retraction of the kite.

The EOS of the kite system does not gather weather information itself, it uses information from near weather stations. The information of interest is the wind speed and wind direction at different locations and heights. The EOS of the kite system consists of an antenna in the buoy to receive the information and uses a computer to determine whether the kite should be retracted or not by the retraction system. The EOS sends the weather information to the attitude control system, which also uses the information to determine the optimal attitude of the kite. If the EOS receives no signal, or cannot communicate with the other devices, it sends a signal to the health monitoring system, which decides whether the kite is retracted.

5.3 Attitude Control System

This section will discuss the Attitude Control System (ACS) of the kite. The question answered in this section is: "How will the kite be controlled?" To answer this main question first two sub-questions will be answered: "How will the kite be attached to the buoy?" and "What mechanism is used to control the kite?" These two questions are coherent, since the type of attachment determines the possibilities for control.

The system can be seen to consist of three parts: the ground segment (on the water surface), the aerial segment and the attachment between these two. The ground segment actually consists of a buoy (with its on board systems), which is located on the water surface and an anchor which is located on the seabed. Now the attachment is investigated. The system should be autonomous, so it should function without human interference. For this reason it is preferred to have only one main tether, since then there will be no entangled lines. Using only one main tether also simplifies the retraction system (section 5.4).

With this known, the control mechanism can be determined. With only one main tether, only the length of this tether and thus the height of the kite can be controlled. The kite position should however be fully controllable, in order to have stability and to be able to steer the kite to an optimal position. Figure 5.5 shows how the kite should be positioned for two different wind directions. The attitude control system is used to get to the optimal position, in which the downwash is directed towards the wind turbine.

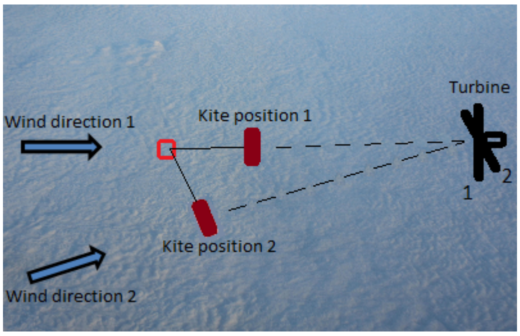

Figure 5.5: The optimal kite position for two different wind directions

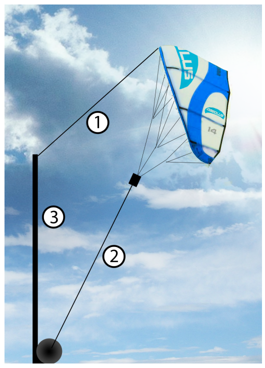

Figure 5.6: Outline of retraction system

To obtain control a control pod is present. The aerial segment now consists of the kite, the control pod and the bridle lines between these. The control pod is an active system - it receives energy through the main tether - which controls the kite by mechanically pulling the control lines to vary the control angles: pitch and roll. By pulling on some of the control lines, the kite attitude is controlled, by which the position of the kite is determined. This mechanism is treated in detail in chapter 12.

In order to control the kites attitude a computer is installed in the control pod. This computer functions as the "automatic pilot". The input for the control pod are the weather conditions (from the EOS), the tether length (from the retraction system) and the current position and attitude of the kite (from GPS sensors on the kite). The autopilot is discussed in detail in chapter 6.1. The output is the required control line length, which actually steers the kite. Note that as was discussed in section 5.1, the control pod also holds a gas cylinder to regulate the pressure in the inflatable tubes of the kite.

Now the ground segment performs two tasks for the control pod. Firstly, it supplies power to the control pod through an electricity cable in the main tether; this is a conventional solution [10]. Note that through a cable in the main tether also information is transferred from the ground segment to the aerial segment. Secondly, the ground segment holds the retraction system, which determines the tether length and cooperates with the attitude control system to obtain the optimal tether length.

5.4 Tether Retraction System

This section discusses the Tether Retraction System (TRS) that is used to retract the kite in non-operating weather conditions or before maintenance. First the requirements for the retraction system are stated. Then the retraction system and the buoy on which it is placed are discussed.

The kite has two configurations: it is either airborne or fully retracted on the buoy. The control pod is used to keep the kite airborne, so it will not hit the water. The retraction system must perform the change between these two configurations. Another important requirement for the retraction system is that it is fully autonomous and therefore it must function without human interference. Because of this requirement the retraction system should not fail and the lines should not tangle up. Another important requirement is that the kite should be able to move up again after it has been retracted.

The retraction system will be placed onto a buoy which is located between two wind turbines. The retraction system will be split up in three parts. The first part is the winch, which retracts the kite. The second part is the buoy to which the winch is attached. The buoy in turn is attached to the seabed with an anchor. The third part is a power generating device to supply energy to the winch and other energy consuming subsystems.

Now the buoy system is discussed. The kite must be retracted if the weather conditions are out of the operation limits. If there is too little wind the kite is fully retracted, but should not hit the water and should easily get airborne again when wind speed increases. Because of these reasons the kite is suspended on a mast, which is placed upright on the buoy. The leading edge of the kite is attached to the top of the mast and the rest of the kite hangs downwards. If wind speed increases, the kite turns to a horizontal position and produces the required lift to get airborne. The system is shown in figure 5.6; this is just before the kite is fully retracted. Here "1" is the leading edge retraction line, which pulls the leading edge of the kite towards the top of the mast with the so called secondary winch. During normal operation this line does not carry much loads, since it is always less taut than the main tether. The main tether is shown along the "2" and "3" is the mast. The minimum height of the mast is defined by the chord length.

In case of extreme weather conditions the kite will not be fully retracted and will be in the air above the buoy, but below the wake of the wind turbine. Here the wind speed is much lower than at higher altitudes [8] and the kite is therefore safe at this low location. The kite is designed to withstand very high wind speeds of 27.3 [m/s] (see chapter 11). Higher wind speeds might occur at high altitude, but it is very unlikely that these occur at lower altitudes.

In short the retraction process works as follows. First the angle of attack of the kite is reduces by the control pod to reduce the lift of the kite. This is called "depowering" the kite. Then the main winch pulls the kite down by reducing the main tether length. At the same time the leading edge line is retracted by the secondary winch. As soon as the kite is low enough, the control pod reduces the length of the bridle lines. Then the secondary winch pulls the leading edge of the kite to the mast. Now the kite is suspended. Releasing the kite again is done by slowly rolling out both winches.

5.5 Health Monitoring System

A lot of unexpected things can happen during the operation of the kite. For this reason it is important to check the state of the system constantly. This is done by the Health Monitoring System (HMS), which is described in this section.

The HMS is used to detect whether something is wrong with the system. If something is wrong, the kite is retracted and an error report is sent to the maintenance team. The maintenance team can then look at the error report and decide whether they have to fix the error or whether the error is temporary and will disappear without maintenance.

The HMS is in contact with the ACS, the EOS and the TRS. When these systems do not send all the information they should send, because of e.g. a malfunction, this is detected by the HMS, which sends a signal to the maintenance team. If they do not function correctly or break down, this is also detected by the HMS. The relations between the systems are shown in chapter 6.1.

Furthermore, the HMS itself measures the tensile force in the main tether. If the force becomes too low, a signal is sent to the ACS and the TRS. First the ACS increases the angle of attack, to create more lift. This prevents the kite from falling from the sky and increases the tether tension to an acceptable level. If the tether force stays below the minimum level, the TRS retracts the kite. During relaunch of the kite it is checked whether the tensile force is higher again and the system has restored itself. If the tensile force becomes too high, the kite is depowered by the ACS and the TRS retracts the kite, since probably the wind speed is too high. When failure occurs of the EOS and the ACS the kite is retracted, this is necessary to reduces the risk of the kite falling into the sea and making uncontrolled manoeuvres. Uncontrolled manoeuvres will increase the risk of tether failure.

Chapter 6

Data handling and Block diagrams

In this chapter, several block diagrams and the data handling are explained. In section 6.1 the data handling block is explained. Further, in section 6.2, the hardware block diagram is shown. In section 6.3, the software block diagram is given. Finally, in section 6.4, the electrical block diagram is explained.

6.1 Data handling

Data handling is important, since the system is required to be fully autonomous. Therefore the data handling is explained in this section. The data block diagram is explained in subsection 6.1.1. In subsection 6.1.2, the data handling for the EOS is further explained. In subsection 6.1.3, the ACS data handling is treated. Finally, the data handling for the HMS and the TRS systems are given in subsections 6.1.4 and 6.1.5 respectively.

6.1.1 Data Handling Block Diagram

Figure 6.1.1 shows the data block diagram. Each block of this diagram is further evaluated in the following subsection.

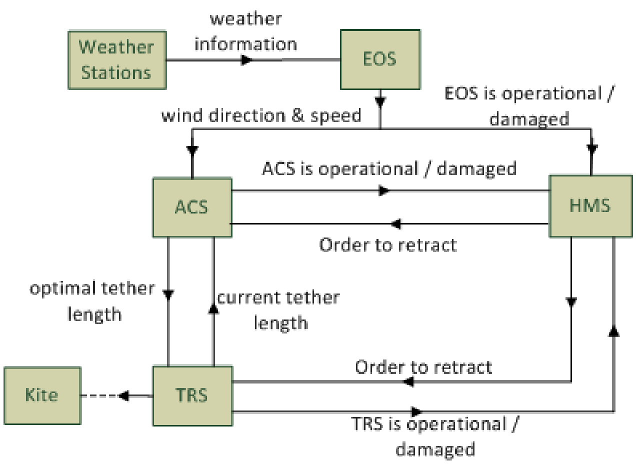

Figure 6.1: Data Handling Block Diagram

6.1.2 Data handling for the EOS

The Environmental Observation System,(EOS), uses the data from several weather stations. This is the same weather data used by OWEZ and in addition EOS uses also data information other than the OWEZ weather station. The EOS uses the wind speed data from the weather stations. In order to get a first order relation between the environmental observation systems at "Meetpost Noordwijk", "IJmuiden" and "K13" and the environmental observation systems located in the OWEZ wind farm at a height of 21 [m], a linear regression of the following form has been used:

$$WS_{weighted} = m \cdot WS_{measured} + c \tag{6.1}$$

This formula can be used to estimate the current airspeed at a height of 21 meters at the position of the buoy, in which the EOS is located. The $WS_{measured}$ parameter stands for the measured airspeeds in the other weather stations. The $WS_{weighted}$ is the estimated airspeed at the EOS location. The parameters m and c have to be inserted into equation 6.1, to obtain a linearized result. For the correct values for m and c, see table 6.1 [9]. The parameters m and c are also dependent on the wind direction. To measure the wind direction, use is made from the environmental observation system located in the OWEZ wind farm. Using all weather stations, long-term predictions can be made more precise. Just using the information from only one weather station, the station located in the OWEZ wind farm, is not sufficient for the calculation of accurate wind speeds and the EOS cannot forecast the wind speeds using only one weather station. Forecasting the wind speeds is important, since the TRS needs more than 5 minutes to retract the kite. If it decides to retract the kite too late, the kite may fall into the sea. To avoid this, it needs to have information from wind stations further 'upstream' of the wind.

Table 6.1: Fitting parameters of the two-step probabilistic linear regression [9]

Wind direction in degree	$m_{Noordwijk}$	$c_{Noordwijk}$	$m_{IJmuiden}$	$c_{IJmuiden}$	m_{K13}	c_{K13}
0 <... ≤30	0.94	-0.39	0.86	-0.17	1.14	-2.10
30 <... ≤ 60	1.02	-1.17	0.81	-0.30	1.38	-4.22
60 <... ≤ 90	0.84	-0.19	0.95	-0.38	1.28	-2.01
90 <... ≤ 120	0.89	-0.64	0.74	-0.29	1.31	-2.15
120 <... ≤ 150	0.83	0.20	0.63	-0.08	1.28	-1.55
150 <... ≤ 180	0.77	0.39	0.64	0.16	1.12	-0.11
180 <... ≤ 210	0.95	-0.41	0.76	0.03	1.04	0.81
210 <... ≤ 240	1.15	-1.95	0.96	-0.55	1.04	0.09
240 <... ≤ 270	1.08	-1.50	0.89	0.10	1.00	-0.55
270 <... ≤ 300	1.04	-1.02	0.98	-0.57	1.03	-0.48
300 <... ≤ 330	0.98	-0.40	0.92	-0.29	0.97	-0.20
330 <... ≤ 360	0.98	-0.44	0.86	0.41	0.98	-0.40

The data received from the weather stations has several communication channels. For our device, only channels 1,4,7 and 9-17 can be used to determine if the kite needs to be retracted or not. The antenna should thus be tuned at these channels to receive appropriate information. The complete channel description can be found in the OWEZ wind farm EOS report [9].

The kite is retracted if the calculated airspeed at 145 meters height at the location of the EOS is above 27.3[m/s] or below 4 [m/s]. The kite is not retracted by wind speeds over 17[m/s] when the kite is in fact useless for increasing the wind farm efficiency, since this requires power. The kite is only retracted when it is absolutely necessary.

6.1.3 Data Handling for the ACS

The Attitude Control System, or ACS, consists of a GPS, gyroscopes (located inside the GPS), the autopilot and the control pod. This system tracks the location and the attitude of the kite and can optimize the location and attitude of the kite using this information. The ACS has three inputs and two outputs. The first input of the ACS is from the EOS. The ACS may abort the mission due to the received data input from the EOS, if the wind speed gets too high or too low, or the wind speed forecasts are not good.

The second data input is from the HMS. When the system is damaged (one of the subsystems), the HMS gets notified and will order the ACS to abort the mission and land. The ACS orders the TRS to decrease the tether length. The third input is from the TRS, the TRS tells the ACS what the current cable length is, this is essential for the ACS in order to optimize the position of the kite.

The first output of the ACS can request a desired cable length to the TRS in order to optimize the position of the kite. The second out put of ACS to send data to HMS of it's status. In case ACS is damaged, HMS is responsible to send data to TRS to retract the kite.

6.1.4 Data Handling for the HMS

The Health Monitoring System (HMS) checks the overall status of the subsystems. The HMS has three inputs and two outputs. It receives health data information from the EOS, ACS and the TRS. If the HMS detects a failure, it will send an order to retract the system to the TRS and informs the ACS about the status. In case when HMS is damaged, there will be no data exchange between ACS and HMS. In that case, ACS will send data to TRS to aboard and to retract the kite. The HMS also monitors the tether tension, if the tension is too weak, it will order TRS to retract.

6.1.5 Data Handling for the TRS

The tether retraction system (TRS) retracts or releases the tether with the kite attached to it when it is needed. This subsystem has two data inputs and two data outputs. The first input is from the ACS, the TRS gets information from the ACS about the desired cable length. The TRS will adjust the cable length to optimize the attitude of the kite. Also It sends data to the ACS of the current tether length. The second input is from HMS, this input is needed in case a subsystem is damaged and kite has to be retracted. Since there is no direct data exchange between kite and some other subsystem, kite is shown in figure 6.1.1 with a dashed arrow.

6.2 Hardware Block Diagram

The hardware block diagram, as can be seen in figure 6.2, is a schematic overview of the hardware elements of the system. This hardware block diagram is separated into two parts. The first part deals with the systems located in the buoy. In the second part, the systems which are located outside the buoy are shown. There are several systems in the hardware block diagram:

- **Buoy**
  In the buoy, the EOS system is located. The EOS receives its signal from other weather stations through an antenna. The EOS is powered by solar cells, during night the EOS is powered by the batteries. The EOS (antenna) sends data to the EOS processor, therefore these hardware components are connected. The EOS processor is connected with the Winch and the HMS. The winch is connected to the HMS and the control pod. The control pot gets information from the GPS and can change the Attitude of the kite.
- **Kite**
  Between the tether and the bridle system, the ACS station is located. This ACS station optimises the attitude of the kite, in order to do this, it needs a particular tether length. It requests a desired tether length to the TRS station, the TRS station in turn communicates to the ACS how long the tether actually is. If the ACS station does not receive information from the TRS station, it send a signal to the HMS station about a malfunction of the system. It receives information about the current position from the GPS and the gyroscopes. The GPS is powered by the solar cells and/or the batteries.

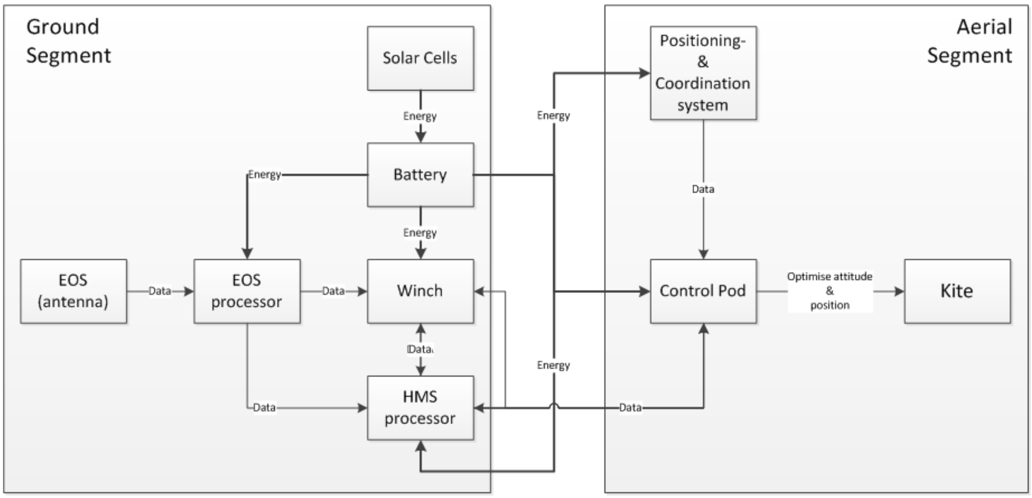

Figure 6.2: Hardware Block Diagram

6.3 Software Block Diagram

The software block diagram, figure 6.3 is used in order to see the different relations between the software of the subsystems. The 'flow' starts when the weather stations transmit their data to the EOS. If the EOS is not able to receive the data from the OWEZ wind farm or any other weather station, the HMS is notified. If it can receive the data it will determine if the weather conditions are safe enough to fly. If the weather conditions are not within the required conditions, the TRS is notified to retract the kite. If the conditions are safe enough, it will enable the TRS and the ACS to let the kite fly in the air in an optimal way. If this is not possible, due to miscommunication between the ACS and TRS systems for example, the HMS is notified of an error and the kite will be retracted.

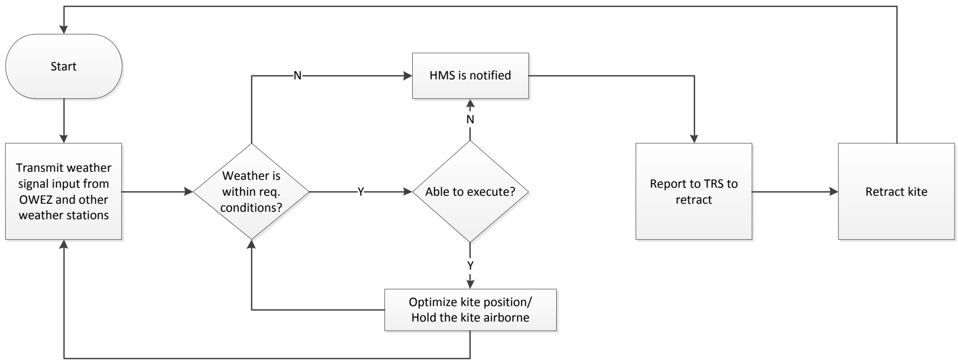

Figure 6.3: Software Block Diagram

6.4 Electrical Block Diagram

The electrical block diagram, figure 6.4, shows the electric connections between the subsystems. As can be seen in the figure, the solar cells powers the batteries. These batteries enables the electric systems to work at night, or when the solar cells cannot deliver (enough) power. The amount of power needed by each subsystem is explained in section 19.2. The EOS, TRS, HMS, ACS and the GPS are powered by the batteries or the solar cells.

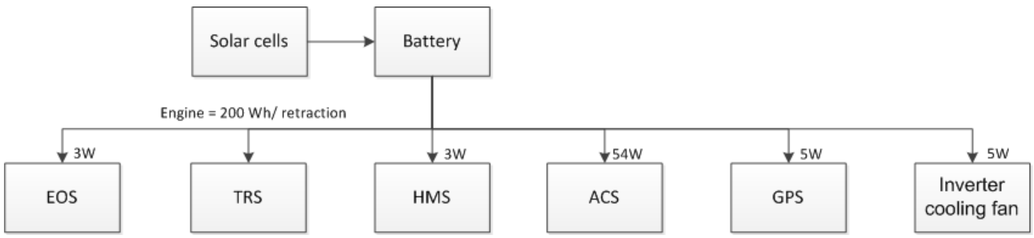

Figure 6.4: Electric Block Diagram

Chapter 7

Functional Analysis

The kite system should perform certain functions to achieve its mission. These functions are displayed in this chapter in two different diagrams, called the Functional Flow Diagram (FFD) and the Functional Breakdown Structure (FBS). These diagrams are attached as figures 7.1 and 7.2. Both diagrams in general and their current structure are explained in the sections below.

7.1 FFD and FBS in General

The FFD and FBS are two different diagrams to illustrate the functions to be done by the device. The FFD indicates the flow, so the sequence of occurrence, of the (sub)functions under the top level functions. The FBS categorizes the sub-functions within function groups. This means that the sub-functions are aggregated under function groups and these function groups under the top level functions. The FFD can be used to see when functions occur, while in the FBS it can be seen to which group the functions belong.

7.2 FFD and FBS Structure

The FFD and FBS for the device consist of 6 top level functions, which are stated below:

- Production
- Transportation
- Installation
- Operation
- Maintenance
- Retire and Recycle

Each top level function and their sub-functions are explained in the sections below.

7.2.1 Production

First the device has to be produced. This is done by first creating parts from raw materials and semi-finished products. Then the parts will be assembled to components, which subsequently will be assembled to result in the sub-assemblies. These sub-assemblies are to be transported to the wind farm. After the parts and components are assembled, the assemblies are inspected to verify whether they work properly and fulfil the requirements. When they do not, they will be repaired or recycled.

7.2.2 Transportation

After the device is produced, it has to be transported to the wind farm. This is done by first loading the device on the transport vehicle. The type of transport vehicle needs to be determined in further research, however, a truck is likely to be used. Secondly, by transporting it to an onshore location near the wind farm and lastly, by loading the aerial segment on a transport vessel and by attaching the buoys behind it, after which it is shipped to the specific location within the wind farm.

7.2.3 Installation

After the device is transported to the specific location within the wind farm, it has to be installed. This is done by more accurately locating the desired position and installing the device, which is explained in section 16.2. This is done by attaching the anchor to the buoy, that is already floating in the water. Next, this anchor is released and sinks to the bottom. Now, the aerial segment can be installed. After the integration is complete, the device is inspected to determine whether it can perform its mission properly on location. When it does not, it will be repaired.

7.2.4 Operation

After the device is installed and the pre-operational inspection is performed, it is operational. When looking at the FFD and FBS, six main operational branches can be identified. Firstly, power to the subsystems needs to be delivered. Secondly, the health status needs to be monitored before the full operation is started. When the health system reports an error, actions need to be taken. Thirdly, the environment is observed. When the conditions are good, the operations can continue. Fourthly, the kite is flown. This means it is released from the ground system and the tether is rolled out. The kite climbs to its desired operational altitude. Fifthly, if the weather is getting too rough or the wind is absent the kite is retracted. Finally, when the kite is retracted, it is suspended on the mast. Each of the aforementioned processes involve a lot of sub-functions, which can be derived from the FFD and FBS.

7.2.5 Maintenance

When the device calls for maintenance, first the problem is investigated. This is done by inspecting the ground segment, the tether and the aerial segment. Secondly, it is determined whether the device can be repaired or parts have to be recycled and replaced, after which this has to be done accordingly. After the repair the device is tested to check whether it performs well, before it continues operation. When scheduled maintenance is performed, different parts of the system are inspected. Again, the device is repaired or parts are recycled and replaced. The time each maintenance action takes is dependent on the severity of potential damage. Four days are scheduled to perform regular maintenance, in which the kite is replaced. During some scheduled maintenance, more actions will have to be performed, like replacing batteries. This will take some more time. However, four days in total for all systems should be enough to inspect or replace the different subsystems and lubricate moving parts. If severe damage has occured, for instance a leakage of the buoy, probably more time is required, since special craftsmanship is demanded.

7.2.6 Retire and Recycle

After at least 20 years of operating, the device has to be retired. This is done by transporting it to the shore, after which it is disassembled. Then it has to be indicated which parts are discarded or recycled. Before the parts are recycled, they are prepared for this.

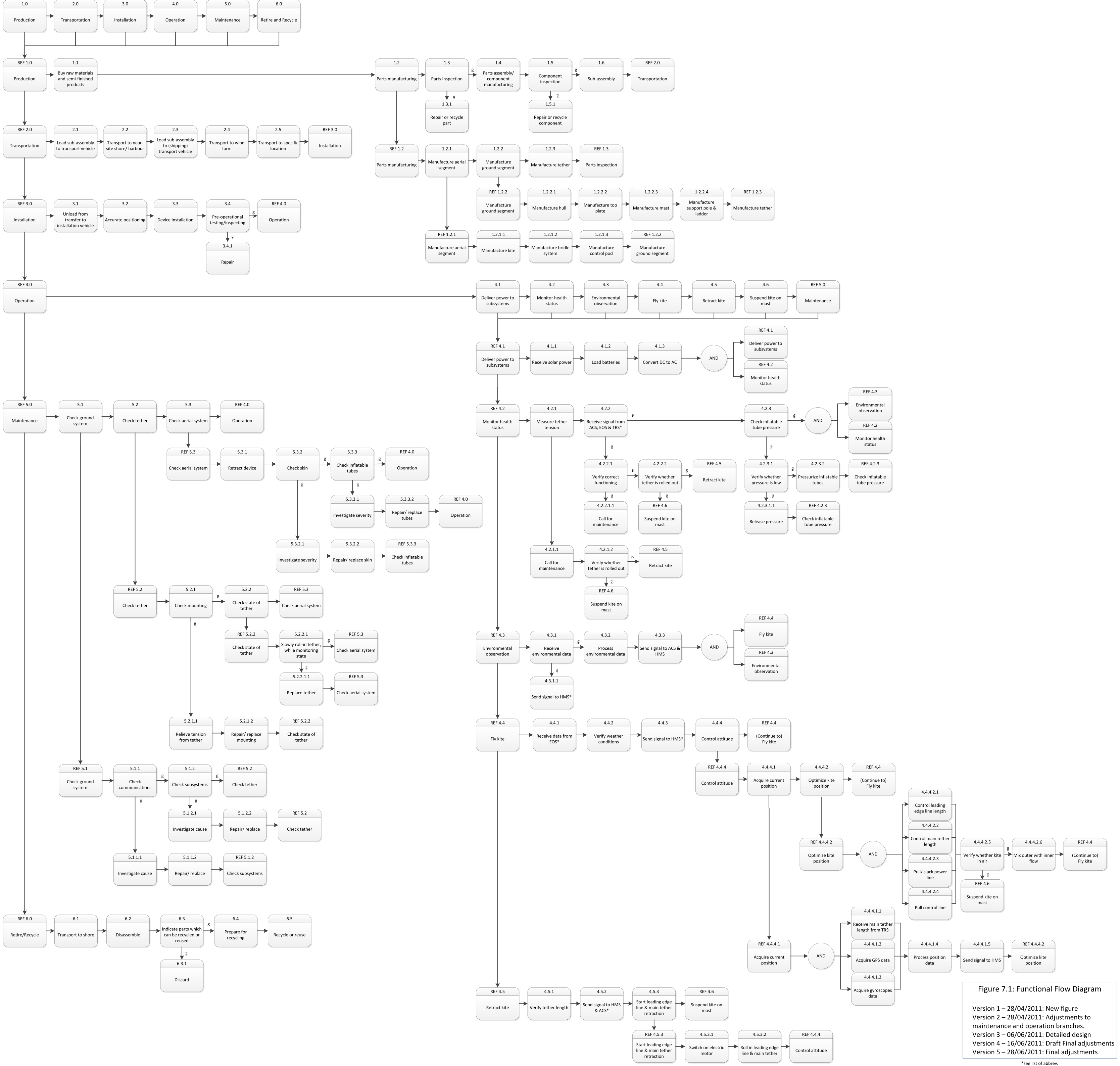

Figure 7.1: Functional Flow Diagram

Version 1 – 28/04/2011: New figure
Version 2 – 28/04/2011: Adjustments to maintenance and operation branches.
Version 3 – 06/06/2011: Detailed design
Version 4 – 16/06/2011: Draft Final adjustments
Version 5 – 28/06/2011: Final adjustments

*see list of abbrev.

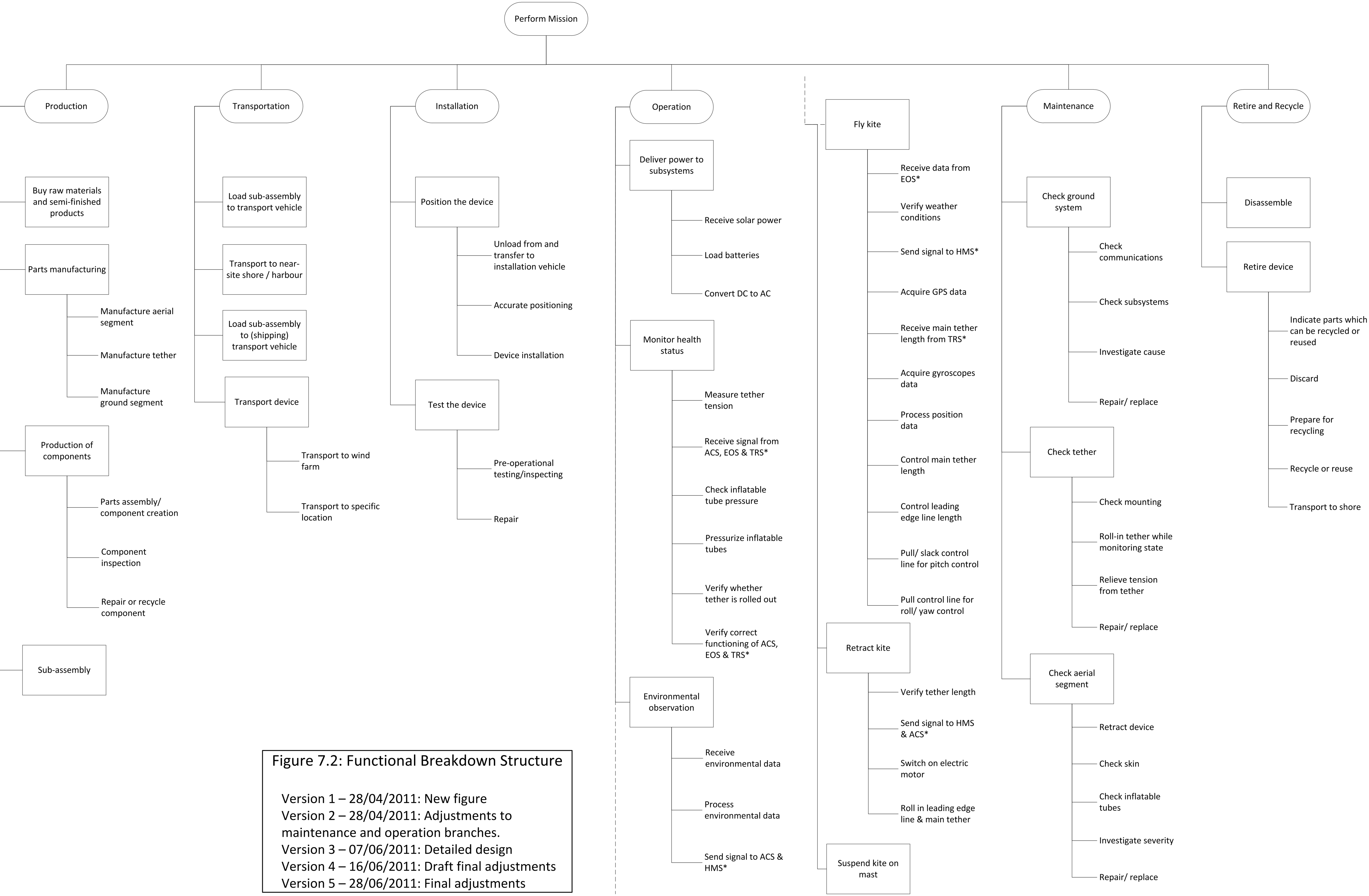

Figure 7.2: Functional Breakdown Structure

Version 1 – 28/04/2011: New figure
Version 2 – 28/04/2011: Adjustments to maintenance and operation branches.
Version 3 – 07/06/2011: Detailed design
Version 4 – 16/06/2011: Draft final adjustments
Version 5 – 28/06/2011: Final adjustments

Chapter 8

Resource Allocation

This chapter will mainly focus on the human resource allocation and the budget breakdown. First of all, the technical budget will be shown in section 8.1. Secondly, the working process within the groups will be explained in section 8.2. Hereafter the individual team functions will be explained and the assigned team member for each of the functions will be given in section 8.3. Finally, the contingency management will be shown in section 8.4.

8.1 Technical Budget

In this section the technical budget will be outlined. Technical budget is a way to control performance risks of the system that will be designed. The technical budget serves as a constraint for the technical parameters. The Technical Performance Measurement (TPM) are the parameters that are needed to complete the project successfully. These parameters are listed in table 8.1.

Throughout the report the different subsystems will define technical budgets for different parameters. it is important that the individual subsystems do not violate each others technical budget. However budgets are often tight and not all subsystems can be created within the allocated budget. Therefore budgetting will be required so that critical areas can be seen and analysed inn order to solve the technical issues. Reallocation of budgets or redefinition of requirements will have to take place in these cases [11].

8.2 Resource Allocation Groups

The total project is split up into various fields e.g. aerodynamic, controllability and structures. For each field there is a team of two members which is working on it. How the persons are chosen is based upon the work from previous report. In the previous phases it became clear that individuals became experts in their respective fields and therefore the same team will be assigned to the corresponding fields.

8.3 Resource Allocation Team Functions

Knowing who has to do what is essential for this project. Several functions and tasks are therefore defined in order to make sure that responsibilities are clear and important actions are not overlooked. These functions and tasks are assigned to individual group members. Table 8.2 shows which functions are defined and which person is assigned to each function.

Note that the functions were shuffled after the conclusion of the conceptual design phase. This is done because then all group members have the chance to get a special function - because there are not enough different functions for all group members. Therefore in table 8.2 a distinction is made for the responsible persons in conceptual phase - running from the start of the project to the end of the conceptual design phase - and in the detailed phase - running from the start of the detailed design phase to the end of the project.

This project is focused on improving a sustainable concept, the wind farm, i.e. making wind farms more sustainable. Because sustainability is an important goal of the whole project, one team member is assigned specifically to this subject. Because of him, the team will not loose sight of sustainability.
Now the responsibilities of each function are defined. For each function it is stated what this function incorporates. In the end, each function will not be too heavy, so every group member can have a clearly identifiable technical contribution to the project.

Table 8.1: Technical Performance Measurement parameters

TPM Parameters
Weight budget
Efficiency Increase
Maintenance Costs
Production Costs
Wind speed and direction envelope
Energy budget

Table 8.2: Team functions and responsible group members.

Function	**Person(s) responsible**	
	Conceptual design phase	**Detailed design phase**
Project manager	C. Broich	A.S. Hamraz
Chairman	J.F.G. Schneiders	R.L.C. Kalthof
Secretary	J.J. Wiegerink	K.J.Groot
Documentation	R.L.C. Kalthof	J.J. Wiegerink
Systems Engineer	G.J.W. Nieuwint	D. Boonman
Controlling and quality assurance	Y. Tang and D. Boonman	Y. Tang and G.J.W. Nieuwint
Sustainability	A.S. Hamraz	R. Deerenberg

Project manager: C. Broich (conceptual phase) and A.S. Hamraz (detailed phase)

- Assigning responsibilities to team members.
- Assuring that all team members understand and accept their responsibilities.
- Keeping the team focussed on developing and executing the plan.
- Making sure that different sub-teams communicate and work in a similar way, if possible. This makes it possible to integrate or compare results of different teams. It also prevents team members from doing work twice.
- Reporting project status to team members.
- Making timely adjustments to the plan.

Chairman: J.F.G. Schneiders (conceptual phase) and R.L.C. Kalthof (detailed phase)

- Preparing and leading meetings.
- Contact with principle tutor and team coaches.
- Arbitrating and resolving conflicts.
- Maintaining an issues log.

Secretary: J.J. Wiegerink (conceptual phase) and K.J. Groot (detailed phase)

- Making minutes, including action points.
- Communicating minutes timely to team members, the principle tutor and coaches.

Documentation: R.L.C. Kalthof (conceptual phase) and J.J. Wiegerink (detailed phase)

- Maintaining the project files.
- Document version control, i.e. preventing version mistakes.

Systems Engineer: G.J.W. Nieuwint (conceptual phase) and D. Boonman (detailed phase)

- Controlling the project time planning and project progress.

- Making timely adjustments to the plan, in collaboration with the project manager.
- Keeping an eye on schedule risks.

Controlling and quality assurance: Y. Tang and D. Boonman (conceptual phase) and Y. Tang and G.J.W. Nieuwint (detailed phase)

- Reviewing deliverables (e.g. reports) and correct content and language errors.
- Assessing work done on relevance to the (virtual) ”customer”.

Sustainability: A.S. Hamraz (conceptual phase) and R. Deerenberg (detailed phase)

- Making sure that sustainability is always on the agenda of the team.
- Critically reviewing designs on sustainability.

8.4 Contingency Management

In this chapter a Technical Performance Measurement (TPM) is done in section 8.1. A TPM ensures that discrepancies between required and actual characteristics of a concept are recognized at an early stage of the project which strongly effects the overall contingency. This is based on components specifications and estimations, which are derived from project related discussions. Table 8.1 shows a contingency scheme for the concept, it can be seen from the table which design part has the most or least contingency.

	CONTINGENCY (%)																			
Design Maturity	Configuration/ Layout	Dimensions	Structural Characteristics	Material Characteristics	Aerodynamic Characteristics	Control and Stability	Electrical System	Mass	Communication/ Status Report	Reliability	Availability	Maintainability	Safety	Maintenance Costs	Series Production Costs	Installation/transport Costs	Total Costs	Operational Profit	Production Time	Overall Efficiency Increase
Concept Generation Phase	50	50	40	40	40	40	50	60	40	35	30	40	25	35	45	50	70	50	45	25
Concept Work-Out Phase	20	20	18	15	18	20	20	20	13	20	20	20	10	16	24	20	30	25	10	10
Detailed Design Phase	12	12	10	12	12	15	8	12	8	10	10	8	7	9	13	15	14	12	9	9
Testing Phase	6	4	5	7	6	9	5	5	5	8	10	8	5	6	10	12	12	10	5	6
Production Phase	2	2	3	2	3	5	2	2	2	6	5	4	2	3	7	8	8	8	4	2

Figure 8.1: Contingency

During the concept generation phase, all the concepts are briefly explained and the feasibility checks are executed. However which concept will be chosen at the end is still unknown during the concept generation phase, that causes a large contingency. During the second stage the work-out phase, the contingency is smaller due to elimination of the less feasible concepts. However there are still three concepts left. That is why there are still some uncertainties. At the detailed design phase, it is clear which concept is chosen and what all the sub-parts are. At the testing phase, the prototype is made. The experiments can be executed which will decrease the contingency even more. The last row of the contingency table is the production phase. At that point, everything should be clear and the minimum amount of contingency can be acquired.

Note that the contingency of the total costs of the concept is rather high in all the phases in comparison with the other aspects. At the early stage, that is because each different design has its corresponding total costs. The total costs can vary a lot for the different designs. In the later stage, production delays can be occur which results in increasing of the total costs. In contrast, the contingency of the safety is rather small in comparison with the other aspects. The requirements for the safety is the same for all the concepts and after the testing phase there should be almost no contingency any more for safety. The contingency for the overall efficiency increase of the wind farm is rather small as well due to the fact that is one of the requirements for the design. At the production phase, the exact overall efficiency increase should be known. All the other aspects are somewhere between the contingency of the total cost and the overall efficiency increase.

Chapter 9

Risk Assessment

In this chapter a technical risk assessment is made. Different kinds of risk are identified and are evaluated for the probability of occurrence and the consequence of the event.

In section 9.1 the technical or performance risks associated with the different subsystems are stated and a risk map is plotted, based on these risks. Section 9.2 will deal with two other kinds of risk. Namely, schedule risk and cost risk. All three categories are strongly related to each other, as for instance a failure or delay will cause extra costs. Finally, a conclusion is drawn upon the technical risk assessment in section 9.3.

9.1 Performance risk

In this section different kinds of performance risk are identified. These, with their handling methods, are stated in subsection 9.1.1 and are plotted in a risk map. A general approach towards the handling of performance risks is presented in subsection 9.1.2.

9.1.1 Risk map

In table 9.1 the performance risks, associated with the different subsystems from the second column, are listed in the third column. Also different risk handling methods are displayed in the fourth column. The subsystems listed in the table can be grouped into three main subsystems. Namely, the aerial segment, the tether and the ground segment. Subsystems no. 1-3 and 5-6 are associated with the aerial segment. Subsystems no. 4 and 7-9 are part of the tether. Subsystems no. 10-19 are part of the ground segment.

Table 9.1: Risk tracking

No.	Subsystem	Risk	Risk Handling
1	Skin	-Rupture. -UV degradation. -Bird/ hail/ rain collision.	-Reinforcements. -UV protective layer. -Design for ultimate loads.
2	Inflatable tubes	-Leaking. -Rupture. -Falling in sea due to lost aerodynamic shape.	-Pressure system. -Reinforcements. -Design winch for fast retraction to maintain aerodynamic shape.
3	Pressure regulation system	-Corrosion. -Overpressure.	-Corrosion protective layer. -Pressure valves.
4	Main tether	-Breaking. -UV degradation.	-Design for ultimate loads. -UV protective layer.
5	Bridle system	-Breaking. -Entangling of tethers. -UV degradation.	-Design for ultimate loads. -Use control pod to sustain tension. -UV protective layer.
6	Attitude control system (ACS)	-Control pod malfunction. -Failure of position monitoring. -Corrosion.	-Corrosion resistant hull.
7	Tension meter	-Corrosion.	-Corrosion protective layer.
8	Leading edge line	-Breaking. -UV degradation.	-Design for ultimate loads. -UV protective layer.
9	Electricity cable	-Breaking.	-Insulate in tether.

10	Tether retraction system (TRS)	-Electric motor fail. -Corrosion.	-Corrosion protective layer. -Water protective hull.
11	Anchor chain	-Breaking. -Corrosion. -Boat collision.	-Signal light. -Corrosion protective layer.
12	Rubber floats	-Leaking. -Boat collision.	-Redundant float design. -Signal light.
13	Battery	-Failure. -Low battery power.	-Redundant battery design. -Redundant solar cell design. -Large battery capacity. -Reliable Nickel-Cadmium battery.
14	Solar cells	-Failure. -Obstructed by foreign object.	-Large battery capacity. -Redundant solar cell design.
15	Earth observation system (EOS)	-Antenna failure. -Data processor failure.	-Insulation.
16	Health monitoring system (HMS)	-Failure. -Power feed failure.	-Redundant battery design. -Redundant solar cell design.
17	Mast	-Corrosion. -Breaking.	-Corrosion protective layer. -Design for ultimate loads.
18	Buoy structure	-Leaking. -Collapsing. -Boat collision.	-Redundancy in design. -Design for ultimate loads. -Signal light.
19	Anchor	-Eroding. -Breaking.	-Design for ultimate loads.

No.	**Verification**	**Risk**	**Risk Handling**
20	Jensen/Frandsen models	-Deviation from measurements.	-Validation in reality.
21	*Patran-Nastran* models	-Accuracy uncertainty.	-Validation in reality.

In table 9.2 a risk map is shown. This is done, using the different subsystems shown in table 9.1. Each number in table 9.2 corresponds to the same number in table 9.1. The risk map shows the consequences of the occurrence of the failure of a subsystem on the horizontal axis. The probability of occurrence is shown on the vertical axis, given that some parts of a design can be non-existing at the time and some, like tether properties, are known because they have a proven design.

Table 9.2: Risk Map

Probability →				
Feasible in theory	21		20	
Working laboratory model				
Extrapolated from existing design			1	5, 18
Proven design		3, 7, 8, 12, 15, 16	10, 13, 14	2, 4, 6, 9, 11, 17, 19
	Negligible	**Marginal**	**Critical**	**Catastrophic**

Performance Consequence →

9.1.2 Risk handling

A general approach towards the handling of the different kinds of performance risks described in section 9.1.1 is presented here.

Firstly, in case of an emergency the aerial segment is retracted, either to a lower altitude or to sea level, dependent on the event. If a severe storm might occur, the aerial segment is retracted to a lower altitude, to decrease the forces on the aerial segment, tether and ground segment, as the mean wind velocity is less at a lower altitude. When, on the other hand, there is no or only a little wind the aerial segment is fully retracted to the ground segment.

Secondly, to reduce the performance risks, different aspects of the kite system are made redundant. Below, two scenario's are considered and the way the risk is handled is described:

- Failure of EOS: if the EOS fails the aerial segment is retracted to a lower altitude. The aerial segment can not receive accurate weather data and therefore is unaware of its environment. To prevent the aerial segment from damaging due to high wind speeds, it is retracted partially. When chosen to retract it in case of failure, it could be damaged when attached to the mast.

- Failure of EOS in low wind: as stated in the previous bullet, the aerial segment is retracted to a lower altitude in case of a failure of the HMS. However, when the wind speed drops below the stall speed of the kite, it should not end up in the ocean. To prevent this from happening, the system is made redundant by implementing a tension meter in the TRS. If tension forces get lower, the system 'feels' that the wind speed is dropping. Therefore the aerial segment is further retracted. On the other hand, when the tension increases, the aerial segment is flown.

Note that the failure of the EOS is an example of a subsystem that could fail. Other subsystems can be thought of, however, the general approach towards handling these risks is stated.

Thirdly, a safety factor is assigned to the design of different components, in order to reduce the probability of a failure. If done so accordingly, this is stated in the chapter in which the component is described.

9.2 Schedule and cost risks

Schedule risk shows the possibility that scheduled milestones are not met. Table 9.3 shows these schedule risks on the left. Furthermore, the identified schedule risks are allocated in table 9.4 taking into account their consequence and probability of occurrence. The amount of influence on these risks is limited. They are taken into consideration during the designing and planning phases of the project. By choosing well known and readily available materials, designing easy transportable subsystems and choosing uncomplicated production methods, these risks are reduced significantly.

Cost risks tell whether there is the possibility that the available budget is exceeded. Table 9.3 shows these cost risks on the right. Furthermore, the identified cost risks are allocated in table 9.4 taking into account their consequence and probability of occurrence. Again, the amount of influence that can be exerted by the project manager on these risks is limited. However, they are taken into consideration during the designing and planning phases of the project. By reducing the performance and schedule risks, also the cost risks are reduced significantly. However, since the margins between being profitable and being not are rather small, all cost risks are identified to be critical.

Table 9.3: Schedule & Cost Risks

No.	Schedule risk	No.	Cost risk
1	Installation delayed due to bad weather/ design flaws	5	Delay causes increased cost
2	Materials and subsystems are not delivered in time	6	Material costs increase
3	Transportation is disturbed/ delayed	7	Labour costs increase/ more labour is demanded
4	Fabrication delayed	8	Cost of transportation increases
		9	Maintenance costs in case of failure
		10	Inflation and Real Interest Rate rise

Table 9.4: Schedule & Cost Risk Diagram

Frequent				
Probable		1	5, 7, 10	
Improbable		2, 3, 4	6, 8, 9	
Impossible				
	Negligible	**Marginal**	**Critical**	**Catastrophic**

9.3 Conclusion

From section 9.1 and 9.2 it can be stated that many different risks, in terms of performance, schedule and cost, exist. These risks are handled with care in order to produce an effective and safe system. All individual risks are treated in order to mitigate the overall risk of the kite system. Some risks, such as corrosion risk, are mitigated by extensive design. Other risks, such as the risk of extra maintenance costs, are mitigated by clear descriptions for production, installation and maintenance.

Chapter 10

Aerodynamics

In this chapter, a relationship is made between the dimensions of the kite and the efficiency increase that can be achieved. The chapter can be divided into four separate parts.

Firstly, the requirements on the reduction of the velocity deficit and increase of mass flow are calculated. This is done in section 10.1. Also the flying altitude of the kite will be determined in section 10.2, and the wind speed at this altitude in section 10.3.

Secondly, correction factors are calculated to correct for different phenomena which reduce the efficiency increase achieved. A correction factor which takes into account variable wind directions is calculated in section 10.4 and one which corrects for the maximum power output of the turbines in section 10.5. The efficiency of the mixing of the airflows is tackled in section 10.6. Finally section 10.7 defines the jet expansion correction factor.

Thirdly, the relation between efficiency increase and surface area of the kite is explained in section 10.8. From this, also the dimensions of the kite are calculated.

Fourthly, in section 10.9, a remark is made on the influence of variable wind speed, and in section 10.10 the assumptions made are evaluated.

For convenience, throughout this chapter an example calculation is made, starting from an optimal wind farm efficiency increase of 3%. Calculations for other efficiency increases are done with Matlab, which ultimately yields the plot in figure 10.18. Furthermore table 10.6 in section 10.8 gives an overview of all calculation steps and related equations.

10.1 Required velocity increase

In this section the required velocity increase and mass flow - for a certain efficiency increase - will be calculated with a method based on the measured wind farm efficiency, in subsection 10.1.1, with a simplified wind tunnel model. Afterwards, this method will be verified with a calculation of the velocity deficit with both the Jensen and Frandsen wake model, in subsection 10.1.2. In section 10.1.3 the simplified model of the wind farm is extended to a model of the wind farm with four rows of wind turbines. Then the final required velocity and mass flow increase is calculated in section 10.1.4.

10.1.1 Calculation of the required velocity increase

An increase of wind farm efficiency is realized by mixing the undisturbed outer flow with the wake region. This will increase the average velocity in the wake region. In this section, the increase in airspeed will be quantified, using the lower wind farm efficiency increase limit of 3% as an example.

For the scope of this section, a wind farm consisting of only two wind turbines behind each other is considered, as shown in figure 10.1. In section 10.4, this model is extended to incorporate different wind directions. The wind turbine on the left is called the first wind turbine, whereas the wind turbine on the right is called the second wind turbine.

Note that the power generated by the second wind turbine, P_2, is less than the power generated by the first wind turbine, P_1, due to the wake effect. The ratio between the generated power in this wind farm and the power which would be generated by the two independent wind turbines $2P_{independent}$ is the wind farm efficiency η_{wf} [12]. This is given by equation (10.1).

$$\eta_{wf} = \frac{P_1 + P_2}{2P_{independent}} \tag{10.1}$$

According to Betz' law, the power generated by a wind turbine P is proportional to the power coefficient C_P, which is defined as in equation (10.20) [13]. Inserting this equation into equation (10.1) yields equation (10.21).

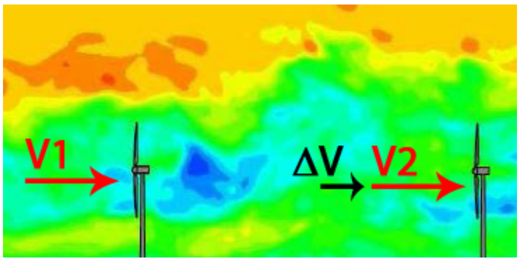

Figure 10.1: Sketch of the small wind farm with velocity definitions

Note that it is assumed that the power generated by an independent wind turbine equals the power generated by the first wind turbine in the wind farm.

$$P = C_P \frac{1}{2} \rho V^3 S \tag{10.2}$$

$$\eta_{wf} = \frac{C_{P_1} \frac{1}{2} \rho V_1^3 S + C_{P_2} \frac{1}{2} \rho V_2^3 S}{C_{P_1} \rho V_1^3 S} \tag{10.3}$$

$$\eta_{wf} = \frac{V_1^3 + \frac{C_{P_2}}{C_{P_1}} V_2^3}{2V_1^3} = \frac{V_1^3 + V_2^3}{2V_1^3} \tag{10.4}$$

The wind turbines in the OWEZ wind farms are variable speed wind turbines [14]. This implies that the power coefficient is constant for the wind turbines [15], as long as $V < V_{rated}$. Where V_{rated} is the rated speed of the wind turbine. It is assumed that this is indeed the case, because the average wind speed at the OWEZ wind farm is lower than the rated velocity of the wind turbines [14][12]. Therefore, the power coefficient $C_{P_1} = C_{P_2}$. Furthermore, because the Mach number of the flow will be smaller than 0.3 [12], the density of the air may be assumed to be constant. Equation (10.21) can now be simplified, yielding equation (10.4).

From equation (10.4), the velocity before the second wind turbine, V_2, can be calculated if the wind farm efficiency and the velocity before the first wind turbine, V_1, are known. The respective equation is given by equation (10.5). Equation (10.6) defines the factor f_2, the velocity factor for a 2 wind turbine wind farm, which will be used later on.

$$V_2^3 = V_1^3(2\eta_{wf} - 1) \implies V_2 = \sqrt[3]{V_1^3(2\eta_{wf} - 1)} = V_1 \sqrt[3]{2\eta_{wf} - 1} = V_1 \cdot f_2 \tag{10.5}$$

$$f_2 = \sqrt[3]{2\eta_{wf} - 1} \tag{10.6}$$

The measured wind farm efficiency of the OWEZ wind farm is 93.4% [2]. The minimum required wind farm efficiency increase - set by the clients - is three percent point, yielding a minimum desired wind farm efficiency of 96.4%. Note that this increase will be used for example calculations. As will be shown later on in this chapter, these calculations will ultimately not lead to the desired increase of 3% point, because correction factors need to be applied. A relationship will be developed where the efficiency increase is variable to obtain the optimal increase and kite dimensions.

Furthermore, from the OWEZ measurements [12], it follows that the average wind speed, from all directions, through the first wind turbine $V_1 = 9$ [m/s]. This is the average wind speed with a Weibull distribution with scale parameter $A = 10.1$ [m/s] and shape parameter $k = 2.3$ [12][16]. In figure 10.2 this probability distribution is plotted, as a Probability Density Function (PDF) and Cumulative Density Function (CDF) at the left and right respectively. This allows for a clear view of the wind speeds that are to be expected. Clearly, wind speeds above 30 [m/s] are not expected under normal circumstances.

From equation (10.6) follows that for the original wind farm efficiency of 0.93 the factor $f_2^{\eta=0.93} = \sqrt[3]{2 \cdot 0.93 - 1} = 0.95$ and in the new situation, with an efficiency increase of 3% the factor $f_2^{\eta=0.96} = 0.97$. With the wind speed distribution and equation (10.5), the required increase in average airspeed is now obtained. The results are shown in table 10.1.

As follows directly from table 10.1 the required ΔV for an efficiency increase of three percent points is on average 0.19 [m/s]. This implies that the air velocity needs to be increased by $0.19/8.95 \cdot 100\% = 1.46\%$. On first sight this seems to be a very low required velocity increase.

Looking at the decrease of the average velocity deficit behind the first turbine however shows something different. The average velocity deficit in the original situation equals $8.95 - 8.51 = 0.44$ [m/s] and in the new

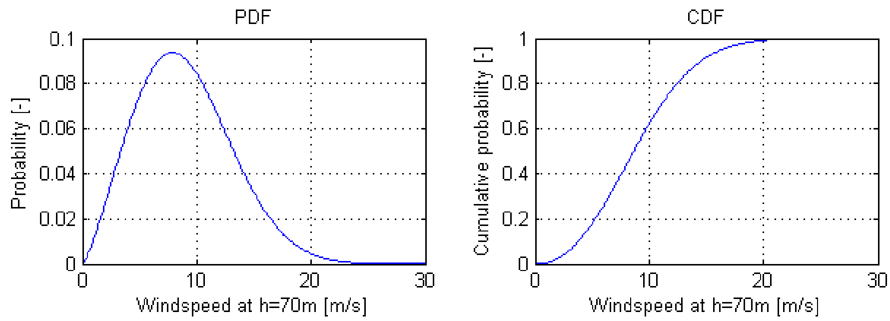

Figure 10.2: Distribution of the average windspeed on 70 [m].

Table 10.1: Calculation of the required increase in average airspeed (simplified wind farm)

Parameter	Average [m/s]
V_1	8.95
$V_{2_{\eta=0.93}}$	8.51
$V_{2_{\eta=0.96}}$	8.70
ΔV	0.19

situation $8.95 - 8.70 = 0.25$ [m/s]. Note the required decrease of the velocity deficit is $\frac{0.44-0.25}{0.44} \cdot 100 = 43\%$.

With the required average velocity increase known, the required change in mass flow $\Delta\dot{m}$ can be calculated with equation (10.7). The velocity should be increased over the surface of the wind turbine rotor disk, which has a diameter of 90 [m] [14] and therefore a surface area of 6362 [m^2]. Furthermore, standard atmospheric conditions at sea level are assumed, therefore the air density $\rho = 1.225$ [kg/m^3]. Calculation of the required change in mass flow with equation (10.7) yields with this data an average mass flow $\Delta\dot{m} = \rho A_{rotor} \Delta V = 1.5 \cdot 10^3$ [kg/s].

$$\Delta\dot{m} = \rho S \Delta V \tag{10.7}$$

It is important to note that certain specific assumptions have been made in the analysis so far:

- All calculated velocities are average velocities, concerning height. In the real situation, there will be a vertical velocity distribution over the wind turbine rotor disk. More will be explained about this subject in section 10.3.
- Only 2 wind turbines located behind each other are looked at. Since the wind will come from different directions and the wind turbines turn accordingly, this has to be accounted for. This is elaborated more in section 10.4.
- The wind turbines are assumed to be operating in speeds below V_{rated}. Therefore, the power coefficients of the first and second wind turbines are equal.

To conclude, the required average velocity increase, 1.46%, and average increase in mass flow, 1500 [kg/s], have now been found.

The calculation presented above are based on the measured wind farm efficiency. These calculations will now be verified with theoretical wake models.

10.1.2 Verification of the required velocity increase

The calculations presented above will be verified with the Jensen and Frandsen wake model. It has to be emphasized that this analysis is performed for a wind farm with 2 wind turbines in a row for simplicity. In subsection 10.1.3, the analysis is extended to 4 wind turbines in a row.

The Jensen model is a well known wake model which follows from balance of momentum. It describes a single wake by assuming the wake behind a turbine has an initial diameter of the same size as the rotor and it spreads linearly downwind as function of distance [17]. More information regarding the Jensen model is readily available in literature - for example in [17]. For this analysis the resulting equations are simply stated.

The Jensen model dictates that the velocity deficit can be calculated with equation (10.8). In this equation, C_T is the thrust coefficient of the turbine, D the rotor disk area, k a constant called the decay factor and X the horizontal distance in the wake behind the turbine.

$$V_1 - V_2 = V_1 \left(1 - \sqrt{1 - C_T}\right) \left(\frac{D}{D + 2kX}\right)^2 \tag{10.8}$$

$$C_T = \frac{3.5(2V_1 - 3.5)}{V_1^2} \tag{10.9}$$

$$k = \frac{0.5}{\log\left(\frac{h_{hub}}{z_0}\right)} \tag{10.10}$$

The thrust coefficient for modern wind turbines, such as the turbines in the OWEZ wind farm, can be calculated with the empiric equation (10.9) [18]. The decay factor k can be calculated with equation (10.10) [17], which is empiric too. As explained in section 10.3, the roughness coefficient $z_0 = 0.0002$ [-] and the hub height is 70 [m]. This yields $k = 0.048$ [-].

The Frandsen model is very similar to the Jensen model, but involves some more calculations [17]. Again, because information on the Frandsen model is readily available - for example in [17] - only the equations used are stated in this section. The velocity deficit can be calculated with the Frandsen model using equation (10.11) to (10.16).

$$\beta = \frac{1}{2}\left(1 + \sqrt{1 - C_T}\right) / \sqrt{1 - C_T} \tag{10.11}$$

$$s = \frac{X}{D0} \tag{10.12}$$

$$\alpha = \beta^{k/2} \left((1 + 2 \cdot 0.05s)^{k-1}\right) s^{-1} \tag{10.13}$$

$$D_X = D\left(\beta^{k/2} + \alpha s\right)^{1/k} \tag{10.14}$$

$$A = \frac{\pi}{4} D_X.^2 \tag{10.15}$$

$$V_1 - V_2 = V_1 \left(1 - \left(\frac{1}{2} + \frac{1}{2}\sqrt{1 - 2\frac{A_0}{A} C_T}\right)\right) \tag{10.16}$$

Solving equations (10.8) and (10.10) for the Jensen model and equations (10.11) to (10.16) for the Frandsen model with the thrust coefficient from equation (10.9) yields the velocity deficits as shown in table 10.2. As can be seen the resulting velocity deficits are close to the previously calculated velocity deficit. Where the Frandsen model yields a better solution than the Jensen model, as expected from Fernando [17]. The relative large difference between the calculated velocity deficit and the Jensen Model can be explained by the fact that in the Jensen model only a model of a wind farm with two rows of wind turbines is considered. In general it can be said the results from Jensen Model and Frandson Model seem to verify the calculation of the velocity deficit. In the next section, this model will be further developed into a model for a wind farm with four rows of wind turbines - such as the OWEZ wind farm.

Table 10.2: Verification of the velocity deficit at $X = 1000$ [m], for 2 wind turbines in a row

Method	$\mathbf{V_1 - V_2}$ **[m/s]**
Measurements (sec. 10.1.1)	0.44
Jensen	0.82
Frandsen	0.57

10.1.3 Model extension to a four row wind farm

The analysis performed in the current section assumes a very important scenario, that only one wind turbines is placed in the wake of another. In this subsection, this model is extended to rows which contain more than 2 wind turbines.

Looking at figure 10.6, in section 10.5, the air stream can be followed, which moves from left to right and passes through multiple wind turbines. Each wind turbine causes the airspeed to decrease with a certain factor, called f in figure 10.6. Therefore, when the flow has passed three wind turbines, the wind speed will have dropped by a factor f^3. Extending this to the number N wind turbines, equation (10.17) or its equivalent, equation (10.18), are found for the wind speed before the last wind turbine V_N as a function of the initial wind speed V_1, the number of wind turbines N and the factor f, the more general equivalent of f_2 defined in subsection 10.1.1:

$$V_N = V_1 \cdot f^{N-1} \tag{10.17}$$

$$\frac{V_N}{V_1} = f^{N-1} \tag{10.18}$$

In the same way, the definition of the wind farm efficiency can be extended for a wind farm with 4 rows of wind turbines, such as the OWEZ wind farm, assuming that this is the maximum number of wind turbines in a row, the result is equation (10.19):

$$\eta_{wf} = \frac{\sum P_N}{N \cdot P_{independent}} = \frac{P_1 + P_2 + P_3 + P_4}{4P_1} \tag{10.19}$$

Now, using the same procedure for the derivation of equation (10.4) in the previous section equation (10.22) is found. In which is assumed that the flow is incompressible since the Mach number is smaller than 0.3 and that the power coefficients are equal, $C_{p_i} = C_{p_j}$, since the air velocity is assumed to be smaller than V_{rated}, as explained in subsection 10.1.1.

$$P = C_P \frac{1}{2} \rho V^3 S \tag{10.20}$$

$$\eta_{wf} = \frac{C_{P_1} \frac{1}{2}\rho V_1^3 S + C_{P_2} \frac{1}{2}\rho V_2^3 S + C_{P_3} \frac{1}{2}\rho V_3^3 S + C_{P_4} \frac{1}{2}\rho V_4^3 S}{2 \cdot C_{P_1} \rho V_1^3 S} \tag{10.21}$$

$$\eta_{wf} = \frac{V_1^3 + \frac{C_{P_2}}{C_{P_1}} V_2^3 + \frac{C_{P_3}}{C_{P_1}} V_3^3 + \frac{C_{P_4}}{C_{P_1}} V_4^3}{4 \cdot V_1^3} = \frac{V_1^3 + V_2^3 + V_3^3 + V_4^3}{4 \cdot V_1^3} \tag{10.22}$$

Now, filling in equation (10.18), into equation (10.22), equation (10.23) is found. Working out this equation, equation (10.24) is obtained.

$$\eta_{wf} = \frac{1 + \left(\frac{V_2}{V_1}\right)^3 + \left(\frac{V_3}{V_1}\right)^3 + \left(\frac{V_4}{V_1}\right)^3}{4} = \frac{1 + (f)^3 + (f^2)^3 + (f^3)^3}{4} \tag{10.23}$$

$$\eta_{wf} = \frac{1 + f^3 + f^6 + f^9}{4} \tag{10.24}$$

Substituting equation (10.25) in equation 10.24, equation (10.26) is found stated below:

$$p = f^3 \tag{10.25}$$

$$\eta_{wf} = \frac{1 + p + p^2 + p^3}{4} \tag{10.26}$$

As can be seen, equation (10.26) is a cubic. This equation can be solved using Mathematica [19], which returns the three algebraic solutions, the first stated in equation (10.27), the second and third forming a complex conjugate stated in equation (10.28):

$$p_1 = -\frac{1}{3}\sqrt[3]{2}\sqrt[3]{3\sqrt{3}\sqrt{27\eta_{wf}^2 - 10\eta_{wf} + 1} - 27\eta_{wf} + 5} + \frac{2^{2/3}}{3\sqrt[3]{3\sqrt{3}\sqrt{27\eta_{wf}^2 - 10\eta_{wf} + 1} - 27\eta_{wf} + 5}} - \frac{1}{3} \tag{10.27}$$

$$p_{2,3} = \frac{\left(1 \mp i\sqrt{3}\right)\sqrt[3]{3\sqrt{3}\sqrt{27\eta_{wf}^2 - 10\eta_{wf} + 1} - 27\eta_{wf} + 5}}{3\ 2^{2/3}} - \frac{1 \pm i\sqrt{3}}{3\sqrt[3]{2}\sqrt[3]{3\sqrt{3}\sqrt{27\eta_{wf}^2 - 10\eta_{wf} + 1} - 27\eta_{wf} + 5}} - \frac{1}{3} \quad (10.28)$$

Now, filling in the values for the current wind farm efficiency, equal to 0.93, the corresponding numerical results are found as stated in equations (10.29) and (10.30).

$$p_1^{\eta=0.93} = 0.95 \quad (10.29)$$

$$p_{2,3}^{\eta=0.93} = -0.98 \mp 1.38i \quad (10.30)$$

Since the wind farm efficiency is a real parameter, the complex conjugates $p_{2,3}$ are omitted. Now, using equation (10.25) inversely, the value for f is calculated to equal $f^{\eta=0.93} = \sqrt[3]{p} = \sqrt[3]{0.95} = 0.98$. Similarly it is found that $f^{\eta=0.96} = 0.99$.

As calculated in equation (10.6), the value for $f_2^{\eta=0.93} = 0.95$. This value is verified in subsection 10.1.2 with the Jensen en Frandsen wake models. As stated before however, this value corresponds to a wind farm with 2 wind turbines in a row.

For the more general equivalent f, for 4 wind turbines in a row, the velocity deficit after one wind turbine is stated in table 10.3 using $V_2 = fV_1 \implies V_1 - V_2 = 8.9 - 0.98 \cdot 8.9 = 0.18$ [m/s], together with the calculated deficits of the Jensen and Frandsen wake models.

Table 10.3: Comparison of the velocity deficit, for 4 wind turbines

Method	$\mathbf{V_1 - V_2}$ **[m/s]**
Measurements (sec. 10.1.3)	0.18
Jensen	0.82
Frandsen	0.57

It can be seen in the table that the velocity deficits are quite different and not in the same range, in absolute sense. This fact can be explained firstly by the fact that the wake models do not take into account 4 wind turbines in a row. Secondly and most importantly, the measured parameters of the wind farm efficiency take into account multiple wind directions, which the wake models do not. Thirdly, the wind turbines are not placed directly behind each other at all different wind directions, which means the actual velocity deficits in front of a wind turbine in the wake is lower than straight behind the first turbine.

Therefore, the measurement result is found to be more precise and will be used in the remaining of the calculations. The comparison with the wake models is used as a verification of the order of the velocity deficit only.

A lot of research is done concerning the latter subject, examples are Guillen [17] and Jensen [20]. In further development of the kite system, the velocity deficit should be determined using a more advanced implementation of more advanced wake models. For this first analysis however, the model described in this subsection, using 4 wind turbines in a row in combination with the measured wind farm efficiency, will be used.

10.1.4 Definition of velocity ratio

In the previous section it was calculated that $f = 0.98$. This means that the velocity after the first wind turbine equals approximately $V_2 = fV_1 = 0.98V_1$. The velocity after the second turbine will be $V_3 = f^2V_1$ and so on. When the velocity deficit between the first and second row is completely 'repaired' by the first kite the velocity after the first turbine becomes $V_2 = V_1$ and after the second turbine becomes $V_3 = fV_1$. However, if the velocity deficit is not completely 'repaired' the velocity after the first and second turbine will be larger. This means that most likely the velocity deficit between the first and second row will be smaller than the velocity deficit between the last two rows. Therefore, optimally, kites of different sizes should be used for different rows. However, because the wind direction changes the first row sometimes becomes the last row, which makes it impossible to effectively vary the kite size. Furthermore, from a manufacturing point of view it is more difficult because different kite production lines should be made.

To overcome this problem, the value of the velocity deficit between two middle turbines is used for the calculations, which leads to average kite dimensions. In further research this problem needs to be tackled with a more advanced simulation program, to come up with more optimal kite dimensions.

The average velocity deficit follows from the average velocity ratio f_{av} as given in equation (10.31). Note that this equation follows from inspection of equation (10.23). Calculating f_{av} with this equation yields $f_{av}^{\eta=0.93} = 0.967$ and $f_{av}^{\eta=0.96} = 0.982$.

$$\left.\begin{array}{l} \eta_{wf} = \frac{1+(f)^3+(f^2)^3+(f^3)^3}{4} \\ \eta_{wf} = \frac{1+3f_{av}^3}{4} \end{array}\right\} f_{av} = \sqrt[3]{\frac{(f)^3+(f^2)^3+(f^3)^3}{3}} \tag{10.31}$$

With the velocity fraction $f_{av} = V_2/V_1$ the values in table 10.4 are calculated. Furthermore, with equation (10.7) the required mass flow to be added is calculated.

Table 10.4: Calculation of the required increase in average airspeed and mass flow (extended wind farm model)

Parameter	Average [m/s]
V_1	8.95
$V_2^{\eta=0.93}$	8.66
$V_2^{\eta=0.96}$	8.79
ΔV	0.13
$\Delta \dot{m}$	978 [kg/s]

10.2 Kite height

In this section it will be determined at which altitude the kite will fly during normal operation. The kite will need to get air from the outer flow into the wake region, which means that it should be positioned in the outer flow. The higher it is positioned however, the farther it is positioned away from the wake region and the wind turbine. This is also not desirable, therefore the kite will be positioned just above the wake.

The diameter of the wake can be calculated with the Jensen and Frandsen wake models [17]. The corresponding equations are given by Jensen with equation (10.32) [17] and by Frandsen with equation (10.33) [17]. In the model of Jensen, the decay factor k is given by equation (10.10). In the model of Frandsen the required input values are given by equations (10.11) to (10.13).

$$D(x)_{Jensen} = D_{rotor} + 2kx \tag{10.32}$$

$$D(x)_{Frandsen} = D_{rotor}\left(\beta^{k/2} + \alpha s\right)^{1/k} \tag{10.33}$$

In section 10.4 it is determined that the kite is positioned at half a distance between the wind turbines. Solving equations (10.32) and (10.33) for $x = 500$ [m] yields the values listed in table 10.5. Note that because the hub height of the turbines is 70 [m] the wake height is given by $h_w = 70 + D(x)/2$.

Table 10.5: Calculation of wake height at $x = 500$ [m]

	Jensen	Frandsen
Wake diameter [m]	140	160
Wake height [m]	140	150

In table 10.5 it is shown that the two models both approximate the wake height at around 145 [m]. Therefore in this first analysis the kite will be placed at 145 [m]. In further analysis this needs to be optimized with more complex mixing models of the wake and the downwash.

10.3 Wind profile

The velocity of the undisturbed flow varies with height. This is caused by the so called boundary layer effect of the earth's surface [8]. The resulting velocity distribution is called the wind profile. In figure 10.3 a wind profile is plotted (based on the log wind profile in [8]).

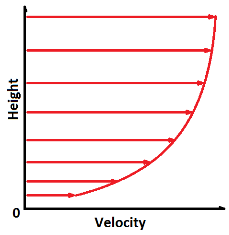

Figure 10.3: Illustration of the wind profile

It is assumed that the wind profile is logarithmic, as given in equation (10.34) [8]. Using this equation, the velocity of the undisturbed flow can be approximated [8]. In this approximation, the roughness coefficient is assumed to be $z_0 = 0.0002$ [m/s], which should be used for the open sea surface [8].

$$V(h) = V_1 \frac{\log \frac{h}{z_0}}{\log \frac{h_1}{z_0}} \tag{10.34}$$

In section 10.1.1 it was shown that the average wind speed at hub height (70 [m]) equals $V_1 = 9$ [m/s]. With equation (10.34) it is then calculated that at the kite height of 145 [m] the wind speed is on average 9.5 [m/s]. Using the results of the previous sections as listed in table 10.4, this yields an airspeed with difference between outer flow and the wake of $9.5 - 8.66 \approx 0.84$ [m/s], which clearly is more than the required 0.13 [m/s], as stated in subsection 10.1.4. Therefore it can be concluded that the airspeed of the outer flow can be used elegantly for the velocity increase of the airflow in the wake.

As stated in the section 10.1, the values of the calculated required airspeeds are averaged over height. In reality, as stated in this section, a wind profile exists, yielding an increase of airspeed with height. For the scope of this report, this wind profile effect is neglected concerning the required velocity increase calculations. The average values are taken in this case, therefore no correction factor is applied to the required velocity increase for effect of the wind profile.

10.4 Wind direction correction

In section 10.1 the required velocity and mass flow increase calculation was shown. This calculation however is only valid when the wind blows only from one direction. As explained before, the buoy will not be able to 'move' substantially. Therefore, the overall efficiency increase induced by the kite - taking into account all possible wind directions - is lower than the efficiency increase in only the optimal direction. In this section a correction factor will be calculated which accounts for the fact that the kite will not always be positioned in the optimal wind direction, as the wind direction changes.
Figure 10.4A shows a map of the OWEZ wind farm, where figures 10.4B and -C state results of wind direction and speed measurements done by the meteo mast [21]. Because the kites can rotate around the buoys only, a substantial efficiency increase is only achieved when the kites are aligned with the wind turbines in the wind farm.

In figure 10.4A, the different possible rotations with respect to the prevailing wind direction are shown. The line with the arrowhead indicates the dominant wind direction, where the lines without arro heads indicate the alternative wind directions in which a wind turbine will be aligned with a kite. This can be seen in figure 10.4A, since all lines, with arrowhead or not, pass through a wind turbine and through the kite's location.

In this analysis it is assumed that the kite will only increase the wind farm efficiency when it is aligned with a nearby wind turbine, as the kite will be able to rotate in these directions. Note that in other situations the kite will still reduce the wake effect to some extent, because the outer air will still be mixed with the wake region. However, to be on the safe side with the estimations of the kite size, only the time when the kite is aligned with a nearby wind turbine is taken into account.

Plotting the wind rose determined in figure 10.4A in figure 10.4B, which shows the frequency of occurrence of each wind direction, the occurrence of the prevailing and alternative wind directions are determined. All occurrences are indicated in percentages next to the wind directions in the wind rose in figure 10.4B.

From figures 10.4A and 10.4B follows directly that the kites are aligned with wind turbines for only $(20+5+11+5+4+12 =)$ 57% of the time. In all other cases the kite will not be aligned and therefore will not increase the wind farm efficiency according to the assumption made above. Therefore a wind direction correction factor

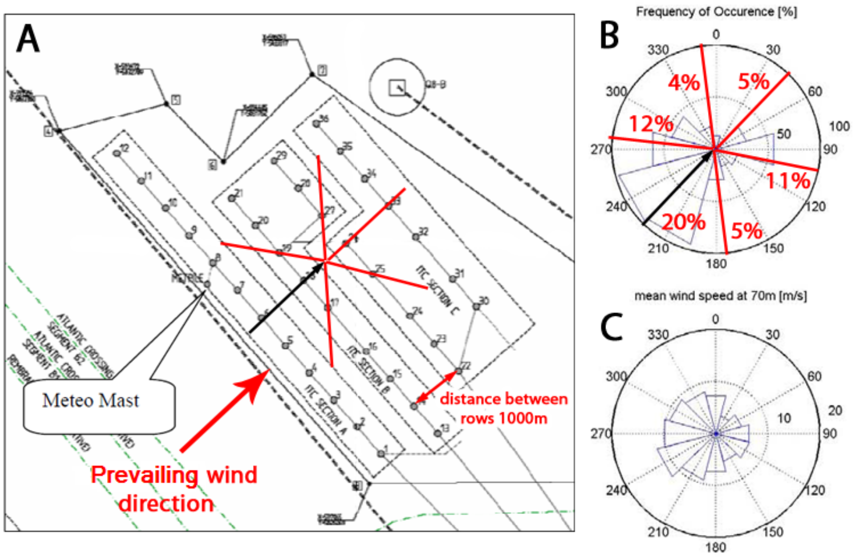

Figure 10.4: Feasible wind directions (figure based on [21])

of $c_{\text{wind dir.}} = 0.57$ should be applied to the required wind farm efficiency increase of 3% to obtain the actual required wind farm efficiency increase in the optimal wind directions.

10.5 Correction for maximum power

When the wind speed increases, the power generated by the wind turbines increases [14]. This happens up to a certain speed, which is called the rated velocity of the wind turbine [14]. For the Vestas V90-3MW wind turbines in the OWEZ wind farm, the rated velocity is 15 [m/s] [14]. This is also shown in figure 10.5. This figure clearly shows that from 15 [m/s] on the output remains 3 [MW] with increasing wind speeds.

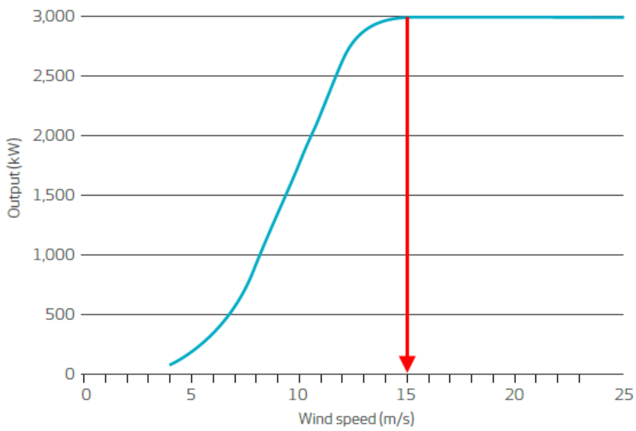

Figure 10.5: Power curve of the Vestas V90-3MW (figure from [14])

Figure 10.5 also implies that there are undisturbed wind speeds for which it is not possible to increase the wind farm efficiency any more, because the wind speeds in the whole wind farm are already above the rated velocity. All wind turbines then already output maximum power. In this section a correction factor will be calculated to correct for this.

Figure 10.6 shows that the velocity in the wake before before the wind turbine after the wind turbine causing the wake is the wind speed in front of the first wind turbine decreased by a factor $f_{av}^{\eta=0.93} = 0.97$ - as calculated in section .

In figure 10.6 it is shown how the wind speed is reduced by this factor after each wind turbine. This means that if the undisturbed wind speed is the rated velocity of 15 [m/s], the velocity in the wake is reduced and therefore the efficiency of the wind farm can still be increased by mixing the airflows. However, when the undisturbed speed is $15/f$ [m/s], the speed through the second turbine equals $\frac{15}{f} \cdot f = 15$ [m/s]. This is the

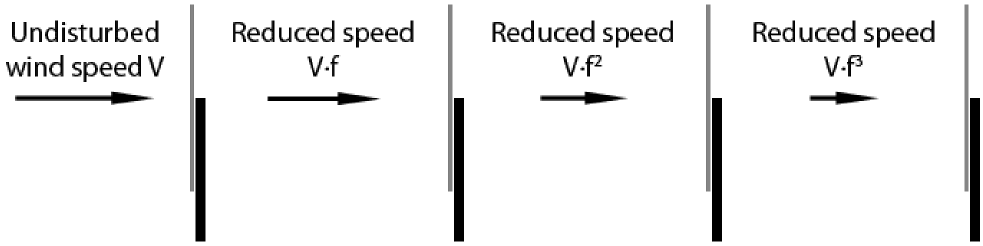

Figure 10.6: Reduction of speed over multiple wind turbines

rated speed and therefore the power output of the second turbine cannot be increased any more. Similarly the wind speeds through the third and fourth wind turbines are the rated speed when the undisturbed wind speed is respectively $15/f^2$ and $15/f^3$ [m/s].

Figure 10.4 shows that in the most common wind directions the wind farm consists of four rows of wind turbines. The first row is in the undisturbed flow, therefore three rows are used to increase the wind farm efficiency. When the velocity is the rated velocity in the first row, the wind farm efficiency can only be increased by increasing the wind speed for the third and fourth row of turbines the wind farm farm. Therefore, the potential efficiency increase is reduced by 1/3. Similarly when the velocity is also the rated velocity in the third row only the fourth can be used and the potential is reduced by 2/3. When the velocity is the rated velocity also in the fourth and last row, the wind farm efficiency is maximum and cannot be increased any more.

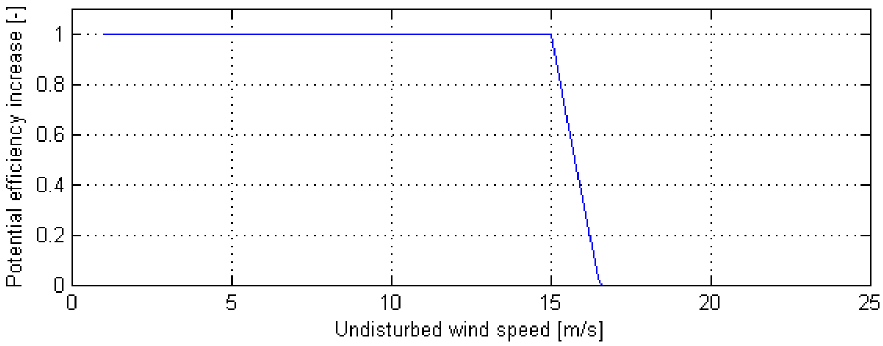

Figure 10.7: Potential efficiency increase (on a scale from 0 to 1) for each wind speed

It is assumed that the potential efficiency increase reduces linearly between the mentioned wind speeds. The resulting potential efficiency increase is plotted in figure 10.7. As can be seen, the efficiency cannot be increased any more when $V_{undisturbed} = 15/f^3 = 15/0.97^3 = 16.5$ [m/s].

$$c_{\text{rating correction}} = \int_4^{25} P(V) \cdot (\text{Potential Efficiency Increase})\,\mathrm{d}V \tag{10.35}$$

Because the potential efficiency increase is plotted on a scale from 0 to 1, the correction factor for the power rating can be calculated with equation (10.35). This equation is the integral over the undisturbed wind speed from the cut in speed of 4 [m/s] to the cut out speed 25 [m/s] of the probability of occurrence of a certain wind speed $P(V)$, as presented in figure 10.2, multiplied by the potential efficiency increase at that speed. This yields the ratio between the amount of time the efficiency can be increased and the total time that the wind turbine is generating power.

The integration is performed numerically with Matlab and yields $c_{\text{power rating}} = 0.93$ [-].

Note that in this section four wind turbines in a row are analysed. From inspection of the layout of the OWEZ and the wind directions in figure 10.4 it follows that often the wind direction is such, that there are more rows of wind turbines in the wake region. This will however only increase the correction factor - making it easier to achieve a certain efficiency increase - because the velocity in the wake region will be decreased further when more rows are added. This effect is not accounted for, to guarantee that the minimum efficiency increase is calculated. and nothing is overestimated.

10.6 Mixing efficiency

The downwash is generated to increase the velocity of the wake flow induced by the wind turbine. In this section the efficiency of the mixing process (or equivalently bending the wake flow downwards) is estimated. This will be done by analysing the results from different wind tunnel tests [22][23].

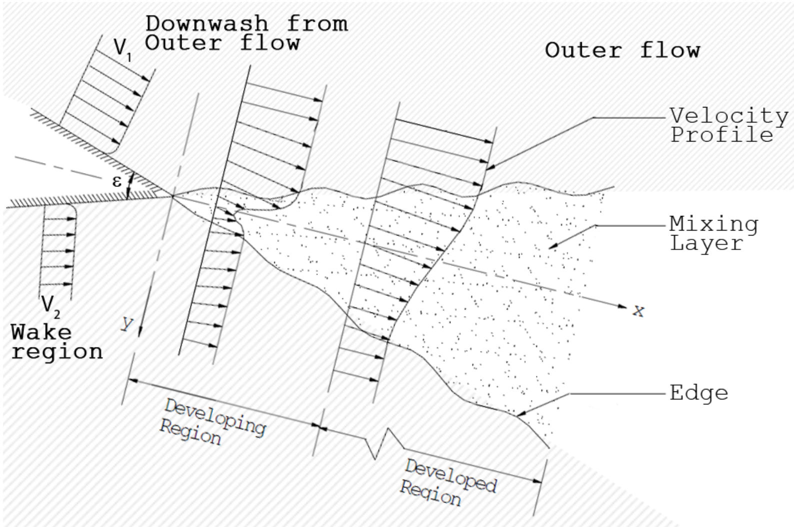

Figure 10.8: Sketch of the mixing layer (figure based on [22])

Figure 10.8 is a sketch, and therefore only a qualitative indication, of the mixing region (or so called 'mixing layer' as used further in this section) between the wake flow and the downwash flow. Also the velocity profiles are shown on different locations. This figure is based on the wind tunnel set-up used in the wind tunnel tests done by Azim [22]. The horizontal airflow, indicated by V_2, is similar to the airflow in the wake of the wind turbine. Also, the diagonal airflow, indicated by V_1, is similar to the downwash airflow, produced by the kite. The angle between these flows is the downwash angle ϵ.

As can be seen in figure 10.8, starting at the point where the flows reach each other, they will start to mix. However, due to the fact that the boundaries of the wind tunnel induce a temporary velocity deficit, the mixing layer has to develop first. The region in which this happens is called the 'developing region' as shown in the figure. The region where the velocity deficit is not present any more is called the 'developed region'. Since the developing region, as a result of the wind tunnel boundaries, is not interesting for the current analysis, this region is not considered.

What is considered, is the following. In figure 10.8, a wavy horizontal line indicates the location where the downwash from the kite reaches the mixing layer. It can be seen that below this line, in the developed region, the stream velocity decreases slowly as one goes downward with respect to the wavy line. This is the interesting part of the experiment considering the mixing efficiency. Because the part of the flow in the mixing layer that has a higher velocity than the flow in the wake region of the wind turbine will eventually induce the wind farm efficiency increase.

It has to be noted, that the flow below the mixing layer, which has the same velocity as the initial flow from the wake flow, is bend down, as can be seen in figure 10.8. This corresponds with the equivalent statement in the introduction of this section, that the wake flow is bend downwards.

The wind tunnel tests from Azim consider mixing angles of 18 [deg] and 20 [deg]. In section 10.8, it will be calculated that this corresponds to the downwash angle of the kite. Furthermore, the velocity of the wake and downwash used in the test are respectively 7 and 10 [m/s]. As was explained in section 10.1, the wind speeds at the height of the kite and turbine are around 9.5 [m/s]. Because this speed and the downwash angle are in the same order as the flow velocities and mixing angles in the wind tunnel test, the wind tunnel tests are considered representative for the mixing problem.

The following characteristics are however different from the case in reality:

- Firstly, the wind tunnel experiments consider laminar flows only [22]. However, the mixing of turbulent flows, which occurs in reality, because of the interactions of the kite and the wind turbine blades with the airflow, is more efficient [24]. Therefore, the final estimation will yield a larger than estimated efficiency increase, considering this effect.

- Secondly, in reality the wake flow of the wind turbine consists of vortices induced by the blades of the wind turbine, which form helices or 'coherent structures' behind it, as shown in figure 10.9. The flow in the wind tunnel has no such patterns at all, therefore the wind tunnel experiment does not include the corresponding characteristics. Regarding the complexity of calculations concerning the coherent structures, the only way to incorporate their effect is to use a wind tunnel experiment or a CFD model that simulate these patterns. Therefore, here the effect neglected. In chapter 26 more is explained on this matter.

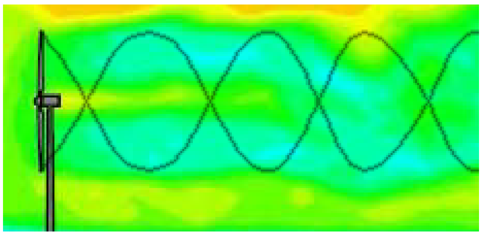

Figure 10.9: Vortices induces by the wind turbine blades forming helices behind the wind turbine.

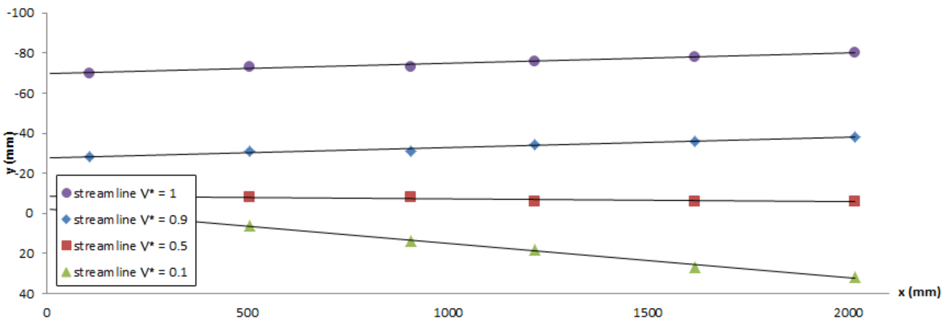

Figure 10.10: Streamlines in the wind tunnel transformed in y-coordinates in [mm] (derived from wind tunnel test [22])

Figure 10.10 shows the streamlines in the wind tunnel used in the experiments described earlier in this section, after the two flows are combined. The vertical location is stated in millimetres in figure 10.10 for clarity. In Azim's report, these are stated non-dimensionally. Below the corresponding transformation is explained. The velocity V is made dimensionless for the streamlines too. This dimensionless velocity V^* is given by equation (10.36).

$$V^* = \frac{V - V_2}{V_1 - V_2} \tag{10.36}$$

As can be seen in figure 10.10 there is a velocity gradient in cross-stream direction. For location $x = 2017$ [mm], the downstream location in the wind tunnel, this gradient is given in figure 10.11, which is derived from the results of Azim [22]. Note that when $V^* = 1$, the velocity equals the downwash velocity V_1. Figures 10.10 and 10.11 show that in a certain region in the stream, the velocity equals the initial downwash velocity (when $V^* = 1$). Furthermore, from figure 10.10 follows that this region is bounded in cross-stream direction by a more or less constant line at $y = -80$ [mm].

For clarity reasons, the velocity profile in figure 10.11 is given in coordinates which have dimensions. The plots given in Azim's report [22] are given in non-dimensional units. These non-dimensional units are transformed using the definition in equation (10.37) [22].

$$\eta = \frac{y - y_{0.5}}{\delta} \tag{10.37}$$

In this equation, η is the so called similarity parameter, or simply the non-dimensional vertical distance in the wind tunnel; y is this vertical distance (or y-coordinate) in millimetres, with respect to the center of the wind tunnel, which is positive pointed downwards as in figure 10.8; $y_{0.5}$ is the y-coordinate (or isovel) corresponding to $V^* = 0.5$ in the mixing layer, which are stated in figure 10.10 and finally δ is the thickness of the mixing layer, which is calculated using the definition shown in equation (10.38) [22].

$$\delta = y_{0.1} - y_{0.9} \tag{10.38}$$

Here, $y_{0.1}$ and $y_{0.9}$ are the y-coordinates or isovels just like $y_{0.5}$ corresponding to $V^* = 0.1$ and 0.9, respectively. Also $y_{0.1}$ and $y_{0.9}$ are stated in figure 10.10.

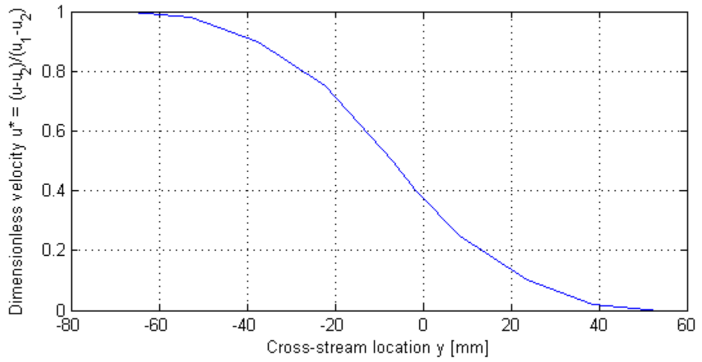

Figure 10.11: Velocity profile of the developed mixing layer (calculated from wind tunnel test data [22])

Now, enough is known to determine the mixing efficiency. The mixing efficiency is defined using the reasoning stated earlier: It is the part of the downwash flow in the mixing layer, which induces a higher velocity than the velocity of the wake (or initially horizontal) flow (V_2). This is equivalent to the complete downwash flow minus the part of the downwash flow which is undisturbed; the part of the downwash flow which is not decelerated - thus not bent into the wake region but bent back to the outer flow. Equation (10.39) explains this reasoning in symbols.

$$\eta_{mix} = f_{dw_{disturbed}} = 1 - f_{dw_{undisturbed}} = 1 - \frac{h_{dw_{undisturbed}}}{h_{dw_{initial}}} \tag{10.39}$$

Here, η_{mix} is the mixing efficiency; $f_{dw_{disturbed}}$ is the fraction of the downwash flow in the mixing layer, which induces a higher velocity than the velocity of the wake flow and is therefore precisely the mixing efficiency; $f_{dw_{undisturbed}}$ is the complementary fraction of the mixing efficiency, the part of the downwash flow which does not mix with the flow from the wake of the wind turbine; $h_{dw_{undisturbed}}$ is the height of the downwash flow which is not mixed with the flow from the wake of the wind turbine and lastly $h_{dw_{initial}}$ is the initial height of the downwash flow.

Note that the heights are used in the calculations instead of areas. This can be done since the width of the wind tunnel cross-section is rectangular: 300 [mm] by 300 [mm] [22]. Furthermore, as stated above the cross-stream coordinate y is defined to be zero in the center of the cross-section and the positive axis is defined downwards as stated in figure 10.8. Therefore, the region where the downwash flow is undisturbed, is bounded between $y = -150$ [mm], the wall location, and $y = -80 (= y_1)$ [mm], the location where $V^* = 1$. This yields the cross-stream height of the undisturbed flow is equal to: $-150 - (-80) = -70$ [mm]. The initial downwash was spread over a cross-stream height of -150 [mm]. Therefore the mixing efficiency can be calculated using equation (10.39):

$$\eta_{mix} = 1 - \frac{h_{dw_{undisturbed}}}{h_{dw_{initial}}} = 1 - \frac{-70}{-150} = 0.53 \tag{10.40}$$

Therefore, the mixing efficiency is equal to 0.53, as stated in equation (10.40).

10.7 Jet expansion correction

Section 10.6 discussed the mixing efficiency in terms of the ratio between the total downwash mass flow and the mass flow that actually ends up in the wake region of the wind turbines. The added mass flow can be seen as a jet in the wake region. In this section it will be verified if this jet does not expand too much until it reaches the wind turbine. If the diameter is larger than the diameter of the wind turbine rotor disk, not all added mass flow goes through the wind turbine, decreasing the effectiveness of the added mass flow.

The expansion of the jet is shown in figure 10.12. In this figure the expansion of the jet is modelled linearly. Looking at the validity of the wake model by Jensen [20][17] and the entrainment model for a turbulent jet by Enjalbert et al. [25], this is a very realistic model for this first analysis.

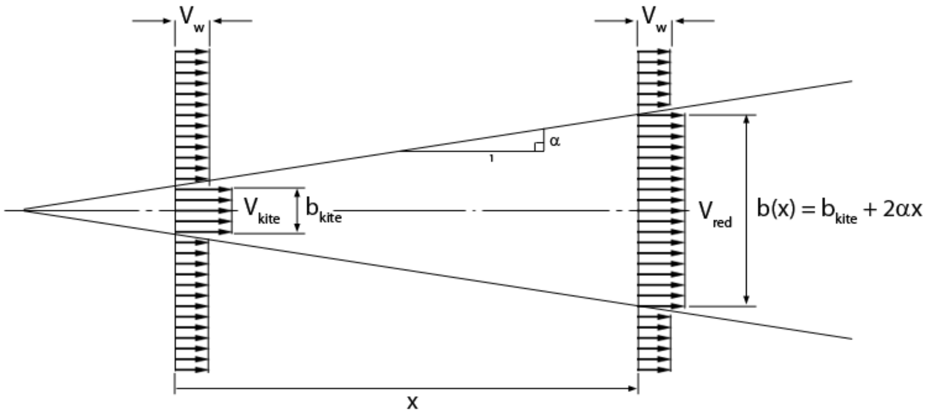

Figure 10.12: Linear jet model (based on the Jensen wake model [20][17])

$$b(x) = b_{\text{kite}} + 2\alpha x \tag{10.41}$$

Modelling the jet linearly allows for calculation of the jet's diameter with equation (10.41). Here $b(x)$ represents the diameter of the jet and x the horizontal distance behind the kite (see figure 10.12). It is assumed that the diameter of the jet equals the diameter of the kite. This implies that the flow bend down by the kite is the flow 'swept' by the kite: the area of circle around the kite, with the kite's diameter. While this seems a somewhat arbitrary area, it yields very good results in different analysis [24] [26].

The linear growth of the jet is defined by the entrainment constant α [17] [20] [25]. The wake of an offshore wind turbine can be modelled with an entrainment coefficient of 0.05 [17] [27]. Because in the wake behind the wind turbine the velocity is lower than the undisturbed flow, whereas in the wake behind the kite the air speed is higher, a slightly different value is found for α. From Enjalbert et al. [25] and Ricou and Spalding [28] it follows that the entrainment coefficient $\alpha \simeq 0.056$ for a turbulent jet.

Using this value, a relation can be plotted between the kite's diameter and the size of the expanded downwash stream at the location of the wind turbine downstream. Note that a location of the kite has to be set and for this analysis it is assumed that the kite is positioned in the middle between two wind turbines. This means the distance between the kite and the next wind turbine is 500 [m]. Using $x = 500$ [m] and $\alpha = 0.056$, figure 10.13 is plotted with equation (10.41).

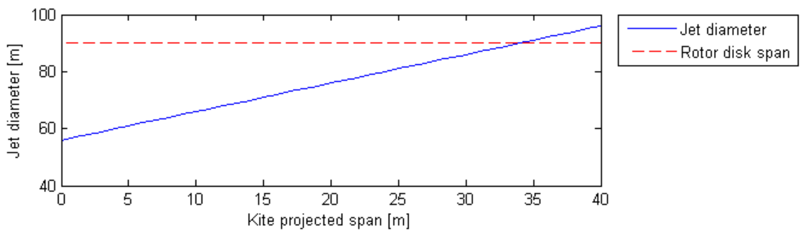

Figure 10.13: Diameter of the jet left by the kite at location of the wind turbine downstream

As can be seen in figure 10.13 the diameter of the jet only gets larger than the diameter of the wind turbine rotor disk when $b_{kite} > 34$ [m]. As can be read in section 11.2 the kites span will only be 16 [m]. With this span the diameter of the jet will be smaller than the rotor disk diameter as can be seen in figure 10.13. Because kites with a span larger than 34 [m] are not feasible and will not be considered, no correction factor is implemented to correct for the reduced effectiveness of these kites.

It should be noted that because the jet coming from the kite is relatively small, the angle the kite makes with the wind turbine is very critical. To solve this problem the kite will feature an active control system to keep it in the best attitude, in the right direction.

Now all relevant correction factors have been calculated. The question may rise though, that if a large downwash is generated, the flow in the wake is bend down which reduces the mass flow through the wind turbine, as shown in figure 10.14. This will lead to a decreasing marginal utility of the system, because increasing the mass flow will lead to more mass flow losses, which will eventually balance to an equilibrium after which the mass flow cannot be increased any further. However the mass flow through the rotor disk is $\dot{m} = \rho A_{rotor\,disk} V_{rotor} \approx 1.225 \cdot 6362 \cdot 9 \approx 7 \cdot 10^4$ [kg/s]. This is approximately 70 times more than the added

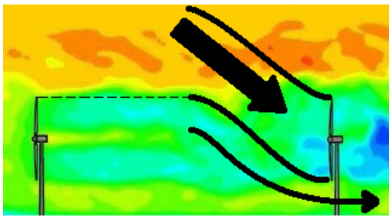

Figure 10.14: Source of decreasing marginal utility, accompanying very large added mass flows.

mass flow of approximately $1 \cdot 10^3$ [kg/s]. Because of this large difference in mass flow, it is assumed that the effect of the wake being bend down, and therefore the effect of decreasing marginal utility, is negligible.

10.8 Relationship dimensions and efficiency

In the previous sections the required additional mass flow and correction factors have been calculated. With this knowledge, in this section a relation will be derived between the dimensions of the kite and the wind farm efficiency increase.

The equations used for this derivation are very similar to the equations used in the conceptual design phase of the project, as presented in the Mid-Term Report. In the conceptual design phase however, the dimensions of different concepts were compared for a fixed wind farm efficiency increase. In this detailed design phase, the wind farm efficiency increase will be a variable and the kite dimensions will be plotted as function of the efficiency increase. This will allow for an optimization of the kites performance (as will be explained later in section 11.2).

The starting point of this derivation will be the calculation of the downwash angle of the kite. The downwash angle of a kite near the kite with an elliptical lift distribution can be calculated with equation (10.42) [24]. Required inputs in this equation are the lift coefficient C_L and aspect ratio AR of the kite. From measurements it follows that for different possible kites - which can be used to achieve the require downwash - the maximum lift coefficient at which the kite remains in the air easily is $C_L = 1.1$ [29]. For calculation of the aerodynamic forces, the drag force should not be neglected. From reference kites it follows that the lift to drag ratio for relevant kites is approximately $L/D = 5$ [29]. This means the drag coefficient is - because $L/D = C_L/C_D$ - equal to $C_D = (C_L/C_D)^{-1}C_L = 0.22$. Furthermore, because a large downwash angle is desired, and also from a structural point of view, the aspect ratio should be made small. From an investigation of different kite solutions it was found that an aspect ratio of $AR = 2$ is achievable [29].

Inserting these values in equation (10.42) yields a downwash angle of 20 [deg]. It should be noted that this downwash angle equals the angle used in the wind tunnel experiments described in section 10.6. This confirms that indeed the correct mixing efficiency was calculated. If the downwash angle turned out to be lower than 20 [deg], the mixing efficiency would also be lower [22][23].

$$\epsilon = 2\frac{C_L}{\pi AR} \tag{10.42}$$

Now the downwash angle is verified with the calculated mixing efficiency, the wind farm efficiency increase should be related to the dimensions of the kite. Note that the surface area of the kite appears in the equation for the lift generated by the kite, which is given by equation (10.43) [24].

$$L = C_L\frac{1}{2}\rho V^2 S \tag{10.43}$$

The lift generated is still an unknown, and therefore the surface area cannot be calculated yet with equation (10.43). In section 10.1 the required mass flow increase was calculated. This mass flow will be used to calculate the lift that has to be generated.

In figure 10.15 a sketch of an airfoil in a free stream is shown. It can be seen that the free stream air flow is bend downwards with an angle ϵ^*, and thus the airfoil generates lift.
The entering free stream flow $\mathbf{V}_E$ in figure 10.15 is given in Cartesian coordinates by equation (10.44) and the departing flow $\mathbf{V}_D$ by equation (10.45).

$$\mathbf{V}_E = V_{inf}\,\mathbf{i} \tag{10.44}$$
$$\mathbf{V}_D = V_{inf}\cos\epsilon^*\,\mathbf{i} - V_{inf}\sin\epsilon^*\,\mathbf{j} \tag{10.45}$$

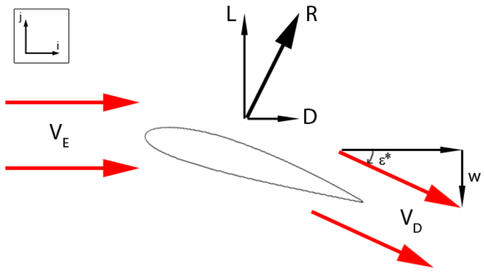

Figure 10.15: Lift by bending the flow

With these airflows known, the forces $\mathbf{F}_E$ and $\mathbf{F}_D$ exerted on the airfoil by the entering and departing stream follow from respectively equations (10.46) and (10.47).

$$\mathbf{F}_E = \dot{m}\left(V_{inf}\,\mathbf{i}\right) \tag{10.46}$$
$$\mathbf{F}_D = -\dot{m}\left(V_{inf}\cos\epsilon^*\,\mathbf{i} - V_{inf}\sin\epsilon^*\,\mathbf{j}\right) \tag{10.47}$$

The total force exerted by the kite on the airflow then follows from the sum of equations (10.46) and (10.47), as shown in equation (10.48).

$$\mathbf{R} = \mathbf{F}_E + \mathbf{F}_D = \dot{m}V_{inf}\left[\left(1-\cos\epsilon^*\right)\mathbf{i} + \sin\epsilon^*\,\mathbf{j}\right] \tag{10.48}$$

The lift force equals the vertical component of this reaction force $\mathbf{R}$ and is given by equation (10.49). The angle ϵ^* in this equation designates the angle with which the air flow leaves the kite.

$$L = \dot{m}V_{inf}\sin\epsilon^* \tag{10.49}$$

Because ϵ^* is a very important parameter in equation (10.49) it will be approximated with two different methods, to verify the solution.

In section 13.1.3 on the calculation of the tether force it is approximated that the tether is positioned under an angle of approximately $\epsilon^* = 11$ [deg] as shown schematically in figure 10.16. The Kutta condition implies that the air flow leaves a body with a sharp trailing edge - such as the kite - such that the flow leaves parallel to the trailing edge [24]. Assuming that the tether is attached perpendicular to the kite as shown in figure 10.16 the angle with which the air leaves the kite is the same angle ϵ^* under which the tether is positioned.

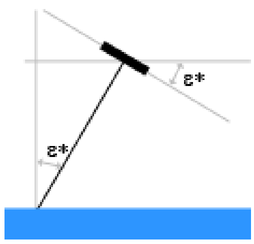

Figure 10.16: Angle ϵ^* determined from geometry

This angle will now also be approximated in an alternative fashion. From Anderson [24] it follows that for wings with an elliptical lift distribution, the air leaves the wing with approximately an angle α_i as given by equation (10.50) [24].

$$\alpha_i = \frac{C_L}{\pi AR} \tag{10.50}$$

Inserting $C_L = 1.1$ and $AR = 2$ into equation (10.50) yields an angle $\alpha_1 = 10$ [deg]. Note that this is very close to the already approximated from tether geometry $\epsilon^* = 11$ [deg]. For this analysis the lowest of the two angle will be used, to prevent overestimation of this angle. Hence $\epsilon^* = \alpha_i = 10$ [deg].
The lift force is now with equation (10.43) written in terms of the surface area of the kite and with equation (10.49) in terms of the angle ϵ^* and the mass flow of the air bend down by the kite. Combining these equations gives the ratio between the surface area of the kite and the mass flow of the air bend down by the kite. This is done in equation (10.51).

$$\left.\begin{array}{l} L = C_L \frac{1}{2}\rho V^2 S \\ L = \dot{m} V \sin\epsilon \end{array}\right\} \frac{S}{\dot{m}} = \frac{2\sin\epsilon^*}{\rho V C_L} \tag{10.51}$$

Apart from the wind speed, all variables in this equation are known from the previous analysis. The wind speed V is the wind speed at height of the kite - 145 [m]. This follows directly from the wind profile given in section 10.3 and on average is $V = 9.5$ [m/s]. Inserting all values in equation (10.51) yields $\frac{S}{\dot{m}} = \frac{2\sin 10\cdot\frac{\pi}{180}}{1.225\cdot 9.5\cdot 1.1} = 0.027$ [-].

In section 10.1 the required mass flow increase was calculated and in section 10.6 it was approximated how much of the downwash mass flow is actually added to the wake region. Combining this knowledge allows for calculation of the required mass flow to be bend down by the kite, which is required to solve equation (10.51) for the surface area S.

In equation (10.52) the calculation of the surface area is summarized. As discussed, the ratio $\left(\frac{S}{\dot{m}}\right)$ needs to be multiplied with the corrected - for the mixing efficiency - required mass flow $\dot{m}_{corr}$. This mass flow follows from dividing the required mass flow by the mixing efficiency of $\eta_{\text{mix}} = 0.53$ calculated in section 10.6.

$$S = \left(\frac{S}{\dot{m}}\right)\dot{m}_{corr} = \left(\frac{S}{\dot{m}}\right)\frac{\dot{m}_{req}}{\eta_{\text{mix}}} \tag{10.52}$$

The required mass flow follows directly from the calculations performed in section 10.1. In this section however the required mass flow increase is related to the efficiency increase in the optimal direction, whereas it should be related to the overall wind farm efficiency increase.

$$\Delta\eta_{\text{wf}} = \Delta\eta_{\text{optimal}} \cdot \prod c_{\text{correction factors}} = \Delta\eta_{\text{optimal}} \cdot c_{\text{winddir.}} \cdot c_{\text{power rating}} = 0.53\Delta\eta_{\text{optimal}} \tag{10.53}$$

For clarification purposes, an example calculation is performed with the equations. It was calculated in section 10.1 that for an optimal wind farm efficiency increase of 3%, a mass flow of approximately $\Delta\dot{m} = 978$ [kg/s] needs to be added. Note that the corresponding real wind farm efficiency increase is much lower according to equation (10.53). This equation gives $\Delta\eta_{\text{wf}} = 0.53 \cdot 3 = 1.59\%$.

The corresponding required surface area follows from equation (10.52). Inserting the calculated mass flow requirement into this equation yields $S = \left(\frac{S}{\dot{m}}\right)\frac{\dot{m}_{req}}{\eta_{\text{mix}}} = 0.027 \cdot \frac{978}{0.53} = 50$ [m^2].

With the surface area of the kite known the dimensions of the kite can easily be calculated. Equation (10.54) gives the relationship between the aspect ratio (which is a known input), surface area and span of the kite. When the span is known, the chord follows directly from $c = b/AR$. Doing this with the calculated surface area yields $b = \sqrt{2 \cdot 50} = 10$ [m] and $c = 10/2 = 5$ [m]. Note that this are not the final dimensions of the kite, but dimensions that follows from the example calculation presented in this chapter. In chapter 11 the final dimensions will be determined.

$$AR = \frac{b^2}{S} \Rightarrow b = \sqrt{AR \cdot S} \tag{10.54}$$

The dimensions calculated with the equations above are based on the kite's lift coefficient $C_L = 1.1$. For this lift coefficient the projected surface area is used as reference area [29]. Therefore, the dimensions calculated with the above equations are the projected dimensions of the kite (see also figure 10.17).

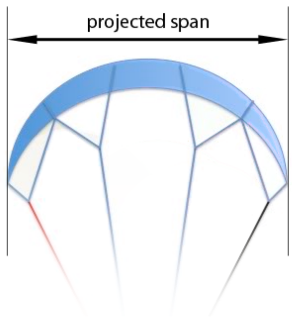

Figure 10.17: Definition of the projected span

Table 10.6: Summary of equations for dimensions calculation

Step	Calculation of:	Guideline, Value or Equation
1	Required velocity increase	Section 10.1.4, equation (10.31)
2	Required mass flow increase	Equation (10.7)
3	Kite height	From section sec:kiteheight; 145 [m]
4	Wind speed at kite height	Equation (10.34); 9.5 [m/s]
5	Wind direction correction	Section 10.4, $c_{\text{wind dir.}} = 0.57$
6	Maximum power correction	Section 10.5, $c_{\text{power rating}} = 0.93$
7	Calculate mixing efficiency	Section 10.6, $\eta_{\text{mix}} = 0.53$
8	Jet expansion correction	Section 10.7, $c_{\text{jet expansion}} = 1$
9	Verify downwash angle	Equation (10.42), $\epsilon = 20$ [deg]
10	Calculate ratio $\frac{S}{\dot{m}}$	Equation (10.51), $\frac{S}{\dot{m}} = 0.027$
11	Calculate surface area	Equation (10.52)
12	Calculate projected span	Equation (10.54)
13	Calculate chord	$c = b/AR$
14	Calculate flat span	Equation (10.55)

For the cost and structural analysis, it is required to know the flat span of the kite. A relationship between the flat and projected span of a bow-kite has been established from analysis of reference kites [29]. This relationship is given with equation (10.55).

$$b_{\text{flat}} = \frac{b_{\text{projected}} + 0.002}{0.8283}; \tag{10.55}$$

For the example calculation, which yielded a projected span of 10 [m] this equation yields $b_{\text{flat}} = \frac{10+0.002}{0.8283} = 12$ [m]. Now finally, with the equations described above, a graph can be made showing the relationship between the wind farm efficiency increase and the dimensions of the kite. This relationship is plotted in figure 10.18. The results of the example calculations are marked with X's.

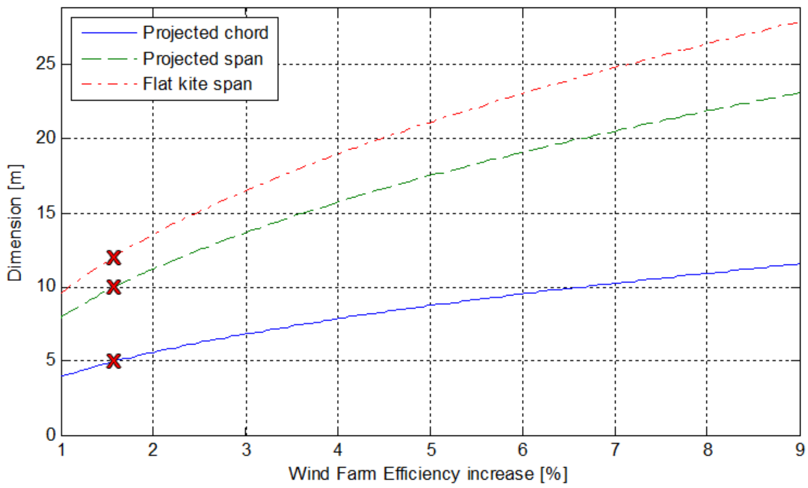

Figure 10.18: Relationship between kite dimensions and wind farm efficiency increase (the X's mark the results of the example calculation)

It is easy to lose track over the different calculations made in this chapter. Therefore table 10.6 is supplied to summarize all equations used for calculation of figure 10.18.
With figure 10.18 and performance, costs and structural limits, in section 11.1 the design space is defined, and then in section 11.2 the final dimensions of the kite are fixed.

10.9 Variable wind speed

In section 10.1 it was explained that the wind speed does not stay constant all the time. Figure 10.2 shows the Weibull distribution of the wind speed at hub height. Furthermore in section 10.5 it was explained that the power output is directly related to the wind speed, when the wind speed is below the rated speed of the wind turbines. However in this chapter, the average wind speed was used to calculate the size of the kite. Therefore, in this section it will be checked if also for other wind speeds the desired wind farm efficiency can be achieved.

The steps listed in table 10.6 have been implemented in a Matlab program. This makes it easy to change the input wind speed and see the results. In the following paragraphs, qualitatively the implications of a lower wind speed will be explained.

When the undisturbed wind speed V_1 is decreased, naturally the wind speed in the wake decreases. However, because equation (10.5) is of the form $V_2 = V_1 \cdot f(\eta_{wf})$, with f not dependent on V_1, the ratio between the wind speed in the wake, with and without kite, does not change when the undisturbed wind speed V_1 changes. The absolute value of the velocity deficit decrease does decrease however. Therefore, also the mass flow which needs to be added to the flow decreases.

The wind direction correction and the correction for maximum power are not dependent on the undisturbed wind speed. Furthermore, in this analysis it is assumed that also the mixing efficiency is not dependent on the wind speed. It is however recommended that this is investigated in further research.

The next step dependent on the wind speed is step 6 in table 10.6. However, note that the mass flow depends linearly on the wind speed. Therefore the undisturbed wind speed appears in both sides of equation (10.51) and can be crossed out of the equation, which means that in this simplified analysis the surface area of the kite is not dependent on the wind speed. This can be explained by the following. When the wind speed is decreased the required mass flow to be added decreases, leading to a smaller kite. However, the lift per unit area also decreases because the wind speed over the kite is lower. This leads to a larger kite. From the equations listed in table 10.6 follows that both effects cancel each other out.

From the considerations presented in this section follows that with varying wind speeds, a kite of the same size achieves the same wind farm efficiency increase for all different wind speeds. Therefore, no correction factor needs to be applied to the wind farm efficiency increase to correct for different wind speeds.

10.10 Problems, assumptions and solutions

In this section, all calculation problems regarding the aerodynamics are repeated for clarity. These are structured in difficulties that are worked out fully, these are stated in subsection 10.10.1, and those that could not be worked out fully and therefore are simplified, these are handled in subsection 10.10.2.

10.10.1 Fully worked out difficulties

The following difficulties are worked out completely. With every difficulty, the corresponding section is indicated and a short description is given.

- **Directional performance (Section 10.4):**

  The wind direction will not be the same throughout time. Most times it will be effective; directed such that the downwash generated by the kite arrives at the downstream wind turbines. Sometimes however, it will be ineffective; directed such that the generated downwash does not reach any downstream wind turbines.

  Therefore, a correction is implemented. This correction enlarges the kite in such a way that it will have a larger effect during its effective operation, which is the case when the wind direction is effective. This larger effect accounts for the times in which the wind direction is ineffective.

- **Power correction (Section 10.5):**

  The wind turbines will not output more than 3MW when the wind speed increases above the rated velocity of 15 [m/s]. This reduces the time the efficiency can be increased, because sometimes an increase in wind speed will not lead to a larger power output. This problem is tackled in section 10.5 with a correction factor.

- **Jet expansion correction (Section 10.7):**

  The downwash 'jet' spreads out downstream behind the kite. In section 10.7 it was found that it does not increase beyond the wind turbine diameter, hence no correction factor needs to be applied for this problem.

- **Decreasing marginal utility (Section 10.7):**

  When an enormous mass flow would be bend down, in the order of the mass flow through the wind turbine, a very large amount of air will diverge from its original path through the downstream wind turbine, as indicated by figure 10.14. The big arrow in the figure indicates a (very) large downwash, whereas the smaller arrow indicates the lost mass flow bended away from the rotor blade disk. A larger kite would lead to more losses and therefore the efficiency increase would eventually reach a maximum.

  This problem, imposing decreasing marginal utility, occurs for very large added mass flows only; as stated before, mass flows in the order of the mass flow through the complete wind turbine rotor disk. The mass flow bend down by the kite is 40 times smaller than that flowing through the rotor disk. Therefore it is assumed that decreasing marginal utility is not dominant, and therefore to be neglected, for the device.

10.10.2 Simplified difficulties

The following difficulties could not be worked out fully, therefore they are simplified. It has to be emphasized that all these simplifications are dealt with using either a wind tunnel test or a CFD model. More on this can be found in chapter 26. Again, with every difficulty the corresponding section is indicated.

- **Local wind profile effects (Section: 10.3):**

  The wind profile, as explained in section 10.3, causes a difference in wind speed on different heights. Therefore, along the rotor blades of a wind turbine a velocity difference is present too, locally. This local effect of the wind profile is neglected in this analysis and the velocity along the wind turbine rotor is taken equal to the average airspeed.

- **Laminar versus turbulent mixing efficiency (Section 10.6):**

  The downwash generated by the kite, flows into the wake of the upstream wind turbine. The interaction of the flows is approximated using wind tunnel experiment results [22] [23]. In the wind tunnel experiments, the flows directed onto each other are laminar. The downwash and the wake flows are however both turbulent. The only way to investigate this situation intensively, is to do a new wind tunnel experiment or use a CFD model. In chapter 26 more is explained on possible methods for further research on this.

  From qualitative analysis it is known that turbulent flows have better mixing properties. Therefore, it is assumed that the performance of the kite will only improve relative to the current analysis; using laminar flows [24].

- **Mixing downwash with vortices and coherent structures (Section 10.6):**

  The upstream wind turbine blades move through the flow. Therefore, the blades firstly generate tip vortices just like wings, which subsequently follow the flow direction and the rotation of the blades, forming helices (or coherent structures), behind the wind turbine.

  This combination of vortices and helices forms a stable flow pattern for wings of aircraft [30] [31]. For wind turbines, these patterns are less stable, yielding a lower effect on the mixing efficiency of the kite. Modelling the vortices and helices is very complex, therefore a wind tunnel test or a CFD model is needed to check whether the effect is negligible, as we assume. See chapter 26 for more information on this.

- **Flow interaction by the kite (Section 10.8):**

  The flow is bend down by the kite to achieve its purpose. To perform this, lift has to be generated by the kite, which yields that the flow is, for example, accelerated above the kite [24] [8].

  Once again, due to the complexity of modelling the latter, its effect is neglected and an average value is used for the flow downstream of the kite.

Chapter 11

Performance

In chapter 10 on aerodynamics, the relationship between the wind farm efficiency increase and the kite's dimensions is given. In this chapter the constraints on the dimensions and efficiency increase are determined, forming a design space. From this design space, together with a cost analysis, the most profitable wind farm efficiency increase and respective kite dimensions will be derived.

This design space is defined in section 11.1. Hereafter, in section 11.2, the final dimensions of the kite are set. When the dimensions of the kite and the wind farm efficiency increase are set, the number of kites required to guarantee this increase is defined in section 11.3. Furthermore the flight envelope parameters of the kite are defined in section 11.4

11.1 Design space definition

Figure 10.18 in chapter 10 presented the relationship between wind farm efficiency increase and kite dimensions. From this plot it is possible to define an infinite amount of different kite configurations. In this section, constraints will be defined on the performance of the kites and on the dimensions. This yields the design space as is presented in figure 11.3, which will be used together with a cost analysis to find the optimum dimensions.

11.1.1 Required performance

The first constraint is the minimum performance set by the clients, requiring a efficiency increase of 3%. The constraint is indicated in figure 11.3 by the vertical line labelled with the number one; it can be seen that the line coincides with the horizontal axis at 3% efficiency increase. Since this is a minimum set by the clients, this is a minimum limit.

11.1.2 Maximum theoretical performance

The second constraint is the maximum theoretical performance. It is assumed that the maximum efficiency is obtained, when the average wind speed through the wind turbine equals the wind speed at the height of the kite.

Using equation (10.23) from section 10.1, equation (11.1) is found. Inserting the velocity at height of the kite, calculated using the wind profile, of $V_{kite} = 9.5$ [m/s] and the velocity $V_1 = 8.9$ [m/s], the velocity of the wake of the wind turbine, yields that the maximum efficiency of the wind farm becomes $\eta_{wf,max} = 1.14$. Therefore, the maximum increase becomes $\Delta\eta_{wf,max} = 114 - 93 = 20\%$

$$\eta_{wf,max} = \frac{1 + \left(\frac{V_{\text{kite}}}{V_1}\right)^3 + \left(\frac{V_{\text{kite}}}{V_1}\right)^3 + \left(\frac{V_{\text{kite}}}{V_1}\right)^3}{4} \tag{11.1}$$

This maximum constraint is not shown in figure 11.3 because for readability the axis system is not extended up to an efficiency increase of 20%. It will be shown in the next section, that other parameters will be more critical for the maximum attainable performance.

11.1.3 Maximum practical performance

The third constraint is the maximum practical performance. This constraint follows from the maximum theoretical performance constraint handled in subsection 11.1.2. However, here all correction factors are taken into account, as given in equation (10.53). Furthermore, it is multiplied with the mixing efficiency. This yields a maximum practical wind farm efficiency increase of 5.8%. This constraint is indicated in figure 11.3 with the line labelled with the number 2. Just like its the maximum theoretical increase, it is a maximum limit within the design space.

11.1.4 Structural limits

From the structural analysis of the kite, performed in chapter 13, the potential limits imposed by the structure on the maximum efficiency increase are looked at. The stresses within the kite, which are the critical parameters, are analysed. It follows that the stresses that occur, for the maximum practical performance, are far below the tensile strength of the used material.

The dimensions of the kite however, do impose a limit on the performance. Figure 11.1 gives a basic schematic of the kite when it is retracted. It is important, when the kite is retracted while the wind turbines are still operating, that the kite is not positioned in the region in front of the next wind turbine rotor disk. Since the kite should not bend flow out of the wake region, lowering the speed in the wake region even further.

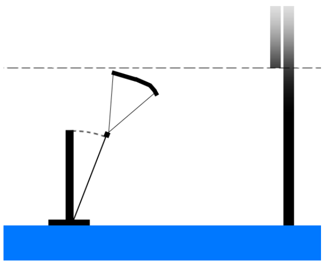

Figure 11.1: Schematic of the structural limit imposed by the tether and bridle system length

For this analysis, it is assumed that the minimum length of the tether, from the buoy to the control pod, equals approximately the length of the mast, to prevent the control pod from hitting the mast or the buoy during sudden gusts. Furthermore, from analysis of reference kites and of the kite layout in section 18.1, it is found that the length of the bridle system from the control pod to the kite has a length of approximately $l_{controlpod->kite} = 1.1c$. It is found in the buoy design that for a kite with a chord length of 8 [m] the mast height equals 11 [m]. For this kite, the length between the control pod and the kite is $1.1 \cdot 8 = 8.8$ [m]. The sum of these becomes 20 [m]. With a safety factor of 1.25 to correct for uncertainty in the length of the kite's cable and angle under which the kite flies; this length is approximately 25 [m]. This is also approximately the distance from sea level to the bottom of the rotor disk. Therefore, a kite with a chord of 8 [m] is considered the largest kite possible.

This limit is shown with line three in figure 11.3, as a constraint on the maximum projected kite span. Note that the span corresponding to a chord of 8 [m] is 16 [m], since the aspect ratio is equal to 2.

11.1.5 Profit distribution

From the cost analysis, performed in chapter 22, a profit distribution as a function of wind farm efficiency increase is derived. It is assumed that with varying kite dimensions, only the buoy and kite costs vary - and thus also maintenance costs. The corresponding cost equations are given with equation (11.2).

$$\left.\begin{array}{l} P_{buoy} = 11633e^{0.0881b_{flat}} \\ P_{kite} = 1370.9b_{flat}^{0.4687} \\ P_{maint.\,kite} = (t_{life}/t_{maint.\,cycle} - 1)P_{kite} \end{array}\right\} P_{var} = P_{buoy} + P_{kite} + P_{maint.kite} \tag{11.2}$$

Furthermore, from chapter 22 the revenue can be calculated. Based on the revenue of €$12.7 \cdot 10^6$ corresponding to a 4.3% wind farm efficiency increase, as calculated in chapter 22, the revenue at different wind farm efficiency increases can be calculated with equation (11.3).

$$\text{revenue} = \frac{\Delta\eta_{wf}}{4.3} 12.7 \cdot 10^6 \tag{11.3}$$

Subtracting the total variable costs from the revenue, yields a measure for the total costs of the system, related to the wind farm efficiency increase. Note, that it is not the real revenue, because kite dimension independent costs are not taken into account. Figure 11.2 shows the result, divided by the measure for the return on investment at 9% wind farm efficiency increase, to get a dimensionless measure. As can be seen in this figure, it is desirable to increase the wind farm efficiency as much as possible to achieve the largest ROI.

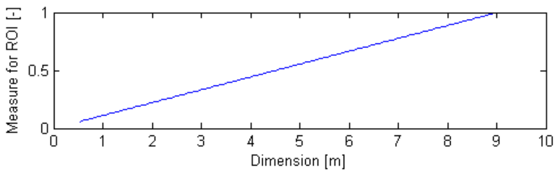

Figure 11.2: Measure for return on investment at different $\Delta\eta_{wf}$

11.1.6 Final design space

By combining all constraints and the relation between the wind farm efficiency and the kite dimensions, as derived in chapter 10, figure 11.3 is plotted.

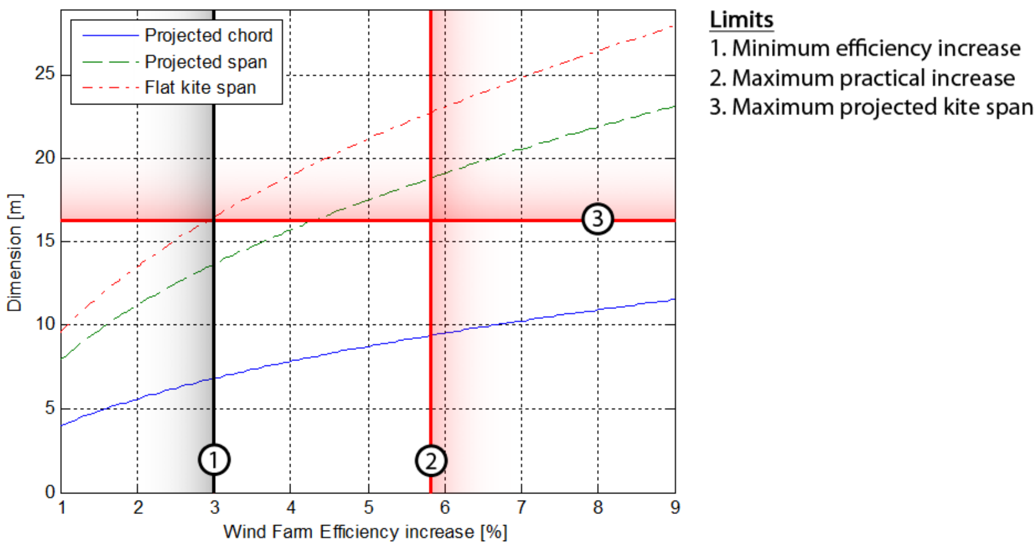

Figure 11.3: Final design space

It can be seen in figure 11.3 that the following constraints are the determining factors for the kite dimensions. Since they enclose - when they form a minimum or maximum limit - the only possible space from which the kite can be designed:

1. Required minimum performance
2. Maximum practical performance
3. Maximum kite span

The lines corresponding to the constraints listed above, form the final design space. With this design space, the final kite dimensions are determined in the following section (11.2).

11.2 Dimensions definition

In the previous section, the final design space is defined. Within the final design space, all possible kite dimensions can be found. However, an optimization is done to find the best set of kite dimensions. As explained in section 11.1.5, the efficiency increase should be maximized to guarantee maximum ROI. Therefore, the maximum dimensions and efficiency increase follow as shown in figure 11.4 from the first maximum constraint. Figure 11.4 shows that this constraint is the constraint imposed by structural considerations. It has to be noted that the particular constraint is an indication for the maximum *projected* span only, not for the flat span.

As can be seen in figure 11.4, a wind farm efficiency increase of 4.3% will be obtained with the kite. The final dimensions of the kite are summarized in table 11.1.

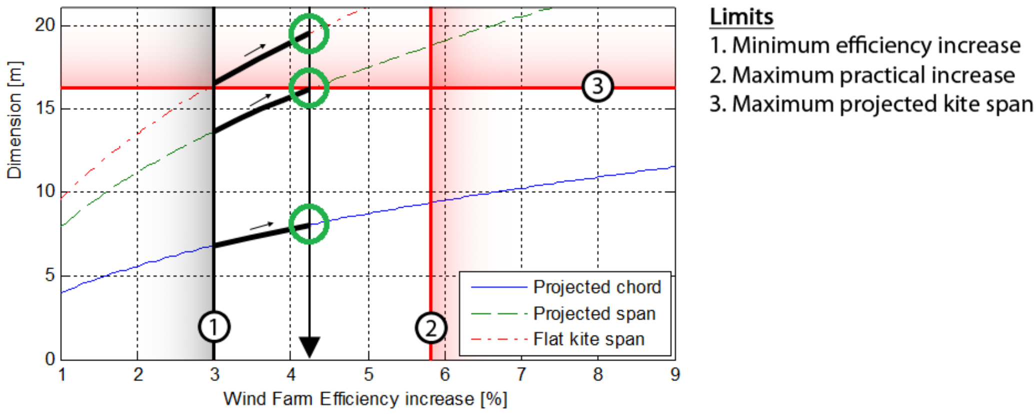

Figure 11.4: Final design space, with final kite dimensions and efficiency increase

Table 11.1: Kite parameters

Parameter	Value	Unit
Wind farm efficiency increase	4.3	%
Projected span	16	m
Flat span	19	m
Chord length	8	m
Aspect ratio	2	-
(Projected) surface area	128	m^2

11.3 Number of kites

The exact number of kites in the wind farm has not been defined yet. In section 10.4 on the wind direction correction, a correction factor was estimated to correct for different wind directions. The kites are required to be positioned such that when the wind blows from the directions defined in section 10.4, each wind turbine in the wake region in the wind farm is aligned with a kite that increases its power output.

Analysis of the OWEZ wind farm shown in figure 11.5 shows that to guarantee this, at least one kite should be placed in the centre of a sub-grid of four wind turbines. Furthermore, kites should only be placed on locations that are in the wake region of the wind farm—when the wind blows from one of the six chosen wind directions. No kites are required outside the wind farm, because these will never be in the wake region. This implies that there are a minimum of 23 kites required, as shown in figure 11.3.

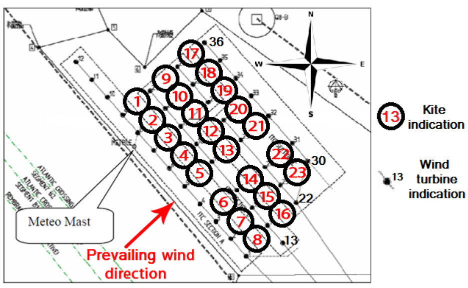

Figure 11.5: Locations of the kites

11.4 Flight envelope parameters

This section is a small sidestep from the aerodynamics and performance calculations. It will be approximated how many times a day the kite should be retracted and will endure extreme weather conditions is terms of wind speed. This follows from the stall speed and the maximum airspeed, which will also be calculated in this section. These parameters are not directly required for the dimensions calculation of the kite, but are required in other chapters of this report and are therefore presented here.

In subsection 11.4.1, the stall speed is handled, where in subsection 11.4.2 the maximum airspeed and therefore the performance ceiling is handled.

11.4.1 Stall speed

The stall speed follows directly from equation (11.4) [24].

$$L = W = C_L \frac{1}{2}\rho V_{stall}^2 S \implies V_{stall} = \sqrt{\frac{W}{S}\frac{2}{\rho}\frac{1}{C_L}} \tag{11.4}$$

From section 13.1.1 follows that the kite and control pod weight is in total 81 [kg]. Furthermore, in section 13.1.3 it was shows that the tether weight is approximately 10 [kg]. This means the total mass the kite has to keep up in the air is $10 + 81 = 91$ [kg].

The lift coefficient of the kite is $C_L = 1.1$, as was explained in chapter 10. Furthermore, in section 11.2 it was set that the surface area is 128 [m^2]. Inserting these values, together with the air density $\rho = 1.225$ [kg/m^3] at sea level, yields that $V_{stall} \approx 3.2$ [m/s]. It is however not desirable to fly the kite at 3.2 [m/s]. The wind turbines cut-in at 4 [m/s]. For safety, it is chosen to already retract the kite at this airspeed.

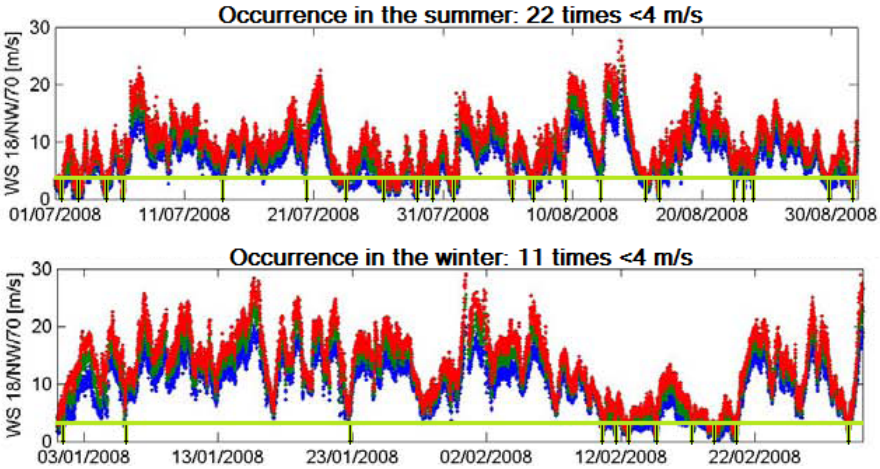

Figure 11.6: Frequency of occurence of $V_{wind} < 4$ [m/s]

Figure 11.6 shows how many times wind speeds smaller than 4 [m/s] occurred in the period of two months in the summer [21]. As can be seen, this occurs approximately 22 times in two months. This implies approximately once every three days. Furthermore, in the winter wind speeds lower than 4 [m/s] only occur 11 times in two months. This implies once every 6 days.

In conclusion, in the summer the kite is retracted most of the time. It needs to be able to be retracted approximately once every three days.

11.4.2 Performance ceiling

Analysing the OWEZ reports [21], it follows that the highest occurring wind speed on hub height (70 [m]) on the location of OWEZ is 26 [m/s]. Therefore, this is taken as the maximum speed that will occur at that specific height. Because this speed is the maximum, the extreme loads that will act on the kite can be calculated. This is explained in this subsection.

In figure 11.7, the wind speed versus time is stated for a period of 2 months in the summer, in the upper plot, and in the winter, in the lower plot. From these plots, the number of times the wind speed reaches 26 [m/s] is counted. In the summer, it occurs 1 time over a time period of 2 months, yielding that an airspeed of 26 [m/s] occurs once in 62 days. In the winter it occurs slightly more often: 6 times in a period of 2 months, yielding that it occurs once in 11 days.

It has to be noted, that this speed occurs at a height of the hub. Therefore, the wind profile, explained in section 10.3, has to be considered to determine the airspeed at the height of the kite. Below, in figure 11.8, the wind profile distribution is shown, calculated with equation (10.34) using a surface roughness z_0 equal to 0.0002, for the airspeed equal to 26 [m/s] at 70 [m], which is the hub height.

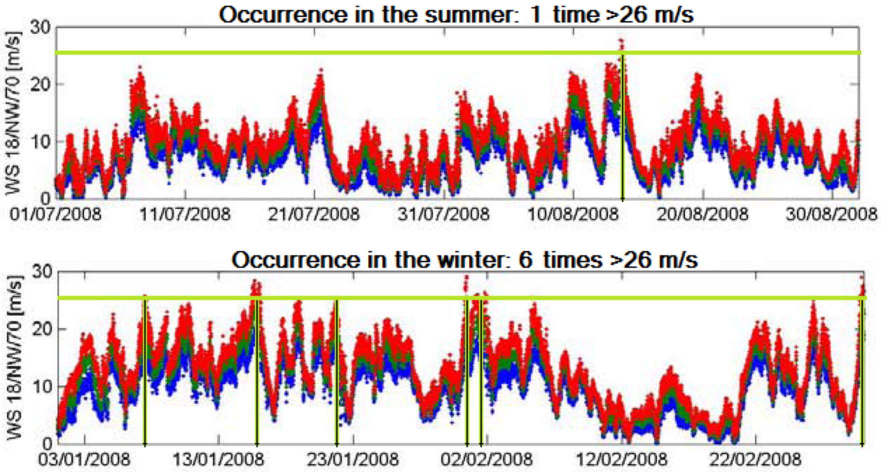

Figure 11.7: Frequency of occurence of $V_{wind} > 26$ [m/s] at the height of the hub

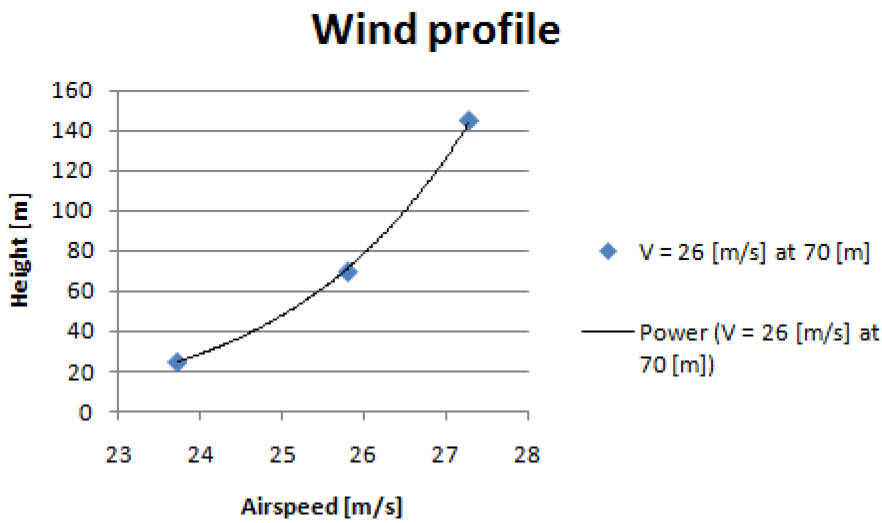

Figure 11.8: Wind profile calculation for $V_{wind} = 26$ [m/s] at hub height

In figure 11.8, the airspeed is indicated at the height of the kite, when the airspeed is 26 [m/s] at the hub height. This airspeed is equal to 27.3 [m/s], which is the maximal airspeed the kite will endure. Filling in this speed in equation (11.4), the extreme lift and drag forces are determined. Using the surface area of the kite, the wing loading is found. The results are stated in table 11.2 below:

Table 11.2: Extreme force on the kite

Parameter	Value	Unit
Extreme lift	65	kN
Extreme wing loading	500	N/m^2
Extreme drag	13	kN

In section 5.4 in chapter 5 is explained that the kite will be retracted in cases of high wind speeds. This will be done at airspeeds of 26 [m/s] at hub height. It can be seen in figure 11.8, that the airspeed under the wake of the wind turbine is considerably lower, in the order of 24 [m/s]. Therefore, for safety reasons, the kites are retracted beneath the wake of the wind turbine, when airspeeds equal to 26 [m/s] or higher are predicted at hub height.

Chapter 12

Stability and Control

This chapter first deals with a basic explanation on the set-up of the control and stability system for the kite in section 12.1. Hereafter the control aspects for the kite are explained further in 12.2 and the stability of the kite will be drawn in 12.3. Summing up, a conclusion will be drawn at the end of kite part. Thereafter, in section 12.4, the stability of the buoy is handled.

12.1 Layout Control System

The basic layout of the control system can be seen in figure 12.1. In the upper part the kite can be seen. It can be seen that a bow kite is used. Bow kites are leading edge inflatable kites which consist of a bridle system on the leading edge. In general they can be described by a flat, swept-back profile with a concave trailing edge [32].

In the lower part the bridle system can be seen. The bridle system is the term for the set of four kite lines just below the kite itself. The four kite lines go down further towards the control pod. The control line is responsible for the control movements of the kite, the power lines are static and are used for depowering the kite.

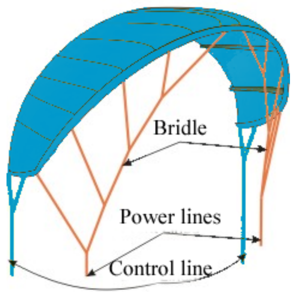

Figure 12.1: Control and Stability Setup

The control pod is a cylinder shaped nacelle in which the ACS station is implemented. Furthermore there are two electric engines for actuation, a winch and a fixed pulley. The winch is connected to one of the engines for retracting and releasing the lines in order to power and de-power the kite. The pulley is used to steer the kite. The control pod will be explained further in detail in section 12.2.2.

12.2 Control Set-up

The control set-up is explained in two ways. First the theoretical approach is outlined, hereafter the practical set-up is explained.

12.2.1 Theoretical Control Set-up

In order to analyse the kite control system further the basic theoretical equations need to be set-up. From these derivations a simulation will be set-up in order to verify the control system.

In order to describe the behaviour of the kite, first a reference system needs to be set-up. First of all a fixed Cartesian coordinate system with X, Y and Z coordinates is chosen, which can also be seen in figure 12.2. The X vector is set-up in such a way that it aligns with the wind velocity. Hereafter a second Cartesian coordinate system ($X^{'}$,$Y^{'}$,$Z^{'}$) is used which is centred at the kite steering unit [33]. This coordinate system accounts for motions with respect to the kite steering unit. For the displayed system it is possible to indicate the kites position as a function of the distance r from the origin (the buoy) and angles θ and ϕ. Further in figure 12.2 the basis vector for that can be seen (e_θ, e_ϕ, e_r) [34].

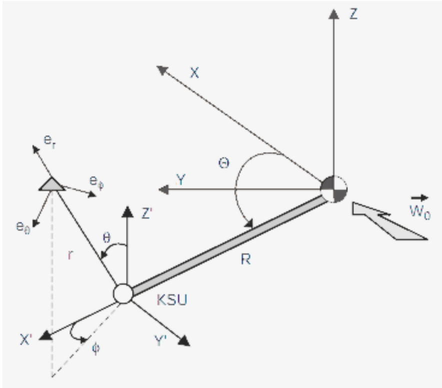

Figure 12.2: Kite Reference System

After setting up the basic parameters, it is now possible to apply Newtons second law for the local coordinate system.[35] This yields:

$$\ddot{\theta} = \frac{F_\theta}{mr} \tag{12.1}$$

$$\ddot{\phi} = \frac{F_\phi}{mrsin\theta} \tag{12.2}$$

$$\ddot{r} = \frac{F_r}{m} \tag{12.3}$$

With the basic reference system and governing equations set-up, it is now possible to use a control system that stabilizes the kite. For the scope of this project it was decided to sketch the basic control pattern in a flow chart to give an overview on how the control system should behave. For the actual control system one can make use of an off-the-shelf control system. After being in contact with Skysails and Kitepower it becomes clear that the development of an auto-pilot from scratch would yield costs in between €200,000 and €750,000. However it was recommended to use an existing auto-pilot and change the parameters for our model. This should lower development costs significantly. Also the total costs of the autopilot are reduced significantly since the development costs are the major contributor. Estimates reach between €3,000 and €5,000 for the autopilot and control system. However this remains an estimate, therefore an uncertainty margin is implemented in the later cost calculation.

12.2.2 Practical Control Set-up

The control system should enable the kite to create as much lift as possible while maintaining a safe and controllable position in the air. In contrast to energy generating kites which have the goal of creating a large tether force by performing an 8-shape flight path, this kite should be stable in the air.

The control system is displayed in figure 12.3. The basic layout of control pod consists of one fixed control pulley (4) and one winch (3). The fixed control pulley is used for rolling and yawing movements of the kite by rotating clockwise and counter clockwise around its axis with a line. By retracting and releasing the tether using the winch, the pitch angle of the kite can be controlled. There are two extra movable pulleys (1 and 2) used outside the control pod in order to combine pitching, rolling and yawing movements in the system. Furthermore, there are total four separate lines used in the system, two of them are used to connect the movable pulleys to the kite. One line is used to connect all the pulleys. It further needs to be noticed that flat cables are used, in order to operate smoother.

In the extreme conditions the kite generates 65 [kN], assume that the power lines (the bridle lines at the middle of the leading edge) resist as much force as the control lines (bridle lines at the outer leading edge). The total force for the trailing edge will be 32.5 [kN] ,and there are in total two control lines, which means each control line should able to withstand a force of 16.1 [kN].

The last line is used to connect the previous line to the winch. The connection between the lines will be one meter right above the winch and will be a knot, so the lines cannot move independently. The system can also be seen in figure 12.4.

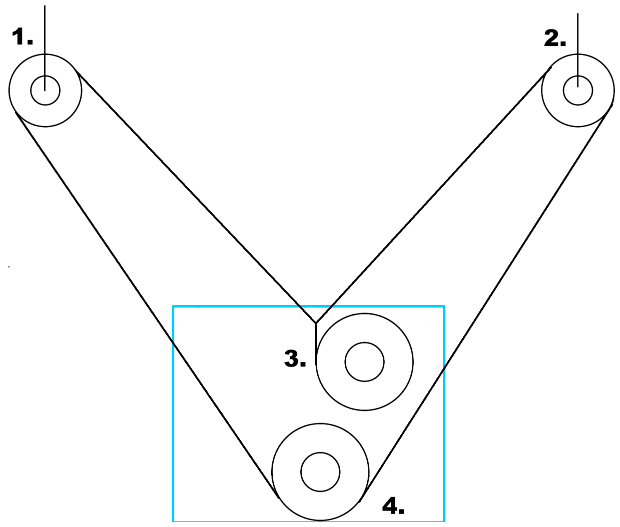

Figure 12.3: Schematic Control Pod Layout

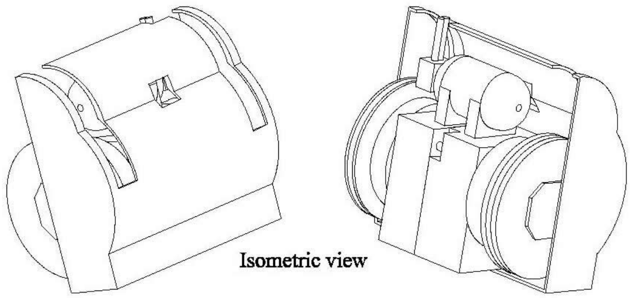

Figure 12.4: Catia Sketch of Control Pod

As stated earlier, the fixed control pulley is used for rolling and yawing motions of the kite. By rotating the fixed control pulley clockwise, the line will rotate from right to the left, a force will be generated to put the right movable pulley down, so does the right part of the kite. This results in a roll motion to the right due to less lift generated on the right part with respect to the left part of the kite. For rolling motion to the left, the fixed control pulley needs to rotate counter clockwise. However this is only possible when the winch is clamped. In order to change the pitch angle, the winch needs to be rotatable. When the winch is retracting the line, a force will be generated to put the movable pulleys down hence the trailing edge of the kite will go down as well. As result the pitch angle increases. To decrease the pitch angle, the winch needs to release the line, so the movable pulleys move upwards.

Furthermore the current position of the kite can be measured in a Cartesian coordinate system. The measurement of the kite position can be done via the Shadowbox GPS receiver [36]. The Receiver uses the following sensors:

- 3-Axes Gyroscopes: It measures the angular velocity (spin rate) and is used to calculate the rotation angles around the X, Y and Z axis.
- GPS module: The GPS unit uses the GPS network to give a low frequency measurement of position and velocity. It also helps to to determine speed, location elevation and the movement pathway.
- 3-axis High G Accelerometer: It measures the acceleration which is used to calculate velocity and position on a much finer scale then the GPS. It is also used to track the gravity vector to get a low frequency measurement of pitch and roll angles.
- 3-axis Low G Accelerometer: Same as above, just more accurate for low-impact movements.
- 1 Barometric Pressure Sensor: It is used to determine small changes in altitude.
- 3-Axis Magnetometers: It measures the earth‘s magnetic field to determine compass heading (Z-axis angle)
- 1 Temperature Sensor: It is used to calculate the air density which is used to translate the atmospheric pressure into an altitude measurement.

The position is not directly calculated from the GPS but instead actually calculated using the inertial data from the accelerometer and gyroscope that are built-in and then corrected using a Kalman filter and the GPS data to account for drift over time. Various tracking programs exist which show the location of the kite and also measures the speed in various directions [37]. Such a typical profile for a kite can be seen in figure 12.5 [38]. The system can also be used to analyse the behaviour of the kite for a prototype.

The GPS unit in mounted on the op of the kite and receives energy from the line that also leads to the pressure regulation system. The GPS unit then sends the signals to the control pod which monitors the kite movements and can counteract in non-intended movements. Also the information about the wind speed and wind direction are transmitted to the control pod. The auto pilot uses all these information in order to keep the kite in the correct position.

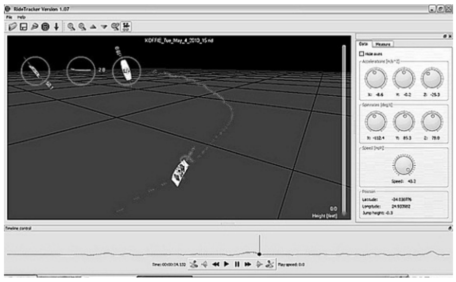

Figure 12.5: Kite GPS Control

12.3 Stability of the Kite

Stability of the kite is essential for its performance. The bow kite is slightly unstable, however the stability of the kite can be improved by using the stabilisation software which keeps the kite continuously stable by using the control system. The stabilisation software is already developed by the ASSET.

There are several criteria for the kites position. First of all the correct pitch angle needs to be set by the control system. Furthermore the correct location in X and Y direction need to be defined. The correct X and Y direction follows from the wind direction. As seen in figure 12.6 the needed location in X and Y direction can be determined from solving the interception of a circle and a line.

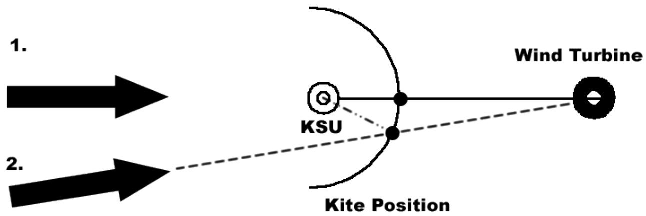

Figure 12.6: Influence of Wind direction

The circle is fixed at the location of the Kite Steering Unit (KSU) with the radius of the kite line. The line has the slope of the wind in the x-y plane with the y intercept at the wind turbine. The system has its origin at the location of the wind turbine. Obviously the solution would yield two results, thus the valid area needs to be defined. The entire system can be solved in Matlab using:

$$[xout, yout] = linecirc(w_{vector}, c, x, y, r) \tag{12.4}$$

Here w_{vector} is the slope of the wind in X and Y direction, c is the y intercept, x is the center of the KSU in x direction, y is the distance of the KSU in y direction and r the radius of the kite line. Based upon the x and y direction the correct height can then also be calculated so that the wind, that is led downwards, reaches the turbine. Furthermore it needs to be noted that the kite can only operate in a range of 30 degrees around the ideal position. Based upon these angles the aerodynamic calculations have been performed. It was estimated that angles beyond the 15 degree angle will lead to a kite position that is far to lean, thus an estimate on the flow behaviour will be difficult.

Using these calculations for the x, y and z coordinates one can feed the control system which consists of the actuators and the retraction system. These inputs can be seen in figure 12.8. The control diagram consists of an inner and out loop. The inner loop consists of the correction for the x and y coordinates using the actuator system. The outer loop is used to reach the correct height using the retraction system. It was chosen to use the inner loop to be the update of the X and Y coordinate since the position needs to be updated more frequently.

The kite can be made stable by using the stabilisation software through the control system, hence the optimal performance can be achieved. When looking at the reference frames, it becomes obvious that there are several models available which can be used for simulation of the behaviour of the kite system [39]. A further analysis can be implemented in order to compare the accuracy of the various models. Furthermore it is recommended to prepare extra wind tunnel testing for the case that the kite position reaches angles beyond 15 degrees. The behaviour of the flow on the wind turbine needs to be further researched.

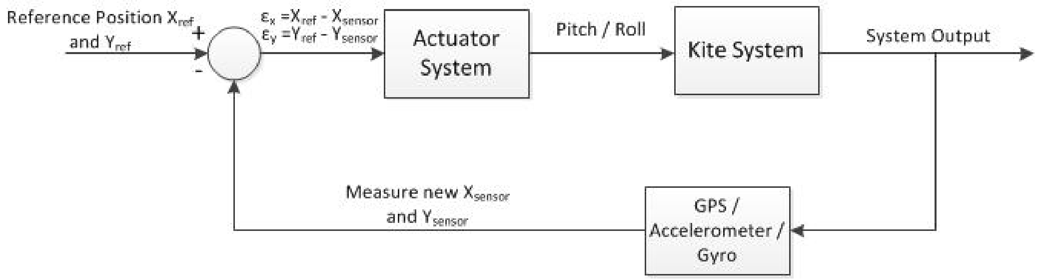

Figure 12.7: Control Flow Actuator

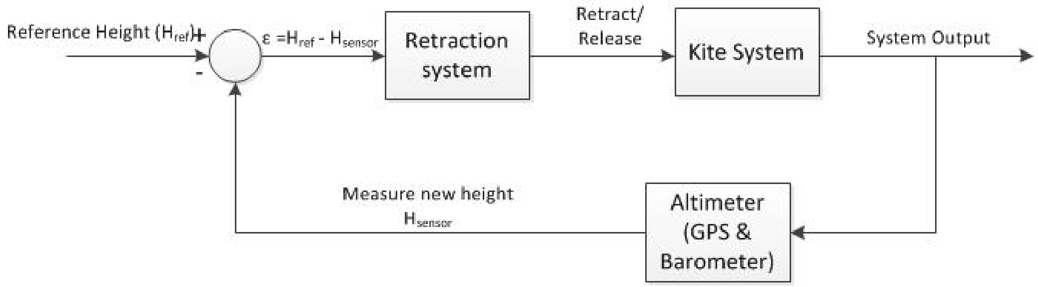

Figure 12.8: Control flow Retraction

12.4 Stability of the buoy

In this section of the report, the stability of the buoy will be discussed. The buoy is subject to more and larger forces than any traditional buoy. An example is the tether force which has a tendency to lift the buoy out of the water. This causes the need for a anchor which was discussed in section 14.4.

In this section, first an explanation of the buoyancy force, and its relationship to the weight under a disturbance, will be discussed in section 12.4.1. Finally the resultant stability will be discussed in section 12.4.2.

12.4.1 Centre of buoyancy

In floating vessels such as ships and buoys, stability is an important design aspect. One important design parameter follows from the centre of buoyancy. A floating object is stable if it tends to restore itself to an equilibrium position after a small disturbance. This depends on the centre of buoyancy, where the resultant buoyancy force acts through [40].

According to the famous principle of Archimedes, "'Any object, wholly or partially immersed in a fluid, is buoyed up by a force equal to the weight of the fluid displaced by the object"' [41]. In other words, the buoyancy force is an upward acting force exerted by the water. This force is proportional to the volume of the submerged part of the buoy. This volume times the density of water $\rho_{water} = 1000$ $[Kg/m^3]$, and the gravity constant $g = 9.81$ $[m/s^2]$ leads to the buoyancy force [N].

Vertical stability is present in most floating objects, aswell as for the Daeolus buoy. For example, if the buoy is pushed down, the added submerged volume will create a greater buoyancy force, which, unbalanced by the weight force, will push the object back up. Rotational stability is a less trivial aspect, but is of great importance. Given an angular displacement, the buoy may return to its original position (stable), move away from its original position (unstable), or remain where it is (neutral) [42]. Rotational stability depends on the relative lines of action of forces on the buoy. The upward buoyancy force acts through the Centre of Buoyancy (CB), being the centroid of the displaced volume of fluid. The weight force of the buoy acts through its centre of gravity. A buoyant object will be stable if the center of gravity is beneath the center of buoyancy, since any angular displacement will produce a corrective moment, forcing the buoy to its initial position [43]. However, the Daeolus buoy has a CG which is located above the CB. In this configuration, the buoy may still be stable. This can be explained by the location of the metacentre.

When the buoy is banked, or 'heeled' in maritime jargon, the centre of buoyancy of the buoy moves laterally. When the buoy is heeled, for example in a clockwise direction, the submerged volume of the buoy is not symmetric as can be seen to the right in figure 12.9. The intersection of a vertical line through the heeled centre of buoyancy, crosses the line through the original vertical centre of buoyancy, this is the location of the metacentre [43]. If the metacentre is located to the right of the centre of gravity (with a clockwise heel), a corrective moment will appear. This is analogous to the aforementioned situation where the CG is located below the CB.

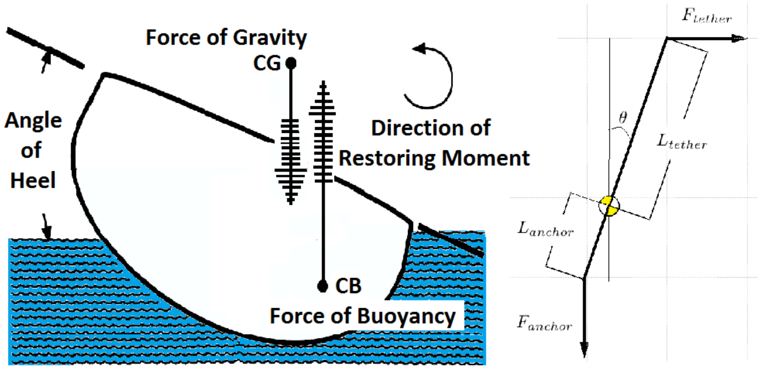

Figure 12.9: Visualisation of the displacement of the centre of buoyancy, and associated metacentre

Thus, for the buoy to be stable, the horizontal distance between the CB and CG must be such that $CB > CG$. This distance is also called the righting arm, a larger righting arm will lead to a stiffer but more stable design. While, when this distance is reversed, a moment is created which will add up to the disturbance.

Using a CATIA model for the buoy, a very precise calculation can be made to determine this horizontal distance between the CG and CB.

Table 12.1: Righting arms for different angles of heel

Righting arms [mm]		
Angle of heel	CB	CG
0^o	0	0
5^o	325	305
10^o	630	605
15^o	980	905

As can be seen from table 12.1, the buoy is in fact stable since $CB > CG$. There will also be a tether and anchor force. These forces will be much larger in magnitude and will be the most important factors in terms of stability. In case these connections are not present, for example when both cables are not connected, the buoy will still be stable.

12.4.2 Anchor and tether force

As determined in section 14.4, the chain weight will lie between 65 [kN] and 215 [kN]. This force will counteract the maximum tether force of 65 [kN] easily, when the main tether is used for load transferring. This is due to the larger moment arm for the anchor, $L_{anchor} = 3.5$ [m] when compared to the moment arm for the winch, $L_{winch} = 1$ [m]. However, when the main tether breaks, this is not so obvious. Therefore, a moment equation should be made for the extreme condition, where the tether force 65 [kN] is acting through the leading edge tether at the top op the mast.

From the FBD indicated in the right of figure 12.9, the equilibrium heel angle can be determined.

$$F_{anchor}L_{anchor} \cdot \sin\theta - F_{tether}L_{tether} \cdot \cos\theta = 0 \tag{12.5}$$
$$215000 \cdot 3.5 \sin\theta - 65000 \cdot 8.5 \cos\theta = 0 \tag{12.6}$$
$$\theta = 39^o \tag{12.7}$$

As can be seen from equation 12.7, the anchor force with corresponding arm length, will produce a larger moment than the tether force at an heel angle larger than 39^o. This will create a corrective moment for the angle of heel. Thus, for the extreme condition, in which the main tether breaks during 27.3 [m/s] wind speed, an equilibrium will be reached at 39^o of heel. And during nominal conditions the tether force is not able to produce a larger moment than the anchor at critical angles of heel.

It should be noted, that the tether force will not be acting in the horizontal direction. In principle the kite will be located at an angle of 10^o as derived from the aerodynamic calculations, this means the angle of heel will never be larger than 10^o during normal operations.

Chapter 13

Aerial segment structures

In this chapter the structural characteristics of the aerial segment are treated. This is done by firstly looking into the structure of the tether and the bridle system in section 13.1. Secondly, the skin of the kite is analysed in section 13.2. Thirdly, the inflatable leading edge is handled in section 13.3.

13.1 Tether and bridle system

The kite stays up in the air because it generates a large lift force which can overcome the kite's weight. Because it obstructs the free stream air flow there also is a drag force. The kite is fixed to the buoy with a tether, which exerts a force on the kite to keep it in a certain position in the air. In this section the tether and bridle system of the kite will be analysed.

To start with the analysis, first the forces on the kite need to be determined. The weight of the kite and control pod is approximated in section 13.1.1. The aerodynamic forces are calculated in 13.1.2. When the total weight, drag and lift force are known, the tether force and geometry can be calculated. This will be done in section 13.1.3.

13.1.1 Weight

The first force to be analysed is the kite's weight. For this preliminary analysis no detailed weight analysis is done for the kite. The weight will be determined from reference kites. Comparing different kites used in the laddermill project [44] a relation can be made to estimate the weight of the kite. It follows that a 25 [m^2] kite (flat area) weighs approximately 11 [kg]. In section 11.2 it was explained that the flat surface area is 152 [m^2] of the kite considered in this analysis. This means the mass of the kite is $11/25 \cdot 152 = 65$ [kg].

For the analysis it is important not only to include the weight of the kite, but also the weight of the control pod; the kite has to keep the pod up in the air. From reference kites it follows that for a small kite with a surface area of 25 [m^2] the control pod weighs approximately 6 [kg] [45]. Note that the reference control pods include a 0.5 [kg] battery [45]. Because the control pod considered here receives its energy through an electrical wire in the tether to the buoy, the battery is not required. Therefore the control pod mass would be approximately 5.5 [kg].

Table 13.1: Kite mass approximation (all values in [kg] unless stated otherwise)

Kite surface area	**25 [m^2]**	**152 [m^2]**
Kite mass (scales with area)	11	67
Battery pack (not present)	0.5	0
Motor system (scales with forces)	1.5	9.1
Other components (do not scale)	4	4
Complete control pod (1.2 safety factor)	6	16
Total mass (control pod + kite)	17	83

It is assumed that the electrical motors and related components, such as the gearboxes, inside the control pod scale with the forces on the kite. Because the lift force scales with the surface area, and all other parameters remain the same, the surface area ratio is used for scaling. The other components - for example the control system - inside the control pod are assumed to remain of the same mass. The mass of the two motors, the motor controllers and gearboxes together is 1.5 [kg] for the 25 [m^2] kite [45]. Scaling this with the surface area yields a $1.5/25 \cdot 152 = 9$ [kg] mass for the Daeolus kite motor system in the control pod. Because the motors will be larger, a safety factor of 1.2 is assumed to correct for added structural weight. Note that the mass of the other components in the control pod of the 25 [m^2] kite is $5.5 - 1.5 = 4$ [kg]. Therefore, the mass of the new control pod for the Daeolus kite becomes $(W_{motorsystem} + W_{other})c_{safety} = (9 + 4) \cdot 1.2 = 16$ [kg]. This means that the ratio between the mass of the control pod of the 25 [m^2] kite and the Daeolus kite becomes $16/6 = 2.7$. For convenience, the calculation of the weight of the kite is summarized in table 13.1.

13.1.2 Aerodynamic forces

In section 10.8 it was explained that the lift coefficient of the kite is $C_L = 1.1$ and the drag coefficient is $C_D = 0.22$. With these coefficients known, the lift and drag forces can be calculated with respectively equations (13.1) and (13.2).

$$L = C_L \frac{1}{2} \rho V^2 S \tag{13.1}$$

$$D = C_D \frac{1}{2} \rho V^2 S \tag{13.2}$$

The lift and drag forces differ with different wind speeds. For this analysis the extreme lift and drag forces will be calculated from the maximum wind speed. In section 11.4 the extreme velocity was explained to be 27.3 [m/s]. Furthermore, the wind speed during nominal conditions is 9.5 [m/s]. For both nominal and extreme conditions the lift and drag forces are calculated and listed in table 13.2.

Table 13.2: Aerodynamic forces on the kite

Nominal conditions (V = 9.5 [m/s])		
Nominal lift	7.5	kN
Wing loading	0.059	kN/m^2
Nominal drag	1.5	kN
Extreme conditions (V = 27.3 [m/s])		
Extreme lift	65	kN
Extreme wing loading	0.5	kN/m^2
Extreme drag	13	kN

With the aerodynamic forces, and the weight of the kite known, the force in the tether can be approximated.

13.1.3 Tether and bridle system forces

Next to the kite, the tether and bridle systems are the main elements of the aerial system. To assess the tether geometry and forces, a finite element method (FEM) analysis is set up. The analysis is very similar to the analysis performed in the conceptual design phase, as presented in the Mid-Term Report. The FEM model is however extended in this detailed design phase. The main additions include that now the electrical wire is included in the tether, the wind profile is taken into account, the control pod is modelled separately and the different cable geometry of the bridle system is taken into account. The implications of these additions will be explained later on in this section.

The tether is modelled as a single line - with an electrical wire in the core and Dyneema around it to carry the forces - from the buoy to the control pod. The bridle system is modelled as a single line from the control pod to the kite. This last part from the control pod to the kite will not contain the electricity cable and will have the special flat shape as explained in chapter 12. Note that the bridle system is modelled by a single line for this analysis. This is done, because one single line of the complete bridle system should be able to carry all the forces, regarding safety measures. Figure 13.1 shows the two different cross sections.

In reality, the bridle system will be much more complex however. Detailed analysis and optimization of the different branches of the bridle system is recommended for a further research topic.

For convenience, the designation 'tether' is used when referring to both the connection between the buoy and the control pod and between the control pod and the kite in this chapter. When a distinction should be made between the two parts, it will be stated explicitly.

In the FEM model, the tether is split up into many small rigid beam elements. Figure 13.2 shows two elements and the forces acting on them. The elements before and after the element apply a horizontal and vertical force, F_x and F_y respectively. Also the (known) weight force dW is present and the element produces lift and drag, dL and dD respectively.

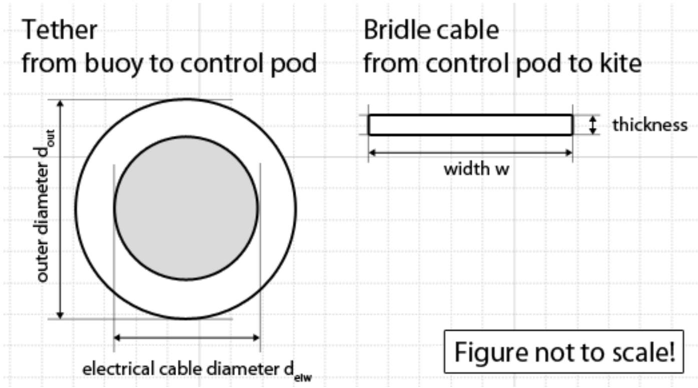

Figure 13.1: Different cross sections of different parts of the tether

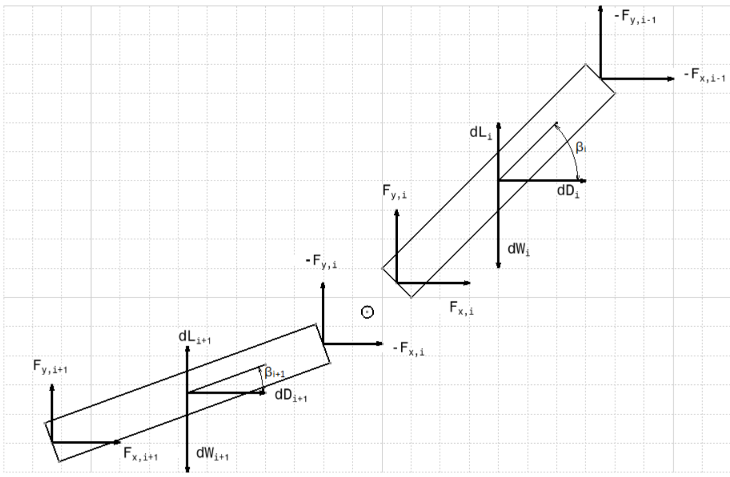

Figure 13.2: Two rigid beam elements and the forces acting on them

The forces acting on the first element, F_x and F_y, to which the kite is attached, follow directly from the weight of the kite and the aerodynamic forces acting on the kite. The horizontal and vertical components of the resultant of the forces acting on the kite are respectively the force components, F_x and F_y, acting on the first element. The direction of the element, the angle β, is equal to the direction of the resultant force which is applied to it by the previous element, since the tether can only exert tensile forces. Once the angle β is known, the aerodynamic forces can be approximated. According to Hoerner [46] the lift and drag forces can be accurately approximated with respectively equations (13.3) to (13.6) [47]. Here ρ is the air density, V is the wind speed, d_t is the tether diameter or width and ds is the element length. The wind speed is calculated with the wind profile equation explained in section 10.3 in the chapter on aerodynamics. Note that this is the undisturbed wind profile. For this analysis the effect of the wake on the cable lift and drag is neglected. Because the wind speed in the wake however will be lower than the undisturbed wind speed, the calculated forces and stresses will be larger than in reality. Therefore, estimations on dimensions and materials will yield a too strong - safe - structure and not a too weak structure.

$$C_L = 1.1\sin^2(\beta)\cos(\beta) \tag{13.3}$$
$$C_D = 1.1\sin^3(\beta) + 0.02 \tag{13.4}$$
$$dL = C_L\frac{1}{2}\rho V^2 d_t ds \tag{13.5}$$
$$dD = C_D\frac{1}{2}\rho V^2 d_t ds \tag{13.6}$$

Now the weight, the aerodynamic forces and the forces applied by the previous element are known, the forces which the current element applies to the next can be calculated using force equilibrium in horizontal and vertical direction. From this the direction of the next element is also found.

This process is iterated until the control pod is reached. The control pod has a mass of approximately 16 [kg], as was explained in section 13.1.1. This leads to a downwards force of $16 \cdot 9.81 = 157$ [N]. Furthermore the control pod will generate lift and drag. Because the lift force will be very small in comparison to the weight of the pod - the control pod is not an aerodynamically shaped object - it is neglected. The drag force is calculated with equation (13.7). The control pod has a very blunt shape. For this analysis it is assumed to be a cube. When the Reynolds number is larger than 10^4, from measurements it follows that the drag coefficient of a cube equals approximately 1.05 [48] when the surface of one side of the cube is taken as reference area. The control pod, modelled as a cube, is assumed to have sides of 0.5 [m]. This is based on reference control pods from the ASSET group at the faculty of Aerospace Engineering of the TU Delft [44]. Note that indeed the Reynolds number is larger than 10^4, because $Re = V \cdot l_{pod}/\nu \approx 10 \cdot 0.5/1.461 \cdot 10^{-5} \approx 9 \cdot 10^5 > 10^4$.

$$D = C_D \frac{1}{2} \rho V^2 S \tag{13.7}$$

The weight and drag of the control pod are added to the next small tether element. Furthermore, the tether geometry and density changed, because now also the electrical wire is embedded in the tether (see also figure 13.1).

When the control pod is added, the forces in the rest of the elements are calculated. This yields the tether geometry as shown in figure 13.3 and the tether force distribution as shown in figure 13.4. For this calculation the average aerodynamic characteristics of the kite concept were used for a wind speed of 9.5 [m/s].

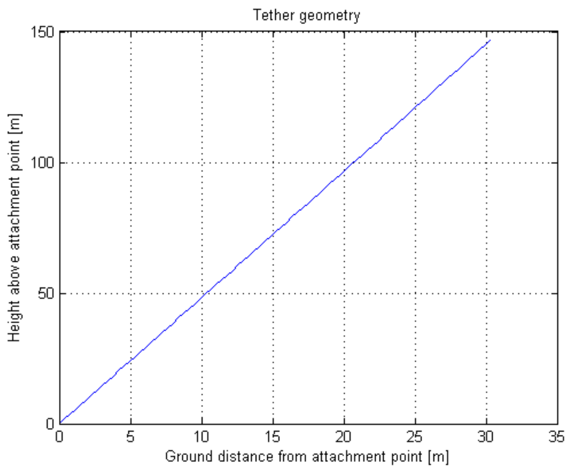

Figure 13.3: The tether geometry (V = V$_{\text{extreme}}$)

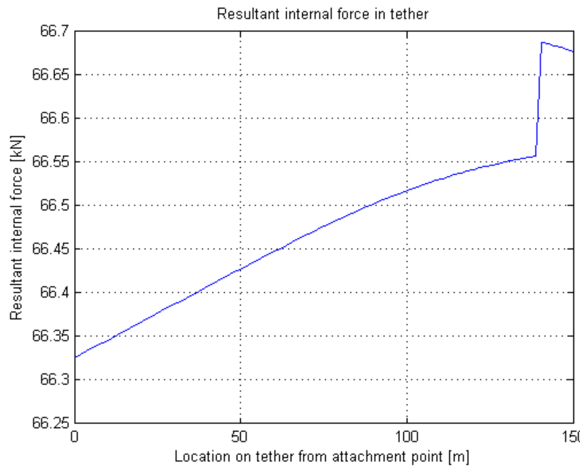

Figure 13.4: The tether force (V = V$_{\text{extreme}}$)

Note that for these calculations, a certain diameter for the electrical cable and the amount of supporting Dyneema needs to be assumed for the first part of the tether (as shown in figure 13.1) and certain dimensions for the second part, the bridle system. When these dimensions are set, the forces can be calculated as explained above and the stresses in the tether and bridle system can be calculated. Most likely the assumed dimensions will not yield an optimal result. Therefore the simulation is done again, with new dimensions. These dimensions are based on the forces calculated with the initially assumed dimensions. From the maximum force in both parts of the tether follows the new surface area of the Dyneema parts of the tether - because only the dyneema will transfer loads - and bridle system as shown in equation (13.8). Here σ_{tensile} designates the tensile strength of Dyneema. Because the Dyneema will not deform substantially elastically or plastically before failing, the tensile strength and not the yield stress is used in these calculations.

$$A_{\text{tether/bridle}} = \frac{F_{\max}}{\sigma_{\text{tensile}}} \tag{13.8}$$

The outer diameter of the tether - the part from the buoy to the control pod - is calculated using equation (13.9) to arrive at (13.10). For this equation the diameter of the electrical wire needs to be known. From Bieber [49], it follows that for an electrical wire between 100-200 [m], which has to supply energy to the control pod (as explained before, approximately 55 [W]), a wire with a diameter of 5 [mm] is sufficient.

$$A_{\text{tether}} = \frac{\pi}{4}(D_{\text{outer}}^2 - D_{\text{ew}}^2) \tag{13.9}$$

$$D_{\text{outer}} = \sqrt{\frac{4A_{\text{tether}}}{\pi} + D_{\text{ew}}^2} \tag{13.10}$$

Lastly, the width of the bridle cable is determined using equation (13.11) to arrive at equation (13.12), using the width to thickness ratio of 4.5 ($w = 4.5t$), which followed from analysis of comparable bridle lines [29].

$$A_{\text{bridle}} = w \cdot t = w \frac{w}{4.5} \tag{13.11}$$

$$w = \sqrt{4.5 A_{\text{bridle}}} \tag{13.12}$$

The new dimensions are inserted into the FEM model, and the maximum forces are again inserted into equation (13.8) and new dimensions are calculated again to close the loop. Note that the forces changed because the cable weight changes when the dimensions are changed. This is done one more time and it is found that the dimensions do not change significantly any more. Now only a safety factor needs to be applied to these dimensions as will be shown.

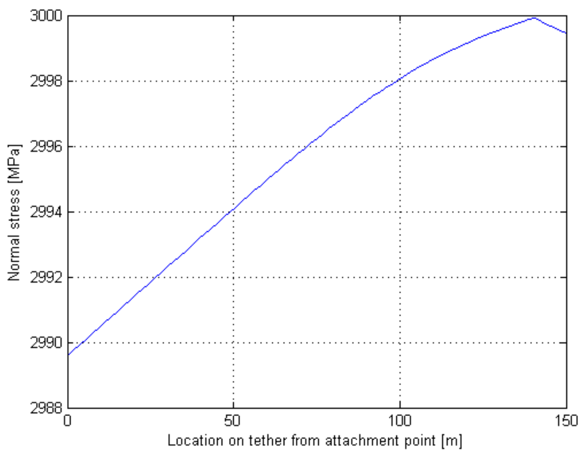

Figure 13.5: Tether normal stress (no safety factor and V = V_{extreme})

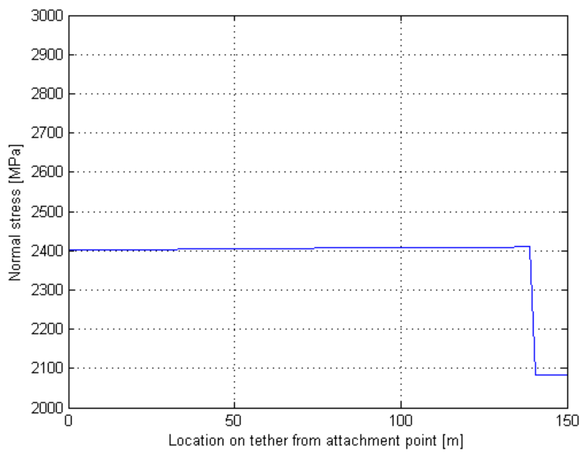

Figure 13.6: Tether normal stress (with safety factor and V = V_{extreme})

Figure 13.5 shows a plot of the stresses in the tether with the dimensions that are found. As can be seen, the maximum stress is exactly the tensile stress of Dyneema; approximately 3000 [MPa], which is as given in chapter 15. This is however not a safe situation, therefore a safety factor of 1.2 is applied to the dimensions. Note that the consequence of the tether failing is catastrophic during nominal operation of the kite, hence it would normally require a higher safety factor. Because the tensile strength of Dyneema however is very high and the manufacturing is relatively straightforward [50] and because an as low as possible tether diameter is desired here, only a safety factor of 1.2 is chosen. Note that with this low safety factor there is little space for inaccuracies in the model. In further development of the tether it is important to verify the accuracy of the model. Furthermore it can be seen that the electrical wire takes up most of the diameter of the tether. This diameter followed from Bieber [49], but needs to be verified in further development and optimization of the tether, because no extensive electrical research is done.

The final tether dimensions are listed in table 13.3. The resulting stress distribution in the kite is given in figure 13.6.

Table 13.3: Tether dimensions (as shown in figure 13.1)

Tether dimensions (from buoy to control pod)		
Electrical wire diameter	5	mm
Total diameter	7.7	mm
Dyneema surface area	27	mm^2
Bridle dimensions (from control pod to kite)		
Width	12	mm
Thickness	2.7	mm
Dyneema surface area	32	mm^2

Convergence analysis and verification of the simplified FEM model was already performed in the conceptual design phase and will not be repeated here. The reader is referred to the Mid-Term Report for more information on this. Note that in figure 13.4 clearly the location of the control pod can be seen, because there is a sudden change in tension force at the location of the control pod. This is due to the weight and drag of the control pod.

13.2 Kite skin

The kite is designed to create a downwash under nominal conditions. However, sometimes extreme weather conditions occur and in all cases the kite should have sufficient structural integrity. Therefore, in this section, the stresses due to the loads on the kite are analysed. The kite consists of two main parts: the skin sections and the Leading Edge (LE). Both parts are handled separately, the former in this section, whereas the latter is handled in section 13.3.

The most suitable program for the analysis of the complete kite is *MSC Adams* [51]. However, this program is far to extensive to work with in the provided time window. Therefore, it is chosen to make an approximation with the program *Patran-Nastran* to get an indication of the maximal stress in the critical parts of the kite.

Firstly, in subsection 13.2.1 the assumptions and simplifications are stated. Secondly, in subsection 13.2.2, the models of the skin sections are explained. Thirdly, the results are stated in subsection 13.2.3. Finally, the accuracy of the model and its results is evaluated on in subsection 13.2.4.

13.2.1 Assumptions

While analysing the skin of the kite, the following is assumed:

- The skin can be modelled as an isotropic bending plate.

  To be able to model the skin in *Patran-Nastran*, it is assumed that the skin can be modelled as an isotropic bending plate, with the average Young's modulus of Dacron of 3.4 [GPa], derived from table 15.1 stated in chapter 15. This is done to keep the model simple; implementing anisotropic behaviour, for example, is time costly.

- All aerodynamic loads act on the skin of the kite.

  This can be assumed since the surface area of the skin is much larger than that of the inflatable tubes. Therefore, no corrections are made for the wing loading on the skin and it is implemented as a distributed load along the surface.

- The distributed load is assumed to be linear until 0.125c, from the trailing towards the leading edge.

  No detailed airfoil characteristics - concerning the inflatable leading edge - are available for kites. Therefore, this linear distribution is chosen.

- The most critical skin sections are the section next to the strut in the center of the kite.

  This can be assumed since this part is directed to the flow the most, comparing with the rest of the skin sections. Therefore, this section is modelled in *Patran-Nastran* (not one of the more curved sections near the tips).

- The thickness of the skin is set equal to 6 [mm], one of the provided thicknesses of Dacron on the market. [52]

13.2.2 Models

Because all aerodynamic loads act on the skin of the kite, the skin between two struts can be analysed to check whether the tensile stress of Dacron is reached in extreme weather conditions. It has to be emphasized that with "kite section", in this section the skin part *between* two struts is meant. This part is modelled in *Patran-Nastran* [53] [54].

This is done using the extreme wing loading as stated in table 13.2. This wing loading is applied to the skin assuming the load distribution along the chord wise direction to be linear from the trailing edge (1c) until 0.125c (as can be seen in figure 13.8). [24] [29]

Because no knowledge of the number of struts is available, 2 models are made with two different numbers of struts. One is modelled dividing the kite in 4 and the other in 8 load carrying kite sections. The model with 4 sections has an area of 8 x 4 ($= \frac{16}{4}$) meters, the model implemented in *Patran-Nastran* is indicated in figure 13.7 to the left. The model with 8 sections has an area of 8 x 2 ($= \frac{16}{8}$) meters, this part is indicated to the right in figure 13.7 below.

For the applied forces in figure 13.8, it has to be noted that, due to the shared boundary conditions at the long sides, the applied forces are halved here, because the skin section next to the modelled section carries the same - halved - force. When more skin sections are modelled next to each other, the complete (not halved) force should be added.

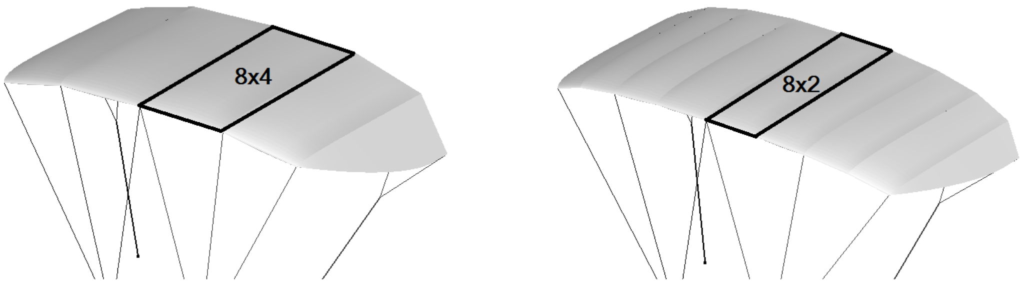

Figure 13.7: Kite lay-outs used in the analysis.

13.2.3 Results

The results are plotted for the different models in figures 13.8 to 13.11. Plotting the applied loads in figure 13.8, the constraint forces in figure 13.9, the stresses in figure 13.10 and the translational displacements in figure 13.11.

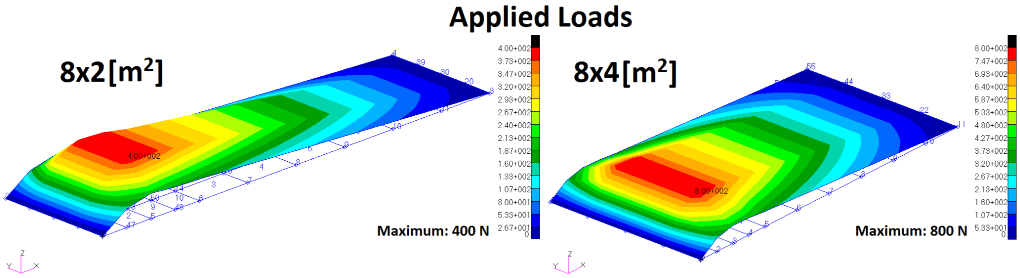

Figure 13.8: The applied loads on the skin for a 8x2 [m^2] and a 8x4 [m^2] kite element.

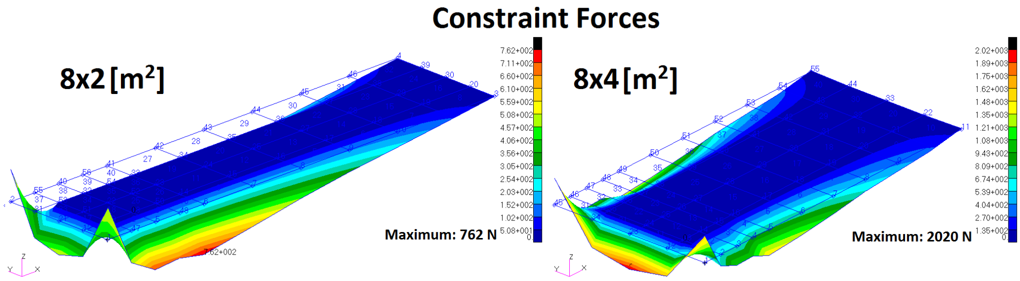

Figure 13.9: The constraint forces acting on the surrounding inflatable tubes for a 8x2 [m^2] and a 8x4 [m^2] kite element.

For the stresses in figure 13.10, it has to be noted that the fringes in this figure indicate the stresses, where the deformation (the geometry shown in the figure) of the figure is equal to the translational displacements result. In figure 13.11, the translational displacements are shown in the fringes and the deformation of the plot.

In all figures, the maximal values are stated. In figure 13.10, with the stresses, it can be seen that the maximal stresses for 8 and 4 skin sections are 0.758 and 2.39 [MPa] respectively.

The average tensile strength of Dacron is equal to 60 [MPa], derived from table 15.1 stated in chapter 15 (and in [55]). Therefore, it can be stated that Dacron can easily handle the extreme weather conditions, since the maximal stresses in the kite are at least $\frac{60}{2.4} = 25$ times smaller.
Below the kites are shown with the stress plots applied to give an impression where the largest stresses occur in the kite. Figure 13.12 shows an impression of the deformation of the kite with the 8 [m] by 4 [m] skin sections, where figure 13.13 shows this for the kite with the 8 [m] by 2 [m] skin sections.

One of the models, or equivalently the number of struts, must be chosen to implement in the kite's design. The first choice considering the weight 'point of view', the skin section of 8 [m] by 4 [m] will be chosen, corresponding to 3 struts excluding the leading edge at the wing tips. Because for this number of struts the

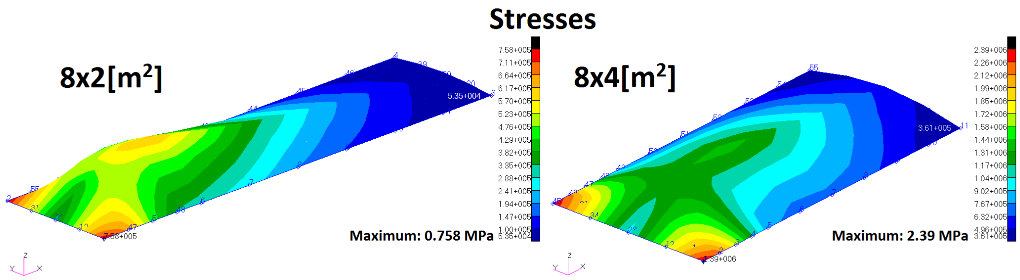

Figure 13.10: Internal stresses in the skin for a 8x2 [m^2] and a 8x4 [m^2] kite element.

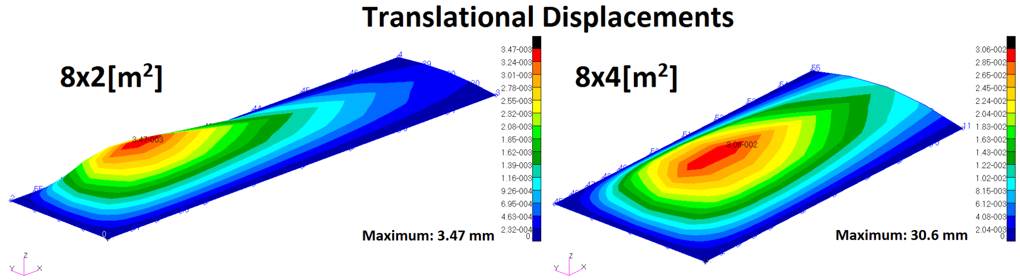

Figure 13.11: Translational displacements of the skin for a 8x2 [m^2] and a 8x4 [m^2] kite element.

weight is as small as possible.

However, when using the skin sections of 8 [m] by 4 [m], the skin will deform considerably more than when skin sections of 8 [m] by 2 [m] are used; centimeters instead of millimeters. Due to the deformation, the characteristics of the loads on the skin will change. Because the model has low accuracy already, as will be stated in subsection 13.2.4, the result for which the lowest deformation occurs is chosen; the skin sections of 8 [m] by 2 [m].

13.2.4 Accuracy

As explained in subsection 13.2.1, along others, one of the assumptions is that the skin can be modelled as a bending plate. This means that the accuracy of the model is low.

The model is therefore used for an indication of the order of magnitude of the stresses in the skin only. Since the found stresses are at least 25 times lower than the tensile stress of Dacron, it is assumed that the lack of accuracy is not critical. Therefore, the conclusions stated above, that the skin is able to withstand the extreme loads, are valid.

13.3 Inflated leading edge

The leading edge of the kite will be an inflated tube. This tube will provide the stiffness needed for the aerodynamic shape of the kite. Furthermore, the rigidity will prevent the kite from folding up in the air or when it is stationed at the buoy. In this section the required pressure inside the inflated leading edge will be determined.

The analysis of the inflatable tube is simplified to the analysis of the maximum bending moment at the location of the bridle attachment points. This bending moment should be lower than the collapse moment, otherwise the inflatable tube will collapse [56][57][58]. A good first approximation of the collapse moment was given by Stein et al. [56][57][58] and is presented with equation (13.13). In this equation the overpressure in the inflated tube is given by Δp and the radius of the tube by r.

$$M_{\text{collapse}} = \pi \Delta p r^3 \tag{13.13}$$

In table 13.2 the aerodynamics forces on the kite are presented and in section 13.2 it was given that there are six bridle cables attached to the leading edge of the kite at five attachment points. This leads to four sections of the inflated leading edge. Because the kite's span is 16 [m], each section has a length of $w = 4$ [m]. For this first analysis, it is assumed that the lift force is equally distributed over the whole kite. This means that per

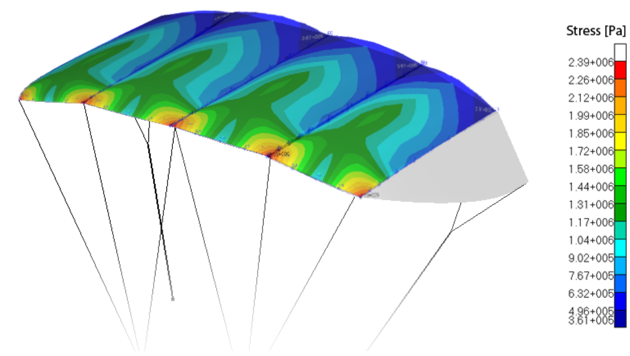

Figure 13.12: Impression of the deformation of and stresses in the kite with 4 sections

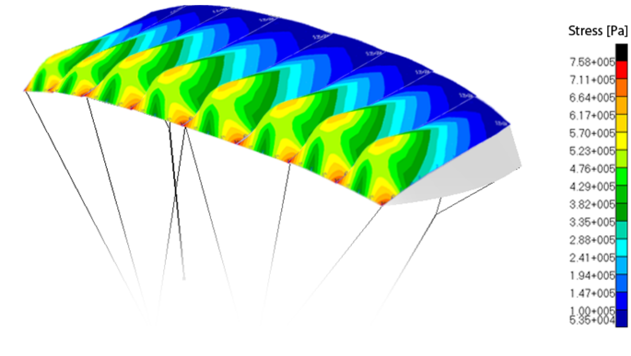

Figure 13.13: Impression of the deformation of and stresses in the kite with 8 sections

section the lift force is $l' = L_{tot}/4 = 65/4 = 16$ [kN]. This force is assumed to act on the middle of the tube section and is supported by a bridle at the left and right end of the section. Therefore, the bending moment caused by the lift force on the inflatable tube sections is $M_{\max} = l'/2 \cdot w/2 = 8 \cdot 2 = 16$ [kNm]. This is the maximum bending moment the leading edge tube has to withstand. Note that this is a common method for first analysis. A similar analysis is also performed by Veldman et al. [59].

The maximum pressure, which the tube has to withstand, is calculated with equation (13.14), which is given by Veldman et al. [59]. This equation gives the maximum stress in circumferential direction. In the optimal case, the bias angle of the fibres in the fabric γ is such that both the stress in circumferential direction and along the tube axis is equal [59]. This optimal angle is calculated with equation 13.15.

$$\Delta p_{max} = \frac{2t}{d}\frac{\sigma_{ult}}{4}\sin^2\gamma \tag{13.14}$$

$$\cos 2\gamma = -\frac{2}{3}\left(\frac{4}{\sigma_{ult}}\frac{8}{t}\frac{M_{max}}{\pi d^2} + 1/2\right) \implies \gamma = \frac{1}{2}\arccos\left[-\frac{2}{3}\left(\frac{4}{\sigma_{ult}}\frac{8}{t}\frac{M_{max}}{\pi d^2} + 1/2\right)\right] \tag{13.15}$$

The radius of the leading edge inflatable tube follows from reference kites [29][44] and is assumed to be $r = 0.25$ [m]. Furthermore it follows that the load carrying Dacron of the inflatable tube normally has a thickness $t = 3$ [mm] and $\sigma_{ult} = 75$ [MPa].

With equation (13.16) - which follows from equation (13.13) - now the minimum pressure in the inflatable tube can be calculated. Inserting $M_{\max} = 1.6M_{\max} = 16$ [kNm] and $r = 0.25$ [m] into this equation yields that $\Delta p_{min} = 336$ [kPa] and that $p = \Delta p_{min} + p_{atm} = 336 + 101 = 437$ [kPa].

$$p = \Delta p_{min} + p_{\text{atm}} = \frac{M_{\max}}{\pi r^3} + p_{\text{atm}} \tag{13.16}$$

Now the maximum pressure differential in the tube will be calculated with equations (13.14) and (13.15). Inserting a thickness of $t = 2$ [mm] into these equations yields a complex maximum stress, which means that the structure is too weak at all pressures. Inserting the thickness of $t = 3$ [mm] yields $\gamma = 71$ [deg] and $\Delta p_{max} = 864$ [kPa]. Clearly $\Delta p_{min} < \Delta p_{max}$, therefore the inflatable tube structure is deemed feasible.

Chapter 14

Ground segment structures

In this chapter the structure of the buoy, the underwater parts, the mast and the connection between these parts will be discussed. First, in section 14.2.2, the structure of the mast will be described and analysed. Hereafter in section 14.2, the buoy will be analysed using the forces exerted by the tether and the connection to the anchor at the seabed. Next, in section 14.3, the required reinforcements and connection methods will be discussed. Finally the anchor and anchor chain are analysed.

14.1 Mast

The vertical pole that is located on the buoy, from now on conveniently called the 'mast', is used to suspend the leading edge of the kite when the wind speed is too low, and the kite needs to be retracted. Normally, no large forces will be exerted on this mast. The dimensions of the mast will be determined from the extreme loading scenario, for when the leading edge line will take up all the aerodynamic loads from the kite. This could happen for example, when the main tether would break. This type of failure should not lead to the collapse of the entire mast. Instead of designing the mast for nominal wind conditions and corresponding tether forces, and then adding a safety factor, the choice is made to design the mast for extreme wind conditions, at the most unfavourable location of the kite, at an angle of 90 degrees from the mast (when the kite is located in the same horizontal plane). This is the most unfavourable position since this will lead to the largest bending forces in the mast. The maximum force that the mast should be able to withstand is 66 [kN], as was explained in section 13.1. The mast will be suspended at two locations, at the bottom of the buoy and on the top of the buoy structure, located 2 [m] apart from each other. The maximum load will act on the top of the mast, at a height of 12 meters from the bottom of the buoy.

In order to determine the forces present in each part of the mast, the principle of virtual work, also called Castagliano's theorem [60] must be used. This is necessary since the problem is statically indeterminate, that is, there are more unknown reaction forces than available equilibrium equations. There are 4 unknowns and 2 non correlated equilibrium equations. In order to reduce the amount of unknowns, it will be assumed that the connection to the buoy, located at the top panel, will only carry horizontal loads. This is visualised in figure 14.1, along with the representation of the principle of virtual work on the simplified Free Body Diagram (FBD).

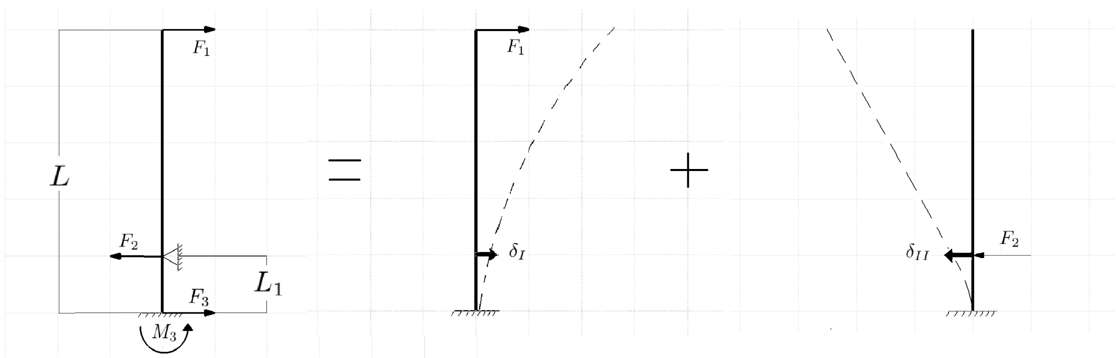

Figure 14.1: FBD's and equivalent virtual structures

As can be seen from figure 14.1, the simplified FBD is decomposed into two different complementary FBD's.

In the first FBD, the horizontal support is removed and the resulting horizontal displacement at that point is given by δ_I. In the second FBD, the tether force F_1 is removed, and the horizontal displacement δ_{II}, as a result of the reaction force F_2 is calculated. These displacements do not happen in reality, since that point is supported. A compatibility equation can be written that describes this, $\delta_I + \delta_{II} = 0$. This equation can now be used in combination with the two equilibrium equations in order to find the reaction forces.

$$\delta_I + \delta_{II} = 0 \tag{14.1}$$

$$\delta_I = \theta_2 \cdot L_1 = \frac{F_1 \cdot L^2}{2EI} \cdot L_1 \tag{14.2}$$

$$\delta_{II} = \frac{F_2 \cdot {L_1}^3}{2EI} \cdot L_1 \tag{14.3}$$

$$\Sigma \overrightarrow{F}_x = 0 : F_1 - F_2 + F_3 = 0 \tag{14.4}$$

$$\Sigma M_3^{\frown} = 0 : M_3 + F_2 \cdot L_1 - F_1 \cdot L = 0 \tag{14.5}$$

$$F_1 = 66[kN] \tag{14.6}$$

$$F_2 = 3564[kN] \tag{14.7}$$

$$F_3 = 3630[kN] \tag{14.8}$$

$$M_3 = 7920[kNm] \tag{14.9}$$

Where θ_2 is the bending angle at location 2. Solving this set of equations will lead to the following results, using the fact that L_1=2 [m], L=12 [m], E=200 $\cdot$ 10^9 [Pa] which is the Young's Modulus of A36 Steel [61], the moment of inertia I=4.20 $\cdot$ 10^-6 [m^4] as calculated with formula 14.10, and finally the loading F_1=66 [kN], which is the maximum force generated by the kite, for the case where the main tether breaks during maximum wind conditions.

Now that the forces involved are known, the mast can be designed. Due to added functionalities to the mast, the geometry is already fixed, as explained in section 17. Since also the minimum height of the mast is fixed, the only remaining design parameters are the 4 thicknesses of the steel plates that make up the mast. Since the maximum load will be perpendicular to the two straight plates of length 600 [mm] and 800 [mm], the highest stresses will be present in these plates. Also, the smallest of these two plates must have a larger thickness since the loads will be more concentrated. Since this type of loading is already very unlikely, the ultimate strength of A36 steel is used, leading to plastic deformation, which has a value of 400 [MPa] [61]. In the unlikely event of such a large loading, the mast is allowed to permanently deform, since designing the mast for the Yield strength will give an unnecessarily large and thus heavy structure. A heavy mast is unwanted, since this will affect the stability of the ground segment, which will create the need for a larger buoy, increasing the mass even further. This will cause a snowball effect were one kilogram of weight added to the mast will add several kilograms to the entire structure.

The required thickness of the plates can be determined by using the engineering bending equation [60]. In its reduced form, the stresses are given by formula 14.10.

$$\sigma_z = \frac{M_x}{I_{xx}} y \tag{14.10}$$

$$I_{xx} = \int_A y^2 dA \tag{14.11}$$

Where I_{xx} is dependent on the thicknesses. Using this method, a optimal thickness for the A36 steel plates, with an ultimate strength of 400 [MPa], can be found. The resultant thicknesses are as shown in figure 14.2. For the structure with these final thicknesses, a finite element structural analysis was made in Dassault Systemes CATIA V5R20 [62]. Here, the structure was clamped at both supports, and subjected to the forces as calculated before.

As can be seen from figure 14.4, the design is confirmed since no stresses higher than the ultimate strength of the used material occur, thus no failure will occur. Also, it can be seen that the highest stresses occur near the first connection to the buoy, visualised by the dark arrows. The maximum stress that is given in the legend in the figure, gives a higher local stress than the ultimate strength of the material. This stress concentration is located in a edge at less than a cm from the support, and is due to local miscalculations by CATIA, due to conflicting mesh sizes for the support and the mast. From figure 14.3, it can also be seen that the maximum displacement caused by the applied load is 200 [mm], which is well within limits to continue normal operation and retraction.

Buckling is a concern in this design due to the large size of the mast, and it only being clamped at one side. The maximum compressive force that the structure can withstand before buckling occurs is given by the Euler buckling formula [63].

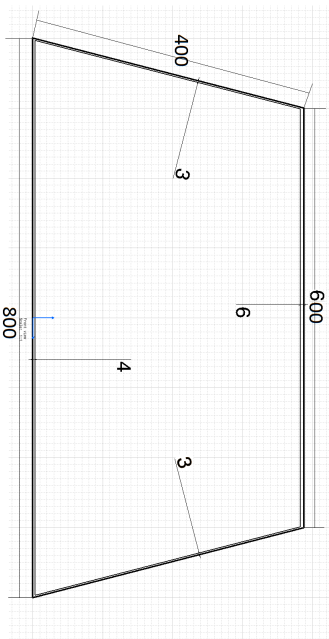

Figure 14.2: Dimensions of the mast

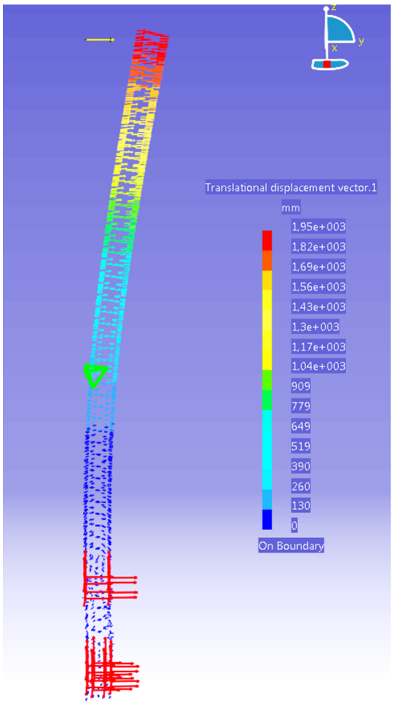

Figure 14.3: Displacements

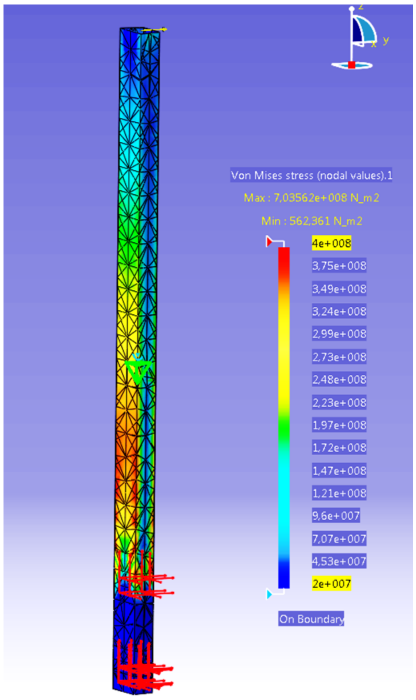

Figure 14.4: Von Mises stresses

$$F = \frac{\pi^2 EI}{(KL)^2} = \frac{\pi^2 \cdot 200 \cdot 10^9 \cdot 4.20 \cdot 10^{-6}}{(2 \cdot 10)^2} = 4.14 \cdot 10^6 [N] \tag{14.12}$$

Where the maximal force, F is dependent on the modulus of elasticity E, the second area moment of inertia I, the unsupported length of the beam L which is $L = 10$ [m] due to the support at the top panel and the column effective length factor K. This K factor is given to be $K = 2.0$ for a beam with one end fixed and the other free to move laterally. The only compressive force acting on the mast is its own weight $W_{mast} = 630$ [Kg] and the weight of the kite $W_{kite} = 81$ [Kg]. This leads to a total compressive force of 6975 [N], which is much smaller than the allowable force. However, during the maximum bending of the mast, the side with 600 [mm] width is under compression. Equation 14.12, cannot be used for this situation. A more complex equation needs to be used [64].

$$\sigma_{critical} = \frac{K_b \pi^2 E}{12(1-\mu^2)} \left(\frac{t}{b}\right)^2 = \frac{1.97\pi^2 \cdot 200 \cdot 10^9}{12(1-0.28^2)} \left(\frac{0.006}{0.6}\right)^2 = 445[MPa] \tag{14.13}$$

Where $\mu = 0.28$ is the poisson's ratio for steel [63], the thickness of the plate in question is given by t, and the width is given by b. The K_b factor which is different from the previous one, is determined by the relationship between width and length, and for the mast it is equal to 1.97 [64]. As can be seen, the critical stress is 445 [MPa] which is higher than the tensile strength of steel, which is, as stated before, rated at 400 [MPa] for steel A36. Thus, the design of the mast is checked and confirmed to not fail under the design conditions.

14.2 Buoy structure

The main function of the buoy is to connect the kite with the ground while the kite is airborne. In a marine environment, such as that of the OWEZ wind farm, use must be made of a buoy. Since the ground segment is floating, a buoyancy force is present which is related to the weight of the structure. Similarly to the design of the mast, the structure of the buoy is designed to withstand the maximum tether force, with its action point located at the top op the mast. This force is larger than the tether force when acting on the winch, as showed in section .

The weight and volume of the structure will also determine the associated buoyancy force and its distribution. The weight of the structure along with the dimensions of the buoy will determine if the structure will float. In sections 14.2.1 and 14.2.2, the final weight will be used to show the required dimensions. However, the weight is dependent on the structure, this was in reality an iterative process where a first estimation for the weight of the structure was used. Hereafter, the design process was repeated until the final optimal design was created. In this final design, the weight of the ground segment is composed of the components given in table 14.1.

Table 14.1: Breakdown of the weight of the ground segment

Weight in [Kg]		
Mast	630	
Top panel of buoy	520	
Lower part of buoy	1490	
Support structures	185	
Winch	600	
Batteries	113	
Total Weight	3538	Kg

The buoyancy force needed to keep the buoy floating will have the same magnitude as the weight, in order to reach an equilibrium. This buoyancy force will be assumed to be evenly distributed over the buoy by the water. As explained in section 12, this will cause the lower 870 [mm] to be submerged. This submerged area will have to transfer this distributed buoyancy force. The total buoyancy force will be multiplied by a safety factor of 1.5 in order to account for increase in weight as for example when personnel is standing on top of the buoy. The buoy is also connected to the ground at the centre position of the bottom panel. This force, also related to the buoyancy force, will be much more demanding for the structure since it is more concentrated. As also explained in section 12, the maximum possible tension force is 215 [kN].

The tether affects the structure of the buoy indirectly in this loading condition, that is, the reaction forces as calculated in section 14.2.2 will induce stresses into the structure of the buoy. It is assumed that the top panel of the buoy will only take the horizontal force F_2, and the vertical force may be neglected. This will be further elaborated in section 14.2.1. The lower structure of the buoy will then be subject to the forces through the mast F_3 and M_3, the maximum force created by the cable connected to the ground and the distributed load of the buoyancy force. It is also assumed that the buoyancy force only has an upward pointing component, this assumption is valid since it will simplify calculations while creating more stresses than in the real case where the buoyancy force is a pressure force. This will be used in section 14.2.2, were the lower structure will be further explained.

14.2.1 Top plate

The needed thickness of top plate of the buoy structure can be determined from the force F_2 generated by the tether via the mast. This force is larger than the tether force when acting on the winch, as showed in section . This can be done by using the simplified formula relating the stress σ with the cross-sectional area A and applied force F_2.

$$\sigma = \frac{F_2}{A} = \frac{F_2}{w \cdot t} \tag{14.14}$$

Equation 14.14 will not give accurate results since the plate is too large to assume a constant stress distribution. Therefore, use was made of Finite Element Analysis in Dassault Systemes CATIA V5R20 [62]. In this model, the weight of the winch of 5886 [N] is taken into account and also the force F_2. Also, in this simulation the support at the location of the winch was assumed to only carry horizontal loads, to keep consistency in the design process. Also the resultant forces from the lower structure were added to the top panel through the edge of the top panel, without taking into account stress concentrations due to the bolted connections since CATIA V5R20 is not capable of accurately predicting these stresses. Instead, the supplied loads from the lower structure were multiplied with a safety factor of 1.2.

In figure 14.5 and 14.6 the plate that will be used with a optimised thickness of 11 [mm] is shown. It can be seen that the plate is asymmetrically loaded. Furthermore, these plots confirm the statement that due to the large size of the plate, equation 14.14 cannot be used. Also, in these Von Mises plots it can clearly be seen that stresses are concentrated at the centre of the plate. Instead of sizing the entire plate for these maximum stresses, the thickness was reduced such that reinforcement 45^o woven glass fibre mats need to be added. This solution will be cheaper in material cost, and will save weight. In the figures it can clearly be seen where reinforcements need to be added, the dark area in the middle will require a single 45^o E-Glass type sheet, with a tensile strength of 3450 [MPa] versus 69 [MPa] of the chopped strand material. This will easily take care of the higher stresses present in the top panel.

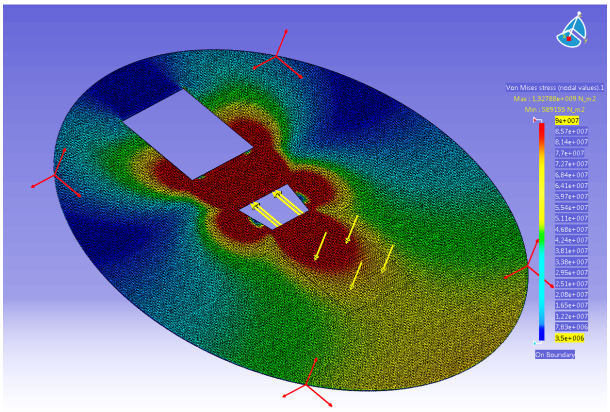

Figure 14.5: Von Mises stress distribution over the top panel of the buoy

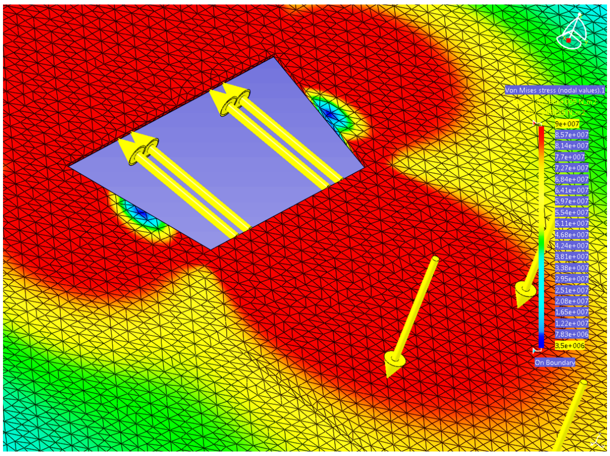

Figure 14.6: Von Mises stress distribution near the hole for the mast

14.2.2 Lower structure

Similarly to the top plate, the needed thickness of lower structure of the buoy can be determined from the force F_3 and moment M_3 generated by the tether via the mast. These forces are larger than the tether force when acting on the winch, as showed in section . Also in this case, equation 14.14 will not give accurate results since the plates are too large to assume a constant stress distribution.

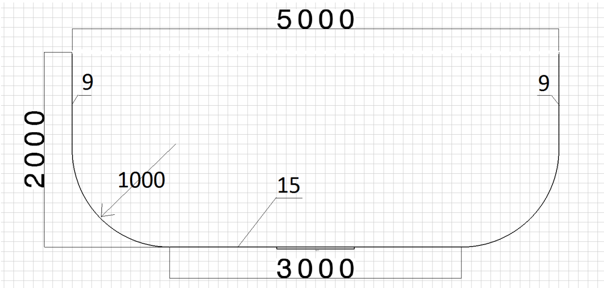

Figure 14.7: Basic dimensions of the lower structure of the buoy

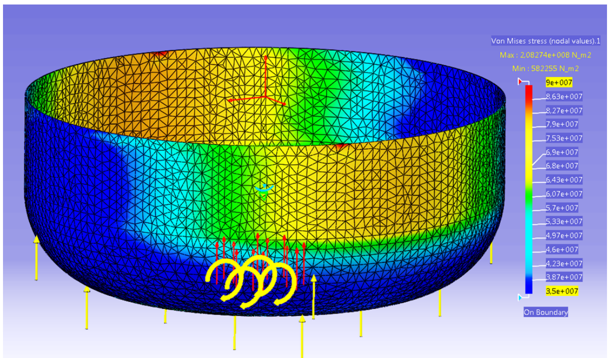

Figure 14.8: Side view of the modelled forces and resulting Von Mises stresses

Therefore, also for the lower structure use was made of Finite Element Analysis in Dassault Systemes CATIA V5R20 [62]. In this model, the forces transferred via the top plate are taken into account, as well as the weight of the winch that is transferred via a support pole to the lower panel as discussed in section 14.3.1. Furthermore, the buoyancy force exerted by the water is modelled, where the maximum buoyancy force is used. The maximum buoyancy force is determined by the maximum amount the buoy can be pulled underwater, by the cable connecting it to the anchor. Lastly, this cable that is connected to the anchor is modelled as a distributed force, distributed over the local bottom reinforcement, this reinforcement will be further discussed in section 14.3.1. Once more no stress concentrations due to the bolted connections are taken into account since CATIA V5R20 is not capable of accurately predicting these stresses.

As can be seen from the Von Mises stress analysis, figure 14.8, the sides of the structure are asymmetrically loaded due to the bending forces from the mast. Also, it can be seen that there is a sharp rise in stresses at the curvature of the buoy. This curvature has a radius of 1000 [mm], found by trail and error in CATIA. This optimal value reduces the stress concentrations at these points to a level below the ultimate tensile strength plus an added safety factor of 1.2. This safety factor is added to account for any flaws in production. Increasing the radius even further would lead to negative effects in terms of stability as can be seen in chapter 12.

When looking at figure 14.9 the bottom plate can clearly be seen. It is here where the forces from the anchor and the mast come together. This can clearly be seen in the high associated stresses. Once more, the effect of the asymmetrical loading produced by the mast can be seen in the corresponding stresses. It should be noted that at the location were the forces are placed in the model, as can be seen more clearly in figure 14.10, the stresses are much lower than at its surroundings. This can be explained by the location of the lower reinforcement which will be discussed in section 14.3. This reinforcement acts as a increase in thickness of the

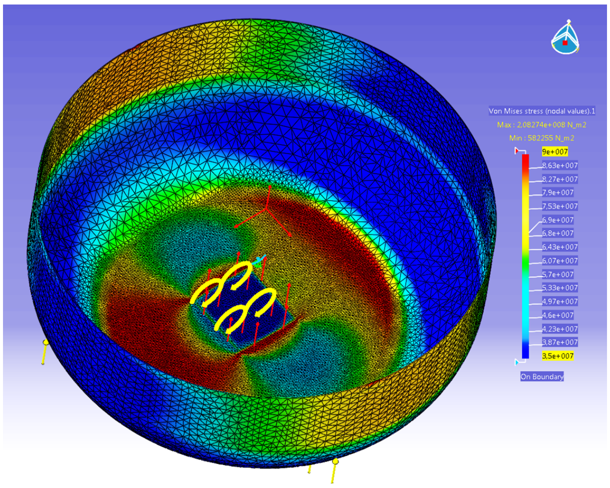

Figure 14.9: Top view of the modelled forces and resulting Von Mises stresses

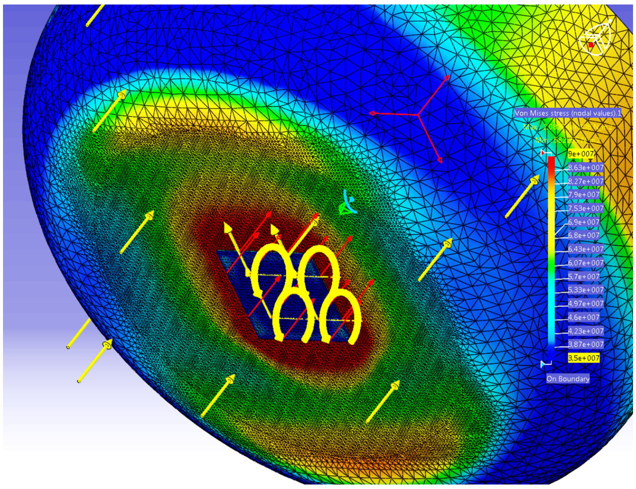

Figure 14.10: Bottom view of the modelled forces and resulting Von Mises stresses

structure, with lower associated stresses. Similarly to the top panel, instead of sizing the entire plate for these maximum stresses, the thickness was reduced such that reinforcement 45^o woven glass fibre mats need to be added. This solution will be cheaper in material cost, and will save weight. In the figures it can clearly be seen where reinforcements need to be added, the dark areas in lower middle part require a single 45^o E-Glass type sheet, with a tensile strength of 3450 [MPa] versus 69 [MPa] of the chopped strand material. This will easily take care of the higher stresses present in the top panel. Also, one extra mat needs to be added for the attachment to the mast in the center of the buoy.

14.3 Reinforcements

The mast needs to transfer loads to the glass fibre structure in a smooth fashion in order to reduce stress concentrations. This is done by locally reinforcing the structure by using glass fibre mats or steel reinforcement sockets. The dimensions of these reinforcement will first be discussed in section 14.3.1. Hereafter, thermal effects and connection methods will be discussed in section 14.3.2.

14.3.1 Dimensions

The reinforcements can be sized when looking at the reaction forces as determined in section 14.2.2. The forces F_2 and F_3 can be used to determine the required size of the reinforcements at the upper plate and lower plate respectively. The thickness of the upper reinforcement can be determined using the load that needs to be transferred to the upper plate and the yield stress of A36 Steel, which has a value of 250[MPa].

$$\sigma_t = \frac{F_2}{A} = \frac{F_2}{w \cdot t} \tag{14.15}$$

$$t_2 = \frac{F_2}{\sigma_t \cdot w} \cdot SF \tag{14.16}$$

$$t_{2_{long}} = \frac{3564000}{250 \cdot 10^6 \cdot 0.8} \cdot 1.6 = 24[mm] \tag{14.17}$$

$$t_{2_{small}} = \frac{3564000}{250 \cdot 10^6 \cdot 0.6} \cdot 1.6 = 32[mm] \tag{14.18}$$

In equation 14.17, where F_2 is the force in the mast at the top plate, as found in section 14.2.2. The required thickness is dependent on the width of the mast, w. An increase in width will lead to a lower required thickness of the reinforcement. For the length of the reinforcements a taper factor of 3.5 will be used. This means that for a thickness of 73[mm] a length of 255[mm] is used and for a thickness of 55[mm] a length of 192[mm] is used. For all previous values a safety factor $SF = 1.6$ was used as follows from 9 about risk and risk handling. These values will cause a proper load transfer to the glass fibre plate.

The lower reinforcement will be made from glass fibre as explained in 16. This requires a different approach, than for the top plate since there is a limit on the maximum thickness that can be achieved using the chopped strand spraying technique. As explained in section structures:ground:buoystructure, the bottom plate already requires an extra layer of 45^o woven E-Glass mat. If an extra reinforcement is also placed to connect the mast to the bottom plate, the structure will transfer its loads properly. Note that there is a minimal ratio between the radius of curvature and the minimal distance between the radius and the end of the reinforcement [65]. Since not much is known about the exact dimensioning of the bottom reinforcement it is assumed that a height of 500 [mm], and length of 300 [mm] and 405 [mm] for the 800 [mm] and 600 [mm] respectively, will be used. This is, however, an area for further research.

The support pole that will be present to support the loads from the winch will be designed using a similar approach to the design of the mast. For a explanation on the design method the reader is referred to section 14.2.2. The driving requirement for the dimensions follow from the compressive force of 5886 [N] generated by the 600 [Kg] winch, and associated buckling limits. A thin walled circular cross section made of A36 steel will be used with $E = 200$ [MPa], since this profile is readily commercially available.

$$F = \frac{\pi^2 EI}{(KL)^2} \tag{14.19}$$

$$I = \pi R^3 t \tag{14.20}$$

$$6000 = \frac{\pi^2 \cdot 200 \cdot 10^9 \cdot \pi R^3 t}{(0.5 \cdot 2)^2} \tag{14.21}$$

In equation 14.21, a column effective length factor, $K = 0.5$ is used as follows for a beam fixed at both extremities. As can be seen from formula 14.21, there are two design parameters, the radius of the circular cross section R and the thickness t. In this design a radius $r = 50$ [mm] with a corresponding thickness value of $t = 1.34$ [mm] was used. Note that a safety factor of 1.6 has been added to these values, using the reasoning following from the risk and risk handling chapter 9.

14.3.2 Thermal effects and connection methods

The connection from the mast to the reinforcements will be performed using bolts. This is done for ease of assembly, inspection and maintenance. Also, the connection must be made between a steel mast and a glass fibre structure. This limits the options for connection methods. For example, adhesive bonding will not be possible due to thermal expansion differences. Other, more obvious, impossible connection methods ones are welding or riveting.

When using two different materials in a design, especially when a connection between these two is present, extra care must be taken to aspects such as connection methods and also how the connection will hold over time. In the case of the connection from the steel mast to the glass fibre structure, there is one important difference in material properties, the thermal expansion coefficient (TEC). The TEC is a measure of how much a material will expand under one degree of temperature increase. The TEC of A36 grade Steel is rated at $\propto_{steel} = 12 \cdot 10^{-6} [K^{-1}]$ and the TEC of glass fibre at $\propto_{glass} = 5 \cdot 10^{-6} [K^{-1}]$ [66]. It is assumed that the temperature range that will be present in the environment at the OWEZ wind farm varies from $-15^o C$ to a maximum of $40^o C$. Assuming the buoy will be assembled indoors at a room temperature of $20^o C$ this will lead to a maximum temperature difference ΔT=35[^{0}C] and the corresponding following strains ($\epsilon_{thermal}$) and associated differences in thermal elongation.

$$\epsilon_{thermal} = \propto \Delta T \tag{14.22}$$

$$\Delta L = \epsilon_{thermal} \cdot L_{initial} = \propto \Delta T \cdot L_{initial} \tag{14.23}$$

$$\Delta L_{steel} = \propto_{steel} \Delta T \cdot L_{initial} = 12 \cdot 10^{-6} \cdot 35 \cdot 2 = 0.84[mm] \tag{14.24}$$

$$\Delta L_{glass} = \propto_{glass} \Delta T \cdot L_{initial} = 5 \cdot 10^{-6} \cdot 35 \cdot 2 = 0.35[mm] \tag{14.25}$$

$$Tolerance = 0.84 - 0.35 = 0.49[mm] \tag{14.26}$$

As can be seen in equations 14.24 and 14.25, the used value for the initial length, $L_{initial}$ is taken as 2[m]. This was done since the bottom of the mast is assumed to be fixed. The location where thermal expansion effects will be important is at the connection to the buoy structure at 2[m] from the bottom. As can be seen from equation 14.26, the maximum difference in length is 0.49[mm]. This value is small enough to conclude that thermal effects can easily be overcome, as long as the tolerances for the bolts used in the connection are not smaller than 0.49[mm].

14.4 Anchor and anchor chain

This section will discuss the basis of the ground segment: the anchor. The function of the anchor is to keep the buoy at its initial location. This requirement is of great importance with respect to the performance and the risk management of the Daeolus kite system. First free body diagrams will be discussed to derive the equilibrium equations and to calculated the loading on the anchor. The calculations discussed in this section are performed with simplifying assumptions which will be stated, to correct for these assumptions safety factors will be introduced. For the design of an anchor it is required that the anchor can be removed from the seabed, this is stated by the Dutch law. The fist subsection will discuss the equilibrium equation of the anchor, the second subsection discusses the equilibrium equations of the buoy, the third subsection treats the chain loading and finally the anchor and chain dimensions are discussed, in the final subsection the final underwater segment layout is concluded.

14.4.1 Anchor equations

This section will derive the equilibrium equations of the anchor, where the anchor is assumed as a point mass. First the free body diagram of the anchor is presented in figure 14.11.

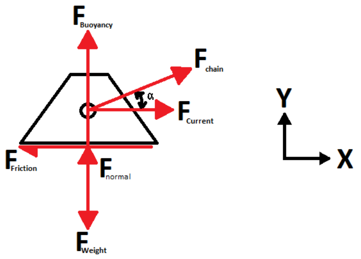

Figure 14.11: Free body diagram of the anchor

Indicated are all the forces working on the anchor:

- F$_{normal}$: The normal force of the ground onto the anchor.
- F$_{buoyancy}$: The anchor is in the water, this causes a buoyancy force.
- F$_{current}$: The wind farm is located at sea where tide currents are present these will exerting forces on the anchor
- F$_{chain}$: The chain to the buoy pulls on the anchor, when waves smash onto the buoy, this will increase the force on the anchor
- F$_{friction}$: Friction between anchor and seabed.
- F$_{weight}$: The weight of the buoy.
- α: Angle of the chain and the horizon.

The buoyancy force is a function of the volume of the anchor and the density of seawater which is $\rho_{water} = 1025[kg/m^3]$. Concrete is a cheap and heavy solution with a density of 2400 [kg/m^3] [67]. Assuming that the whole anchor is made of concrete, the buoyancy force can be computed as.

$$F_{buoyancy} = \rho_{water} V g = 10000V \tag{14.27}$$

Where V stands for the volume in $[m^3]$ of the anchor and g stands for the gravitational constant which is 9.81[m/s^2]. F_{weight} can be written as function of its volume.

$$F_{weight} = \rho_{concrete} V g = 24000V \tag{14.28}$$

With this known the first equilibrium equation in y-direction can be computed.

$$\sum F_Y \uparrow_+ : F_{buoyancy} - F_{weight} + F_{chain} \sin\alpha + F_{normal} = \tag{14.29}$$

$$10000V - 24000V + F_{chain} \sin\alpha + F_{normal} = \tag{14.30}$$

$$-14000V + F_{chain} \sin\alpha + F_{normal} = 0$$

The required volume is a function of the chain force and the angle at which the chain reaches the anchor, which is at itself a function of the length of the chain. With an increasing chain length α will go to zero. In the same manner the equilibrium equation in the x-direction can be constructed. For the scope of this project $F_{current}$

is assumed to be zero because of the existence of the boundary layer. This means that near the seabed the current velocity decreases to zero. $F_{friction}$ can be written as.

$$F_{friction} = F_{normal}\mu_{friction} = (F_{weight} - F_{buoyancy})\mu_{friction} \tag{14.31}$$

Where $\mu_{friction}$ stands for the friction coefficient. On wet sand $\mu_{friction}$ equals 0.5 [68]. Note that $\alpha = 0$ in this case.

$$\begin{gathered}\sum F_X \rightarrow_+ : F_{current} + F_{chain}\cos\alpha - F_{friction} = \\ F_{chain}\cos\alpha - F_{friction} = F_{chain}\cos\alpha - 7000V = 0\end{gathered} \tag{14.32}$$

Equation 14.31 and 14.33 are characteristic for the calculation of the volume of the anchor. These three equation contain four unknowns where F_{chain} is to be determined by the determination of the force on the buoy and the sizing of the chain.

14.4.2 Buoy equations

This section will discuss the equilibrium equations of the buoy, using these equations the anchor chain dimensions can be determined. From this the chain length will be determined. For the calculations the worst case scenario parameters are used, in these conditions the anchor should withstand all forces and may not move to another location by hopping over the seabed. In figure 14.12 the free body diagram is given for the buoy. This figure

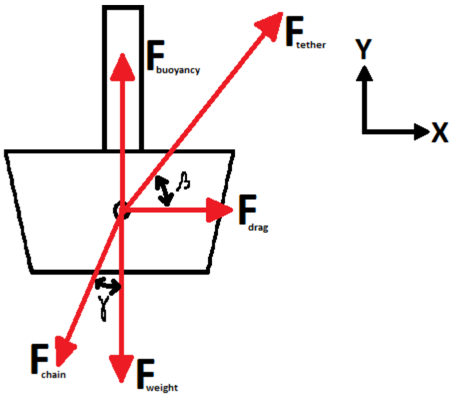

Figure 14.12: Free body diagram of the buoy

contains the following forces:

- F_{bouy}: The buoyancy force of the buoy.
- F_{tether}: The tether force at the buoy.
- F_{drag}: This force contains three sub forces, the water current force, the wave force and the wind drag which are all working in the same direction.
- F_{chain}: This is due to the weight of the chain, together with F_{weight} defines the total weight.
- F_{weight}: The weight of the buoy.

All the forces in x-direction working on the buoy should be transferred through the anchor chain and are absorbed by the anchor. For the determination of the chain weight only the vertical forces are of importance.

The maximum allowable buoyancy force of the buoy is determined by its volume which is 26 $[m^3]$ below sea level. This is derived from the Catia drawing. Which corresponds with 255 [kN] buoyancy force, note that the buoy in this condition has a deck height of 0.5 [m] with respect to the water surface which is the critical deck height. The mass of the buoy is 4000 [kg] $\approx 40[kN]$. $F_{chain}\cos\gamma$ is the weight force of the chain on the buoy: $F_{y,chain}$. The vertical tether force $F_{tether}\sin\beta = F_{y,tether}$ is valued to be the lift force of the kite in extreme weather conditions, since the kite system should withstand extreme weather conditions. The equilibrium equation becomes.

$$\sum F_Y \uparrow_+ : F_{buoy} - F_{weight} + F_{y,tether} - F_{y,chain} = 0 \tag{14.33}$$

With this equation the weight range of the chain $F_{y,chain}$ can be determined. When assuming that the kite produces zero lift the buoy operates with its maximum allowable buoyancy force of 255[kN]. This will result in a maximum allowable $F_{y,chain_{max}}$ of.

$$F_{y,chain_{max}} = F_{buoy} - F_{weight} = 255 - 40 = 215[kN] \tag{14.34}$$

For extreme weather condition where the kite produces 65 [kN], it should be prevented that the buoy is raised up into the air in this situation $F_{buoy} - F_{weight}$. The minimum chain weight therefore is.

$$F_{y,chain_{min}} = F_{buoy} - F_{weight} + F_{y,tether} = F_{y,tether} = 65[kN] \tag{14.35}$$

With the results of equation 14.35 and 14.34 the weight range of the chain is determined to be 65-215 [kN], note that the buoyancy force of the chain itself is not jet taken into account. The equilibrium equation in x-direction will be discussed in the next subsection.

14.4.3 Chain loading

This subsection will discuss the dimensions and weight of the anchor chain. As discussed in the previous section the weight range of the chain is defined as 65-215 [kN]. As stated by the OWEZ [5] the water depth in the wind farm is in the range of 15-20 [m], a minimum of 65 [kN] should support the buoy. The minimum water depth is taken as measure for the effective chain length, 15 [m], since this is the effective weight of the chain till it lays on the seabed when the tide is low. The minimum and maximum chain weight become.

$$W_{chain_{min}} = \quad 65/15 \quad = 4.3[kN/m] \tag{14.36}$$

$$W_{chain_{max}} = \quad 215/15 \quad = 14.3[kN/m] \tag{14.37}$$

These chain weights correspond to 440-1500 [kg/m], which in not feasible. Therefore a different solution has to be found. A weight of 65 [kN] should be attached below the buoy to compensate for extreme weather conditions, since otherwise the buoy is lifted out of the water. Again note that the stated 65 [kN] is defined as a point mass where its buoyancy force is neglected, when the actual weight is attached this has to also compensate for the buoyancy force. If this weight is included the chain weight range becomes: 0-150 [kN], this value is calculated by subtracting 65 [kN] from each value. With this range the chain only fulfils the function of transferring all horizontal loads on the buoy to the anchor which is preferable, from this the required friction force for the anchor can be calculated.

In extreme weather conditions the chain should withstand all external forces, all horizontal components of the free body diagram of the buoy and the anchor should be added to calculated what the dimension of the anchor should become.

$$F_{x,anchor} = D_{extreme} + F_{drag_{max}} + F_{drag_{chain}} \tag{14.38}$$

The exact calculation of $F_{xanchor}$ is out of the scope of this project therefore assumptions are made to give a indication of this value. F_{anchor} is the sum of three drag forces working on the buoy: the wind force, the current force and the wave force. The coherency between these forces are: with increasing wind speed the current speed and the wave forces increase. Due to the relative high viscosity of water compared to air the wind drag force is neglected with respect to the current drag. The second reason for this is due to the wind profile due to the boundary layer: at the water surface the wind velocity is low. For the drag force calculation the wave force is neglected, to account for this the maximum current force is doubled for the calculation of the current drag. The current speed has a quadratic relation with respect to the current velocity, this is shown in equation 14.39. The frontal surface of the chain will be negligible in all situation, when compared to the surface of the buoy, therefore $F_{drag_{chain}}$ is assumed to be zero.

$$F_{drag_{max}} = \frac{1}{2} C_T \rho V^2 S = \frac{1}{2} \cdot 0.024 \cdot 1025 \cdot 2^2 \cdot 10 = 0.5[kN] \tag{14.39}$$

In this equation, ρ stands for the density of seawater. V the current velocity, S the frontal surface area and C_T drag coefficient which is 0.024 [69]. The frontal surface area of the buoy in the water is 7 $[m^2]$. This is a multiplication between the buoy depth $h = 1.4[m]$ and the buoy diameter $d_{buoy} = 5[m]$, $1.4 \cdot 5 = 7$. Summing this with the additional weight surface results in S=10 [m], the mentioned buoy depth is drawn form the technical Catia drawing. The maximum current velocity is 1 [m/s] [70]. Multiplying this by 2 for the correction of the wave force gives: $V = 2[m/s]$. Substituting these values results in a drag force of $F_{drag} = 0.5[kN]$. Now the total horizontal force can be computed in extreme weather conditions. The drag force of the kite in extreme weather conditions is 13 [kN].

$$F_{x,anchor} = D_{extreme} + F_{drag_{max}} = 13 + 0.5 = 13.5[kN] \tag{14.40}$$

The effective force working on the chain is 13.5 [kN]. An other import chain strength parameter is the weight of the anchor. It should be possible to lift the anchor with the anchor chain since it should be possible to remove the anchor from the seabed. The exact chain dimensions will be discussed in the next section.

14.4.4 The anchor and chain dimensions

In this section first the weight of the anchor is determined together with the anchor chain length. Second the shape and finally the dimensions of he anchor are determined. Equation 14.31 and 14.33 are characteristic for the volume of the anchor. The angle α is an unknown, for now α is assumed to be 0 this can be done since the anchor chain will be long enough to meet this requirement. This can be done if the anchor chain has a larger length as the water depth which results in a parabola shape of the anchor chain. Substituting the values $F_{chain} = 13.5[kN] = 13500[N]$ and $\alpha = 0[deg]$ results in equation 14.42

$$F_{chain}\cos\alpha - 7000V = 13500 - 7000V = 0 \tag{14.41}$$
$$V = \frac{13500}{7000} \approx 2[m^3]$$

The most important aspect of the anchor is that it does not move. For navigation buoys a safety factor of 1.5 is applied [71] to the anchor volume. For the ground segment at least a safety factor of 1.5 should be chosen. Due to the fact a kite is continuously pulling on the buoy a safety factor of 2 is used, which results in an anchor volume of $2 \cdot 2 = 4[m^3]$.

Because the current force on the anchor is neglected the anchor should have an outline that has a low drag, therefore the anchor will get a cross-section of a trapezium, the bottom and top are circular. This is shown in figure 14.13 and figure 14.13.

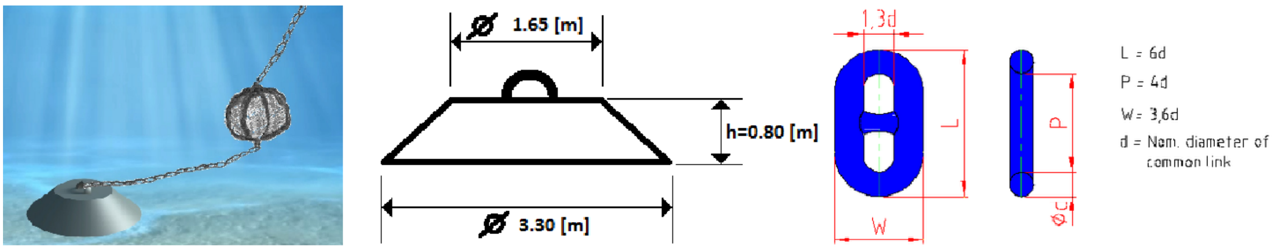

Figure 14.13: Underwater segment, layout and dimensions

The length of the chain must be longer than 20 [m] which is the largest depth at high tide. With increasing chain length the swing path increases. The swing path is the imaginary circle on the seabed where the buoy can be located as function of the chain length, the origin of the circle is the anchor. A swing path radius the same as the water depth results in $\alpha = 0$ [72], an assumption made previous. The corresponding chain length is $20\sqrt{2} = 28.3[m]$. Referring back to the previous subsection the chain should be able to deal with a anchor weight of.

$$F_{weight} = \rho_{concrete}Vg = 2400 \cdot 4 \cdot 9.81 = 94[kN] \tag{14.42}$$

With a safety factor of 1.5 on the chain strength [71], the anchor chain should withstand a force of 141 [kN] which corresponds to a chain thickness of d=19 [mm] steel [73], the dimensions of the chain are visualized in figure 14.13.

14.4.5 Underwater segment

This subsection will give a brief description of how the underwater segment looks like. Down from the buoy the anchor chain hangs down with the required weight of 65[kN] at its end. From the weight a second chain is hanging down and is attached to the anchor. With this configuration the buoy will be stable since the weight is keeping it up and the angle α is zero. The anchor absorbs all horizontal forces.

Chapter 15

Materials

In this chapter the materials that are used for the kite system are discussed. In section 15.1 the materials used for the aerial segment are explained. This is followed by section 15.2 which discusses the materials used for the tether. Finally, section 15.3 presents the materials used for the buoy and the anchoring system. Table 15.1 shows all relevant properties of the materials that are used for the kite system.

15.1 Aerial Segment

The aerial segment consists of three components. Namely, the structure of the kite, the bridle system and the control pod. The materials used for the kite are explained in section 15.1.1. The materials used for the bridle system are the same as for the tether, which will be discussed in 15.2. Section 15.1.2 deals with materials used for the control pod.

15.1.1 Kite

The materials used for the structure of the kite have to withstand aerodynamic forces and structural loads. Besides these, the material has to have a good UV-radiation resistance and in addition it has to be a sustainable material. Therefore Dacron is the most suitable material. Dacron is a woven material that is the main material to be used for the kite. Dacron is a Polyethylene Terephthalate (PET) polymer which has good resiliency properties, high abrasion resistance, high UV- resistance, high flex strength, high durability and low costs [74]. Furthermore, it has a good reputation and a lot of experience with the application of the material is present, because it is broadly applied for different purposes in the maritime industry, for example in sail cloths [75].

For the inflatable tube, Mylar is used. This is a polyester which is applied as a flexible, strong and durable film with properties making it suitable for many industrial applications. The excellent dielectric strength, moisture resistance and physical toughness make Mylar a very versatile and functional insulating material [76].

The UV-radiation plays a very important role in the life time of the kite. Although Dacron has a good UV-radiation resistance, it is preferable to protect it with an extra layer, to be sure that a life time of at least two years is guaranteed. As it is shown in table 15.1, a Tedlar film will be applied, using an adhesive, on the surface of the kite. Tedlar is supplied with both sides treated for adherability, to enable bonding to a wide variety of substrates. Treated surfaces have excellent compatibility with many classes of engineering adhesives, including polyesters, epoxies, rubbers and pressure-sensitive mastics [77].

Tedlar is the trade name of Polyvinyl Fluoride (PVF), which is tested in outdoor conditions for more than 30 years [78]. This material is tested to perform well in temperatures between -73 to 107 ° C, which obviously is in the range of temperature differences in the operational environment, namely OWEZ [79]. Furthermore it has an excellent hydrolytic stability, high dielectric strength and dielectric constant which are very preferable. This is because of the fact that the kite is continuously operational in outdoor conditions where, for example, thunderstorms can be expected.

15.1.2 Control Pod

The control pod is located at the intersection of the bridle lines and the main tether. The bridle lines lead from the control pod to the kite. The shell of this pod is waterproof and protects the electronic components against humidity and shocks. The framework of the control pod is made out of carbon fibre, a composite material. This is the same material as used for the control pod of SkySails [80]. A carbon fibre is a rubbery carbon material with good mechanical properties. For example, it is light in weight, has a high specific tensile strength and a high specific elastic modulus. Furthermore it has a good electric conductivity, heat resistance, low thermal expansion coefficient, chemical stability, self-lubrication property and high heat conductivity [81].

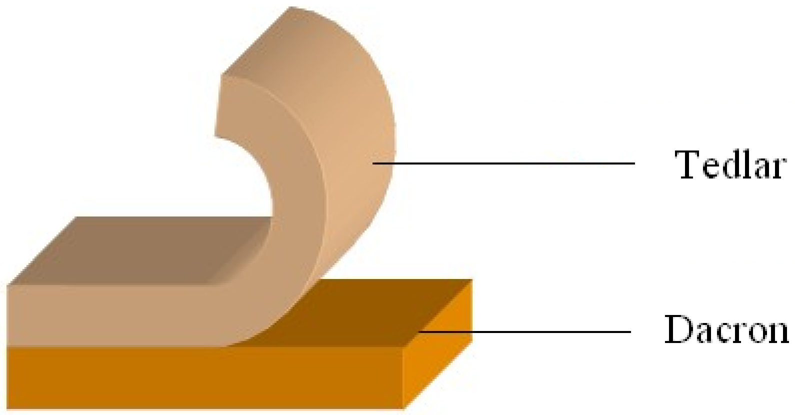

Figure 15.1: Dacron covered by Tedlar

The material that is used for the housing of the HMS, EOS, GPS and Gyroscopes and chips is also carbon fibre. No price is given for this materials in 15.1, since these components are Commercially Off-The-Shelf (COTS). The cost of these are discussed in chapter 22.

15.2 Tether

The material used for the tether, and the bridle lines, should be able to support the loads generated by the kite under tough conditions for a lifetime of 20 years. This puts some major requirements on the material to be used. The most important environmental conditions are the salty sea environment and humid conditions and the exposure to UV-radiation. A proven solution is the material Dyneema SK-78. This material is a standard in the maritime sector [82]. Dyneema, having a high strength and low weight, is the world's strongest fibre [83]. The Young's modulus of Dyneema is The density of Dyneema is 0.96 [kg/m^3], while the specific density of water is 1.0 [kg/m^3]. This makes the cable able to float when it falls into the water [84]. Also, Dyneema is a hydrophobic material and therefore does not absorb water. Furthermore, the material has good resistance to photo degradation and is chemically inert, which eliminates the need for protective covers. When looking at the aspects of using a winch for the tether retraction system, a Dyneema tether is highly suitable. Dyneema is 15 times stronger than steel wire and 8 times lighter than steel wire [85]. Opposed to steel wire, Dyneema does not loose its strength so it will not kink. This will simplify the design of the winch. Furthermore, Dyneema is able to resist overlapping, unlike steel wire which will crush and loose its strength if overlapped on the winch drum.

Also, safety is increased when using Dyneema. This material does not splinter like steel wire does, increasing the safety for the maintenance crew. The safety increase is however most noticeable in the unlikely event of the tether breaking. Dyneema has virtually no recoil, unlike steel wire where recoil is extremely dangerous.

15.3 Ground Segment

In this section the materials used for the ground segment are explained. The ground segment consists of three main parts, namely the mast, the buoy and the anchor. Section 15.3.1 explains the material used for the mast, section 15.3.2 deals with the material used for the buoy and section 15.3.3 explains the materials that are used for the anchoring system.

15.3.1 Mast

The material that is used for the mast is steel. This is an alloy consisting mainly of iron and carbon. This material is used in countless diverse applications due to its mechanical properties and the experience which is built up during many years of application. There are different types of steel available, hence the type used depends on what the purpose of the application is. In the kite system the important roles of the steel mast are to support the kite when it is inoperative and to transfer the bending loads while it is. It should be able to transfer these bending loads even under extreme conditions. The selected type of steel should have the right properties to withstand the salty seawater environment, meaning being corrosion resistant. Taken these requirements into account, the select type of steel alloy is A36. The composition of this alloy is 98.0 % Iron, 0.29 % Carbon, 1.0 % Manganese and 0.28 % Silicon, based on weight. The mechanical and thermal properties of this alloy are given in 15.1. Steel is largely applied in maritime industries because of its mechanical properties and corrosion resistance in seawater [86]. Besides for the mast, steel is used for the maintenance ladder of the buoy. Next, steel is used for the anchor chain. The mast, the maintenance ladder, and the anchor chain have similar requirements. Since all three deal with the same environment, the same type of steel can be used for all these components.

15.3.2 Buoy

The buoy is made of fibre glass. Besides fibre glass, steel is a possible candidate material which can be used for the ground segment. Steel is commonly used in maritime and offshore environments for a very long time. But comparing steel with fibre glass, steel has some disadvantages. Although steel has a good general corrosion resistance, it is vulnerable to pitting corrosion [87]. Suggest a buoy made of steel and it's protected layer is damaged during the maintenance procedure. This will cause corrosion in a salty an moist environment. Furthermore the steel is less sustainable as is explained in chapter 20. Fibre glass has a higher strength-to-weight ratio and is stronger than steel in lengthwise direction [88]. Therefore fibre glass is a better solution for the structure of the buoy. In table 15.1 the properties of the fibre glass used for the buoy are presented.

The question may arise why the mast is not made of glass fibre. This is mainly because of bending moments. Glass fibre is able to withstand very large loads when in tension, however steel has better properties in coping with compression loads. The mast is designed not to break when it experiences bending moments. Therefore the mast is made of steel. Furthermore, to improve the mechanical properties of the fibre glass even more, it has been reinforced with E-Glass mats. The E-Glass mats are 45 ° - directional mats. The process of applying these mats is explained in chapter 16. The properties of the E-Glass are shown in table 15.1. The protection edge, on the outside of the buoy hull, and the air pockets, which are positioned inside the buoy hull, are made of rubber. Reinforcement of the air pockets is not necessary since the air pressure inside the air pocket is equal to the surrounding air pressure. Just like other materials, the properties of this material can be found in table 15.1.

15.3.3 Anchoring System

The anchor system consists of two parts, a precast concrete block to keep the buoy on the predetermined position and a steel chain to connect the buoy with the concrete block. The chain is made of steel with the same properties as it is stated in section 15.3.1. Concrete is a composite material which consists of cement and other cementitious materials. For this application a precast concrete block is used. This is corrosion resistant and furthermore it can deal with heavy loads [89]. A concrete block is used for the anchoring because this material is relatively cheap.

15.4 Conclusion

During design, special attention has been given to the best harmony between cost, reliability, durability and the sustainability of these materials. To deal with these demands best, the materials used for the kite system are Dacron, Dyneema SK-78, Glass Fibre, rubber, steel alloy A36, Tedlar, Concrete and Carbon Fibre Composite. The properties of these are tabulated in 15.1.

Table 15.1: Materials

Material	**Part**	**Tensile Strength [MPa]**	**Yield Strength [MPa]**	**Modulus of Elasticity (longitudinal) [GPa]**	**Possion's ratio**	**Creep**	**Cost [$US/ kg]**	**density** [g/cm^3]	**elongation** [%]	**Thermal Conductivity [W/m K]**	**Thermal expansion coefficient** [10^-6K-1]	**Specific Heat [J/kg K]**
Dacron [61]	Kite	48.3-72.4	59.3	2.76-4.14	0.37-.044	-	5.5	1.35	30-300	0.15	117	1117
Dyneema SK.78 [84][90]	Tether	3000	-	110	0.3	< 4 %	130-160 ($US/m) Relative [91]	0.96	3-4	0.2	-12	1850
Glass Fibre [92]	Buoy	69	-	6.9- 17.3	0.35	-	4.2 [61]	1.04-1.46	< 2.6	0.17	5	710-920
Rubber (Styrene-butadiene (SBR)) [93]	Air pockets, Buoy protection edge	41-45	-	2.1-2.4	0.35	-	10 [61]	1.05	-	0,17	80	-
Steel Alloy A36 [61]	Mast. Anchoring chain	400-500	220- 250	207	0.3	-	1 [61]	7.85	23	51.9	12	486
Tedlar (Polyethylene Terephthalate (PET)) [78]; [61]	Coating of kite	55-90	34- 41	2.14-2.7	0.4	4%	3 ($US/ m^2) Relative [94]	1.37-1.72	90-250	-	0.67-0.97	1.01-1.76
Concrete [61]	Anchoring Block	282-551	-	25.4-36.6	0.2	-	0.06 [61]	2.4	-	1.25-1.75	10-13.6	850-1150
E-glass fibers-epoxy matrix [61]	Buoy	3450	-	72.5	0.22	-	3.7	2.58	4.3	1.3	5	810
Carbon Fiber Composite [95]	Control pod, HMS, EOS	110	-	18	0.77	-	-	1.33	2	-	2.15	-
Mylar [76]	kite (inflatable-tube)	234	-	5	-	-	14 ($US/ m^2) Relative	1.4	92	100	115	1170

Chapter 16

Manufacturing, integration and maintenance

In this chapter first the manufacturing processes are described in section 16.1. The focus is on the top level process steps, but also individual manufacturing processes are discussed. In section 16.2 the integration of the kites and buoys in the offshore wind farms is treated. Also onshore wind farms are discussed shortly. Lastly, in section 16.3 the maintenance is treated.

16.1 Manufacturing

Now the manufacturing of the aerial segment, the tether and the ground segment are explained. The emphasis is on how sub-assemblies are manufactured. Making the final assembly from these sub-assemblies is treated in section 16.2.

The Aerial Segment

The kite will be woven from Dacron fibres, as was stated in chapter 15. The manufacturing of the kites will be outsourced to companies in China, Vietnam or India. This is done since it is not profitable to invest in own equipment and contract own people, because the number of kites made for this application is relatively low. Furthermore there is much experience in these countries and almost all kites in the world are produced there [47]. To prevent using child labour, the child labour company list published by the American Bureau of International Labor Affairs [96] will be reviewed and all contracts with Asian companies will be checked by the Dutch Ministry of Economic Affairs in their child labour programme [97].

The companies to which the kite is outsourced start with creating the Mylar bladders that will form the inflatable tubes. To create one tube two Mylar sheets are used. One of the sheets has a hole in it, to which the pressurization ventil is bonded. Both sheets are cut, cleaned and degreased (pre-treatment). Then the two sheets are bonded to each other using adhesive. For this, first a primer is applied and then the adhesive is applied. After that, the bond is cured at an elevated temperature. An adhesive bond is used since it is airtight, has a long lifetime due to the absence of stress concentrations and is strong [98]. Since the adhesive bond is hard to access and repair, it will be designed with the safe-life philosophy. This will make sure that the bond does not fail.

Then the Dacron fibres are woven around the bladders, forming the kite. This is done using sewing machines, but also requires hand work. This is the reason why it is outsourced to experienced companies. During the weaving also the bridle lines are implemented in the kite. Weaving the bridle lines in the kite itself yields a strong link between the two. Once the weaving is finished, the Tedlar coating is applied to the outside. The coating is formulated with organic solvent and is processed at high temperatures [99]. This yields a Tedlar film with good weather resistance and a long lifetime.

The result is a fully manufactured kite with bridle lines and a separate control pod.

The Tether

The tether is manufactured from Dyneema and has an electricity cable inside of it, which supplies the control pod with energy. Figure 16.1 shows how the tether is created. The smaller Dyneema cables are braided over the electricity cable. This forms the thicker tether shown in the top of the figure. The result is a tether with the right length rolled on a spindle. This makes it easy to assemble it. The company Gleistein Ropes is specialized in this type of tether [10]. At first instance, the manufacturing of the tether will be outsourced to this company to lower initial investment costs of the project. At a later stage one might consider making the tether oneself, if this would yield larger profits. Also the leading edge line will be made from Dyneema. Here no electricity cable is needed, so this line is commercially off-the-shelf (COTS).

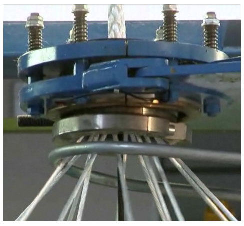

Figure 16.1: The manufacturing of a tether with an electricity cable inside it

The Ground Segment

The ground segment is manufactured in two phases. First the buoy structure is created, then the separate systems are attached to it. Manufacturing the buoy structure is done in a number of steps. These steps are described below and figures 16.2 and 16.3 give a visual representation. Note that since the buoy is made of glass fibre, this requires special manufacturing processes. First five components are made, which are then combined in a sub-assembly.

The first of the five components that is constructed is the hull. This is the bottom plate of the buoy together with the sides. This is done in the following eight steps:

1. **Constructing a wooden mould for the hull** A wooden mould that will determine the hull shape is constructed. It is made out of wood, since mould costs are then low and the series length is medium-sized, about 50 hulls can be made [98]. Preferably two craftsmen are needed to construct the mould in a precise manner, but keep costs low. Note that the draft angle of the hull eases removing the hull from the mould later. The mould should be well supported to withstand the loads from the vacuum bagging (which is explained at step 6).

2. **Placing the anchor chain ring** Once the mould is created, the ring to which the anchor chain is attached is placed at the bottom of the mould. The fibre glass can then be sprayed onto this ring to attach it to the hull.

3. **Applying glass fibres onto the hull mould** First a release film is applied to prevent sticking of the hull to the mould. A gel coat is often applied next to make the outer surface smooth. For this component no gel coat is applied, since it is not necessary to have a smooth outer surface. Now the glass fibres are applied onto the release film with a spray-up process. In spray-up a spraygun chops continuous glass fibre roving in a predetermined length between 10 and 40 [mm]. For this application a length of 30 [mm] is used, since this yields relatively long fibres, which are fit to withstand the loads in the large hull. The chopped rovings are mixed with resin inside the spraygun, this minimizes health hazards for the operators. The spray-up process is fast and uses inexpensive glass roving, so personnel and material costs are relatively low [100]. Once the spray-up is finished, the fibre glass is distributed nicely over the hull and into edges with rollers handled by the craftsmen. Once this glass fibre layer has hardened enough, glass fibre mats are applied using hand lay-up at certain locations (see figure 16.2), to reinforce the hull at these locations. The locations that need reinforcement were identified in chapter 14.

4. **Constructing the reinforcements for the bottom mast, the support pole and the ladder** The reinforcements for the bottom mast, the support pole and the ladder are created in the same way as the hull. First glass fibre is applied using spray-up and then nicely distributed with rollers. After that fibre glass mats are applied to reinforce the structure. The results are three "buckets" in which the mast, support pole and ladder can be placed later.

5. **Binding the reinforcements to the hull** Once the reinforcements have hardened enough, they are placed onto the hull and bound to it with flox. Flox is a mixture of resin and finely milled cotton fibres, which functions as an adhesive [101]. It is also commonly used for kit aircraft and gliders [102]. Fibre glass mats are also applied to bind the reinforcements to the hull. These mats will help transfer loads from the mast to the hull.

6. **Vacuum bagging of the hull** Now the hull shape is complete, the reinforcement-resin mixture is cured to form a composite component. This is done with vacuum bagging. Here a vacuum is applied to the

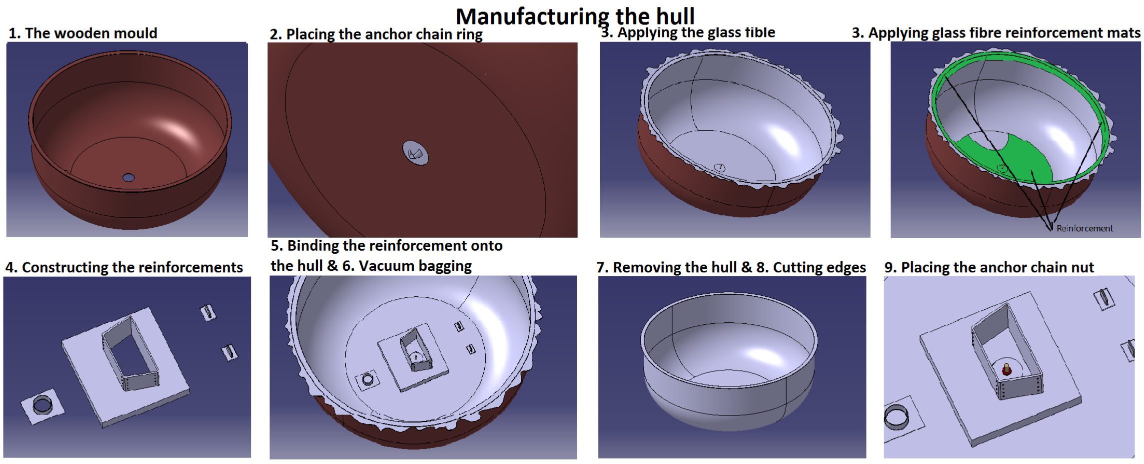

Figure 16.2: Manufacturing the hull in steps

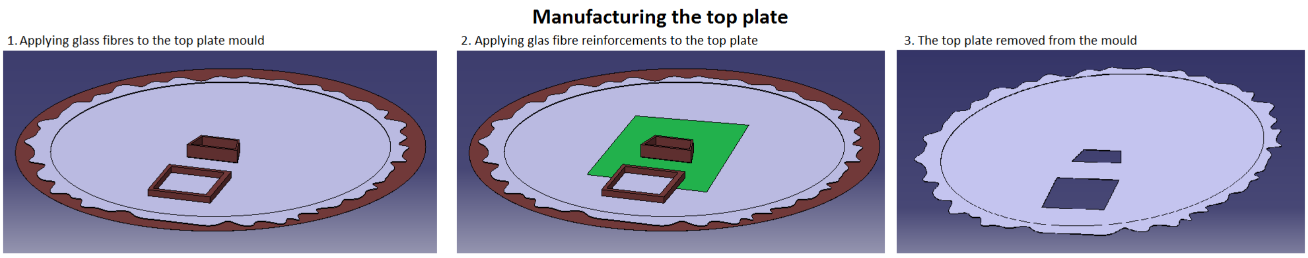

Figure 16.3: Manufacturing the top plate in steps

component, giving a pressure of 1 bar. This pressure speeds up the curing and lowers the void content, which yields better mechanical properties. In this process the hull is covered with several films. The hull is covered with peel-ply (to remove the other films after curing), release film (to minimize bonding between product and waist material), bleeder fabric (to store the excess of resin), breather fabric (to be sure that all air can flow to the vacuum pump) and a vacuum bagging film (to create a vacuum between the foil and the product) [98]. Note that vacuum bagging is used for curing, since it is a low-cost process which is not confined to one location (such as an oven). This makes it possible to create the hull close to the wind farm where it will be used.

7. **Removing the hull from the mould** Once the hull is fully cured, it is removed from the mould by ticking it out and lifting it out. The draft angle of the mould and the release film make it possible to easily remove the hull.

8. **Cutting the edges and smoothing them** The waist material is now cut from the edges and the edges are smoothed.

9. **Placing a nut to secure the anchor chain ring** A nut is placed to the bolt which is part of the anchor chain ring, to attach it firmly to the hull.

Secondly, the top plate is constructed. This is done in the following five steps:

1. **Creating a wooden mould for the top plate** This is done in the same manner as for the hull. The top plate mould is actually just a flat plate with upright parts to create the openings for the mast and the hatch.

2. **Apply glass fibres onto the top plate mould** This is also done in the same manner as for the hull. Figure 16.3 shows at which places fibre mats are placed to reinforce the top plate.

3. **Vacuum bagging of the top plate** This is also similar as for the hull.

4. **Removing the top plate from the mould** Again similar as for the hull.

5. **Cutting the edges and smoothing them** Again similar as for the hull.

Thirdly, the mast is created. This is done in the following five steps:

1. **Punching holes in the mast sheets for hatches** The mast is created from four thick metal sheets. In three of them openings are present to allow electricians to the electrical systems inside of the mast and to be able to bolt the mast to the hull. These holes are created in the sheets by punching. With this technique the sheet is placed on a die and the punch applies shear to the sheet, removing a slug from the sheet and thus creating a hole.
2. **Welding reinforcements around the holes** Since the mast is weakened by the holes, reinforcements are welded around these holes.
3. **Welding the mast together** The four sheets are then welded together to form the mast. The strong weld is watertight, which is necessary because of the electrical systems inside the mast.
4. **Welding the top plate reinforcement** The top plate reinforcement is welded together from separate thick metal sheets. This reinforcement joins the top plate and the mast, thus supporting the top plate.
5. **Bolting the top plate reinforcement to the mast** Once the top plate reinforcement is constructed, it is bolted to the mast. Using bolts makes it easy to remove the reinforcement during maintenance or repair.

Fourthly and fifthly, the support pole and the ladder are created. This is done in the following two steps:

1. **Weld a support plate to a commercially off-the-shelf (COTS) circular pole** A support pole is located between the hull bottom and the top plate right under the location of the main winch. This is to transfer the loads resulting from the weight of the winch. A circular cross-section, metal, COTS support pole is used for this. One end of the pole can be sunk in the reinforcement already located in the hull. The other end holds the support plate to which the top plate is attached. This support plate is welded to the pole.
2. **Weld a support plate to a COTS ladder** A ladder is present between the top plate and the hull to allow maintenance people to enter the hull through a hatch. The ladder also transfers a part of the weight of people on the top plate. A support plate is also welded to the ladder and the ladder can be sunk into the reinforcement already located on the hull.

Now all components are finished and are assembled to form the ground segment sub-assembly. Assembling the components is done in a dry dock This is done in the following four steps:

1. **Bolting the mast, support pole and the ladder to the reinforcements on the hull** The mast, support pole and ladder are sunk into the reinforcements which are already present on the hull. Then bolt holes are drilled. Note that a different drill is needed for the metal and for the composite parts. Once the holes are drilled, the holes may be honed to create a smooth surface, but this is not necessary. Finally bolts are placed and tightened. For the mast this is done through a hole in the mast. For the support pole and the ladder a bolt simply runs through the whole piece, so no openings are needed (since both the bolt end and the nut can be reached from the outside). Using bolts allows easy maintenance and repair.
2. **Placing the rubber air pockets in the hull and fixing them with cables** Four large rubber air pockets are placed in the hull and inflated. They are loosely attached with cables, to fix them to their positions. This must be done at this stage, since in the next step the top plate is fixed to the hull.
3. **Bolting the top plate to the hull** Now the top plate is placed on the hull and bolt holes are drilled through the top plate and the rim of the hull. Once this is done, the bolt holes are honed, to create a smooth and more watertight surface. Then bolts are placed to attach the two to each other. Using bolts again allows easy maintenance and repair.
4. **Placing bolts between the top plate and the mast, support pole and ladder** Finally the mast, support pole and ladder are fastened to the top plate with bolts. Again first the holes are drilled and honed. Then the bolts are placed.

Now that the sub-assembly is finished, the separate systems are added. The following systems are installed in the given order:

1. **Ladders** A COTS ladder is installed to the mast to allow inspection and maintenance of the mast. Also two COTS ladders are installed to the sides of the buoy for the case someone falls off the buoy at sea.
2. **Hatches** The hinge and hatch are bolted to the top plate to cover the opening to the hull. Also hinges and hatches are placed on the openings in the mast, used for bolting and access to the electrical systems inside the mast.

3. **Pulleys for the leading edge line** The leading edge line runs from a winch on the top plate, via the top of the mast to the leading edge of the kite. Several pulleys are installed on the mast to lead the line in the right path.
4. **Alert lamp** An alert lamp is placed on the top of the mast.
5. **Winches** Two winches are bolted to the top plate. For this first bolt holes are drilled. The main winch retracts the main tether and the secondary winch retracts the leading edge line.
6. **Fender** A large fender is installed over the rim of the buoy at the side to which ships moor. This is at the side of the kite to allow easy kite to buoy assembly.
7. **Mooring bollards** Three mooring bollards are bolted to the top plate. For this first bolt holes are drilled. The mooring bollards are located at the same side as the fender. One bollard keeps the ship close to the buoy, the other two prevent forward and backward movement of the ship.
8. **Electrical systems** The electrical systems and wiring are then installed by the electricians. Most electrical systems are inside the lower part of the mast, but wiring to the two winches, to the main tether, to the solar cells and to the alert lamp is also needed.
9. **Solar cells** Once all systems are placed, the electricians which just installed the electrical systems install the delicate solar cells. This is the last step of this sub-assembly to prevent damage to them.

Now the buoy sub-assembly is finished. This sub-assembly goes on the final assembly and integration.

16.2 Integration

In this section the assembly and the integration of the kite system is discussed. The input for the assembly and integration is given by the previous section: manufacturing. The buoy, the anchor, the anchor chain, the kite, the tethers and the control pod are up to this point separate parts with respect to the final assembly. For the installation of the kite system first the buoy is installed and secondly the kite.

16.2.1 Ground segment

The assembly and integration of the ground segment can be split up in three stages, first the preparations, second the transport to the wind farm and finally the installation. The preparation is a very important aspect, since a good preparation reduces integration costs. Up to this stage the buoy is still at the dry dock. Below, the preparation phase is listed, for this phase the anchor, the anchor chain, the main tether, the leading edge line and the buoy itself are included. The preparation:

1. The main tether and the leading edge line are winched up onto the winch on the buoy.
2. The anchor chain is attached to the buoy, the attachment is located at the lower side of the buoy. The loose outer end of the anchor chain is temporarily attached to the upper side of the buoy. The reason for installing the chain to the buoy at the dry dock is because when the buoy is already in the water the attachment is under water which would increase installation costs since divers are required.
3. All buoys are prepared and put in the water. All buoys are tied up and a train formation is created. Each buoy contains mooring bollards for this attachment.

The transportation is performed with a boat. To make the transportation as efficient as possible, the buoys will be placed in train formation behind each other and are towed behind the boat. Depending on the capacity of the ship the amount of ground segments can be determined, a total of 23 kite systems are required for the OWEZ wind farm as stated in section 11.3. Small cargo ships with a crane can transport 8 ground segments and have a sufficient lifting capacity to lift the anchors [103]. The transportation:

1. Hoist the anchors on the boat.
2. Attach the buoy train formation to the boat.
3. The boat with the train structured buoys and the anchor on the deck is transported to the wind farm

The installation of the ground segment has to be performed precise, since the location of the anchor determines the location of the kite within the wind farm and thus influences the performance of the system. The installation:

1. The loose end of the anchor chain is attached to an anchor. With this attachment the ground segment is finalized and is only to be placed on the seabed.
2. The anchor is lifted of the deck an is placed on the exact location

16.2.2 Aerial segment

The assembly and integration of the kite can be split up in two phases, first the preparation and second the installation. The aerial segment contains the control pod and the kite. When the kite is installed onto the buoy the kite system can be activated and is ready to use. Below the assembly and integration is listed. The kite and the control pod are supplied apart from each other and first have to be assembled. In this phase, the kite tubes are deflated and for this reason the kite is not rigid which is preferable for transport in a later stage. The preparation:

1. Attach the bridle lines to the attitude controls in the control pod.
2. Attach the pressure regulation system to the kite tubes
3. Attach the GPS to the kite.

The transport of the kite to the wind farm is performed by boat. During transportation the kites are kept deflated. When the boat arrives at the wind farm the second assembly and integration phase will be performed. Note that during this phase it is preferred to have no wind. The installation:

1. The aerial device is attached to the main tether and to the leading edge line. This is done by connecting the electrical wire of the main tether to the electrical devices in the control pod and the Dyneema outer cable to the load carrying structure of the control pod. The leading edge line is directly attached to the center point of the leading edge of the kite.
2. The control pod contains the pressure regulation system which regulates the pressure in the tubes of the kite. In this stage of the installation the kite hangs deflated to the mast. As stated in chapter 5 a pressure reservoir is used to regulate the pressure in the tubes, in this case because the kite is not in operation, it is preferable to pump up the kite with a compressor to not loose unnecessary reservoir pressure. When the kite is fully pumped up the pressure reservoir is installed.
3. With the previous step the kite system is ready to use, all electrical devices on the buoy and in the control pod are activated.

16.2.3 Integration Gantt chart

The above discussed assembly and integration will be visualized in this section. A Gantt chart is given for the integration phase. The installation of the 23 kite systems will take 30 days. In figure 16.4 this can be seen, as discussed above the integration can be split up in three phases: The preparation phase, the transportation phase and the installation phase. The preparation phase is significantly the most time-consuming phase. The reason for this is that one day of installation is way more expensive than one day of preparation, due to the fact that a boat is required. Therefore it is important that the installation phase is kept as short as possible.

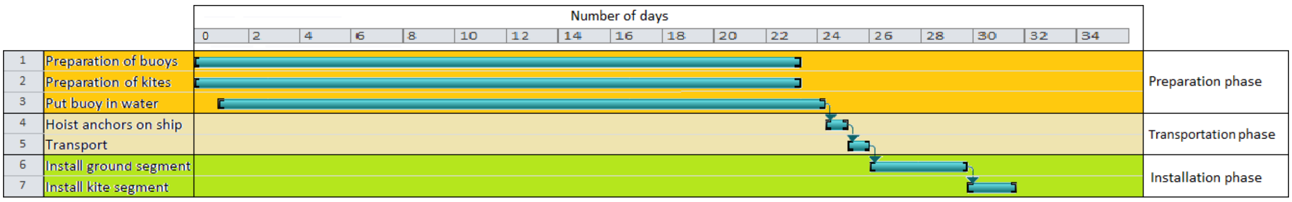

Figure 16.4: Gantt chart of the integration of the Daeolus kite system

16.3 Maintenance

In this section the maintenance of the kite system is discussed. The maintenance can be split up in three parts: the aerial segment, the tether and the ground segment. These segments have different maintenance requirements. In chapter 9 the risks per part are discussed in the risk tracking table: table 9.1. This map is the driving table for the inspection which will result in maintenance. In the first column the part can be seen, the next column displays risk an thus where attention should be paid to during inspection. The final column states how the possible error or failure can be fixed. This section will discus what type of degradation could be present and how it can be recognized in the same order as stated in the risk tracking table. Next to what is stated in table 9.1 some extra important parts have to be inspected and maintained which are not mentioned in the table.

1. *Skin*:
   - Rupture
     - Ripped
   - UV-degradation
     - Kite skin gets dull colour
     - Skin becomes more rough and begins to flake
     - When rubbed between hands does not make cracking sound
     - Skin looses strength, can easily be ripped
   - Bird/hail/rain collision
     - Small holes in kite skin
2. *Inflatable tubes*:
   - Leaking
     - Kite tubes are soft, tends to flutter or flapper in wind like a flag
     - Empty gas cylinder, in case of leaking pressure regulation system
   - Rupture
     - Small undetectable hole in Mylar (kite should be check)
     - Large hole in tube, also Dacron is ripped
3. *Pressure regulation system*:
   - Corrosion
     - Kite tubes are soft, tends to flutter or flapper in wind like a flag
     - Kite lost its form and lift, lays in the water
   - Over pressure
     - Tapping the tube results in noticeable high sound compared
     - Pressure relief valve is broken: corroded, salt layer
4. *Main tether*:
   - Breaking
     - Aerial device is in the water
   - UV-degradation
     - Tether gets dull colour
     - Begins to flake
5. *Bridle System*:
   - Breaking
     - Kite flutters of flappers like a flag
     - Kite is in the water
     - Kite is making uncontrolled manoeuvres
   - Entangling of tethers
     - Kite is making uncontrolled manoeuvres
     - Kite is in the water
   - UV degradation
     - Bridle gets dull colour
     - Begins to flake
6. *ACS*:
   - Control pod malfunction
     - Kite is making uncontrolled manoeuvres
     - Kite is in the water
     - No data form ACS to HMS
   - Failure of position monitor
     - Incomplete data transfer to HMS
     - Kite is in water
   - Corrosion
     - Late correction of kite manoeuvres
     - Excessive corrections to kite manoeuvres
   - Power feed failure
     - Broken electrical wires
     - No data transfer from ACS to HMS
     - Kite is in water
7. *Tension meter*:
   - Corrosion
     - Limited data transfer to HMS
8. *Leading edge line*:
   - Breaking
     - Line is in water
     - Aerial segment is loosely attached to the ground segment
   - UV-degradation
     - Tether gets dull colour
     - Begins to flake
9. *Electricity cable*:
   - Breaking
     - No energy supply to sub-systems
10. *TRS*:
    - Electric motor fail
      - Kite can not be retracted in case of positive power input
    - Corrosion
      - Materials degradation
      - Anti corrosion layer is damaged
    - Power feed failure
      - No power input to TRS
11. *Anchor chain*:
    - Breaking

  - Buoy is not at its initial location
- Corrosion
  - Material degradation
- Boat collision
  - Buoy is not at its initial location

12. *Rubber floats*:
    - Leaking
      - Hole in floater
      - When exposed to bright light, hair cracks can be seen on glass fibre structure
      - Water in floater
    - Corrosion
      - Degradation of material
13. *Battery*:
    - Failure
      - No output power
      - Power input does not result in power output
    - Unloaded
      - No power output
      - Power input results in power output
14. *Solar cells*:
    - Failure
      - No power output during sun exposure
    - Obstructed by foreign object
15. *EOS*:
    - Antenna failure
      - No data output
    - Data processor failure
      - No data output
16. *HMS*:
    - Failure
      - No output commands in extreme weather conditions
      - No reaction after reset
    - Power feed failure
      - No input power
17. *Mast*:
    - Corrosion
      - Material degradation
    - Breaking
      - No power generation and supply to electrical systems
      - Mast detached from floater
18. *Buoy structure*:
    - Breaking
      - No power generation and supply to electrical systems
      - Mast detached from floater
19. *Anchor*:
    - Corrosion
      - Material degradation
    - Breaking
      - Buoy is not at its initial location
    - Boat collision
      - Buoy is not at its initial location

Next to the parts stated above: the buoy and the winches need extra inspection of the following sub parts.

The winch requires some extra inspection of the next three points: First the attachment between the reel and the tether, the tether is stuck through the reel with a hole and comes out at the opposite side. At this location the tether should not display any form of leeway. The second inspection aspect is that the reel should contain at least 12 windings in all situations. Third the brakes of the winch are inspected on effectiveness and corrosion.

Chapter 17

RAMS

In this chapter, a reliability, availability, maintainability and safety (RAMS) analysis is made for the kite system. The reliability will be explained in section 17.1, the maintainability in section 17.2, the availability in section 17.3 and finally the safety will be explained in section 17.4.

17.1 Reliability

This section describes the reliability, which is the ability of a system to perform its function. This reliability can be improved by using different design principles, namely:

- Safe-life: A certain part is designed to last for the lifetime of the particular subsystem, i.e. 2-20 years. The advantage is that the probability of a failure is reduced drastically and no or only little maintenance is required. The disadvantage is that the part is over-dimensioned and is therefore more expensive and adds weight to the structure. Even if the part is performing well at the end of its lifetime it is replaced.

- Fail-safe: A certain part is designed to cause no real harm to the rest of the system if a failure occurs. Either the part is made redundant or the working of the system is made redundant as is explained in section 9.1.2. A failure of a part should not lead to a catastrophic failure of the entire system. The worst outcome should be the retraction of the device, after which maintenance needs to be performed.

Table 17.1 shows the different subsystems with their associated design principle. The different subsystems are further elaborated in chapter 5. The design principles are assigned to the different subsystems, using common sense and looking at the subsystem requirements, to be fulfilled.

In general it can be stated that in order to make the kite system as reliable as possible, the possibility of using standardised or commercially off-the-shelf (COTS) parts should be considered, because they have proven reliability performance and their behaviour is easier to predict. The subsystem that has the shortest lifetime is the kite itself. After two years of operating, it needs to be replaced.

Figure 17.1 shows a Fault Tree Analysis (FTA). From this figure the effect of a failure of a subsystem to the working of the total system can be derived. Again, the reliability of the system is increased by redundancy in design, as can be seen from the 'and' gates in the figure. The 'or' gates, on the other hand, tell that only one of the conditions below has to be fulfilled in order to fail the function above. If, for instance, the skin is ruptured, the kite fails and therefore the primary function is not performed. If, however, one of the solar cells fail, there are many other to perform the primary function of the device.

17.2 Maintainability

Maintainability describes the ease, safeness and effectiveness of maintenance actions. As stated in section 17.1 the kite is the subsystem, which has the shortest lifetime. After two years it has to be replaced. This is the moment at which overall scheduled maintenance will be performed. When this is done, it should be clear to the maintenance people what actions to take to make sure that the kite can continue operation. This has to be done in a safe manner, so maintenance people are not exposed to danger. The quicker and more effective the maintenance is performed, the lower the costs are. The maintenance procedures are further elaborated in chapter 7, showing in the logistics chart and in section 16.3. It is likely that the maintainability evolves throughout the lifetime of the kite system, since at this time only little experience is present, while there will be a learning curve by the repeating character of performing maintenance.

The kite system will operate continuously throughout the two years without maintenance. Only when the

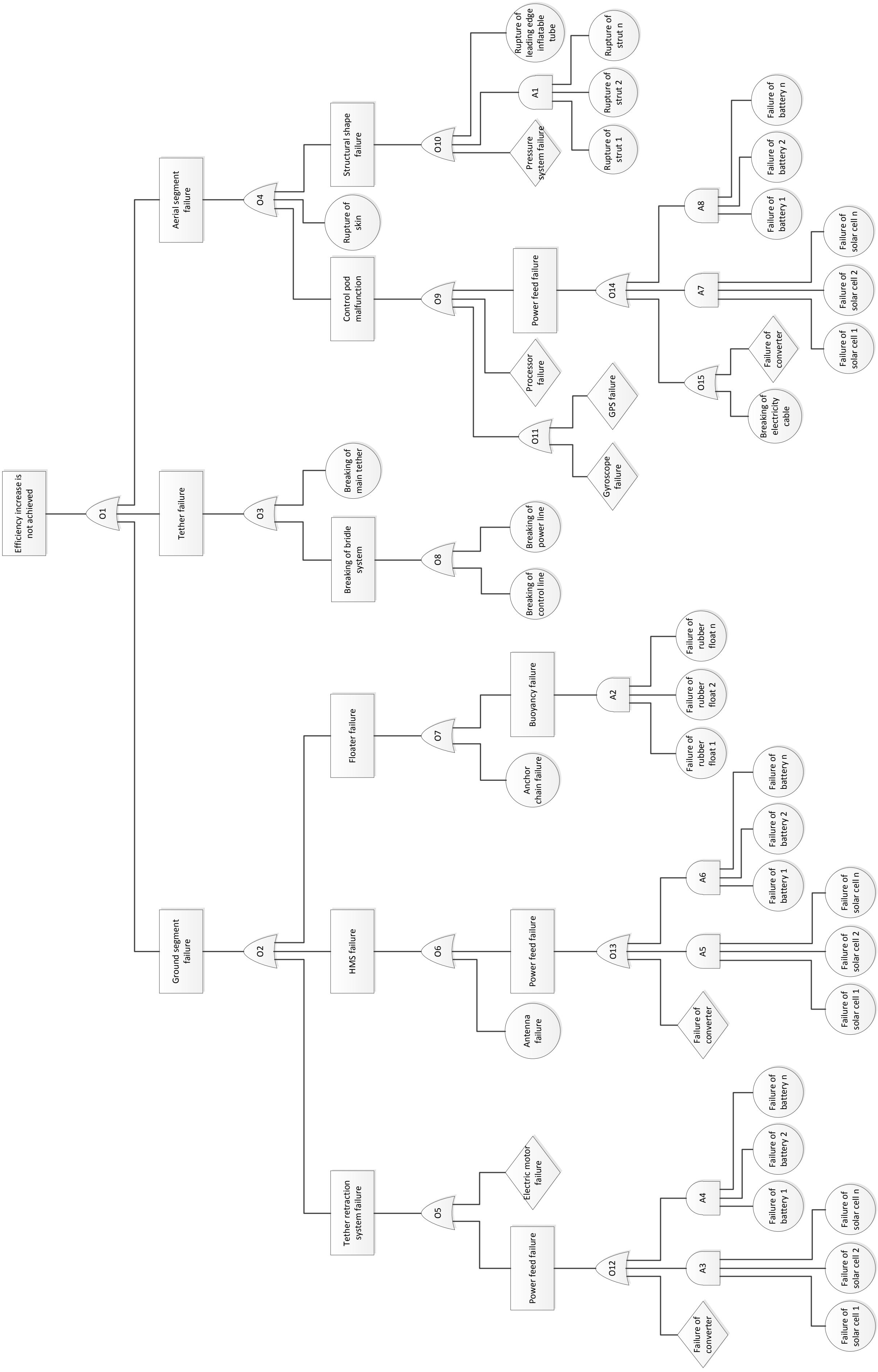

Figure 17.1: Fault Tree Analysis

Table 17.1: Design method

No.	Subsystem	Safe-life	Fail-safe
1.	Anchor	•	
2.	Anchor chain	•	
3.	Rubber floats		•
4.	Antenna	•	
5.	Solar cells		•
6.	Batteries		•
7.	Electric motor	•	
8.	Winch	•	
9.	Mast	•	
10.	Main tether	•	
11.	Electricity cable	•	
12.	Gyroscopes	•	
13.	Tensionmeter		•
14.	GPS	•	
15.	Bridle system	•	
16.	Skin		•
17.	Inflatable tubes		•
18.	Gas cylinder	•	
19.	Pressure tubes	•	
20.	Buoy structure	•	
21.	Leading edge line	•	

wind velocity increases above or reduces below a certain level, the system is inoperative. However, this is not considered here, as also the wind turbines are unavailable at this time. After these two years, maintenance will be performed, after which the kite will continue operating for another two years.

To increase the maintainability of the system, different measures are taken:

- A cage ladder is installed on the mast to reach the top and perform maintenance in a safe manner.
- The kite can be retracted to buoy level and is attached to the top of the mast using the leading edge line.
- The retraction of the kite can be started manually.
- Maintenance people can use the present energy source for their tools.
- Light is present for maintenance and collision avoidance.
- All subsystems are easy accessible and within arm reach from the cage ladder.
- Replaceable subsystems are lightweight.
- Safety hooks can be attached to different spots on the buoy.
- Anti-slip pattern and drainage holes are present.
- A ladder is present on the side of the buoy in case maintenance people fall into the sea.
- A rescue buoy is present in case maintenance people fall into the sea.
- Mooring bollards, which are used to secure the boat, are present .
- A fender is present where the maintenance boat will dock to prevent damage to the buoy and boat.

All aforementioned measures are meant to increase the ease, safeness and effectiveness of maintenance actions.

17.3 Availability

The availability can be explained using operational availability, which is strongly related to the reliability, and downtime, which is strongly related to the maintainability. Availability can be seen as the result of reliability, as explained in section 17.1, and maintainability, as explained in section 17.2. Also maintenance is considered, as is described in section 16.3.

The availability can be described using the Mean Time Between Maintenances (MTBM) and the Mean Time To Maintain (MTTM). As stated in section 17.2, the MTBM equals two years or roughly 17000-18000 hours. The MTTM can be approximated to be 4-6 hours per kite system. Multiple kite systems can be maintained at the same time, adding up to a total maintenance time of 4-5 workdays, or 80-104 hours, taking into account the nights.

Inserting the values for the MTTM and MTBM from in equation 17.1 yields the availability:

$$A = \frac{MTBM}{MTBM + MTTM} \tag{17.1}$$

From equation 17.1 it follows that the availability of each kite system equals more than 99

17.4 Safety

In this section the safety of the kite system is discussed.

Firstly, a safe work environment is important during installation of the device. The workers should have clear descriptions of the installation plans. Furthermore they should wear protective glasses, helmets, gloves and suits. These are preconditions, however also attention is paid to the safety during installation of the system itself. The buoy is assembled on shore. This means there is a stable surface on which the different complex and potentially unsafe parts are installed. The final installation in the wind farm is only considered with the deployment and anchoring of the buoy and the attachment of the kite to it. This is done when the weather and sea are calm and there is a clear visual. The attachment of the kite is done by climbing the cage ladder, while being secured to the buoy.

Secondly, a safe system is very important during maintenance. When maintenance is performed, people are in a potentially hazardous position. The buoy is moving, as the sea is moving. The buoy is slippery as it is wet. These are only examples of critical aspects for which measures are taken, to reduce the risks for maintenance people. Section 17.2 deals with the most important of these safety issues, resulting in more easy and more safe maintenance operations.

Finally, the system should be safe to retire. No toxic waste material is present. The system, when it is shut down, has no moving parts. The kite is detached in the same manner as it was installed in the beginning of its life. Afterwards the buoy and anchoring can be hoisted onto a transport vessel. On shore it can be disassembled further.

Chapter 18

Configuration of the Aerial Segment

In this chapter the configuration of the aerial segment is presented. The aerial segment consists of the kite and bridle system, which are treated in section 18.1, and the control pod, which is treated in section 18.2.

18.1 The Kite

In this section the lay-out of the kite is presented. The kite is seen here to consist of the actual kite and the bridle lines running from it to the control pod (which is described in section 18.2). The lay-out was mainly determined by the aerodynamics (chapter 10), the performance (chapter 11), the structural characteristics (chapter 13) and the control (chapter 12) of the kite. Now first the kite itself is discussed. Thereafter the bridle system is discussed.

The kite is shown in figure 18.1. As can be seen, an inflatable leading edge is present, which bends backwards to a chordwise direction. From this leading edge, seven inflated struts run in chordwise direction. The leading edge and struts transfer the main loads, and for this reason, the bridles are attached at the leading edge - strut connection or to the leading edge. The membrane is present between the struts and leading edge to close the kite and yield the aerodynamic shape, leading to the efficiency increase.

Figure 18.2 shows the bottom view of the kite. The dimensions are given in the figure: the projected span is 16 [m] and the chord is 8 [m]. Furthermore, the distance between each two struts is 2 [m]. Not given in the figure is the strut diameter, which is 0.50 [m]. Figure 18.3 shows the right view and figure 18.4 shows the front view of the kite. In these two figures, the dimensions are given as well. The projected span is 16 [m], but the flat span is 19 [m]. In figure 18.4 a VLEC length is given. Here VLEC stands for the Vertical Distance due to the Leading Edge Curvature. In words, this means that the outer points of the kite are lower than the middle of the kite, due to the bow shape of the kite. The front view also shows the bridle system. This will be discussed next.

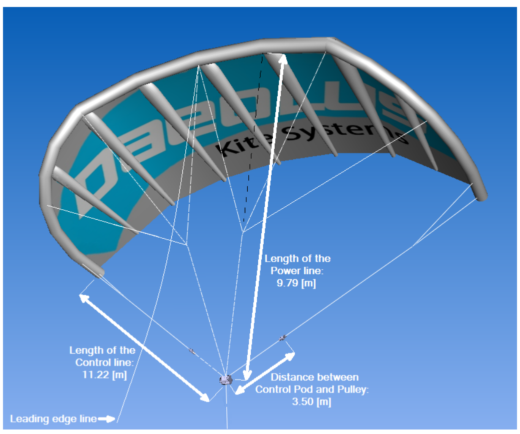

Figure 18.1: Three-dimensional view of kite

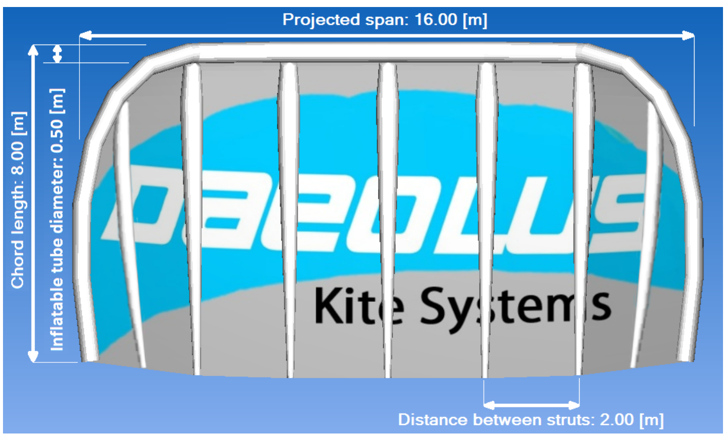

Figure 18.2: Bottom view of the kite

Now the bridle system is discussed. In figure 18.4, the lengths of the different lines are given. Note that the projected lengths are given: the line height (vertical), line width (spanwise) and line depth (chordwise). Distinction should be made in this chapter between the three-dimensional *length* l and the two-dimensional

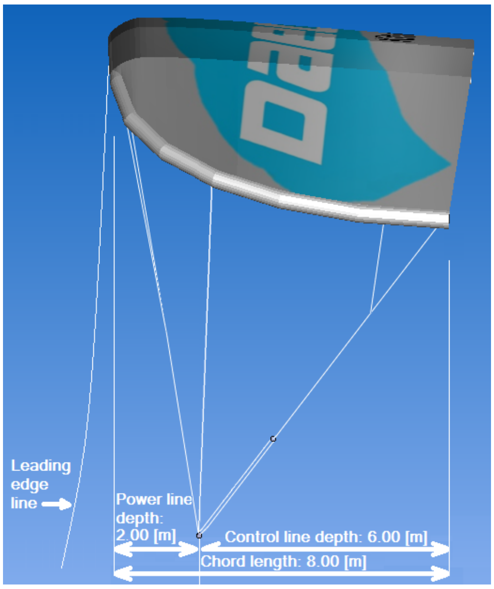

Figure 18.3: Right view of the kite

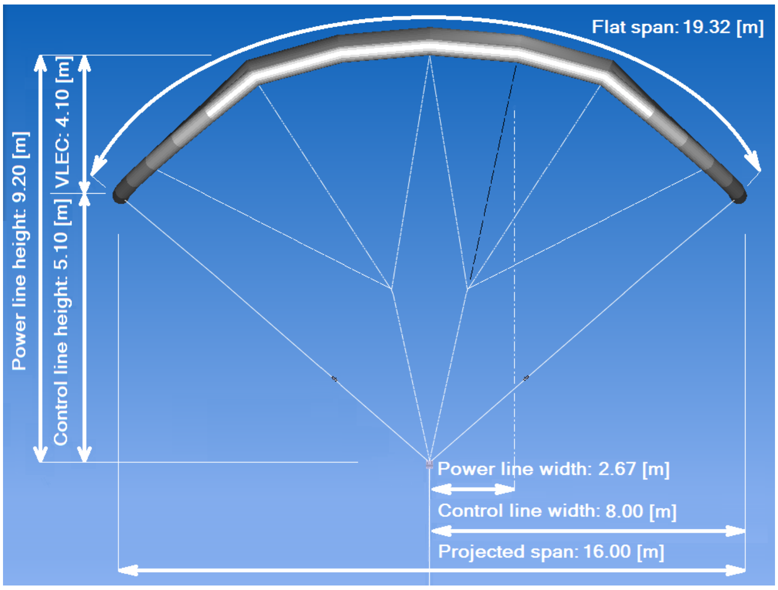

Figure 18.4: Front view of the kite

height h, width w and depth d. Two types of bridle lines can be distinguished. Firstly, there are the power lines (subscript pl), which are attached to the front of the kite and remain taut during operation. Secondly, there are the control lines (subscript cl), which are attached more to the back of the kite and can be pulled at to control pitch and roll. More information about the lines and the control is given in chapter 12. The goal of the bridle lines is to control the kite and to distribute the forces to more points on the leading edge. Disadvantages of a complex bridle system are the drag of the lines and the chance of strangling.

The lengths of the bridle lines are designed in a stepwise manner. The main design constraint is the fact that the bridle lines should not sag during normal operation nor when the kite is suspended on the mast. Now the steps in which the bridle system is designed are presented. Simple sketches are used to visualize the design steps.

1. Power line length: The power lines cannot be retracted by the control pod: their length is fixed. The first step is to design these lines. This is done for the case when the kite is suspended on the mast. Figure 18.5 shows this situation. Since the control pod cannot be rolled onto the winch and since it is preferable for control to have a large distance between kite and control pod, it assumed that the control pod will be just on the winch, when the kite is suspended on the mast. This assumption is fixed in the design and this allows the power line length to be determined. The figure shows that the suspended power line height $h_{pl,suspended}$, the vertical projection of the line length when the kite is suspended, is 9.41 [m]. Figure 18.5 shows that the chord c is 8.00 [m], that the winch width w_{winch} is 1.00 [m], that the mast length l_{mast} is 10.00 [m] and that the winch height h_{winch} is 1.00 [m]. From geometric considerations, equation (18.1) was constructed and used to calculate this value. The power line length l_{pl} can now be determined with equation (18.2) (simply Pythagorean theorem) using the power line width w_{pl}. This power line width is 2.70 [m], as found by the computer program Surfplan [104], which can define these lengths by calculating distances from the fact that the lines should be taut. This results in a power line length of 9.79 [m].

$$h_{pl,suspended} = c + \sqrt{w_{winch}^2 + (l_{mast} - c - h_{winch})^2} = 8.00 + \sqrt{1.00^2 + 1.00^2} = 9.41 \quad [m] \tag{18.1}$$

$$l_{pl} = \sqrt{h_{pl,suspended}^2 + w_{pl}^2} = \sqrt{9.41^2 + 2.70^2} = 9.79 \quad [m] \tag{18.2}$$

2. Operational power line height: Now the (projected) power line height during operation, $l_{pl,operational}$ can be determined. Figure 18.6 shows how this was done. From geometry and the Pythagorean theorem, equation (18.3) was determined. The power line width w_{pl} was found to be 2.70 [m] using Surfplan. The power line depth d_{pl} was determined to be 2.00 [m]. This means that during normal operations, when looked upon from above, the control pod is at a quarter chord from the leading edge. This point was chosen since the resultant lift force acts approximately at this point (see chapter 10) and having the control pod under this point is advantageous for the force transfer through the main tether. Using this and equation (18.3) yields an operational power line height of 9.20 [m]. This value can also be seen in figure 18.4.

$$l_{pl}^2 = w_{pl}^2 + d_{pl}^2 + h_{pl,operational}^2 \implies 9.79^2 = 2.70^2 + 2.00^2 + h_{pl,operational}^2 \implies h_{pl,operational} = 9.20 \quad [m] \tag{18.3}$$

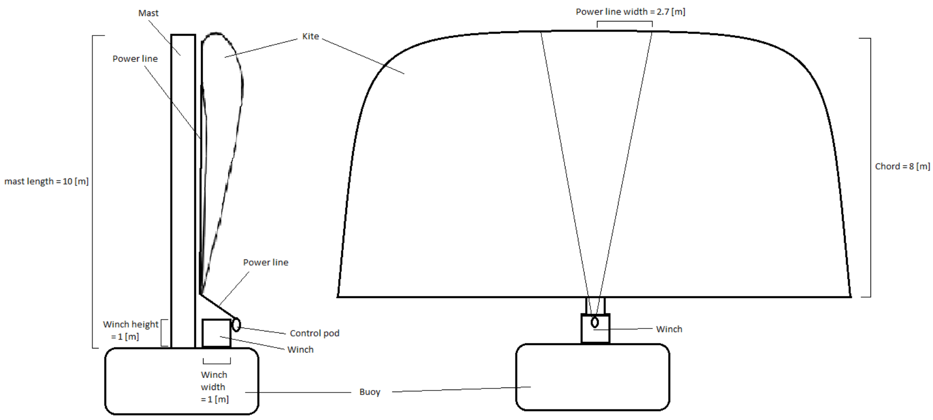

Figure 18.5: Determination of the power line length

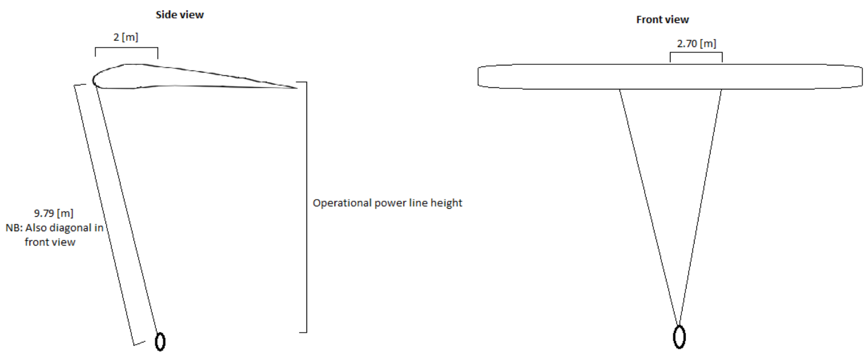

Figure 18.6: Determination of the operational power line height

3. Operational control line length: Now that the control pod location is defined with respect to the kite, the length of the control lines during operation, $l_{cl,operational}$, can be calculated. The length of the control lines is adjustable (in order to control the kite), but here their length is calculated for when the kite is horizontal. This is done using the Pythagorean theorem again, which is shown in equation (18.4). The operational control line height is equal to the operational power line height minus the vertical distance between the middle leading edge and the outer trailing edge (due to the leading edge curvature). The operational power line height was 9.20 [m], the vertical distance between middle and outer trailing edge (VLEC in figure 18.4) is 4.10 [m], so the operational control line height $h_{cl,operational}$ is 5.10 [m]. The control line width is equal to half the kite span, since the control lines are attached to the outer points and the control pod is in the middle. This gives a control line width w_{cl} of 8.00 [m]. The control line depth d_{cl} is 6.00 [m], since the control pod is at a quarter chord from the leading edge, so three quarters of chord from the trailing edge. A chord c of 8.00 [m] thus yields this value. Using equation (18.4) this yields an operational control line length of 11.22 [m].

$$l_{cl,operational} = \sqrt{h_{cl,operational}^2 + w_{cl}^2 + d_{cl}^2} = \sqrt{5.10^2 + 8.00^2 + 6.00^2} = 11.22 \quad [m] \tag{18.4}$$

4. Suspended control line length: When the kite is suspended on the mast, the control line length is reduced by the control pod to its minimum value. This is needed since when the kite is suspended on the mast, its trailing edge is quite close to the winch, where the control pod is located. To prevent sagging, the control line length is reduced. Figure 18.7 shows the geometry of the control line when the kite is suspended. Using the Pythagorean theorem again, the suspended control line length $l_{cl,suspended}$ is found to be 8.12 [m], using equation (18.5). In this equation the span b of 16.00 [m] is used.

$$l_{cl,suspended} = \sqrt{(b/2)^2 + w_{winch}^2 + (L_{mast} - c - h_{winch})^2} = \sqrt{8.00^2 + 1.00^2 + 1.00^2} = 8.12 \quad [m] \tag{18.5}$$

In chapter 12 it was explained that the control line includes two pulleys, which are pulled at when the kite is steered. These pulleys cannot be retracted by the control pod in case the kite is suspended on the mast. Since the control line length is 8.12 [m] when the kite is suspended on the mast, the distance from the pulleys to the kite may not be longer than this 8.12 [m] (since this would mean the pulleys are retracted into the control pod, which is not possible). The amount of control line that is retracted by the control pod is equal to the operational length (11.22 [m]) minus the suspended length (8.12 [m]). This means the control pod retracts 11.22

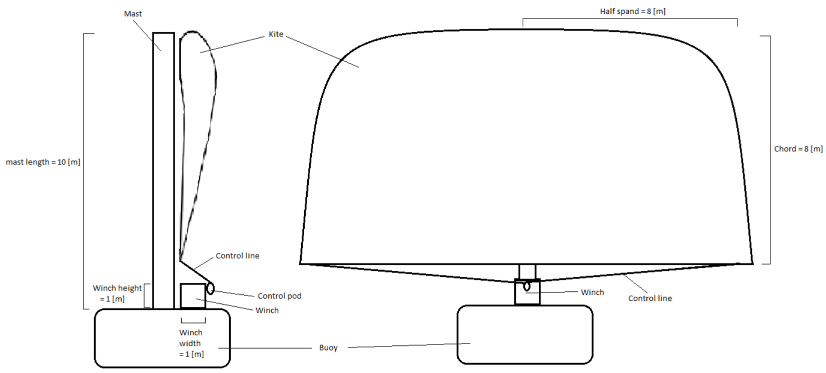

Figure 18.7: Determination of the suspended control line height

- 8.12 = 3.10 [m]. The pulleys must therefore be located at at least 3.10 [m] from the control pod. It is chosen to introduce a safety factor here and to make the distance between the pulleys and the control pod 3.50 [m]. This length is shown in figure 18.1.

18.2 The Control Pod

In this section the layout of the control pod will be explained in detail. At first, two isometric views are given in figure 12.4 for a general idea what the control pod looks like. Hereafter an explode view is given in figure 18.8 to show the different parts of the control pod. Finally the front view, back view, top view and side view are given for a more detailed overview of the control pod in figure 18.9.

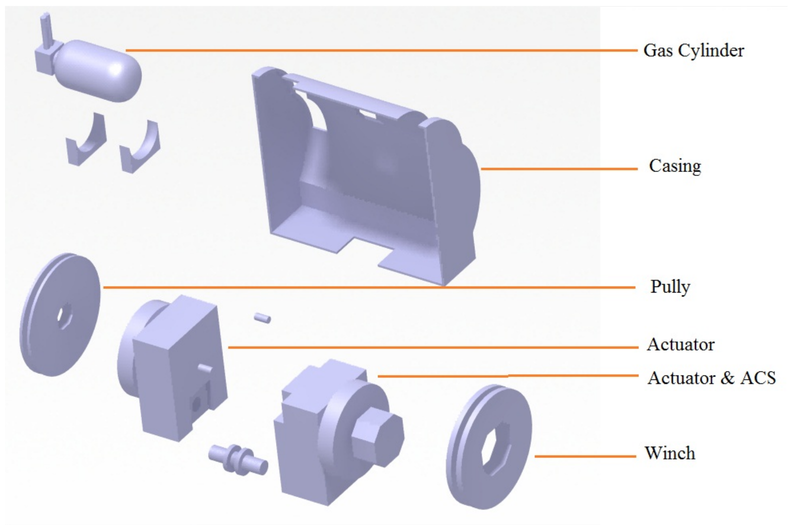

Figure 18.8: CATIA Exploded View of Control Pod

It can be seen in figure 18.9 that the main parts of the control pod are a pulley on the left, a winch on the right, a rectangular box in the middle, a gas cylinder on the top and a rigid casing on the outside for protection. The pulley is used for controlling roll of the kite. In order to prevent slip of the line, pins are placed on the pulley. The winch is used for retracting and releasing the cable to control the pitch. Both of them are directly connected to the actuators which are placed in the rectangular box. Furthermore, the ACS computer is stored in the rectangular box as well. On the top of the box, the gas cylinder is placed in order to refill the gases in the inflatable tubes inside the kite. In front of the gas cylinder, there is a small rectangular box which holds the control valves for regulating the pressure in the tube. On the outside there is a rigid casing for the protection of the entire control pod. In the drawing, only the left part of the casing is shown for the clarity of the drawing. The casing is fully symmetric, hence the left part is representable for the whole casing. Besides the main parts, there are also parts for connecting the tether. On the bottom of rectangular box, there is a reinforced connection for connecting the tether towards the buoy. On the top left and right, there are two connections for connecting the power lines of the kite.

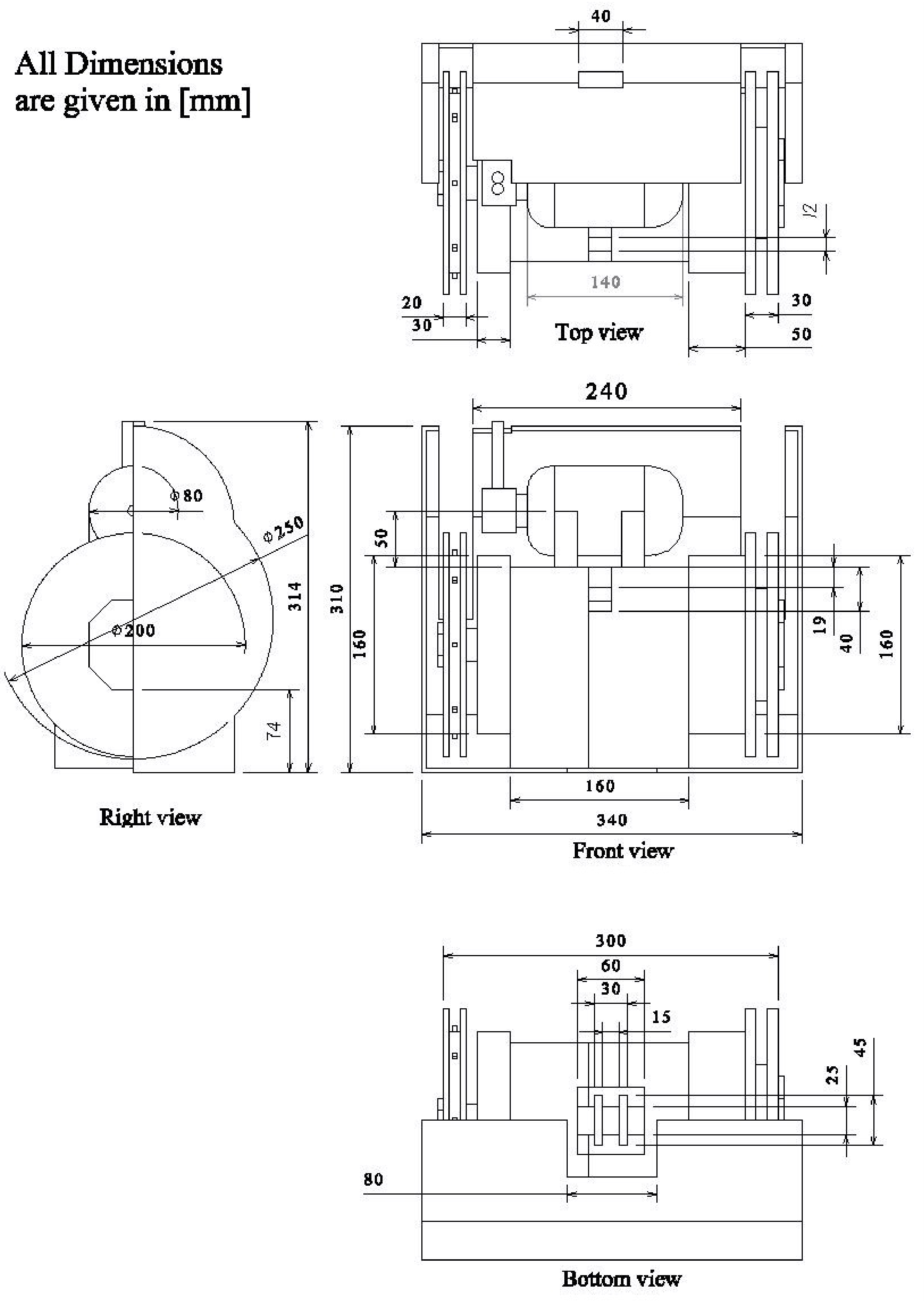

Figure 18.9: CATIA Detailed Sketch of Control Pod

Chapter 19

Configuration of the ground segment

For the configuration of the ground segment, it is important to consider several subsystems.

The different subsystems for the ground segment are solar panels, battery and inverter, antenna and EOS, HMS, TRS, the buoy, the mast and the air pockets.

Firstly, the solar panels are treated in section 19.1. The battery and the inverter are secondly discussed in section 19.2. The chip, housing the TRS, EOS and the HMS, and the antenna are explained in section 19.3. The engine of the TRS is also specified in 19.3. The buoy body is defined in section 19.4 and the mast is explained in section 19.5. Finally, the air pockets are defined in section 19.6. Figure 19.1 shows the whole picture of the ground segment.

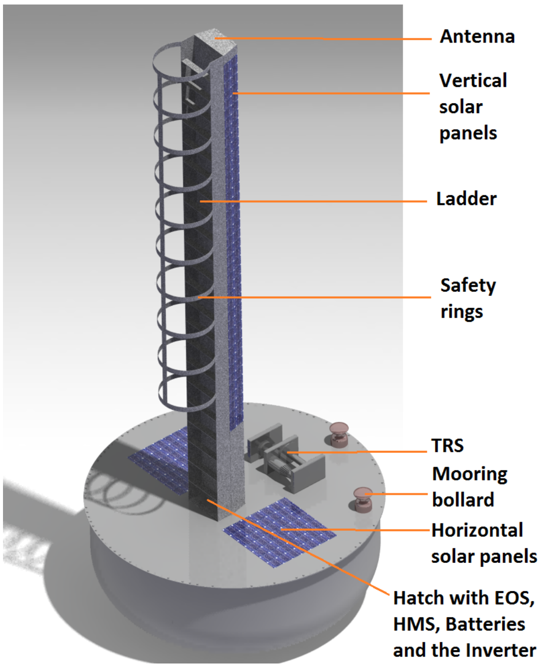

Figure 19.1: The overview of the ground segment

19.1 Solar panels layout

For powering the components of the whole system, use is made of solar panels. The reason for using this kind of power, is to prevent 'tapping' the electricity from the OWEZ power net. This is done because this process is relatively labour intensive and expensive. Furthermore tapping the electricity from the OWEZ power net, electricity cables must be digged up in order to transport the electricity. The components which are dependent from electricity are limited. To supply this small amount of electricity, a small area of solar panels are needed that can be placed on the buoy. This is more efficient and also very sustainable and is easy maintainable.

In order to use the solar panels efficiently, there are four reasonable options where these panels can be installed. These options are:

- to place the solar panels perpendicular w.r.t. the buoys surface
- to place the solar panels parallel w.r.t. the buoy surface
- to place the solar panels with an angle of 45 ^{o}
- to let the solar panels move actively to always directly face the sun

Designing the solar panels parallel and perpendicular w.r.t. the buoy's surface is most preferable because the panels can be installed to the structure of the mast and to the buoy's surface. When placing the panels with an angle, an additional supporting structure is needed, which means extra cost due to use of additional material and labour. A rotating solar panel system requires an even bigger power unit, which is the main disadvantage of this system. In addition, this type of solution needs a supporting structure and housing frames to prevent that sea water enters the moving parts. This all means that extra material is needed, this is more labour intensive and, it demands frequent maintenance. Taking all this disadvantages into account, it is decided to use the combination of placing the solar panels parallel and perpendicular w.r.t. the buoy's surface.

The power produced by solar panels is stored in batteries, which is explained in section 19.2.

For the chosen configuration of the solar panels, a comparison has to be made for the power production during summer and winter conditions.

For this, equation 19.1 [105] can be used, and figure 19.2, which visualize the parameters used in the formula.

- The slope β is the angle between the line normal to the solar panel and the line normal to the horizontal plane.
- The latitude ϕ. The OWEZ wind farm, has a latitude of approximately 52^o.
- The declination angle δ, which is the angle between a line between the sun and the earth and the equatorial plane. Its value is 23.5^o on June 21 and minus 23.5^o on December 21.
- The surface azimuth angle γ. This is the angle between the line normal to the solar panel and the south.
- The argument of perigee ω. When the sun is at it highest point, ω is equal to zero degrees. Each hour, the perigee increases with 15 ^{o}, so that in 24 hours, ω is turned 360^o.

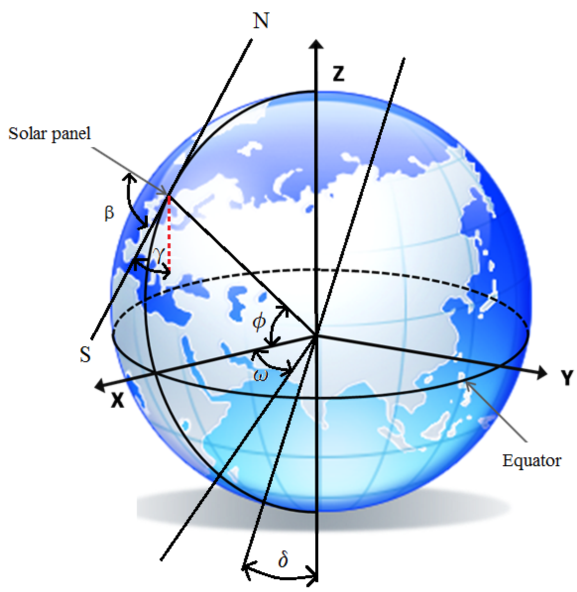

Figure 19.2: Several angles

$$cos\theta_i = (cos\phi \cdot cos\beta + sin\phi \cdot sin\beta \cdot cos\gamma)cos\delta \cdot cos\omega + cos\delta \cdot sin\omega \cdot sin\beta \cdot sin\gamma + sin\delta(sin\phi \cdot cos\beta - cos\phi \cdot sin\beta \cdot cos\gamma) \quad (19.1)$$

For a parallel configuration of the solar panel, β=0 degrees, so equation 19.1 can be simplified into equation 19.2.

$$cos\theta_i = cos\phi \cdot cos\delta \cdot cos\omega + sin\delta \cdot sin\theta \quad (19.2)$$

For a vertical layout of the solar panel, $\beta = 90[^0]$. Substituting this into equation 19.1 gives equation 19.3.

$$cos\theta_i = sin\theta \cdot cos\gamma \cdot cos\omega + cos\delta \cdot sin\omega \cdot sin\gamma - sin\delta \cdot cos\theta \cdot cos\gamma \quad (19.3)$$

If the earth is projected on a flat plate, the average solar intensity is $I_{solar} = 1367[W/m^2]$ [105]. One can plot the expected power output of the solar panels with this fact, together with the solar angles and the formulas 19.2 and 19.3. The output during the winter days (when δ is equal to minus 23.5[^{o}]) for the horizontal and the vertical panels are plotted in figure 19.3.

The perpendicular solar panels are installed to the structure of the mast, as shown in figure 19.1. To obtain a true comparison, the panel area is taken to be same as the usable area of the side of the mast, namely $3.2[m^2]$. For this configuration, γ is also taken to be equal to 30.96 ^{0}. This is the case because this direction occurs most frequently. Therefore, the buoy will let the vertically placed solar panels point to that direction since the dominant wind direction is South West. This dominant wind direction is responsible to point the buoy to the same direction as the kite pulls the ground segment. The second vertically placed solar panel is on the other side of the mast. This ensures power generation even when the buoy is rotated 180 ^{0} for any reason.

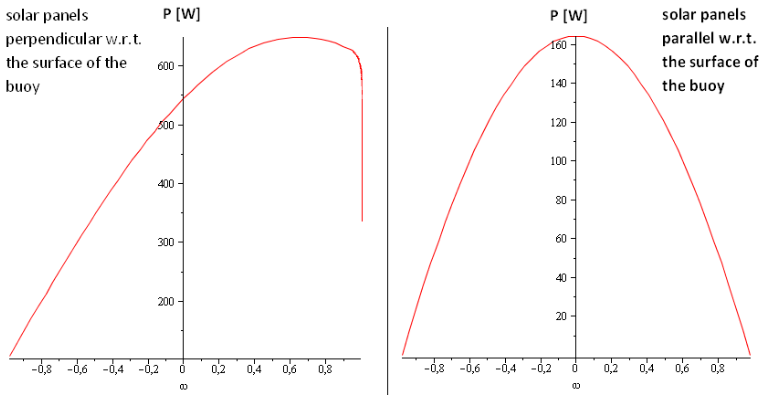

Figure 19.3: Power output of the horizontal and vertical placed solar cells during winter conditions

In figure 19.3, the vertical axis gives the power output in Watts, and the horizontal axis gives the argument of perigee ω. The parameter ω is displayed in radians. When ω is equal to 0, the sun is at it highest point. Each hour, ω increases with 0.2618 radians (or 15 degrees). As shown in the figure, sunrise occurs at ω=1.0. The sun is at it highest point at 12:40, since 1 rad ω equals $1{*}180^o/\pi\ /15$ = 3.82 hours. Also, it can be seen that sunset occurs at ω = -1.0 [rad]. Sunset thus occurs at 12:40 plus 3.82 hours which is at 16:30. The total amount of sunlight hours is equal to $2 \cdot \omega$ = 7.64 hours. The total amount of sunlight hours can also be calculated with equation 19.4, all values need to be inserted in degrees.

$$sunhours = 2/5arccos(-tan\delta \cdot tan\phi) \tag{19.4}$$

In figure 19.3 one can see that the vertical solar panel performs best, since it can create the most output. Furthermore, it can be seen that the highest output occurs when ω=0.6 [rad]. This is (1^{rad}- 0.6^{rad}) $\cdot$ $180/\pi/15$ = 1.53 hours after sunrise, at 11:08. This is due to the orientation of the vertical solar panel, which points somewhat in the Eastern direction most of the time(δ=30.96 [^{0}]). The difference in power output between the horizontal and the vertical solar panels can be explained due to low inclination of the sun on the 21st of December. The maximum inclination is 14.4 degrees above the horizon. Thus, comparing the vertical solar panels with horizontal panels, relatively more solar radiation flux is created using the vertical panels compared to the using the horizontal panels.

During the summer, the inclination angle of the sun is higher, with δ=23.5[^{0}] on June 21st. Therefore, the solar radiation flux of the horizontal panels is higher than for the vertical solar panels. This phenomenon can be seen in figure 19.4.

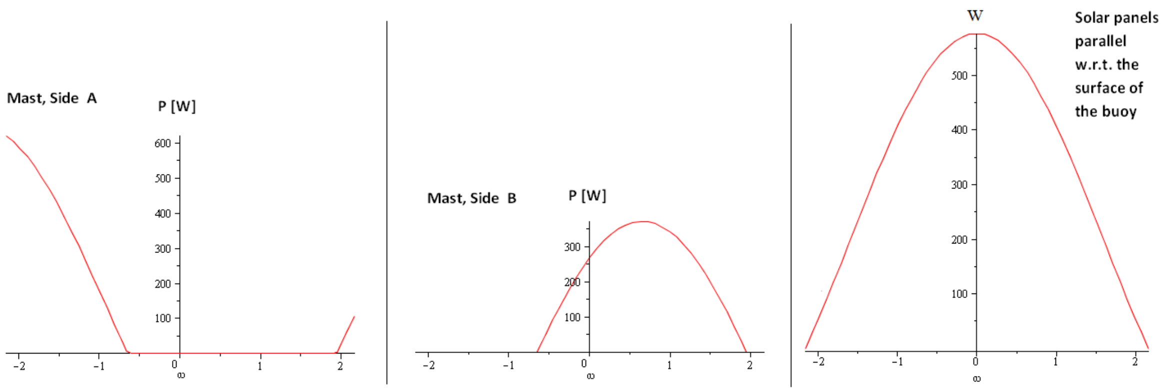

Figure 19.4: Power output of the horizontal and vertical placed solarcells during summer conditions

As can be seen in figure 19.4, the panels parallel to the surface perform better since it create the highest output, as expected. The panels installed vertically to the side A and B of the mast produce almost no output during the largest part of the day time in the summer. This happens since during the summer the sun is located at the highest point in the sky. Therefore, a shade will be created on the vertical side of the mast, which creates no power output in the formulas used. Side A and B, where the solar panels are placed vertically, complement each other, in order to cover the whole sky. However this only works optimally during the winter. In the summer, the sun has a large inclination, therefore there is very limited sunlight on vertically placed panels.

So, panels perpendicular w.r.t. the buoys surface perform optimally in the winter, and panels parallel w.r.t. the buoys surface performs optimally in the summer. That is why a combination of both is used to prevent any power shortages and guarantee a constant power supply through the whole year.

The area of the panels perpendicular w.r.t. the buoys is two times $3.2[m^2]$ and the area of the panels parallel w.r.t. the buoys is two times $2[m^2]$. The area under the graphs shows the total power output, which is 4623 [Wh]. This is the power produced during the shortest day in the whole year, namely on December 21st.

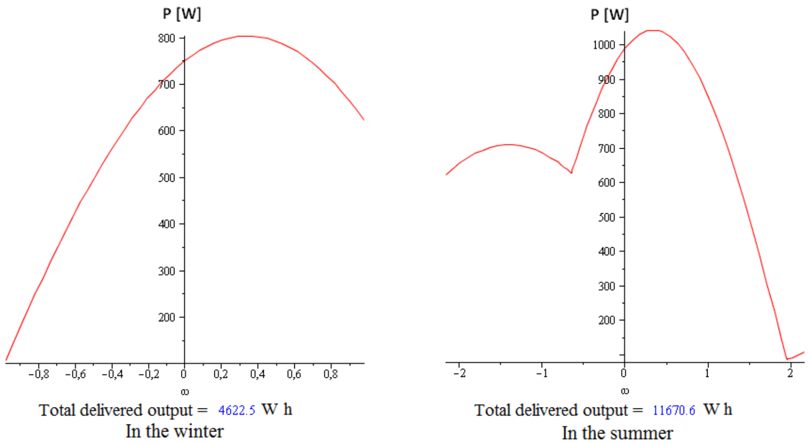

Figure 19.5: Total power output of a combination of vertically and horizontally placed solar panels during winter

The total power output during the summer, is given to the right in figure 19.5. As can be seen in the figure, the power output increases sharply in the morning. This is due to the horizontally placed solar panels. During the morning, the vertically placed solar panels are in the shadow of the mast. During sunset, a second power peak can be seen to the right in figure 19.5. This is due to the contribution of the vertically placed solar panels. The area beneath the graph shows the total power output, which is 11,671 [Wh]. This is power produced during the longest day in the whole year, namely on June 21st.

In conclusion, the combination of the solar panels put perpendicular and parallel w.r.t. the surface of buoy is the best solution. This configuration guarantees constant power for the whole system throughout the whole year independentlt of seasonal effects.

There is also an option available to put the panels at an angle of $\beta = 45^0$, which is quite common in other applications. For the panels placed on the roof top of a house for example. For the purposes of our design, this has several disadvantages. The first disadvantage is that this will require additional support structures, this means the use of extra material. At the other hand, when panels are installed with $\beta = 90^0$ w.r.t. each other, the panels are simply installed to the structure of the mast and the surface of the buoy. The second problem is, that during the winter while the buoy is turned due to the wind, blowing from a non-dominant direction, the solar panels would be turned into the shadow of the mast.

When using vertical and horizontal solar panels around the mast and on the floor, the buoy can be turned 360 degrees and still produce power. If use is made of 2 solar panels, placed at an angle of $\beta = 45$ degrees, the power supply is not guaranteed for all wind directions. The horizontal and vertical placement of solar panels is also best for maintenance, since it is better reachable than the inclined solar panels. Also, during the winter an inclination of $\beta = 45$ degrees is less efficient than an inclination of 90 degrees for the power output. If an equal area of the solar panels is placed at an angle of $\beta = 45$ degrees during the winter, the buoy would suffer power capacity problems, placing vertical solar panels in addition to the 45 degree inclined solar panels, would yield a similar result, since the vertical solar panels attached to the mast would be located in the shadow of the 45 degree inclined solar panels. Therefore, use is made of the horizontally and vertically placed solar panels.

During the summer, as can be seen to the right in figure 19.5, a total power output of 11.67 [kWh] per day is realized. During the winter, a power output of 4.2 kWh a day is generated. This is for a sunny day. However, solar panels also create power when it is cloudy and they even create power when in the shade or not in direct sunlight. However, this is not included in the calculations, in these calculations it is assumed that the output is equal to zero when not in direct sunlight or in the shade, this (partially) compensates for the existence of bad weather, which is also not included in the calculations.

Furthermore, an efficiency of 15% is assumed for the solar panels, since this is common for 'cheap' solar panels. It is assumed to be absolutely sure that even after 20 years, enough power can be delivered, since the solar panels have some degradation, but this is only about 0.5 to 1% of total power output a year [106]. Therefore, this is in fact the power generation of solar panels after a service life of 20 year, since use can be made of solar panels with a gain of 20%, this has been included in all the graphs. The generated power is therefore higher when using new solar panels.

19.2 Batteries and inverter

There is also a power demand at night or during clouded conditions. Therefore use is made of batteries, to avoid power blackout. The batteries store sufficient power to sustain an energy output during night. Therefore, use is made of a nickel-cadmium battery. Nickel-cadmium has the advantage over other types of batteries which has a great depth of discharge[107], this is useful when a lot of power is needed in a small time span. The higher the dept of power, the faster energy can be extracted from the batteries. Also, it is a very light and cheap when compared to other batteries [107].

The battery has to be big enough to ensure power supply to EOS, HMS, TRS, GPS, control pod, power inverter.
For the antenna, a choice can be made between an active or passive antenna. Since the antenna only needs to receive data, use is made of a passive receiving antenna. Therefore, this antenna does not require power.

The EOS system does require some power. The EOS decides whether to retract the kite, due to analysing the weather condition. To decide this, a computer chip is needed. A good chip for this purpose is the 'Chip Thin client PC', this chip only requires 3 [W] to operate [108]. Also, this chip has enough capacity to also hold the HMS and TRS control functions.

The GPS that is used is the Shadowbox, this GPS system only uses 5 [W] to operate [38].

Most energy demand is driven by the control pod of the kite and the TRS engine.

The TRS engine uses 1065 [W] when retracting the kite, the kite is retracted for 675 seconds or less, this is specified by the manufacturer[109]. The batterie is large enough to enable the instant power supply of 1065[W] [107]. This engine is further described in section 19.3. Thus, per complete retraction the TRS engine uses about 200 [Wh].

It is assumed, that on average the kite is retracted once every 3 days, as stated in section 11.4.1. But, for a worst case scenario, 3 times for a single night is assumed.

The control pod also uses a lot of energy, a normal control pod uses up about 20 [W] [29].

Our control has a weight ratio with the normal control pod of 2.7 (13.1.1), therefore the power use is estimated at 2.7 times 20 [W] = 54 [W].

In conclusion, the total power needed is tabulated in table 19.1:

Table 19.1: Power usage for several sub systems

Device:	**Power Usage:**
Chip(EOS, TRS, HMS)	3 [W] constant
GPS	5 [W] constant
TRS engine	200 [Wh] per retraction
Inverter cooling fan	5 [W]
Control pod	54 [W] constant
Total constant power:	67 [W]
Total watt hours required:	2208 [Wh] (for 3 retractions)

The battery is located inside the mast, this is the best option, since it is that protected from water and rain.

Further, the power received from the solar panels is direct current, this has to be converted to an alternating voltage for common use. For this, a power inverter is needed. This inverter is sensitive to rain, therefore the inverter has to be placed inside the mast as well. This inverter is cooled by a 5 [W] Fan, to avoid overheating.

For a worst case scenario, the battery has to store 2208 [Wh] of energy, see table 19.1. A nickel-cadmium battery can store 30 [Wh] per kilo, and have a density of 8.75 g/cm^3[107]. Also, it has good life cycle characteristics, after three years its capacity is still more than 70% after 1500 cycles [107]. Every 4 years, the battery needs to be replaced in order to maintain a relative high efficiency. Also, since the power gained must be converted to alternating voltage, an inverter has to be used, for this, an efficiency of 90% is assumed. After 4 years at the end of the life cycle, with 3 retractions a night the battery needs to be 0.013 [m^3]. It also needs to fit inside the mast. The mast is 400 [mm] high and 600 [mm] width, so using this dimensions, it needs to be at least 5.6 [cm] thick. The battery dimensions are 0.4 [m] by 0.6 [m] by 0.056 [m]. The energy during the day is directly extracted from the solar panels whenever possible. If the solar panels cannot supply the systems with enough energy, the rest of the energy is extracted from the battery.

19.3 Antenna, EOS, TRS, HMS

The receiving antenna is passive, so no electricity is needed to operate the antenna. This antenna receives weather information from weather stations. Also, a normal size antenna can be used, since the weather stations are close to the receiver. The antenna is located on the top of the mast, this ensures good receiving capabilities and keeps the antenna safe and dry. In the right of figure 19.8, the hatch for the maintenance of the antenna, on top of the mast, is shown. The weather data received by the antenna are processed in a computer chip, located in the lower section of the mast to remain dry. For this job, as mentioned above, a 'Chip Thin client PC' is used. This is due to its low power consumption and it requires fewer raw materials to be produced since it is very small, so it is very sustainable. Finally, it creates far less heat than a normal chip, since it has no moving parts [108]. This chip also houses the HMS and the TRS, how this further works is explained in section 6.1. Placing the chip inside the mast will keep the chip dry. If the chip is broken, the TRS engine is ordered to retract.

The TRS also needs an engine, for this, use is made of an already existing engine. This engine is the HADEF 42/87 E model 5108. To this engine a tube is attached. On this tube, two cables are rolled up. Namely the cable to the control pod of the kite and the cable via the mast to the leading edge of the kite. These cables are separated from each other to avoid constriction. An overview and the dimensions of the TRS is given in figure 19.6.

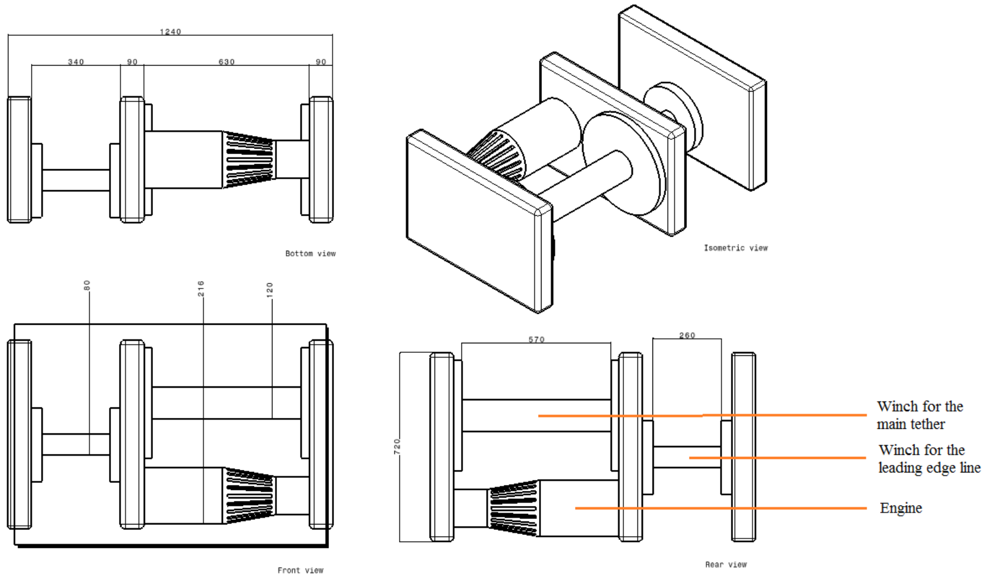

Figure 19.6: The overview of the TRS

19.4 Buoy Body

The body shape can be clearly seen to the left in figure 19.7:

This is a very common design shape for buoys. This has several reasons, the roundness enables the buoy to resist water currents. Further, the slope at the sides of the buoy body is to minimize the amount of waves that can flow over the buoy. When maintenance is performed, this is important for the safety of the maintainers. Also, it is easy to manufacture, as can be seen in section 16.1. In the body surface, horizontal solar panels are installed. Also, a hatch is there for maintenance and the inspection of the air pockets and the inspection of the anchoring of the mast, since the mast is anchored inside the buoy body. In order to anchor boats to the buoy, mooring bollard are also installed on the buoy body. The TRS engine also stands on the surface of the buoy body. Since the mass of the TRS is approximately 600 [Kg], it is supported by a pole inside the buoy body, for structural reasons, this can be seen in the view inside the buoy body to the left in figure 19.8. On the lower part of the buoy body, the anchoring chain can be attached as can also be seen to the left in figure 19.8

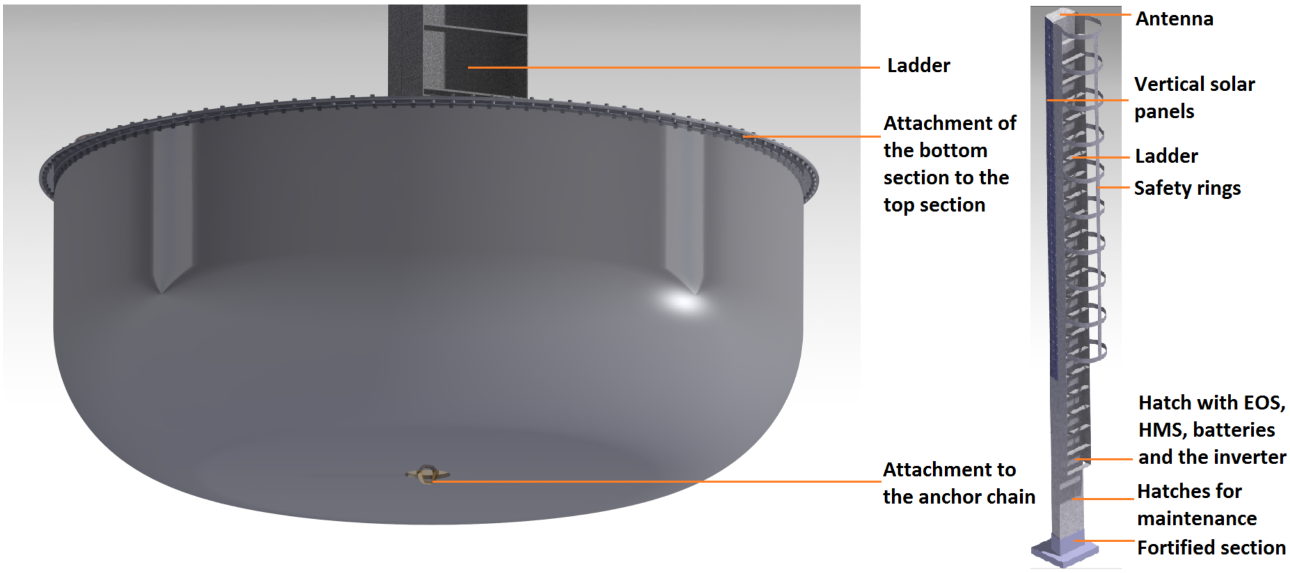

Figure 19.7: The shape of the buoy body, to the left and the mast, to the right

19.5 Mast

The mast is for the storage of the antenna, batteries, inverter and the computer chip and to allow the kite to attach to it at the top. The mast is located in behind the center of gravity. This is to stabilize the buoy, since the TRS engine is located in front of the center of gravity. The Mast is heavier than the TRS so to have zero moment about the center of gravity, the mast is located closer to the center of gravity than the TRS is. Further, the mast can be viewed to the right in figure 19.7. On the short sides, vertical solar panels are attached to the mast. When maintenance is performed, the ladder on the back side can be used to inspect the solar panels and the antenna. The batteries, chip, inverter and antenna, are located in the lower hatch in the mast since they are rather heavy and placing them in the lower part is better for the overall stability of the buoy. These devices are placed inside a water proof hatch. To ensure absolute safety of the maintainers, rings are attached to the mast which are there to help prevent injury for the person that climbs the ladder, since the ladder is 10 meters high. The mast is anchored inside the buoy body, as can be seen to the left in figure 19.8. On top of the mast, the antenna is located, the hatch can easily be reached for maintenance using the ladder. In the body of the buoy, the mast has also two hatches, this is in order to be able to inspect and tighten the bolts for the anchoring of the mast.

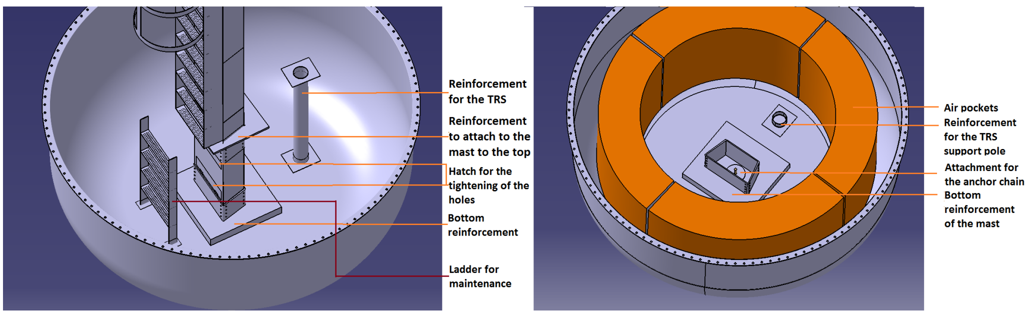

Figure 19.8: The anchoring of the mast to the buoy body, to the left and the air pockets in the buoy, to the right

19.6 Air Pockets

To remain float, air pockets made from rubber are installed inside the buoy. There are four air pockets. The air pockets are well enough to keep the buoy floating, even if the middle of the buoy is filled with water. There are four air pockets, this is to minimize the risk of sinking, since one of the air pockets could be leak. If two air pockets are filled with water instead of air, the remaining two air pockets still enable the buoy to float. The air pockets can be viewed to the right in figure 19.8.

Chapter 20

Sustainability

In the following chapter, the sustainability of the design will be discussed. The core goal of this DSE is to create a device that increases the efficiency of wind farms. The device will enhance the efficiency of an already sustainable energy source, therefore it is very important that the device itself is also sustainable.

The characteristics for sustainable materials is that they must be non-toxic, recyclable, renewable, durable and long lasting. Costs play an important role in the decisions made, since this system should be economically attractive for the wind farm owners. Also, the system must perform its function for 20 years, which creates the need for durable and sustainable materials. Also environmental impact has to be taken into account. In the following chapter, the sustainability aspects of the aerial segment will be discussed in section 20.1, the tether segment will be explained in section 20.2 and the ground segment in section 20.3.

20.1 Aerial segment

For the aerial segment, the materials and associated production processes will be evaluated in terms of sustainability in chapter 20.1.1 and chapter 20.1.2 respectively. Hereafter, the environmental aspects will be discussed in chapter 20.1.3.

20.1.1 Materials

The material that will be used for the cloth of the aerial segment, is called Dacron. Dacron is the brand name for a type of polyethylene terephthalate (PET). This material has good UV resistance, as discussed in chapter 15.1. However, there is still a need for the use of Tedlar, a UV protective layer. Furthermore, the inflatable tubes that will be used for creating the desired aerodynamic shape, are made of Mylar. Mylar is a film which is made of PET, therefore Dacron and Mylar will be discussed simultaneously. The materials Dacron and Mylar are high strength and low weight materials, allowing for more material to be delivered in less packaging and using less fuel for transport, thereby reducing CO_2 emmisions. PET is very durable [110] as shown in past experience in the offshore industry. PET is also completely recyclable. Products commonly made from recycled PET include PET bottles, clothing, rope, automotive parts, construction materials, protective packaging and many more [111].

Tedlar is a material that will protect the Dacron from the UV radiation. Tedlar is a type of Polyvinyl Fluoride Film. Used primarily in backsheets that protect photovoltaic modules. Tedlar is very durable since it is the only UV protection film with more than 25 years of proven field performance [112]. Furthermore, Tedlar is stable at normal temperatures and storage conditions. In terms of aquatic toxicity, toxicity is expected to be low because of negligible solubility in water, as is stated by the Toxic Substances Control Act from the U.S. Federal Regulations [113].

20.1.2 Production

The kite is produced by weaving strands of Dacron into the desired shape. The actual production process, although labour intensive, does not produce any significant negative side effects to the environment. When looking at the process of recycling Dacron, there are several options, such as source reduction, incineration, bio- and photodegradation and pure recycling. Today, about 69% of the plastics ends up in landfills [114], which is not a very sustainable way of getting rid of the waste material. Therefore, care must be taken to make sure the kite is recycled and not put into a landfill by monitoring the recycling process. Furthermore it should be stated that the UV protective layer Tedlar, is made by the company DuPont. This science company's main goal is to create solutions that help protect human health, safety and environment [115]. Therefore, by working together with this company, overall research into sustainability will be promoted.

20.1.3 Environment

The aerial segment will be airborne during most of its operational time. This may lead to birds hitting the kite. Since the leading edge of the kite is a soft membrane, and the rest of the kite is made from a soft material, less damage will be inflicted onto birds hitting the kite. Furthermore comparing to the wind turbine- blades, the noise produced by kite is very low [116]. This is very important when applying the system to onshore wind farms, where resistance against building wind farms is growing by nearby inhabitants due to noise pollution. Also, marine life will not be disturbed by the kite. When the aerial segment is retracted, it is suspended at a height at which no marine life that may be situated on top of the buoy will be struck. Lastly, and most importantly, there will be no emissions produced during operations.

20.2 Tether

In the following section, the sustainability aspects of the tether will be discussed. The materials and associated production processes will be evaluated in chapter 20.2.1 and chapter 20.2.2 respectively. Hereafter, the environmental aspects will be discussed in chapter 20.2.3.

20.2.1 Materials

For the tether, Dyneema will be used. Dyneema is easily recyclable, either by using pyrolysis or dissolution/reprecipatation [117]. Dyneema is a very strong fibre, this makes it possible to use less material for the same applied load when compared to a steel cable, for example. This in turn requires less packaging and less fuel for transport, thereby reducing CO_2 emissions. Also, Dyneema is very durable as it is virtually not affected by cyclic loads. In addition, Dyneema is commonly used in maritime environments [118]. From past experience in this field, it is known that Dyneema is not hazardous for marine life. Also, Dyneema is a high strength and low weight material, allowing for more products to be delivered in less packaging and using less fuel for transport.

20.2.2 Production

Dyneema is largely used by marine industries like offshore platforms. Also for marine applications, Dyneema is woven around electricity cables, similarly to what is needed for this design. This means the already existing production processes can be used to produce the tether for this system. Overall, the production of Dyneema produces no hazardous by-products and requires low amounts of energy to produce. This is due to the method of weaving the individual strands of Dyneema fibres into the final Dyneema cable, this only requires mechanical power and no additional heat or chemical sources are needed.

Furthermore it should be stated that Dyneema, is made by the Dutch company DSM. This company has been included in the top rank of the chemical sector in the Dow Jones Sustainability Index [119]. Therefore, by working with this company, overall research into sustainability will be promoted.

20.2.3 Environment

Dyneema is being used in the maritime sector since its discovery, and no negative effects to the environment are known so far. There are two characteristics of Dyneema that reduce the environmental impact of Dyneema. The first one is the low specific density of 0.97 which causes Dyneema to float. For the unlikely case of the tether falling into the sea, the cable will not disturb any of the underwater marine life. The second point is that Dyneema is hydrophobic, which means it does not absorb any moisture. This eliminates the spreading of substances through osmoses.

20.3 Ground Segment

For the ground segment, the materials and associated production processes will be evaluated in terms of sustainability in chapter 20.3.1 and chapter 20.3.2 respectively. Hereafter, the environmental aspects will be discussed in chapter 20.3.3.

20.3.1 Materials

The ground segment uses a lot of different materials. The structure of the actual buoy is made of fibreglass. Fibreglass is much more sustainable than aluminium or steel, since it does not interacts with the environment. For the mast of the buoy and the connection to the concrete, steel must be used as was explained in chapter 14. This is also the best option in terms of sustainability since making the mast out of glass fibre or another sustainable material will lead to a heavy and inefficient design. This is because glass fibre does not perform well under bending loads, causing the need for much more material to be used when compared to steel. This causes the required amount of material to be such that the environmental impact of using a smaller amount of steel compensates for the difference in sustainability.

The anchor is a concrete block, this material is made from ingredients that are readily available in nature. Energy requirements for transportation are low because it is produced locally from local resources, reducing CO2 emissions. Also, the concrete anchor will only need to be installed once for the design lifetime of 20 years, since concrete is highly durable.

20.3.2 Production

In terms of production and recycling there are significant environmental benefits of choosing a glass fibre buoy instead of a metal one. First of all, no large smoke plumes or other environmental pollution from the manufacture of fibreglass products. However, fibreglass is not biodegradable, but upon disposal it can be pulverized and used as a filler in concrete, this will improve the binding capability of the mix. Another method of recycling fibreglass is by chopping up the old fibreglass part and then by using a process of filtration, separating the strands and resin powder. The strands are turned into chopped fibre cloths and the powder into filler used to thicken the resin, also called microballoons or flox. There are many companies that recycle fibreglass with a high degree of efficiency. Using fibreglass instead of steel, aluminium or other such materials also means that these natural resources are less demanded. This will lead to a reduction of the environmental impact resulting from the production of metals and the disposal of the associated waste.

20.3.3 Environment

The environmental impact to for example marine life, needs to be as low as possible for the ground segment. Amongst other reasons this leads to the choice for a buoy design instead of a structure fixed to the seabed such as a mono-pile. During the hammering of the mono-piles, which were used to build the wind turbines on at the OWEZ wind farm, a lot of noise was produced. The noise during hammering operations is mostly heard underwater. The sound produced can be heard from a much larger distance than sound moving through air. This is due to the difference in density and associated speed of sound. The speed of sound in sea water is dependent on a lot of factors such as depth, suspended sediment and air bubbles, with an average of 1560 m/s [120] which is about 4.6 times the speed of sound in air. The associated sound pressure levels (SPL), for the hammering of the mono-piles was around 170 SPL [dB] [121]. This amount of dB can affect nearby marine life. According to the Ocean Mammal Institute, these effects may include death and serious injury caused by hemorrhages or other tissue trauma, strandings, temporary and permanent hearing loss or impairment, displacement from preferred habitat and disruption of feeding, breeding and other behaviours vital to survival [122].

When looking at the release of hazardous materials and substances, the glass fibre buoy is much safer when compared to other materials. The natural corrosion of steel in sea water is not hazardous for the environment, it does however cause less material to be recycled since the rusted metal is not recyclable. Hard plastics that are structurally and economically viable materials for the buoy structure, have negative environmental side effects. Recent research has shown that hard plastics decompose in sea water, releasing the organic compound Bisphenol A (BPA). This compound is an endocrine disruptor which can affect growth, reproduction and development in almost all aquatic organisms, ranging from plants to fish [123]. Therefore, hard plastics were not considered for the design. Furthermore, glass fibre does not react in any way with sea water. Therefore, as well because of the stated above, fibre glass is the best material in terms of environmental protection.

20.4 Conclusion

When looking at the sustainability of the total design, it is safe to say that this design solution is the most sustainable solution to increase the wind farm efficiency by this large amount. Sustainability aspects are taken into account in every sub-part of the design. The choice of materials is such that the lowest possible impact to the environment is created. This is necessary since the goal is to increase the sustainability of an already sustainable solution for the generation of energy.

The attention to sustainability is also evident in the use of wind energy to increase the efficiency of the wind farm in the form of a kite. This kite requires no additional energy source to perform its function. There are certain elements in this design that do require an energy source, such as the retraction system in the form of a winch and several health monitoring and observation systems. These are powered using a sustainable energy source, namely the sun. Also, the winch that will retract the kite was chosen to be electrically powered. This will in turn eliminate any emissions and use of fossil fuels. All of these design considerations make this a zero emission, durable, extremely sustainable and most importantly a cost effective solution for the given problem.

Chapter 21

Market Analysis

To design and launch a product for exploring an existing market, a market analysis needs to be performed in order to ensure the success of the product to be launched. Firstly, the wind energy market development will be discussed in section 21.1. Subsequently, the wind energy market trends and the SWOT analysis will be explained respectively in section 21.2 and section 21.3.

21.1 Wind Energy Market Development

The wind energy market has experienced a vast growth in the last decades which can be seen to the left in figure 21.1. One of the main reasons for the growth is the urge for seeking an alternative energy source due to depletion of fossil fuels. Subsequently this has led to huge investments into research and development for wind energy applications. However, several governments plan to bail out from the wind energy subsidies within the next 15 years. Therefore it is needed to develop cost-efficient wind farms within the given time constraints.

There are several estimations for the growth of wind energy in the future which are based upon estimations from institutions, government and private companies. In most cases from the last decade the actual growth was higher than the predicted growth. Estimations range from growth rates between 20 percent and 25 percent [124]. Also, there are large regional differences since a large wind energy industry has already been established in the US and in Europe. However, the asian countries led by China and India have also commenced developing and building large offshore wind farms.

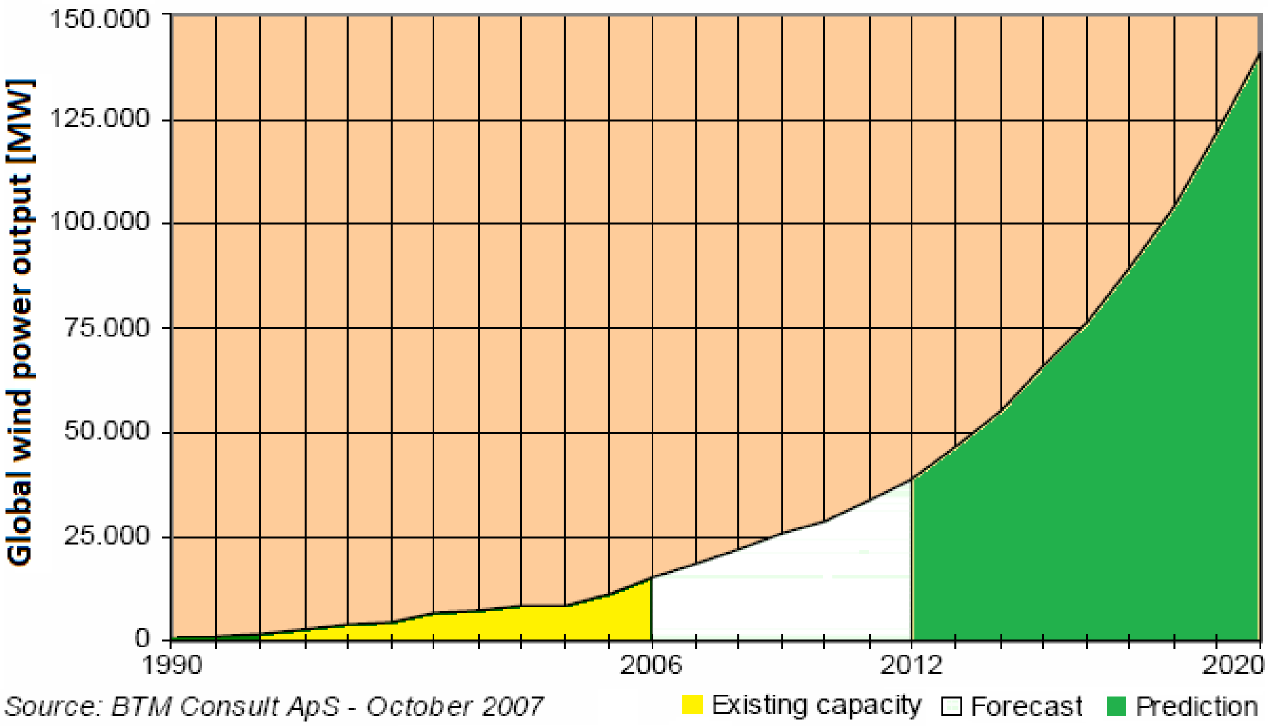

Figure 21.1: Predicted Market Growth

21.2 Wind Energy Market Trends

Much research is done on improving the efficiency of wind farms. The several solutions are found. The first solution is using a yawing nacelle, which enables the turbine to generate electricity for different wind directions, thus increasing the overall efficiency. Furthermore the blades of the wind turbines are adjustable and react on the changing wind speed, which eventually also leads to an increase in overall efficiency. The second solution is clever placing of the wind turbines. This is done by modelling the airflows and using CFD techniques[17]. However, the first and the second solutions are already applied in the most of the wind farms.

During this project the focus will be on a different approach, which is, mixing the undisturbed upper airflow with the reduced wind speed behind a wind turbine. This will lead to an innovative device, which will increase the efficiency of a wind farm by a substantial amount. At last, a study was initiated in April 2011 by the University of Colorado, which also investigates the effects of wakes within wind farms in order to increase the efficiency and decrease the structural loadings [125].

21.3 SWOT Analysis

Many tools are available for a good market analysis. The SWOT analysis is an important tool which can be used for market analysis. In a SWOT analysis, the aspects such as Strengths, Weaknesses, Opportunities and Threats will be analysed. Strengths and Weaknesses are internal factors that create value or destroy value. They include assets, skills or resources that a company has at its disposal, compared to its competitors. They can be measured using internal assessments or external benchmarking. Opportunities and Threats are external factors that create value or destroy value. A company has no influence on them. But they emerge from either the competitive dynamics of the industry/market or from demographic, economics, political, technical, social, legal or cultural factors. The SWOT analysis for Daeolus can be viewed in table 21.1.

Table 21.1: SWOT Analysis

Strengths	**Weaknesses**
- Increases the efficiency - Is cost effective - Low maintenance required - Recyclable - Innovative	- Almost no user experience yet - Strongly dependent on the trend towards wind farms - Short life time of 4 years
Opportunities	**Threats**
- Fossil fuels are becoming scarce - Wind energy industry in growth phase - Sustainability is becoming more important to society - Various locations can be used for placing the wind farm (sea/land) - Wind is a never ending resource - Wind energy is one of the cheapest forms of alternative energy generation	- Low energy production compared to fossil fuels - Dependent on subsidies - Strong competition from other sustainable energy sources - Ups and Downs in the production due to change in wind speed

Chapter 22

Financial Analysis

In order to determine the total cost of the system, a cost analysis will be made. The cost analysis consists of three parts. Firstly the cost breakdown, in which the different cost aspects will be outlined, is shown in section 22.1. This gives an estimate of the final total costs with a margin. Hereafter a detailed cost analysis will be performed in which the individual costs aspects will be analysed (section 22.2). This is based upon the cost estimates and material needs from the different subsystems. Also for the buoy and the kite system cost functions are used. When including the total revenue (due to the efficiency gain) and taking into account the cost, it is possible to plot a graph for the maximum profit. This can be used in order to size the kite according to the maximum profit principle. Another advantage of the cost function is the usage for the application on other wind farms. When using different kites, for example for different turbines, then the cost function enables an easy and quick cost estimation. Subsequently the cost buffer will be calculated (section 22.6 and implied so that the final cost (section 22.4 overview can be established. The cost buffer is implemented in order to account for uncertainty. Hereafter the calculations for the Return on Investment (ROI) are displayed. First the revenue is calculated (22.5) and thereafter the calculated costs from chapter 22 are used to calculate the final return on investment (22.6 and the other important financial aspects like the break even point.

22.1 Cost Breakdown

The cost breakdown can be split up into recurring and non-recurring costs as it can be seen in figure 22.1.

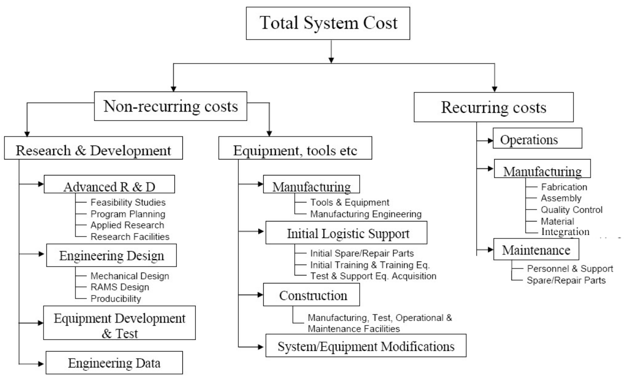

Figure 22.1: Cost Breakdown Structure

22.1.1 Non-recurring and recurring costs

In order to monitor the entire cost of the kit system it is needed to first determine the initial investment costs. By doing so, the production facilities can be developed and production processes generated. When looking at the production, it can be seen that there are three main segments, namely the aerial segment, the ground segment and the tether segment. All these different cost aspects can be seen from figure 22.1.

Furthermore there are the initial costs for installation. Installation includes the transport from onshore to the offshore location.

The recurring costs are costs which will occur throughout the lifetime of the Daeolus Kite System. The recurring costs can be split up further. First there are maintenance costs which consists of replacements for the kites and tether. Also maintenance will be needed for the buoy (retraction system). Additionally there is the operation costs which is the control of the entire system from a control unit that is positioned onshore. This control unit needs to be monitored as well. It is basically a small computer which is monitored by a staff member of the offshore wind farm in order to ensure correct operation.

22.2 Detailed Cost Analysis

In this section the cost of individual subsystems will be analysed, this will be done using cost functions. Since the kites and the buoys are the main cost driver it is necessary to analyse them further. Also suggestions for improvements in order to reduce costs further will be given.

22.2.1 Kite Cost Analysis

The kite cost have been determined via price lookups from different kite production facilities [126]. Additionally a safety factor of two has been used in order to account for specific requirements of the kites such as a special UV coating. Two is chosen since there is quite some uncertainty on how much more detail is needed. Based upon that an interpolation has been made which can be seen in figure 22.2. The interpolation follows a price lookup for various bow kites with a length of 1 - 20 metres.

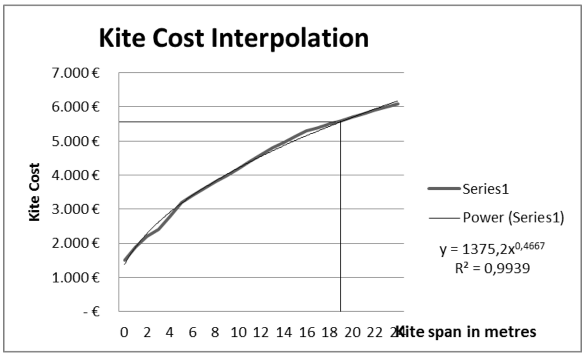

Figure 22.2: Kite Cost Function

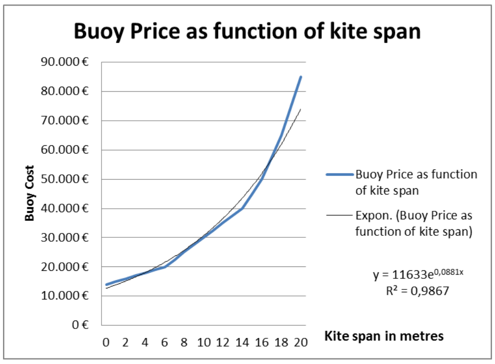

Figure 22.3: Buoy Cost Function

It was decided to use a power function since with increasing kite sizes (above 14 metres span) the rate of change of the kite cost is negative. Also the least square error is the smallest for that (R2 = 0.993). Further in the area of 6 to 14 metres the cost increase is rather linear.

The final price of the kite will be €5,600 which results from the kite cost function (taking as an input a span of 19 m). Also this price has been verified by the ASSET department of TU Delft which predicts similar prices for kite with these dimensions [127]. The total price for the 23 kites then adds up to **€128,800**.

22.2.2 Buoy Cost Analysis

As stated in section 15.3, the buoy is made from several materials. For the buoy, the total costs of the raw material are shown in table 22.2.2.

Table 22.1: Cost and weights of the buoy

Type	Price in €	Remarks
Lamp	20	
Antenna	100	
Chip	250	Chin Thin Client PC [128]
Inverter	200 [129]	
Cooling Fan	10	
Batteries	400	Nickel Cadmium
Bolts	500	
Solar Panels	7280 [130]	2 x 3.2m and 2 x 2m
Buoy Chain	1500	
Concrete Block	2000	
Engine	1200 [109]	HADEF 42/87 E model 5108
Glass Fibre	3700 [131]	
Steel	4000 [132]	
Total	22,960	

Table 22.2: Product Costs

Type	Amount	Price	Total Cost in €
Tether	92	130	11,960
Control Unit	23	5000	115,000
Winch	23	10000	23,000
GPS Unit	23	500	11,500
Battery	23	500	11,500
Total			173,000

The prices are based upon the actual material prices and the interpolation data for changing parameters. Not included are the man hour costs which will be listed separately.

Different prices for buoys have been researched via various B2B platforms [133] and buoy producers [134]. Based upon that, a price interpolation has been made, as it can be seen in figure 22.3.

For the Buoy cost function it can clearly be seen that there is a strong exponential growth. Thus it can be concluded that with an increasing kite size there will be an enormous increase in buoy price as well. The cost is based upon actual cost estimates and looked up values from various B2B platforms. Also an estimate is included for the labour involved [133].

Taking into account that the total kite span is 19 [m], the kite cost function can now be used to estimate the final buoy price (including labour, production and material costs). Looking up the value in the cost function leads to a price of €62,000 for a single buoy or **€1,423,000** for 23 buoys.

The total costs are now based upon the estimation for the material costs and the prediction from the cost function of the buoy.

22.2.3 Secondary Product Costs

Besides the previously listed main product costs, there are various other product costs which contribute to the total price of the buoy system. First of all there is the main tether which is needed for the bridle system and the kite line. Besides that there is the winch to release / retract the kite, the control pod unit and the GPS/Gyroscope unit to measure the position and its actions. The prices were looked up based on the manufactures values where possible. For other cases it was not possible to use direct lookup, thus estimations from B2B platforms were chosen [133]. That will later influence the cost buffer as well. The cost overview for the secondary products can be seen in table 22.2. For the Tether a total of 4 tether per kite is taken into account, this adds up to a total of 92.

22.2.4 Installation Costs

The costs for the installation of the kite system are split up in four main expenses: labour hours, harbour costs dry dock costs and boat costs. In the preparation phase only labour and dry dock costs are required. With a team of 20 men one kite system per day can be produced, however also the dock preparation is required. When all buoys are in the water a boat is needed with the crane. The installation of the ground segments will take 3 days. The installation of the aerial segment takes 2 days. The boat will require 10 men. Summing this up in a table results in €627,000 estimated installation costs. The detailed overview for that can be seen in table 22.3. The values are based upon reference values stated by DOWEC for various installation options [135].

Table 22.3: Installation Costs of entire System

	Amount	Days / hours per day	Mobilisation Cost	Price	Cost in Euro
Man-hour Preparation	20	30/8	-	50 per hour	240,000
Man-hour Installation	10	5/24	-	50 per hour	60,000
Dry Dock	1	30/24	-	1000 per day	30,000
Harbour	-	30/24	-	100 per hour	72,000
Vessel	1	5/24	100,000	25,000 per day	225,000
TOTAL					**627,000**

22.2.5 Maintenance

The maintenance costs consist of three different costs elements. First there are the product costs which are needed to replace items. Secondly there are the labour costs which are required to perform the maintenance. Lastly there is equipment needed in order to perform the operation such as transport vessels. The total maintenance costs can be derived from the different previously mentioned parts. The product costs that need to be replaced are dependent on how many years they last. While the kite lasts two years and thus needs to be replaced 9 times, the GPS unit and the battery last 4 years and lastly the cable will reach 10 years, thus it only needs to be replaced once. At the end of the 20 year lifetime, the buoys can still be used for other kite application, only the kites, the cable and the secondary products needs to be discarded. This can be done in the same maintenance

Table 22.4: Costs of Replacing Products

	Lifetime	Cost per Cycle in K €	Total Cost in K €
Kite	2	129	1,159
Cable	10	12	12
GPS Unit	4	11.5	46
Battery	4	11.5	46
TOTAL			**1,263**

Table 22.5: Maintenance Costs (Transport) of entire System

	Amount	Days / hours per day	Mobilisation Cost in €	Price	Cost in K €
Man-hour Installation	10	5/24	-	50 per hour	60
Dry Dock	1	30/24	-	1000 per day	30
Harbour	-	30/24	-	100 per hour	72
Vessel	1	2/24	25,000	25,000 per day	75
Total per cycle					**237**
Total for nine cycles					**2,133**

22.3 Cost Buffer

For the different cost aspects cost buffer have been estimated which are needed in order to provide a cost prediction. Obviously prices are subject to fluctuations, thus cost buffer need to be included.

Table 22.6: Cost Buffer Overview

	Cost Buffer in %
Kite Cost	5
Secondary Product Costs	10
Buoy Costs	5
Installation Costs	10
Maintenance Costs (Materials)	7.5
Maintenance Operation Costs	10

As it can be seen in table 22.6 there are several cost buffers are applied. The lowest cost buffer is assigned for the cost of the kite and the buoy since the prices have been looked up from various B2B platform and also be approved by external experts (ASSET). Therefore only a 5 percent cost buffer has been implemented. The highest buffer has been implemented for the secondary products, the installation costs and the operation costs. This is due to unpredictable events like weather conditions and wave behaviour for the installation and the maintenance. Also the secondary products receive a higher margin since they are not designed to such a detail like the kite and the buoy. The maintenance costs for the material and product replace, a cost buffer of 7.5% has been implemented since it is a mix of the main products like the kite and also the secondary products.

22.4 Cost Overview and Conclusion

Summing up all the results from the previous sections, it is now possible to state that the predicted total cost will be €6,895,000. This includes the cost buffer as it is shown in table 22.6.

Table 22.7: Cost Buffer Overview

	Estimated Costs in K €	Costs including Buffer in K €
Kite Cost	129	135
Secondary Product Costs	173	190
Buoy Costs	1,423	1,494
Installation Costs	627	690
Maintenance Costs (Materials)	1,263	1,358
Maintenance Operation Costs	2,133	2,345
TOTAL COST	5,748	**6,213**

Furthermore using the buoy and the kite cost function it is also really easy to predict the costs of the the entire system for other wind farms. In general the only variable costs are the kite and the buoy costs which significantly change the price of the entire system. Also they need to be sized for different turbines. Since the calculation has been implemented into an Excel Sheet and a Matlab file it becomes clear that cost estimation for other wind farms can be adapted accordingly.

22.5 Revenue and Profit Calculation

The cost benefits are essentially the 4,3% points of extra efficiency of the wind farm if the device is deployed. As stated before, in order to calculate the benefits, one needs to calculate the average energy produced by the wind farm, in this case the OWEZ wind farm.

The OWEZ wind farm consists of 36 Vestas V90-3MW turbines. Each Vestas V90-3MW turbine has a nameplate capacity of 3 [MW], with a capacity factor of 0.35 on average [136]. The capacity factor of a wind turbine is the ratio of the actual output of a wind turbine over its output if it had operated at full nameplate capacity. If the turbines would be placed separately, the average yearly energy output would be:

$$37.8\ [MW] \cdot 24\ [h] \cdot 365\ [days] = 331\ [GWh] \tag{22.1}$$

However, the turbines are placed inside a wind farm. This results in a decrease in the overall efficiency. Shell and Nuon together evaluated the wind farm efficiency between the periods of January 2007 until March 2008. The wind turbine availability in that period was 90% [4] and the wind farm efficiency was 93.4% [4] during the considered period. This results into the following equation, concerning the total average yearly power output of the OWEZ wind farm:

$$291\ [GWh] - 278.4\ [GWh] = 12.8\ [GWh] \tag{22.2}$$

The price of 1 kWh equals €0.17 on average [137] (in The Netherlands, May 2010). This €0.17 consists of €0.11 subsidies per kWh from the Dutch government and since the wind farm is on average available $2 \cdot 10^3$ to $6 \cdot 10^3$ hours available per year, €0.06 per kWh by selling the energy to the power net [137]. This is further explained in the reference source. However, the project should be cost efficient without subsidies in the near future. Therefore, only the €0.06 per kWh of selling the energy is considered. The benefits if the device improves the wind farm efficiency by 4.3%, would be:

$$12.8\ [GWh] \cdot €0.06 \cdot 1,000,000 = €769k\ /year \tag{22.3}$$

Since the wind farm was opened in 2006, and is scheduled to close in 2026, the benefits will count for the 15 years to come. But, the project should also be applicable to future wind farms, therefore the total revenue over the period of 20 years will be considered. So the fact that this is not the case for the OWEZ wind farm is ignored. Now the total benefits over the entire life cycle will become:

$$€769k\ /year \cdot 20\ [year] = €15M \tag{22.4}$$

What has not been taken into account is the increase in energy price. For the next decades, a bigger increase is expected due to the introduction of sustainable energy sources. However the prediction differ between 2% and 5% increase. Due to an unclarity this has not been taken into account yet. However the inflation can be estimated to be 2%, therefore a conservative estimate of 2% is used [138]. The resulting income can then be calculated using:

$$\text{Total Revenue} = \sum_{n=1}^{20} €769k\ /year \cdot 1.02^{i-1} = €18.7M \tag{22.5}$$

However, the time value of money also plays a significant role, so the present value of the money should be calculated. Since the future interest rate, and bank account rate is uncertain, an estimation of 4% on year basis is used [139] [140]. The present value will then become:

$$\text{PV} = €0.934M \cdot \frac{1 - \frac{1}{1.04^{20}}}{0.04} = €12.7M \tag{22.6}$$

In which the €934k origin from the outcome of equation 22.5 divided by the following years.

To check feasibility, the amount of €12.7M is used. If the cost of a project is more than the amount of €12.7M, the project is not feasible.

Also the profit after twenty years can be determined. Taking into account that the revenue accumulates to €12.7M and the total cost for a lifespan of 20 years amounts to €6.21M, it can be concluded that the profit is €6.49M.

22.6 Return on Investment

Return on Investment (ROI) describes the ratio of money gained from the investment relative to the amount invested [141]:

$$\text{ROI} = \frac{\text{Gain from Investment} - \text{Cost of Investment}}{\text{Cost of Investment}} \tag{22.7}$$

From that it can be seen that the ROI is usually expressed as a percentage. Also for this case, the annual average return will be calculated, since maintenance will occur on different levels (ropes, kites, gases and so on).

In section 22.5 the total revenue and the total investment have already been determined. Therefore the ROI can now be determined:

$$\text{ROI}_{kite} = \frac{12.7 - 6.21}{6.21} = 1.04 \tag{22.8}$$

Expressed as a yearly average that leads to 5.2%, since 104% is derived for 20 years.

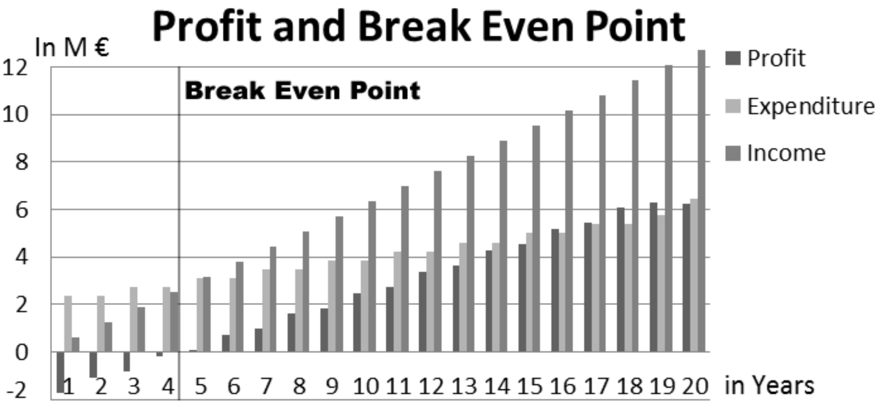

Figure 22.4: ROI and Break Even Point

In order to get a clearer picture figure 22.4 has been created. The image shows the cumulative income, the expenditure and the cumulative profit as a function of time (20 years). Also marked is the break-even point which occurs just precisely after 4.5 years. For the income the average annual extra energy yield has been considered. For the expenditure the initial investment costs are taken together with the average maintenance costs considering a maintenance cycle of two years.

22.7 Conclusion

From the ROI calculations, it can be seen that the values are relatively small compared to other regular investments. When looking at actual offshore wind projects the ROI is at around 12-18 percent, however this is only when taking into account subsidies, which account for around 70 percent of the revenue. Without the subsidies one would receive a negative ROI, which means making losses. Therefore, this application will lead to a higher ROI for standard wind turbines thus increasing the net profit.

Chapter 23

Other wind farm applications

In this chapter the application of the kite system to other wind farms around the world is presented. Firstly, section 23.1 shows the characteristics of a few large wind farms. Secondly, in section 23.2 a distinction is made between onshore and offshore wind farms. Thirdly, in section 23.3 the applicability of the kite system to other wind farms is verified. Fourthly, in section 23.4 whether and in what sense the device can be scaled to other wind farms is presented. Fifthly, in section 23.5 the restrictions to the application of the kite system to other wind farms is laid out. Finally, a conclusion regarding the applicability of the kite system to other wind farms is drawn in section 23.6.

23.1 Other wind farm characteristics

In this section, a short overview of two other noticable wind farms is presented. One onshore and one offshore wind farm will be considered. A comparison to OWEZ is made.

Currently a large onshore wind farm is being built, namely the Clyde Wind Farm, in Scotland. The wind farm will have an installed capacity of 350 MW, more than three times the capacity of OWEZ [142]. When looking at the layout of the wind farm, it can be seen that roughly 70 [%] of the turbines will be located in a matrix format, with a turbine spacing of 500-1000 [m] [143] and rotor diameters of 93 and 101 [m]. The other turbines will be aligned in a single row. The average wind velocity at the wind farm at 80 [m] above ground level is 7-8 [m/s] [144].

Currently on of the largest offshore wind farms in the world is the Thanet Wind Farm (TWF) off the coast of England, with an installed capacity of 300 MW, roughly three times the capacity of OWEZ. When looking at the layout of the wind farm, it can be seen that the turbines are arranged in matrix format. Each turbine is 115 [m] tall and is placed in water depths of 20-25 [m]. The horizontal turbine spacing is at least 450 [m] [145] and the rotor diameter of each turbine equals 90 [m]. The average wind velocity in the wind farm at 100 [m] above sea level is 10-11 [m/s] [146].

The above stated parameters for both the onshore and offshore wind farm are in the same order of magnitude as the parameters of OWEZ for which the kite system is designed. Therefore, on first evaluation the device is likely to be applicable to these other noticeable wind farms. In section 23.2 a comparison is made between onshore and offshore wind farms in general. In section 23.3 the applicability of the kite system to other wind farms in general will be further elaborated.

23.2 Onshore vs. offshore

In this section a distinction is made between the application of the kite system to an onshore wind farm and the application to an offshore wind farm.

Where OWEZ, for which the kite system is designed, is an offshore wind farm, also large onshore wind farms exist. The application of the kite system to these onshore wind farms has some advantages and some disadvantages.

One of the most important advantages of applying the kite system to an onshore wind farm, instead of to an offshore wind farm, is that the installation of the device is much less complicated. When installing the device in an offshore environment, the waves and tides cause the installation platform to be moved and vibrated. Also the system needs to be anchored to the bottom, which lies upto 20 [m] below the water level, and is therefore difficult to reach.

A second advantage is that maintenance to the device in an onshore wind farm can be performed in a less difficult, more safe and therefore cheaper manner. Again, because of the stable and relatively easy accessible surface on the shore. Also, less or less trained maintenance personal is required, resulting in lower costs.

A third advantage is that the kite will not be able to fall into the water, making it difficult to get up in the air again. However, now the risk of collision with the ground is present.

A fourth advantage is that the system can be connected to the electricity grid relatively easy. No costly and risk bearing solar cells and batteries will have to be implemented.

A fifth advantage is the fact that there is less risk of corrosion, because of a relatively unsalty environment. Other practical problems, with respect to the insulation of different subsystems from water, do not have to be solved.

A disadvantage of applying the kite system to onshore wind farms, instead of to offshore wind farms, is due to regulations. At this stage no attention is paid to the overall appearance of the kite system. It should be thought of how to blend the kite system into the existing environment visually.

Another noticeable disadvantage is that the mean wind velocity above land is less than above sea, yielding a lower wind farm energy output [147].

23.3 Multi applicability verification

In this section it is verified whether the kite system can be applied to other wind farms.

The dimensions of the aerial device are driving for the applicability to other wind farms. These dimensions are fixed and are all directly dependent on the kite span. The kite span and wind farm efficiency increase of OWEZ are listed in table 23.1. Different wind farm parameters are checked for their influence to the wind farm efficiency increase. In the Matlab programming code different values for the listed parameters are implemented and the efficiency increase sensitivity to these changes is shown in table 23.2. As can be seen, the first column shows the altered parameters. The second column shows the OWEZ parameters, for which the kite system is designed. The third column shows that each parameter is lowered by 5 [%], resulting in new parameters in the fourth column. The fifth and sixth columns show the changes to the efficiency increase. It can be stated that the rotor diameter has a great influence to the resulting efficiency increase. A smaller rotor yields a higher efficiency increase, which is desirable.

Table 23.1: Kite parameters

OWEZ efficiency increase	**Projected span**
4.3 [%]	16 [m]

Table 23.2: Multi applicability verification

Parameter	**OWEZ**	**Change parameter by [%]**	**New value**	**Efficiency increase [%]**	**Difference [%]**
Current wind farm efficiency	93 [%]	-5.0	88.35 [%]	4.0	-2.4
Wind direction correction	0.57	-5.0	0.54	3.89	-5.1
Rated velocity	15 [m/s]	-5.0	14.25 [m/s]	3.97	-3.2
Rotor diameter	90 [m]	-5.0	85.5 [m]	4.56	11.2

Typical other wind farm parameters, which are also important for the applicability of the kite system, are listed below. These parameters, however are either difficult to verify or are incorporated in the *wind direction correction* parameter in table 23.2.

- **Turbine height:** wind measurements at the hub height are necessary to verify the efficiency increase sensitivity to this parameter.
- **Turbine spacing:** this is incorporated in the *wind direction correction* parameter as is explained in section 10.4. If the spacing of the wind turbines is different, the wind directions in which the kite is aligned with the turbines are different. Looking at figure 10.4, the angles in figure 10.4A and -B are different from the angles in OWEZ. Meaning a different *wind direction correction*, when assuming the same wind speed distribution. Note that it is assumed the wind turbines are placed in a box shaped format.

- **Wind speed variation:** the independence on this parameter is explained in section 10.9.
- **Wind speed distribution:** this is incorporated in the *wind direction correction* parameter as is explained in section 10.4. Figure 10.4C shows a wind speed distribution of OWEZ. If this is different for an other wind farm, assuming the turbine spacing to be the same, this yields a different *wind direction correction.*

The aforementioned parameters can be different for every wind farm. When willing to apply the kite system to a different wind farm, it should be verified whether and in what sense the wind farm is different from OWEZ. These parameters can be implemented in the aerodynamic calculations in chapter 10.

23.4 Scaling to other wind farms

In order to increase the applicability of the kite system, the device should be scalable to other wind farms. In section 23.3 it was described whether the device, with its current dimensions and characteristics, can be applied to other wind farms, with different specifications than OWEZ. Now, in this section, whether and in what sense the device can be scaled to other wind farms is presented. It should be noted, that the different wind farm parameters are used to calculate the kite dimensions, following the aerodynamic calculations in chapter 10. From this it should be noted that the calculations are performed for 4 turbines standing behind each other. In this section, the scaling is performed to yield a 4.3% wind farm efficiency increase.

Subsection 23.4.1 deals with the structural scaling of the aerial segment. Subsection 23.4.2 deals with the costs, following the outcomes of the structural scaling.

23.4.1 Structural scaling

Section 23.3 shows the parameters that are different for each wind farm. To some of these, the device can be scaled. The dimensions of the aerial segment are driving for the scaling of the other different subsystems. These dimensions are strongly dependent on the desired wind farm efficiency increase, local wind properties and the dimensions and characteristics of the wind farm and individual turbines. If, for example, the kite span needs to be higher to gain an efficiency increase of 4.3%, the lift generated by the kite will be larger, which will result in a higher tension force in the tethers. As a consequence the ground segment will have to cope with larger forces. All aforementioned subsystems therefore have to be scaled, either up or down, depending on the specific wind farm characteristics.

When looking at the aforementioned parameters, it can be stated that some of them do and some do not influence the aerial segment's dimensions. Some need further research to be able to draw conclusions upon. Firstly, the individual influence of each parameter on the required kite span is evaluated, while keeping the other parameters constant. Secondly, four dimensional plots are presented in which a combination of multiple parameters is shown. The parameters and their influence on the required kite span are listed:

- **Turbine height:** wind measurements at the hub height are necessary to verify whether and in what sense the system needs to be scaled to this parameter.
- **Turbine spacing:** this is incorporated in the *wind direction correction* parameter as is explained in section 10.4. If the spacing of the wind turbines is different, the wind directions in which the kite is aligned with the turbines are different. Looking at figure 10.4, the angles in figure 10.4A and -B are different from the angles in OWEZ. Meaning a different *wind direction correction*, when assuming the same wind speed distribution. Note that it is assumed the wind turbines are placed in a box shaped format.
- **Wind speed variation:** the independence on this parameter is explained in section 10.9.
- **Wind speed distribution:** this is incorporated in the *wind direction correction* parameter as is explained in section 10.4. Figure 10.4C shows a wind speed distribution of OWEZ. If this is different for an other wind farm, assuming the turbine spacing to be the same, this yields a different *wind direction correction.*
- **Rated velocity:** a higher wind turbine rated velocity, means a larger wind velocity range in which the efficiency can be increased, following the reasoning in section 10.5. According to this, the aerial segment's dimensions can be scaled down, when this rated velocity is higher. On the other hand, when this rated velocity is lower, the aerial segment has to be scaled up. This can be seen in figure 23.1. At the lower wind velocities, this difference is the largest. When a wind turbine has a rated velocity in the range of 10-20 [m/s] - the OWEZ turbines are at 15 [m/s] - only a small scaling will have to be applied, as the change in required span is minimal.

- **Current wind farm efficiency:** if the current wind farm efficiency is lower than the efficiency of OWEZ, a larger kite is required to come to the same wind farm efficiency increase of 4.3%. This can be seen in figure 23.2. The kite span is in the range of 15.8-17.6 [m] for a wind farm efficiency of 75-95% respectively. This comes down to an extreme lift of 63-78 [kN], following equation 10.43, again assuming the maximum wind velocity equals 27.3 [m/s] and the aspect ratio of the kite equals 2. This outcome yields reasonable structural changes, either up or down.

- **Rotor diameter:** a larger rotor diameter yields a larger required mass flow increase to give the same wind farm efficiency increase of 4.3%. As can be seen in figure 23.3 there is a linear relationship between the rotor diameter and the kite span. Looking at a rotor diameter range of 70-130 [m], the kite span is in the range of 12-23 [m]. This corresponds to an extreme lift of 36-120 [kN], following equation 10.43, assuming the maximum wind velocity equals 27.3 [m/s] and the aspect ratio of the kite equals 2. This outcome yields large structural changes, either up or down, when the device needs to be scaled.

- **Wind direction correction:** the *wind direction correction* is a combination of the aforementioned wind speed distribution and turbine spacing. This is further explained in section 10.4. A larger value yields a smaller required kite span to come to the same efficiency increase of 4.3%. This is shown in figure 23.4.

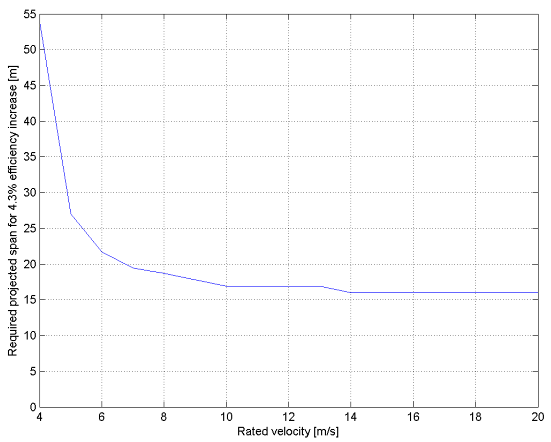

Figure 23.1: Relation between the rated velocity and the projected kite span.

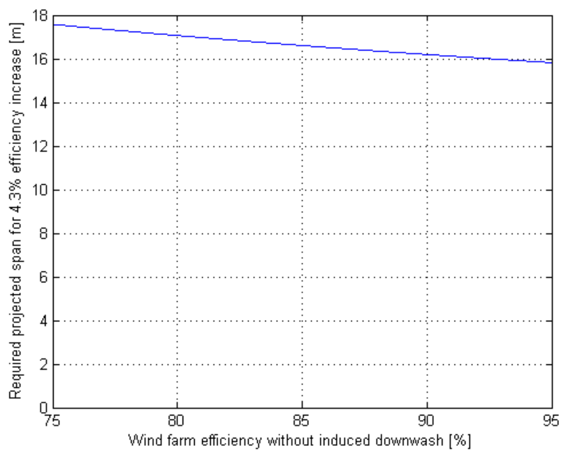

Figure 23.2: Relation between the current wind farm efficiency and the projected kite span.

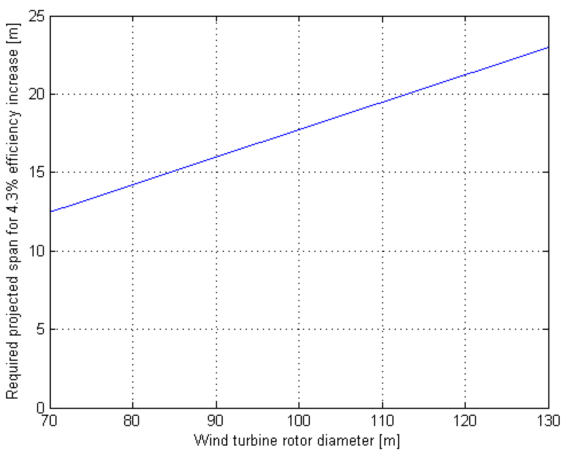

Figure 23.3: Relation between the rotor diameter and the projected kite span.

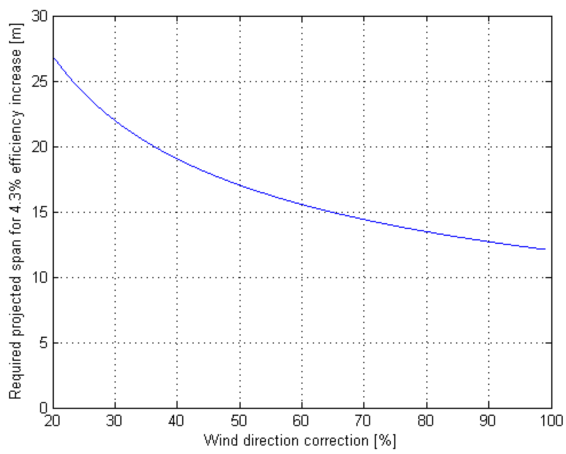

Figure 23.4: Relation between the wind direction correction and the projected kite span.

Now, while the verification of the individual influence of the different aforementioned parameters on the required kite span is performed, they can be combined. Figure 23.5, 23.6 and 23.7 represent the four dimensional plots of the kite span for a constant wind farm efficiency increase of 4.3%, for three different values of the *wind direction correction* factor, namely 0.40, 0.57 and 0.70, respectively. Each plotted surface represents a certain rated velocity. The top surface represents a rated velocity of 9 [m/s], the middle surface a rated velocity of 12 [m/s] and the lower surface a rated velocity of 15 [m/s]. To plot a surface, corresponding to a higher rated velocity, will give no additional useful information, as follows from figure 23.1. The required kite span can be read from the vertical axis when the other wind farm parameters are implemented.

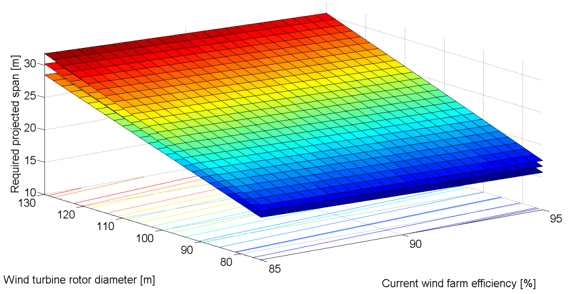

Figure 23.5: 4D-multi applicability plot for a *wind direction correction* factor of 0.40

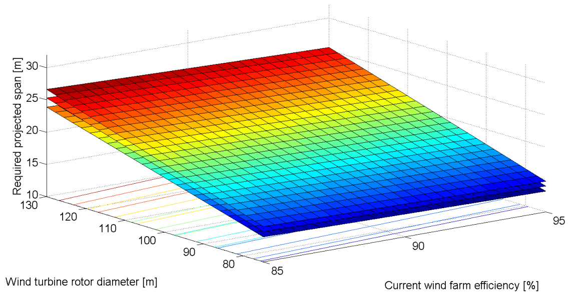

Figure 23.6: 4D-multi applicability plot for a *wind direction correction* factor of 0.57

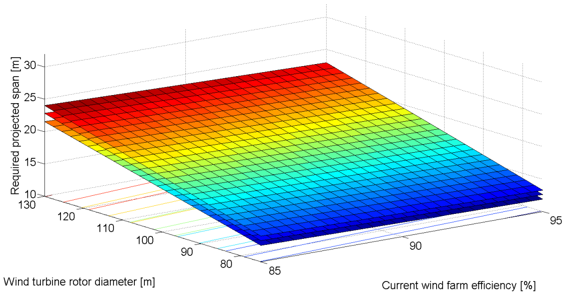

Figure 23.7: 4D-multi applicability plot for a *wind direction correction* factor of 0.70

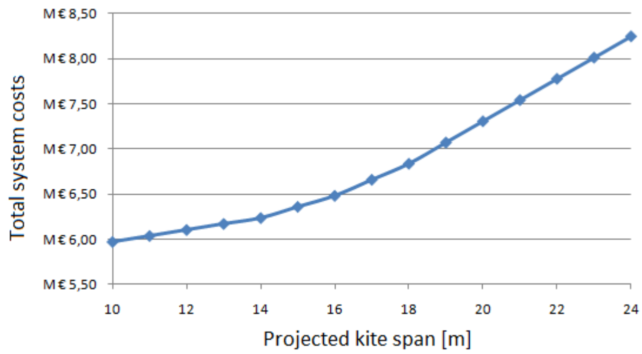

Figure 23.8: Total system costs vs. the projected kite span

23.4.2 Costs

In chapter 22 a cost analysis is performed. The costs of the aerial segment, the tether and the ground segment are estimated. Using these estimations and comparing them to the results from subsection 23.4.1 a cost window can be constructed. Figure 22.2 shows the cost estimation of the kite. Comparing this figure with the results in figure 23.3 and 23.2, the costs per kite are in the range of €4.5-6.1k. Next, the costs of the ground segment are analysed. Figure 22.3 shows the costs of the buoy as a function of the kite span. Again, comparing this figure to the results in figure 23.3 and 23.2, the costs per buoy are in the range of €35-125k. Secondary costs are assumed to remain constant and make up for €7.5k, as can be seen in subsection 22.2.3.

Next to this, it is assumed that the installation and retirement costs remain constant. The maintenance costs are changing by a small percentage. These three costs make up for approximately 70% of the total costs. It can be stated that these are highly dependent on the specific conditions at the considered wind farm. The total costs per kite system, excluding these, add up to €50-143k for projected spans of 12-24 [m] respectively, as can be seen in figure 23.8.

A clear distinction can be made between applying the kite system to an onshore and to an offshore wind farm. Installation, maintenance and retirement costs will be reduced significantly when applied to an onshore wind farm. These are assumed to be a factor 2-2.5 lower in an onshore environment [148]. Also the costs of the ground segment will be considerably lower. No complex buoyant glass fibre structure will have to produced. The anchoring can be omitted. Solar cells are unnecessary, since the system can be connected to the electricity grid relatively easy. Adding up these different assumptions, it can be estimated that the total system costs are roughly a factor 2 lower when applying the kite system to an onshore wind farm.

23.5 Restrictions

In this section a short overview of different restrictions to applying the kite system to other wind farms is presented.

Firstly, when designing for the OWEZ wind farm, a more or less rectangular shaped layout is considered, in which the wind turbines are arranged in parallel rows and columns. This results in different wind turbines standing behind each other for the most common wind direction. If, however, in a different wind farm the wind turbines are aligned in a single row, the 3% efficiency increase might not be achieved, making the device not profitable.

Secondly, if the wind turbines in a different wind farm are standing too close to each other, i.e. less than approximately 400 [m], there is too little room for the kite system to be applied. The distance between the kite and wind turbine should be sufficiently large, in order to make sure the kite does not get tangled up in the turbine rotor.

Thirdly, if the kite system is applied to a wind farm in a very UV radiant region, the lifetime of the kite is lessened. Appropriate measures should be taken in order to cope with this problem.

Fourthly, if the wind turbines in a wind farm are located on different elevations, the wake effects on the wind farm efficiency are very different and most probably less. Therefore an additional wind farm efficiency increase of at least 3% is less likely to be achieved.

23.6 Conclusion

When the measures, described in section 23.1 to 23.5 are taken, the device can be applied to other wind farms around the world, both onshore and offshore. If one is willing to accept a less optimal performance, the currently designed kite system can be applied to different wind farms, when it is verified whether te wind farm characteristics are within reasonable range of the OWEZ wind farm characteristics. If one desires an optimal configuration, specially designed for a particular wind farm, the device can be scaled. This multi applicability shows the potential of the kite system, both economically and environmentally.

Chapter 24

Compliance Matrix

For this project, there were several requirements set by the client that had to be fulfilled, these were:

- Increase the wind farm efficiency with a minimum of 3%.
- The life time of the device should be at least 20 years.
- The minimum interval between maintenances should be at least 2 years.
- The device should be cost efficient.
- The device should be applicable to the OWEZ wind farm and scalable to other wind farms.

The first point is achieved, since the actual wind farm efficiency increase due to the application of the device is 4.3 percent points. The efficiency increase of the wind farm is actually higher than the 4.3 percent point mentioned above, but this is when the wind blows from the dominant south-west direction. For the other wind directions, the device is less efficient, but on average the wind farm efficiency is 4.3%. Therefore the average efficiency is lower than the efficiency it creates when the wind blows from its dominant direction.

The life time for the kite is only 2 years, but the kite can be replaced every time during maintenance. Thus, the kite poses no threat for the required minimum 20 years of life time for this device. The buoy system is not easy replaceable, but this poses no problem since the life time of the buoy is more than the required amount of 20 years. So, in conclusion, this point can also be met.

The minimum time between maintenances is more than 2 years, since the device is fully autonomous, and has several back up systems. As can be seen in chapter 22, the device is also cost efficient. It creates a huge amount of cost benefits, this outweighs the costs. Thus, the return on investment is also positive, this requirement is clearly met.

The actual design was for the OWEZ wind farm, so it is guaranteed applicable to the OWEZ wind farm. The OWEZ wind farm has a prevailing wind direction, this is good for the device. If the device is placed on other wind farm, these wind farm should also have a prevailing wind direction. If this is not the case, design changes have to be made. For this, the device is considered moderately applicable to other wind farms, since it is not applicable for all the wind farm. An overview of the compliance is given in table 24.

Table 24.1: The compliance table

Requirement:	**Is the requirement met?**
3% wind farm eff. Increase	yes
20 Years lifetime	yes
2 years maintenance interval	yes
cost efficient	yes
applicable to OWEZ	yes
applicable to other wind farms	moderately

In conclusion, it can be stated that the device can meet all the requirements stated before.

Chapter 25

Project design & development logic

In this chapter the project design and the future development phases of the kite system after the DSE are presented.

Six phases can be identified in which the design of the system will evolve to a fully operating device. These phases are worked out in more detail, showing in the Gantt Chart in figure 25.1. The sequence in which the different actions are performed is shown in the Work Flow Diagram in figure 25.2. The different identified phases, with the estimated required work weeks and resources required, are shown in table 25.1. In the first column the project development phase is shown. The second column shows the duration and the third column the resources needed.

Table 25.1: Project design & Development logic

Phase	**Duration**	**Resources**
Set-up business	14 weeks	staff
Research phase	18 weeks	staff
Testing phase	24 weeks	staff, equipment tool, materials
Planning production & installation phase	18 weeks	staff, equipment tools, materials, investors
Production & installation phase	19 weeks	staff, equipment tools, materials, investors, transport
Start operations	-	staff
Total Estimated Time	**111 weeks**	-

In the following, the different phases are worked out further:

- Firstly, financial and logistic preconditions have to be dealt with. A business has to be set up, in which a business plan is written and market analyses are performed. Next to this, investors are contacted and arrangements with these are made. Throughout the further development of the system, continuously contact is sought and maintained with investors and clients.
- Secondly, the detailed design should be picked up where it stopped at the end of the Design Synthesis Exercise. All assumptions and calculations on aerodynamics, structures, materials and performance should be validated and worked out in more detail. Risk analyses and cost calculations should be verified and investigated in more depth. When this is done, a CFD model can be created in which the behaviour of the kite and the airflows can be predicted more accurately. From this model the system can be further optimised.
- Thirdly, laboratory tests can be performed. A small scale model is made, which performance is tested in the wind tunnel. From the acquired data the design can be further optimised. After this, a full-scale model is built. Different characteristics of this model are tested, either on strength, functions and performance. These tests are performed for the different subsystems, namely the ground segment, the tether and the aerial segment. Next to this testing, a full-scale test can be performed in which the full system is operating under normal conditions and ultimate conditions. After this, the findings are documented and processed.
- Fourthly, if all tests are passed, the production and installation phase need to be prepared. To do so, a production plan has to be written. Also maintenance and dismantling plans are written. Contact is sought with different potential manufacturers. On the cost prices is negotiated, after which contracts are set up. Similar steps are taken in planning the installation.

- Fifthly, the different subsystems can be manufactured, after which they are transported and sub-assemblies are made. When all subsystems are manufactured, they can be installed. The sub-assemblies are shipped to the wind farm location and are installed on-site. When this is finished the systems can be checked and their correct functioning is verified.

- Finally, after 111 weeks, the full operation of the kite systems can be started.

Note that the amount of time required to finish each phase is strongly dependent on the available resources, i.e. staff, funds, materials, etc. A thorough set-up of the business will result in a good human resource allocation, from which the other actions will take less time.

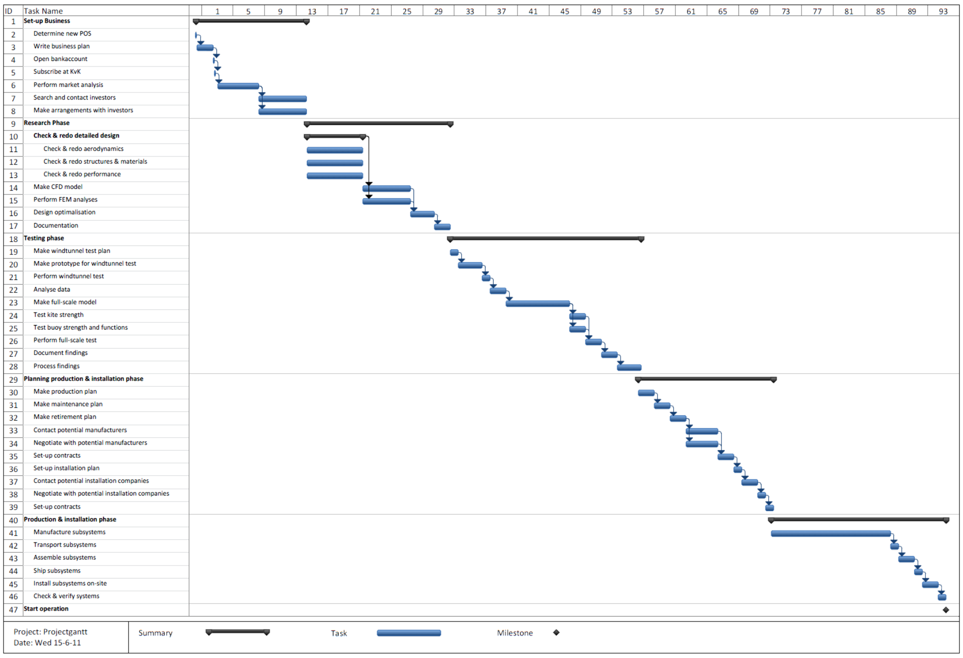

Figure 25.1: Project Gantt Chart

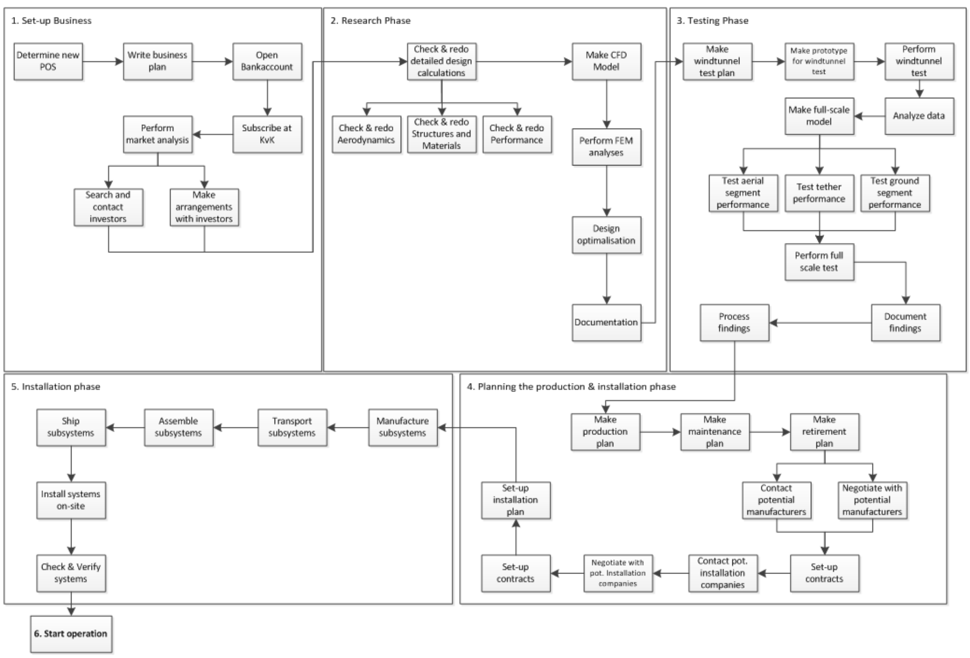

Figure 25.2: Project Work Flow Diagram

Chapter 26

Suggested follow-up research

In this chapter suggested following research is presented. This is an advise for people that will perform research on this subject in the future. In this report many theoretical calculations were done, which showed the potential of the device. Now the potential is shown, more extensive research can be done on the precise behaviour of the system. This can be done with for instance computer simulations or by using prototypes. By doing this extensive research, assumptions can be dropped yielding more accurate predictions. This can help to optimize the design. First, the suggested aerodynamic research is presented in section 26.1. Then, suggested structural & materials research is treated in section 26.2. After that section 26.3 treats the suggested research on stability and control. Note that the different tests may be performed simultaneously. Once all previous research is completed, the final operational research is performed, which is treated in section 26.4.

26.1 Aerodynamics

The aerodynamic calculations in this report assumed fully laminar flows and were quite theoretical. In section 10.10 the main assumptions made for the aerodynamic calculations in this report were stated. The main goal of the suggested research is to become able to drop these assumptions. Furthermore it must lead to an optimized design. The first step is doing Computational Fluid Dynamics (CFD) calculations. After that wind tunnel tests are performed and finally a full scale prototype is made and tested.

26.1.1 CFD

The first thing that should be done is programming the flow around the kite. Doing this on a computer makes it possible to improve the design without building prototypes, which is more expensive and gives less design freedom. Complex CFD calculations can become expensive too however. This is because the programs have to be made by costly engineers and since computer processing time is expensive as well. This is the reason why the CFD calculations are only used to assess some specific effects. More complex effects, such as turbulent mixing, are addressed with a wind tunnel model. Since kites are relatively cheap, wind tunnel tests can be done in a cost effective manner. The goals of CFD calculations are the following:

- Verify the theoretical calculations in this report.
- Assess and quantify the effect of a wind gradient (different velocity at different heights) on the kite performance. This instead of the average velocity over the rotor disc, used in the calculations in this report.
- Assess and quantify the decreasing marginal utility, i.e. the bending of the lower flow (in reality: the wake flow) induced by the downwash.
- Assess and optimize the flow interaction by the kite, particularly the downwash.
- Assess and optimize the velocity increase of a laminar flow (representing the wake) by a downwash of faster flow (representing the outer flow).

Only a rigid kite in an undisturbed flow will be modelled. The turbines will not be modelled in order to keep the model simple and prevent very expensive turbulence modelling. Looking at the goals of the CFD calculations, one can distinguish three types. The first goal is checking of previous calculations. The second and third goal must complement the theoretic calculations by estimating efficiency factors of different effects. The fourth and fifth goal are used to optimize the kite design.

26.1.2 Wind tunnel tests

Once the kite is optimized using CFD calculations the system can be further investigated with wind tunnel tests. If performed well, these tests can model reality better than the theoretical and CFD calculations. A physical model of the system is needed however. Two set-ups will be used: one with just the kite and one modelling both the turbine and the kite. A distinction between the two set-ups is made, since modelling both a turbine and kite needs a lot of scaling (to fit it inside a wind tunnel). This would cause the tests to become less accurate. Testing with only a kite as well, will give better approximations of reality. This type of test will be discussed now. The goals of the wind tunnel test with just the kite are the following:

- Validate the theoretical and CFD calculations.
- Assess and optimize the flow interaction by a kite, particularly the downwash.
- Assess and optimize the structural strength of the kite and investigate effects of extreme weather conditions (see section 26.2).

These goals are accomplished by suspending a kite in the wind tunnel on a rigid support rack and running the tests. Using Particle Image Velocimetry (PIV) the speed and direction of the airflow can be observed. PIV can measure a whole 3D velocity field, in contrast to other techniques which typically measure velocity at one point [149]. PIV measures this by taking two images shortly after each other and observing the distance travelled by individual particles. From the this distance travelled and the known time difference, the velocity field is calculated. Tracking the particles is done with a laser, since it can form a very thin sheet and follow particles even when the flow is very fast [150].

The actual kite has a projected span of 16 [m]. Since this does not fit in a wind tunnel, the kite has to be scaled. However, if the kite is scaled, the flow must change as well in order to have similar properties as in reality. In order for two flows to be similar, the geometry, the Mach number and the Reynolds number for both flows must be equal [24]. Since the real kite is scaled to a tunnel model, the geometry does not change (only the size changes). In order to have the same Mach and Reynolds number in the wind tunnel as in reality, one can change the wind tunnel airspeed. It is however not possible to have both the same Mach number and Reynolds number at the same time, since this would require a very high pressure wind tunnel [24]. Rather, two separate runs must be done: one with the right Mach number and one with the right Reynolds number. One could also consider performing a wind tunnel test with the right Froude number, since the wind velocity is in the low subsonic region and an open-channel flow are researched [151]. When a scale model is used, the required wind tunnel velocity for the right Froude number is quite low [151], so this does not pose a constraint on the wind tunnel. Now the Mach number is discussed first.

Equation (26.1) shows the Mach number M for reality (subscript r) and for the wind tunnel (subscript t). As can be seen the Mach number is dependent on airspeed V and the speed of sound a. It is assumed that a is proportional to the square root of absolute temperature T [24]. This fact yields equation (26.2).

$$M_r = \frac{V_r}{a_r} \propto \frac{V_r}{\sqrt{T_r}} \quad and \quad M_t = \frac{V_t}{a_t} \propto \frac{V_t}{\sqrt{T_t}} \tag{26.1}$$

$$\frac{V_r}{\sqrt{T_r}} = \frac{V_t}{\sqrt{T_t}} \tag{26.2}$$

Now the wind tunnel airspeed, which is required to have an equal Mach number as reality, can be calculated. This is done in equation (26.3). Here V_r is the nominal real airspeed of 9.46 [m/s] (from section 10.3), T_r is the temperature at 145 [m] altitude (the altitude of the kite), which is 287.2 [K] [152]. T_t is the temperature in the wind tunnel, which is assumed to be at sea level, so T_t=288.2 [K]. The result shows that the airspeed is only a bit larger than in reality.

$$V_t = V_r\sqrt{\frac{T_t}{T_r}} = 9.46 \cdot \sqrt{\frac{288.2}{287.2}} = 9.48[m/s] \tag{26.3}$$

Now the required wind tunnel velocity for an equal Reynolds number as reality is calculated. Equation (26.4) shows the Reynolds number Re for reality (subscript r) and for the wind tunnel (subscript t). As can be seen the Reynolds number is dependent on airspeed V , density ρ, geometric dimension c (span in this case) and viscosity μ. It is assumed that μ is proportional to the square root of absolute temperature T [24]. This fact yields equation (26.5).

$$Re_r = \frac{\rho_r V_r c_r}{\mu_r} \propto \frac{\rho_r V_r c_r}{\sqrt{T_r}} \quad and \quad Re_t = \frac{\rho_t V_t c_t}{\mu_t} \propto \frac{\rho_t V_t c_t}{\sqrt{T_t}} \tag{26.4}$$

$$\frac{\rho_r V_r c_r}{\sqrt{T_r}} = \frac{\rho_t V_t c_t}{\sqrt{T_t}} \tag{26.5}$$

Rewriting gives equation (26.6). The density ratio can be calculated with the equation of state for an ideal gas, $p = \rho RT$. This calculation is shown in equation (26.7). Since R is the universal gas *constant* it drops out of the equation. Note that an unpressurised wind tunnel, which will be used, has a pressure ratio of 1.

$$V_t = V_r * (\frac{\rho_r}{\rho_t}) \cdot (\frac{c_r}{c_t}) \cdot \sqrt{\frac{T_t}{T_r}} \tag{26.6}$$

$$\frac{\rho_r}{\rho_t} = (\frac{p_r}{p_t}) \cdot (\frac{T_t}{T_r}) \tag{26.7}$$

From the definition of the Reynolds number, one can deduce that if the model is scaled down, the tunnel airspeed must increase. Figure 26.1 shows the relation between the (scaled) projected span and the required tunnel airspeed. This is done to simulate nominal conditions (V_r = 9.46 [m/s]) and for extreme conditions (V_r = 27.28 [m/s], the maximum allowable airspeed). As was expected from equation (26.6), these relations are inversely proportional. The figure also shows five wind tunnels (the circles), which are considered for testing. Three of them are the subsonic wind tunnels in Delft, which are preferred because of their location. The other two wind tunnels were previously used for Delft kite research [153], but are not in Delft. Table 26.1 shows which number represents which wind tunnel. The locations of the circles indicate the maximum speed of the tunnels as well as the tunnel width, which is the maximum kite projected span. As can be seen in the figure only the Large Lowspeed Facility in Markenesse can be used to test both the nominal and the extreme conditions. The projected span of the kite that will be used will be 7.0 [m] (the design point in the figure). This leaves a total space of one meter between the kite and the tunnel, which is needed to not disturb the flow too much. Once all tests are done, one final test will be performed. The airspeed will be increased to the maximum airspeed of the tunnel (104.2 m/s) to investigate the structural failure of the kite. This corresponds to a real airspeed of 45.4 [m/s] (calculated using equation (26.6)), well above the wind speeds above the North Sea. The kite will probably fail before the maximum wind tunnel speed is reached.

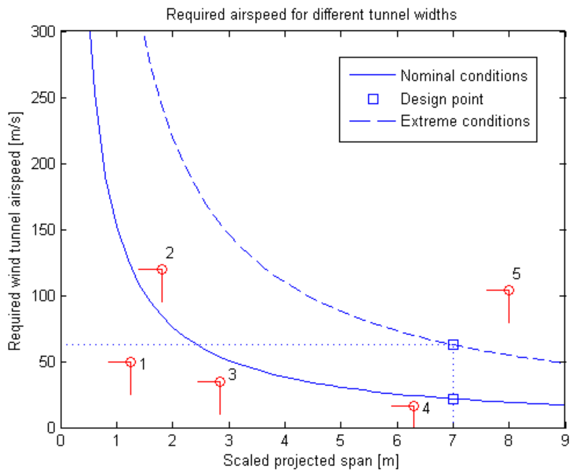

Figure 26.1: The relation between the (scaled) projected span and the required tunnel airspeed

Table 26.1: Characteristics of the considered wind tunnels

Number	Name	Location	Width [m]	Height [m]	Max speed [m/s]
1	Boundary Layer Tunnel	Delft	1.25	0.25	50.0
2	Low Turbulence Tunnel	Delft	1.80	1.25	120
3	Open Jet Facility	Delft	2.85	2.85	35.0
4	Boënwindkanal	Stuttgart	6.30	6.30	16.7
5	Large Lowspeed Facility	Markenesse	8.0	6.0	104.2

The second set-up models both a turbine rotor and a kite. In this wind tunnel test the mixing of the downwash and the coherent structures from the rotor is investigated. The goal is to gain more knowledge about this subject and to estimate the value of a factor which describes this mixing with respect to the laminar mixing assumed in the CFD and theoretical calculations. These tests can be used to further optimize the design. It should be noted however, that these tests can become expensive, due to the complexity of the model: both a turbine and a kite must be created. The main goal is only to gain extensive knowledge about the mixing and one might choose to skip these tests and go to the prototype testing right away. In the prototype testing the performance of the system is assessed, which is the main point of interest anyway.

In this chapter the wind tunnels in table 26.1 are discussed, which are normal wind tunnels. One might also consider using an atmospheric wind tunnel, which can simulate the actual atmospheric wind very accurately. One can choose to perform research in such a wind tunnel as well, but this is not treated further in this chapter. Because of the size of the situation which is to be modelled, some adaptations must be made. Remember from the calculations earlier this section, that if the model is scaled down, the wind tunnel airspeed must become higher in order to have Reynolds number similarity. Figure 26.2 shows three possible wind tunnel models. The left one resembles the real situation, where the rotor is situated on the nacelle on the tower. This however results in a very high model, which needs to be scaled down a lot. That is why the model shown in the middle is considered. Here the tower is not as long as in reality. This reduces the height of the model, which is advantageous. Still the helices from the rotor are fully created in a wind tunnel test. A model with an even smaller height is shown in the right. Here only a half rotor is modelled. By doing this one cannot model the full helices, but only the upper part. This however is the most interesting region when investigating the mixing. Figure 26.3 clarifies this model with a front view. The blades are now turned one by one over 180 degrees. Note that they are not on the same driving shaft, since they rotate separately. This implies that the wind tunnel run has only a short period in which there are helices. The test might have to be run many times, to assess the mixing. Using only a half rotor leads to some inconsistencies, since the helices are not created in the same way as in reality. However, since *turbulent* mixing is being investigated, it is much more important to have the right Reynolds number, which determines the turbulence.

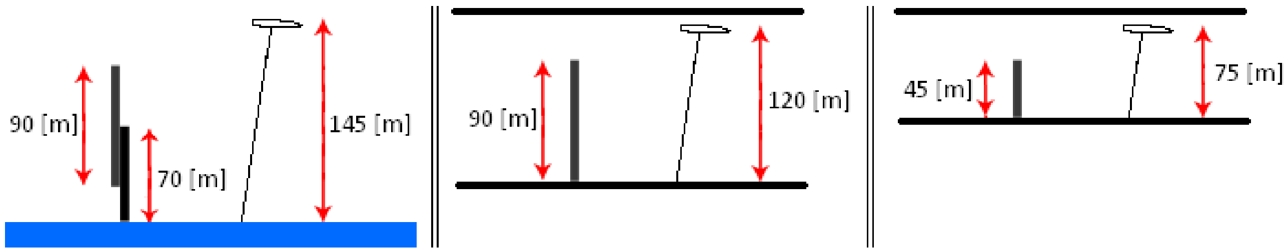

Figure 26.2: A tree showing all wind tunnel tests

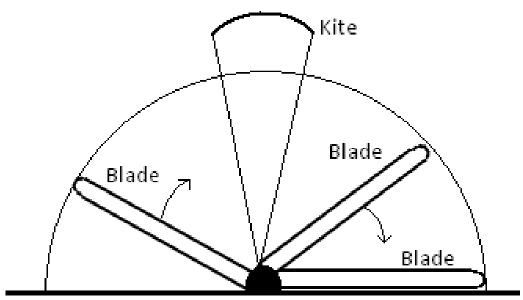

Figure 26.3: A wind tunnel model with only half a rotor

Now again a relation can be created between the required wind tunnel velocity and the scaled model height, using the same equations for equal Reynolds numbers as before. Figure 26.4 shows this relation, which is again inversely proportional (as expected). Again the circles represent the wind tunnels in table 26.1. From the figure it is concluded, that with these wind tunnels it is not possible to run the model at exactly the same Reynolds number as in reality during nominal conditions (V = 9.46 [m/s]). For this reason the best approximation of this situation is used. This means using the half rotor model at the right of figure 26.2 in the Large Lowspeed Facility in Markenesse. The model height (corresponding to the 75 [m] in right of figure 26.2) will be 5.8 [m]. This leaves some space between the model and the tunnel ceiling, which has a height of 6.0 [m]. This means the projected span of the kite is scaled down to only 1.28 [m]. Since in this model the kite is close to the tunnel ceiling, it is advised to use a rigid model of the kite. This is to prevent the kite from flapping to the ceiling. The wind tunnel is run on its maximum airspeed, which is 104.2 [m/s]. Using equation (26.6) it is found that for this model this tunnel airspeed corresponds to a real airspeed of 8.02 [m/s], just a bit under the nominal 9.46 [m/s]. Note that the test is also run with a similar Mach number. This results in a tunnel airspeed of 9.48 (see equation (26.3)), since the tunnel temperature has not changed. The flow in both runs is again investigated using the PIV technology.

Since much wind tunnel runs should be done, a tree showing all tests is given in figure 26.5 for clarity.

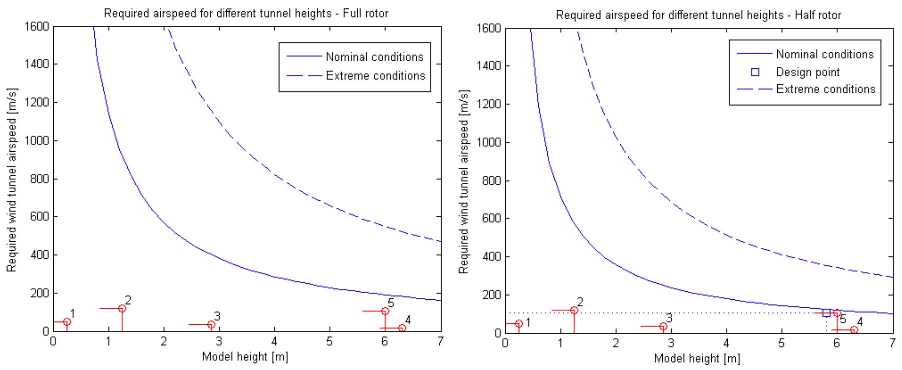

Figure 26.4: The relation between the (scaled) model height and the required tunnel airspeed

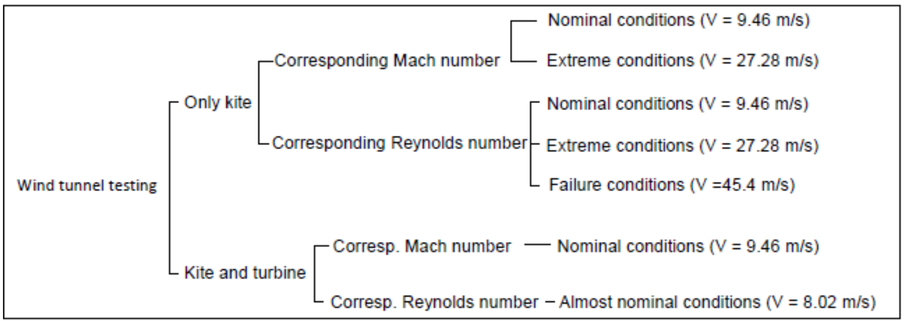

Figure 26.5: A tree showing all wind tunnel tests

26.1.3 Prototype tests

Once the design has been optimized using wind tunnel tests, it is time to build the first real prototype. This is one full scale kite, which is implemented between two turbines in an existing onshore wind farm. For this prototype also the winch, the tether, the control pod and the bridle system are needed. With this prototype test the actual performance of the system is assessed: how much is the output of the second wind turbine increased? In order to test this, the kite is launched to its normal position first. At this moment the power output of the second wind turbine is measured. Then the kite is moved to the side, such that it does not increase the output of the second turbine any more. Now the power output is measured again. This is done quickly to assure that the wind velocity and direction has not changed much between the two measurements. The test is done multiple times and for different airspeeds to fully assess the performance. If successful these test results will persuade potential customers.

26.2 Structures & materials

In this section an approach to the further development of different structural and material characteristics, that will have to be investigated in more depth, is presented. Different methods for getting to a more detailed, more accurate design are stated.

26.2.1 Aerial segment

Firstly, the structural characteristics of the aerial segment can be investigated in more depth. This is done to verify the earlier calculations and to give a more accurate prediction of the structural behaviour of the system. This can be done by drawing the kite in the *MSC Adams kite simulation toolbox*, by Ir. J. Breukels, TU Delft [51]. From an trial and error process the kite design can be further optimized.

Next, the built wind tunnel scale model can be loaded under extreme wind velocities, to verify at which wind velocity the kite will fails. Then, a full-scale prototype of the kite can be built. This prototype can be tested onshore under nominal and extreme conditions. Real conclusions about the structural performance of the kite can be drawn at this stage. Furthermore, the performance of Dacron, covered by Tedlar, can be further investigated. This is done to get a more clear overview of the influence of UV to the performance of the different kite materials.

26.2.2 Tether

Secondly, the structural characteristics of the main tether can be evaluated. To assess the tether geometry, forces and behaviour, a Finite Element Method, or FEM, analysis can be set up. This can be done using *MSC Patran-Nastran*. Nominal and ultimate forces, exerted by the kite, are drawn into the set up. To analyse the slacking and movements of the tether, periodic loads are implemented. From this, a more accurate design of the tether can be made. This in turn will influence the design of the ground segment, as will be explained in subsection 26.2.3.

After the FEM analysis, a real part test can be performed, in which the tether's tensile strength is checked. This is done by exerting nominal and ultimate loads on a short piece of tether in a laboratory set-up. This, to verify the cross-sectional dimensions and material characteristics of the tether, without having to build a costly full-scale model. Furthermore, the influence of the sun on Dyneema can be investigated in more depth.

26.2.3 Ground segment

Thirdly, the structural characteristics of the ground segment can be evaluated. At the present stage, the dimensions of the ground system are derived from the forces exerted by the surrounding water and by the tether, which follows from the lift and weight generated by the aerial segment. However, how the stresses and displacements behave exactly inside the ground segment structure is yet unknown. To get a more clear image of the behaviour of these and to be able to optimize the ground segment further, again a FEM analysis can be made. This can be done using *MSC Patran-Nastran*, in which the ground segment is drawn. The tether force and the water loads are implemented, from which an accurate overview of the stresses and displacements inside the ground segment can be derived. This is done for both the nominal and ultimate loads. Now, stress concentrations and high displacements can be identified and appropriate measures can be taken, optimizing the ground segment design.

26.3 Kite stability & control

In this section different kite stability and control uncertainties are dealt with.

At the present stage, a lot is unknown about the exact behaviour of the kite, in terms of stability and control. A short overview of different issues that have to be solved, in order to get to a successful design, is given:

- Stability of the kite: calculate how stable the kite truly is and define in what manner the control pod can help stabilizing it.
- Control line characteristics: calculate the forces in the control line and quantify the amount of power needed by the winches inside the control pod for correct kite performance.
- Testing the control line wearing: while controlling the kite, the control line is moving along winches and pulleys. Slipping will cause wear of the control line. This wear should be investigated and quantified.
- Autopilot testing: by building a prototype of the kite and control pod, the autopilot functioning can be tested and verified. Also the stability of the kite, while being guided up through the wake, can be verified.

When the aforementioned uncertainties are dealt with and measures are taken to improve the kite and control pod design, the system is ready for further development in terms of stability and control.

26.4 Operations

When all previous research is done, the operations of the kite will be tested using a full scale prototype in an onshore environment. The goal of these tests is not to optimize the kite any more, but to investigate whether the system functions as expected. First the tether retraction system (TRS) is tested. The kite is launched and retracted multiple times. Besides the functioning of the TRS, the main point of interest is the behaviour of the kite in the wake of a turbine. This is assessed by letting the kite move up and down in the wake for an extended period and investigating its stability.

After the TRS is tested, the Health Monitoring System (HMS) is tested. The different subsystems are turned off one by one and it is observed whether the kite does what it should do in case of such an emergency. Also the kite is left in the air, when it is expected that there will be no wind. It is then observed whether the HMS retracts the kite, after noticing the absence of wind with the tether tension meter.

Once the kite is actually placed in an offshore wind farm for the first time, the operations are evaluated regularly during the first couple of months. This is to detect and repair errors and failures in the system.

Chapter 27

Conclusion

The purpose of this report was to come up with a detailed design of a device that can fulfil all requirements set by the client. The main goal was to increase the efficiency of the OWEZ wind farm by at least 3%. In the end, the design should be able to perform its functions, while being sustainable and profitable, posing little or no risks to its surroundings and human beings.

The design of the kite system was done for OWEZ, afterwards the applicability of the device to other wind farms was verified. When looking at the kite concept, three main structural parts were identified, namely the aerial segment, the tether and the ground segment.

Each of these was worked out in detail. This was done in the following way. From aerodynamic calculations, considering the given requirements, the loads and stresses present in the subsystems were identified. From these, the structures and materials were selected and the overall system performance was evaluated. From the achieved efficiency increase and the system costs, the overall profit of applying the kite system to OWEZ was estimated.

By iterating the aforementioned method for different wind farm efficiency increases, the design was optimized.

For this project, there were several requirements set by the client that had to be fulfilled. These are shown in the first column of table 27.1. The second column shows the results.

Table 27.1: Results

Requirement	**Result**
$\geq$ 3% wind farm efficiency increase	4.3% increase
20 years lifetime	20 years
2 years maintenance interval	2 years
cost efficient	> €6M profit
applicable to OWEZ	yes
scalable to other wind farms	to be determined

When looking at the results, it can be stated that all requirements, when applying the kite system to OWEZ, are satisfied. A wind farm efficiency increase of 4.3% is achieved by a kite with a projected surface of 128 [m^2] and a projected span of 16 [m]. This kite is actively controlled by a control pod. The main materials used in the different segments are: Dacron for the kite, Dyneema for the tether and Glass fiber for the Buoy. This system provides a profit of more than €6M, while the device performs its functions for 20 years. The first subsystem that has to be maintained is the kite, which will be after two years, satisfying the corresponding requirement. Next to the fact that the kite system is applicable to OWEZ, it can be applied to other wind farms, depending on their characteristics. Whether the kite can be scaled and in what sense this can be done, to apply it to other wind farms is yet to be determined.

All functions can be performed in a sustainable way, posing negligible risks to its surroundings and human beings.

To get to a fully operating and effective device, further research has to be performed to verify the findings in this report. The calculations should be extended, after which CFD and FEM models can be made. When the outcomes are processed and are satisfying, a wind tunnel test can be performed, in which the performance of the kite can be measured. Again, when the outcomes are processed and are satisfying, a full-scale model can be built. Now, it can be verified whether and in what sense the device acts like it was analysed.

Bibliography

[1] W.A.A.M. Bierbooms, *Project Guide DSE: Wind Farm Efficiency*, 2011. Issue 1.

[2] A. Curvers, P.A. vd Werff, "OWEZ wind farm efficiency," tech. rep., NoordzeeWind, August 2009.

[3] M.P. de Jong, "OWEZ corrosion inspections." `http://www.noordzeewind.nl/files/Common/Data/OWEZ_R_111_20101020_corrosion_2009_R01.pdf`, 2009.

[4] "Wake efficiency." `http://www.noordzeewind.nl/files/Common/Data/OWEZ_R_183_20070101-20080301_wake_efficiency-20090813.pdf`, 2011.

[5] "OWEZ general report." `http://www.noordzeewind.nl/files/Common/Data/OWEZ_R_141_20080215%20General%20Report.pdf`, 2008.

[6] "OWEZ metingen wind, golven en stromingen." `http://www.noordzeewind.nl/files/Common/Data/OWEZ_R_122_Wave_20050701_20081231-20100107.pdf`, 2009.

[7] "Kiting for non-kiters." `http://jimbodouglass.blogspot.com/2010/03/kiteboarding-stuff-for-non-kiters-to.html`, 2011.

[8] T. Oke, *Boundary Layer Climates*. Methuen, 1987.

[9] S. Barth, "Comparison of OWEZ wind speed and wind direction measurements with meetpost Noordwijk, Ijmuiden and K13," tech. rep., NoordzeeWind, 2008.

[10] "Geo marine ropes for special lines." `http://www.gleistein.com/en-geo-marine-ropes/special-lines/skysails-ropes`, 2011.

[11] "Systems engineering summary." `http://www.aerostudents.com/thirdyear/systemsEngineering.php`, 2009.

[12] H. Korterink, P.J. Eecen, J.W. Wagenaar, "Meteorological measurements OWEZ, half year report 01-01-2008 - 30-06-2008." `http://www.ecn.nl/docs/library/report/2008/e08062.pdf`, 2008.

[13] A. Betz, *Introduction to the theory of flow machines*. Pergamon Press, 1966.

[14] "Vestas V90-3.0 MW Offshore." `http://www.vestas.com/en/wind-power-plants/procurement/turbine-overview/v90-3.0-mw-offshore.aspx#/vestas-univers`, 2011.

[15] N. Timmer, "Introduction to wind energy: Aerodynamic theory." Delft University of Technology, 2010.

[16] W. Weibull, "A statistical distribution function of wide applicability," *Journal of Applied Mechanics*, vol. 18, no. 3, 1951.

[17] F. B. Guillen, "Development of a design tool for offshore wind farm layout optimization," Master's thesis, Delft University of Technology, 2010.

[18] P. Frohboese, "Thrust coefficients used for estimation of wake effects for fatigue load calculation," tech. rep., Windtest Kaiser-Wilhelm-Koog GmbH, 2010.

[19] "Wolfram mathematica." `http://www.wolfram.com/mathematica/`, 2011.

[20] N.O. Jensen, "A note on wind generator interaction," tech. rep., Riso National Laboratory, 1983.

[21] H. Korterink and W. J. Eecen, P.J., "Meteorological measurements OWEZ." `http://www.ecn.nl/docs/library/report/2008/e07073.pdf`, 2008.

[22] M.A. Azim, "Mixing layer flow with initially non-parallel streams," tech. rep., Bangladesh University of Engineering and Technology, 2005.

[23] A.K.M. Sadrul Islam, "Plane mixing layers from parallel and non-parallel merging of two streams," tech. rep., Islamic University of Technology, 2003.

[24] J. Anderson, *Fundamentals of Aerodynamics*. McGraw-Hill, 2001.

[25] N. Enjalbert, "An entrainment model for the turbulent jet in a coflow," *C.R. Mecanique*, vol. 337, 2009.

[26] "Momentum theory of lift." `http://www.onemetre.net/design/downwash/Momentum/Momentum.htm`, 12 June, 2011.

[27] "Wake effect model." `http://www.wasp.dk/Products/WAsP/WakeEffectModel.html`, 2011.

[28] N. Enjalbert, "Measurements of entrainment by axisymmetric turbulent jets," *Journal of Fluid Mechanics*, vol. 11, 1961.

[29] A. vd Berg, L. Denies, T. Dikici, D Dykstra, "Analysis of kite performance for power generation," tech. rep., Delft University of Technology, 2011.

[30] T. Gerz, F. Holzäpfel, and D. Darracq, "Aircraft wake vortices: Position paper," tech. rep., WakeNet, 2001.

[31] P. Saffman, *Vortex dynamics*. Cambridge University Press, 1992.

[32] "Flat inflatable kites, flat leis, bow kites." `http://kitesurfingschool.org/Flat%20LEI.htm`, 2007.

[33] "Power kites for wind energy generation." `http://www.kitegen.com/pdf/IEEECSM200712.pdf`, 2007.

[34] "Reference system of kite." `http://www.skysails.info/deutsch/infothek/hintergrundinformationen/skysails-im-luftraum/`, 2010.

[35] G.J.J. Ruijgrok, "AE3-202 Flight Dynamics Reader." `http://blackboard.tudelft.nl/bbcswebdav/courses/18809-101103/FlightDynamicsLN_V2.pdf`, 2011.

[36] "Shadowbox manual." `http://www.shadowboxlive.com/downloads/SHADOWBOX_Manual_Low_Res_DEC_09.pdf`, 2009.

[37] "Kite GPS measuring." `http://shadowboxlive.com/`, 2011.

[38] "Kite forum." `http://www.kiteforum.com/viewtopic.php?f=1&t=2364150&start=10`, 2010.

[39] "An engineering methodology for kite design." `http://www.lr.tudelft.nl/fileadmin/Faculteit/LR/Organisatie/Afdelingen_en_Leerstoelen/Afdeling_AEWE/Applied_Sustainable_Science_Engineering_and_Technology/Publications/doc/Thesis_Jeroen_Breukels_Compressed.pdf`, 2010.

[40] J.F. Kemp, P. Young, *Ship stability: notes and examples.* Stanford Maritime, 1977. 2nd ed.

[41] J. Harland, *Seamanship in the age of the sail.* London: Conway Maritime Press, 1984.

[42] J. Comstock, *Principles of Naval Architecture.* New York: Society of naval architects and marine engineers, 1967.

[43] J. Black, "Ship stability and buoyancy." `http://www.globalsecurity.org/military/library/policy/navy/nrtc/14057_ppr_ch12.pdf`, 2011.

[44] "Kitepower." `http://www.kitepower.com/`, 2011.

[45] A. de Wachter, "Componentgewichten control pods," 2011.

[46] S. Hoerner, *Fluid dynamic lift.* USA: Hoerner Fluid Dynamics, 2011.

[47] J. Breukels, *An Engineering Methodology for Kite Design.* PhD thesis, Delft University of Technology, 2010.

[48] K. Hedlund, "Wing-, cube- and aeroelastic simulations in unicorn," tech. rep., Royal Institute of Technology, 2010.

[49] T.B. Davis, C. Nelson, *Mechanical Trades Pocket Manual.* Audel, 2004.

[50] S. Kurtz, *The UHMWPE handbook.* Academic Press, 2004.

[51] J. Breukels, "MSC ADAMS kite simulation toolbox." `http://lr.tudelft.nl/index.php?id=25830&L=1`, 2011.

[52] J.D. Rumisek, C.E. Wade, D.E. Brooks, C.V. Okerberg, M.J. Barry, J.S. Clarke, "Heat-denatured albumin-coated dacron vascular grafts: physical characteristics and in vivo performance." `http://www.ncbi.nlm.nih.gov/pubmed/2942709`, August 1986.

[53] "Computational Fluid and Solid Mechanics (CFSM), course AE3031, Delft University of Technology." `http://blackboard.tudelft.nl/webapps/portal/frameset.jsp?tab_tab_group_id=_10_1&url=%2Fwebapps%2Fblackboard%2Fexecute%2Flauncher%3Ftype%3DCourse%26id%3D_31610_1%26url%3D`, 2010.

[54] MSC Software, "Patran release guide." `http://www.mscsoftware.com/support/prod_support/patran/documentation/patran_2008r1_doc_release.pdf`, 2008.

[55] A.K. vd Vegt, L.E. Govaert, *Polymeren, van keten tot kunststof.* VSSD, 2005.

[56] S. Veldman, O. Bergsma, and A. Beukers, "Bending of anisotropic inflated cylindrical beams," tech. rep., Faculty of Aerospace Engineering, Delft University of Technology, 2004.

[57] C. Wielgosz, "Bending and buckling of inflatable beams: Some new theoretical results," tech. rep., Faculty of Sciences of Nantes, 2005.

[58] K.L. Apedo, "Theoretical analysis of inflatable beams made from orthotropic fabric," tech. rep., Universite de Lyon, 2009.

[59] S.L. Veldman, C.A.J.R. Vermeeren, H.E.N. Bersee, O.K. Bergsma, "Conceptual design of a high altitude kite," tech. rep., Universite de Lyon, 2009.

[60] T.H.G. Megson, *Aircraft Structures for Engineering Students.* Elsevier Science & Technology, 2010.

[61] W. D. Callister, Jr., *Materials Science and Engineering, An Introduction.* John Wiley and Sons, Inc., 2007.

[62] "Dassault Systemes CATIA V5R20." `http://www.3ds.com/products/catia/portfolio/catia-v5/catia-v5r20/`, 2011.

[63] R.C. Hibbeler, *Mechanics of Materials.* Prentice Hall, Englewood Cliffs, 1997. 3rd ed.

[64] C. A. Featherston, C. Ruiz, "Buckling of flat plates under bending and shear," *Proc Instn Engrs*, vol. 212, 1998.

[65] U. Meier, "Strengthening of structures using carbon fibre/epoxy composites," *Construction and Building Materials*, vol. 9, 1995.

[66] P.A. Tipler, G. Mosca, *Physics for Scientists and Engineers, Volume 1.* New York, NY: Worth publishers, 2008. 6th ed.

[67] G. Elert, "Density of concrete." `http://hypertextbook.com/facts/1999/KatrinaJones.shtml`, 2001.

[68] "Friction coefficient." `http://www.supercivilcd.com/FRICTION.htm`, 2011.

[69] "Voortstuwing en weerstand." `http://www.studeersnel.nl/cms/downloads/1300924103/2006juni_met.pdf`, 2010.

[70] Koninklijk Belgish instituut voor Natuurwetenschappen, "NOS stroming voorspelling." `http://www.mumm.ac.be/NL/Models/Operational/Currents/animation.php?depth=depth-mean#tbl`, 2011.

[71] M. Segeren, June 2011. Offshore department, Delft University of Technology.

[72] G. Headifen, "anchoring a sailboat." `http://www.nauticed.org/blog/tag/swing-of-an-anchor/`, March 2009.

[73] DAMEN, Anchor and chain factory, "Density of concrete." `http://www.akfanchorchain.nl/activities.html`, 2001.

[74] "Fiber guide." `http://www.doylesails.com/design/fiber.html`, 2011.

[75] "Discussion about sailcloth." `http://macksails.com/sailclth.htm`, 2011.

[76] "Polyester film or mylar film properties." `http://www.tapplastics.com/uploads/pdf/Prod%20Data-%20Polyester%20Film.pdf`, 2011.

[77] "DuPont Tedlar PVF films and adhesives." `http://www2.dupont.com/Tedlar_PVF_Film/en_US/index.html`, 2011.

[78] "Polyvinyl fluoride film." `http://www2.dupont.com/Tedlar_PVF_Film/en_US/assets/downloads/pdf/Tedlar_GeneralProperties.pdf`, 2011.

[79] "Polyvinyl fluoride film, product and properties guide." http://www.welchfluorocarbon.com/DuPontHighPerformanceFilm_TeflonFEPTeflonPFATefzelETFETedlarPVFKaptonPI/H-51252-2_DuPontTedlarPVFProductInformation.pdf, 2011.

[80] "Steering system." http://www.skysails.info/english/products/the-skysails-technology/system-components/steering-system/, 2011.

[81] "What are carbon fibers." http://www.carbonfiber.gr.jp/english/, 2011.

[82] "Ropes for off-shore mooring and installation." http://www.dyneema.com/en_US/public/dyneema/page/segment/Offshore.jsp, 2011.

[83] "Dyneema, the world strongest fiber." http://www.dyneema.com/en_US/public/dyneema/page/about/Dyneema.htm#Dyneema-content, 2011.

[84] "FibreMax Dyneema cables." http://www.fibremax.nl/data/www.fibremax.nl/upload/files/Dyneema%20Cables.pdf, 2011.

[85] "The right fibre for whatever challenges lie ahead." http://www.marlowropes.com/index.php?option=com_content&view=article&id=285&Itemid=330, 2011.

[86] W. S. Association, "Offshore platforms." http://steeluniversity.org/content/html/eng/default.asp?catid=176&pageid=2081271912, 2011.

[87] M.P. Ryan, D.E. Williams, R.J. Chater, B.M. Hutton, D.S. McPhail, "Why stainless steel corrodes," *Macmillan Magazines, Nature*, vol. 415, no. 770-774, 2002.

[88] Strongwell, "Compare extren vs. steel." http://www.strongwell.com/PDFfiles/Extren/EXTREN%20vs%20Steel%20Comparison%20Flyer.pdf, 2011.

[89] B. Precast, "A little book of concretel." http://www.britishprecast.org, 2011.

[90] "Dyneema high-strength, high-modulus polyethylene fiber." http://www.dyneema.com/en_US/public/dyneema/downloads/Comprehensive_factsheet_UHMWPE.pdf, 2011.

[91] "Dyneema winchline." http://www.alibaba.com/product-free/113237787/Dyneema_Winchline.html, 2011.

[92] "Polyester (thermoset)." http://www.efunda.com/materials/polymers/properties/polymer_datasheet.cfm?MajorID=P-TS&MinorID=6, 2011.

[93] "Technical information - Polyacrylonitrile-butadiene-styrene." http://www.goodfellow.com/catalogue/GFCat2C.php?ewd_token=tfHG0v2Z2Yds8SnaVEjPF9cWoZizYW&n=KEM28LOJH28wdVCiHVI5M6pNiQIc2P&ewd_urlNo=GFCat24&type=30&prop=3, 2011.

[94] "Low price tedlar film tpe film, solar EVA backsheet." http://www.alibaba.com/product-gs/349976258/low_price_tedlar_film_tpt_tpe.html, 2011.

[95] "Mechanical properties of carbon fibre composite materials, fibre/epoxy resin (120 Â°C Cure)." http://www.performance-composites.com/carbonfibre/mechanicalproperties_2.asp, 2011.

[96] "Independent final/midterm evaluation of the community-based innovations to reduce child labor through education project (circle) in asia." http://www.dol.gov/ilab/projects/asia/CIRCLEI&IIAsia_Winrock_feval.pdf, 2007.

[97] "Stop kinderarbeid - school de beste werkplaats." http://www.stopchildlabour.eu/stopkinderarbeid/Nederlands/Nieuws/Artikelen/%28offset%29/40, 2009.

[98] O.K. Bergsma, J. Sinke, C.A.J.R. Vermeeren, *Materials & Manufacturing 2 reader.* Delft University of Technology, 2006.

[99] "Tedlar pvf resins." http://www2.dupont.com/Tedlar_PVF_Film/en_US/products/resins.html, 2011.

[100] S. Mazumdar, *Composites Manufacturing: Materials, Products, and Process Engineering.* CRC Press, 2002.

[101] R. Alexander, "Basics of composite construction." http://exp-aircraft.com/library/alexande/composit.html, 1999.

[102] P. Kember, *Europa motor glider - introduction*, 2009. Issue 1.

[103] canadian coast guard. http://www.marinfo.gc.ca/en/flotte/Tracy.asp, 2010.

[104] "Surfplan kite software - products." http://www.surfplan.com.au/sp/products.htm, 2011.

[105] "Sustainability course Delft University of Technology (AE3T11)," tech. rep., Delft University of Technology, 2010.

[106] "Degradation of solar panels." http://www.renewable-energy-sources.com/2009/07/30/pv-panels-efficiency-degradation-factors/, 2011.

[107] W.J. Larson, "Space mission analysis and design," 1995.

[108] "Pc chip thin client." http://www.microsoft.com/windowsembedded/europe/greensolutions/chip-pc-reduces-college-energy.html, 2011.

[109] "HADEF engine description." www.sternkopf.de/upload/dokumente/HADEF%20fig42_87e.pdf, 2011.

[110] "Rynite pet, thermoplastic polyester resin." http://plastics.dupont.com/plastics/pdflit/americas/rynite/H72128.pdf, 2010.

[111] PETRA - The PET Resin Association, "An introduction to pet." http://www.petresin.org/pdf/AnIntroductiontoPET.pdf.

[112] D. E. View, "A comparative analysis of photovoltaic backsheet material performance." http://www2.dupont.com/Photovoltaics/en_US/assets/downloads/pdf/Tedlar_Backsheet_ExpertView.pdf, 2010.

[113] D. Polymers, "Tedlar pvf transparent films material safety data sheet," tech. rep., Toxic Substances Control Act, U.S. Federal Regulations Authority, 2004.

[114] R. S. Stein, "Polymer recycling: Opportunities and limitations," *Colloquium Paper*, vol. 89, 1992.

[115] "2010 sustainability progress report." http://www2.dupont.com/Sustainability/en_US/DuPont_2010_Sustainability_Progress_Report.pdf, 2011.

[116] D. J. Alberts, "Addressing wind turbine noise," tech. rep., Lawrence Technological University, 2006.

[117] D.S. Achilias, E. Antonakou, C. Roupakias, P. Megalokonomos, A. Lappas, "Recycling techniques of polyolefins from plastic wastes," tech. rep., Laboratory of Organic Chemical Technology, Department of Chemistry, Aristotle University of Thessaloniki, 2008.

[118] "DSM Dyneema in maritime." http://www.dyneema.com/en_US/public/dyneema/page/segment/Maritime.jsp, 2011.

[119] "No.1 in 2009 dow jones sustainability index." http://www.dsm.com/en_US/downloads/sustainability/triple_p_2009_11_13.pdf, 2011.

[120] W. Wilson, "Equation for the speed of sound in sea water," *The Journal of the acoustical society of America*, vol. 32, no. 10, 1960.

[121] D. de Haan, D. Burggraaf, S. Ybema, R.H.R. Lambers, "Underwater sound emissions and effects of the pile driving of the OWEZ windfarm facility near Egmond aan Zee," tech. rep., NoordzeeWind, 2007.

[122] "Acoustic impacts on marine life." http://www.oceanmammalinst.com/pdfs/Acoustic-Impacts-on-Marine-Life.pdf, 2011.

[123] J. Sajiki, J. Yonekubo, "Inhibition of seawater on bisphenol A (BPA) degradation by Fenton reagents," *Environment International*, vol. 30, no. 145-150, 2004.

[124] "Worldwide wind turbine market and manufacturing trends." http://www.folkecenter.net/mediafiles/folkecenter/pdf/Market_and_Manufacturer_Trends.pdf, 2008.

[125] "Wind turbines: In the wake of the wind." http://www.sciencedaily.com/release/2011/04/110426151040.htm, 2011.

[126] "Power kite prices." http://powerkiteshop.com/, 2011.

[127] "ASSET department, Delft University of Technology." http://www.spiegel.de/wissenschaft/technik/0,1518,763535,00.html, 2011.

[128] "Thin client PC." http://www.bizrate.com/desktop-computers/oid2440838967.html, 2011.

[129] "Grid-tie solar system inverters." http://www.solarelectricsupply.com/Inverters/inverters.html, 2011.

[130] "Solar panels." http://www.ecobusinesslinks.com/solar_panels.htm, 2011.

[131] "Glass fibre price list." http://www.cybglassfibre.co.uk/glass-fibre-price-list.asp, 2011.

[132] "Steel fibre price list." http://www.meps.co.uk/world-price.htm, 2011.

[133] "Alibaba B2B platform." http://www.alibaba.com, 2011.

[134] "Steel ocean buoy prices." http://www.uscg.mil/hq/cg4/cg432/2b_buoysfoam.asp, 2011.

[135] "Installation of a wind turbine in one step." http://www.ecn.nl/fileadmin/ecn/units/wind/docs/dowec/10074_000.pdf, 2010.

[136] "Offshore windpark egmond aan zee, owez." http://www.noordzeewind.nl/index.php?url=project_5.html, 2011.

[137] "Introduction to wind energy course of the TU Delft AE3W02TU." http://blackboard.tudelft.nl/bbcswebdav/xid-2134703_2, 2010.

[138] "Statistical data warehouse." http://sdw.ecb.europa.eu/, 2011.

[139] "Inflatie 2010." http://www.homefinance.nl/economie/inflatie/inflatie-nederland-cpi.asp, 2010.

[140] "Risicovrij en te voet." http://www.rijksoverheid.nl/documenten-en-publicaties/kamerstukken/2009/09/15/kamerbrief-inzake-lange-termijn-discontovoet.html, 2010.

[141] "Return on investment." http://www.investopedia.com/terms/r/returnoninvestment.asp/, 2009.

[142] "Clyde wind farm project details." http://www.sse.com/Clyde/ProjectDetails/, 2011.

[143] "Clyde wind farm layout." http://www.scotland.gov.uk/Resource/Doc/917/0064217.pdf, 2006.

[144] T. Boehme, "Hindcasting hourly wind power across scotland based on met station data," tech. rep., Wiley Interscience, 2007.

[145] "Thanet non technical summary." http://www.warwickenergy.com/pdf/ThanetNTSlr.pdf, 2005.

[146] "Global offshore wind farms database." http://www.4coffshore.com/offshorewind/, 2011.

[147] "Europe's onshore and offshore wind energy potential," tech. rep., EEA, 2009.

[148] "Growth opportunity in global onshore and offshore operation & maintenance market." http://www.lucintel.com/LucintelBrief/OpportunityinOnshoreandOffshoreOMMarket.pdf, 2011.

[149] "Lavision: Particle image velocimetry." http://www.lavision.de/de/techniques/piv.php, 2011.

[150] M. Raffel, C. E. Willert, S. T. Wereley, and J. Kompenhans, *Particle Image Velocimetry: A Practical Guide*. Springer, 1998.

[151] Z. Zhang and Y. Tamura, "Wind tunnel test on cable dome of geiger type," *Journal of Computational and Nonlinear Dynamics*, vol. 2, no. 3, 2007.

[152] "Standard atmosphere calculator." http://aero.stanford.edu/StdAtm.html, 1997.

[153] "Windtunnel kite research with a flysurfer pulse2." http://www.youtube.com/watch?v=uX8dy7sDm1o, 2009.